

Technische Universiteit Delft

# Master Thesis

Assessing the impact of spectral fringes on astronomical line fluxes

Manar, el Akel (4271548)

# Master Thesis

Assessing the impact of spectral fringes on  
astronomical line fluxes

Aerospace Engineering- October 2018

by

Manar, el Akel (4271548)

Principal Mentor: Dr. Brandl B. TUDelft

Second Mentor: Dr. Lahuis E. SRON

Cover page – Tech Insider: [\[17\]](#) [cited 14 June 2018]

This page is intentionally left blank

# Summary

The following report aims to provide an initial approach to the user for quantifying the diverse methods for correcting the fringes within astronomical spectra. This study is developed as part of the Master thesis conducted at the Aerospace Engineering Faculty of Delft University of Technology.

Determining the composition of the environment in space has always been a key feature for understanding it. Perceiving what cannot be seen by the human eye on images was realized by means of spectrometers, combined with focal plane detectors. Spectral features depicted on the delivered spectra provide scientists with vital information on the observed entities. However, further analysis showed that multi-beam interference of the light spectrum occurred within this instrumentation, misleading the results. This physical principle, also called as the Fabry-Pérot principle, generates fringes, that appeared to be present in many space telescope instruments such as the STIS, SWS/LWS, Spitzer IS, HIFI and the MRS. Therefore, the need to find a reliable solution for correcting these fringes has been a key requirement within the astronomy, especially for the future spectrometers and dedicated detectors to be sent in space on board the James Webb Space Telescope in 2019.

The main purpose of this new telescope is to see what the HST could not see; by using longer wavelengths and thus using the infrared to look at the universe, contrary to the HST, which used the optical wavelengths range and ultraviolet. Placed on the second Lagrange point (L2), the JWST is expected to distinguish further objects than the HST as those are more red-shifted. Furthermore, the size the JWST has significantly been increased allowing a larger field of view and a better spatial resolution. The JWST will observe at a wide range of wavelengths (5-28  $\mu\text{m}$ ), allowing it to improve the spectral knowledge of planet atmosphere and determine their energy balance. The telescope has four scientific instruments on board: a near-infrared camera (NIRCam), a near-infrared spectrograph (NIRSpec), a fine guidance sensor/near infrared imager & slitless spectrograph (FGS/NIRISS) and a mid-infrared instrument (MIRI).

Different methods have been developed throughout the years for correcting these fringes. Nonetheless, it appeared more arduous than a simple data correction due to the nature of the fringes. Each fringe pattern is unique, notably due to its light source characteristics. Therefore a definite algorithm could not be applied to all spectra and deliver highly reliable results. However, no specific study has reported all the methods for quantifying their impact on the astronomical line fluxes. The current option selected by most scientists for defringing is the combination of the pixel flat-fielding and the sine-wave fitting, as it appears currently as the most robust combination for processing the data, despite its flaws.

This study considered three main defringing methods: the sine-wave fitting, the Fourier filtering and the multiplicative method. Each of them were developed and tested in two stages namely the theoretical and the practical aspects, based on created data set and MIRI data, respectively. All the methods developed were quantified based on two criteria: the graphical representation (i.e. how good is the final spectrum quality) and the amplitude match of the spectral features found w.r.t the intrinsic ones. However, this later criterion could not be considered for the MIRI data set as its intrinsic spectral features were unknown. The study was further investigated by developing and testing specific combinations of the discussed defringing methods and their optimized versions. At this stage, an algorithm perfectly correcting the fringes was not found, but this study does rank the different methods and propose a method providing reliable and satisfying results. This report provides not only an overview of the different methods to any

reader, but also quantifies their impact on astronomical line fluxes. The second aim of this report is therefore to be considered as a basis for further development on de-fringing methods.

All the algorithms used in this study have been developed independently to any existing algorithms and can be obtained on request via email ([m.elakel@student.tudelft.nl](mailto:m.elakel@student.tudelft.nl)). An overview of the code architecture can be found in [Appendix A](#).

This page is intentionally left blank

# Preface

This document represents the work of six months for a master thesis realized at the Aerospace Engineering Faculty of Delft University of Technology. This report studies the effect on the different defringing methods on astronomical line fluxes, which are tested on the data expected by MIRI, instrument intended to the James Webb Space Telescope. Its purpose is to provide information on this subject to any person who has a general interest in the Fabry-Pérot effect within spectrometers instrumentation.

This paper reports the entire study realized. However, for the sake of clarity, for each section of the different algorithmic tests in the *Theoretical Model*, a conclusion has been made summarizing the outcome from the corresponding section; allowing the reader to skip the previous subsections without losing information.

I would like to express my gratitude towards my mentors, Bernhard Brandl and Fred Lahuis; for giving me the opportunity to work on this project and for their expertise and guidance during this research. I would also thank Migo Mueller for his precious advice, and my family for their continuous support.

*Manar, el Akel (4271548)*  
*Delft, the 30th of August 2018*

This page is intentionally left blank

# Contents

<b>Summary</b>	<b>iii</b>
<b>List of Figures</b>	<b>xi</b>
<b>List of Tables</b>	<b>xix</b>
<b>Nomenclature</b>	<b>xxii</b>
<b>1 Introduction</b>	<b>1</b>
<b>2 Problem Definition</b>	<b>3</b>
2.1 Aim of the study . . . . .	3
2.2 Assessment criteria . . . . .	4
2.2.1 Detectability . . . . .	4
2.2.2 Photometric accuracy . . . . .	5
<b>3 Spectral Fringes</b>	<b>6</b>
3.1 Origin of the spectral fringe pattern . . . . .	6
3.2 Instrumental fringes within MIRI . . . . .	8
<b>4 Traditional Defringing methods - Theoretical Model</b>	<b>9</b>
4.1 Flux Spectra . . . . .	9
4.2 Method 1: Fourier Filtering . . . . .	13
4.2.1 Theoretical Background . . . . .	13
4.2.2 All Cases . . . . .	13
4.2.3 Conclusion . . . . .	21
4.3 Method 2 : Sine Wave Fitting . . . . .	23
4.3.1 Theoretical Background . . . . .	23
4.3.2 Case (1) . . . . .	25
4.3.3 Case (2) . . . . .	33
4.3.4 Case (3) . . . . .	41
4.3.5 Conclusion . . . . .	49
4.4 Method 3 : Multiplicative method . . . . .	52
4.4.1 Theoretical Background . . . . .	52
4.4.2 Case (1) . . . . .	53
4.4.3 Case (2) . . . . .	55
4.4.4 Case (3) . . . . .	57
4.4.5 Conclusion . . . . .	59
4.5 Conclusion: Method's Comparison . . . . .	60
<b>5 Traditional Defringing Methods - MIRI Application</b>	<b>65</b>
5.1 MIRI Data sets . . . . .	65
5.1.1 Data Selection . . . . .	65

5.1.2	Data Quality Required . . . . .	66
5.2	Fourier Filtering. . . . .	66
5.2.1	FM Data Set 1 for Channel 2B . . . . .	67
5.2.2	CV3 Data Set 2 for Channel 1C . . . . .	69
5.3	Sine Wave Fitting . . . . .	72
5.3.1	FM Data Set 1 for Channel 2B . . . . .	72
5.3.2	CV3 Data Set 2 for Channel 1C . . . . .	74
5.4	Multiplicative method . . . . .	76
5.4.1	FM Data Set 1 for Channel 2B . . . . .	76
5.4.2	CV3 Data Set 2 for Channel 1C . . . . .	77
5.5	Conclusion . . . . .	78
<b>6</b>	<b>Method Combinations - Theoretical Model</b>	<b>80</b>
6.1	Combination 1: Fourier Filtering - multiplicative method Modification. . . . .	80
6.1.1	Case (1) . . . . .	81
6.1.2	Case (2) . . . . .	82
6.1.3	Case (3) . . . . .	83
6.1.4	Conclusion. . . . .	85
6.2	Combination 2: Sine Wave Fitting - multiplicative method Modification . . . . .	85
6.2.1	Case (1) . . . . .	85
6.2.2	Case (2) . . . . .	87
6.2.3	Case (3) . . . . .	88
6.2.4	Conclusion. . . . .	89
6.3	Anticipated Conclusion. . . . .	89
<b>7</b>	<b>Optimization - Theoretical Model</b>	<b>91</b>
7.1	Combinations. . . . .	91
7.1.1	OPTIMIZATION 1 - Combination 1: Fourier Filtering - multiplicative method . . . . .	91
7.1.2	OPTIMIZATION 2 - Combination 2: Sine Wave fitting - multiplicative method . . . . .	97
7.1.3	Conclusion. . . . .	103
7.2	Single . . . . .	106
7.2.1	OPTIMIZATION 3 - Sine Wave Fitting . . . . .	106
7.2.2	OPTIMIZATION 4 - multiplicative method . . . . .	111
7.2.3	Conclusion. . . . .	115
7.3	Conclusion . . . . .	117
<b>8</b>	<b>Optimization - MIRI Application</b>	<b>122</b>
8.1	OPTIMIZATION 1 - Combination 1 : Fourier Filtering - Multiplicative Method . . . . .	122
8.1.1	FM Data Set 1 for Channel 2B . . . . .	122
8.1.2	CV3 Data Set 2 for Channel 1C . . . . .	123
8.2	OPTIMIZATION 2 - Combination 2 : Sine Wave Fitting - Multiplicative Method . . . . .	125
8.2.1	FM Data Set 1 for Channel 2B . . . . .	125
8.2.2	CV3 Data Set 2 for Channel 1C . . . . .	127
8.3	OPTIMIZATION 3 - Sine Wave Fitting . . . . .	128
8.3.1	FM Data Set 1 for Channel 2B . . . . .	129
8.3.2	CV3 Data Set 2 for Channel 1C . . . . .	130

---

8.4	OPTIMIZATION 4 - Multiplicative Method . . . . .	131
8.4.1	FM Data Set 1 for Channel 2B . . . . .	131
8.4.2	CV3 Data Set 2 for Channel 1C . . . . .	132
8.5	Conclusion . . . . .	133
<b>9</b>	<b>Conclusion</b>	<b>135</b>
	<b>Bibliography</b>	<b>137</b>
<b>A</b>	<b>Code Architecture</b>	<b>139</b>
A.1	Tool Requirement . . . . .	139
A.2	Tool Overview . . . . .	139
<b>B</b>	<b>Jwst Pipeline</b>	<b>142</b>

# List of Figures

3.1	Scheme of Fredy-Pérot principle . . . . .	7
4.1	Four Peaks introduced in the spectrum . . . . .	10
4.2	Different components of spectrum for Case (1) . . . . .	11
4.3	Different components of spectrum for Case (2) . . . . .	11
4.4	Different components of spectrum for Case (3) . . . . .	12
4.5	All cases spectra . . . . .	12
4.6	Case (1): Fourier Filtering method - Amplitude Fourier Applied. On top: entire wavelengths range, on the bottom: zoom of the central region . . . . .	14
4.7	Case (2): Fourier Filtering method - Amplitude Fourier Applied. On top: entire wavelengths range, on the bottom: zoom of the central region . . . . .	14
4.8	Case (3): Fourier Filtering method - Amplitude Fourier Applied. On top: entire wavelengths range, on the bottom: zoom of the central region . . . . .	15
4.9	Case (1): Fourier Filtering method - Amplitude Fourier Applied with 4 regions- Entire spectrum . . . . .	15
4.10	Case (1): Fourier Filtering method - Amplitude Fourier Applied with 4 regions- Zoom of filtered regions . . . . .	15
4.11	Case (2): Fourier Filtering method - Amplitude Fourier Applied with 4 regions- Entire spectrum . . . . .	16
4.12	Case (2): Fourier Filtering method - Amplitude Fourier Applied with 4 regions- Zoom of filtered regions . . . . .	16
4.13	Case (3): Fourier Filtering method - Amplitude Fourier Applied with 4 regions- Entire spectrum . . . . .	16
4.14	Case (3): Fourier Filtering method - Amplitude Fourier Applied with 4 regions- Zoom of filtered regions . . . . .	16
4.15	Case (1): Fourier Filtering method - Comparison among original spectrum, filtered one and subtracted one . . . . .	17
4.16	Case (2): Fourier Filtering method - Comparison among original spectrum, filtered one and subtracted one . . . . .	17
4.17	Case (3): Fourier Filtering method - Comparison among original spectrum, filtered one and subtracted one . . . . .	18
4.18	Case (1): Fourier Filtering method - Comparison among observed peaks spectrum and the filtered one . . . . .	19
4.19	Case (2): Fourier Filtering method - Comparison among observed peaks spectrum and the filtered one . . . . .	19
4.20	Case (3): Fourier Filtering method - Comparison among observed peaks spectrum and the filtered one . . . . .	19
4.21	Case (1): Comparison among Intrinsic peaks spectrum and the filtered one . . . . .	20
4.22	Case (2): Fourier Filtering method - Comparison among Intrinsic peaks spectrum and the filtered one . . . . .	20
4.23	Case (3): Fourier Filtering method - Comparison among Intrinsic peaks spectrum and the filtered one . . . . .	21
4.24	All cases: Fourier Filtering method - Match of peaks flux w.r.t. to Intrinsic Fluxes - Graphical Representation . . . . .	21
4.25	All cases: Fourier Filtering method - Match of peaks flux of Region 1 and observed ones w.r.t. to Intrinsic Fluxes - Graphical Representation . . . . .	23
4.26	Case (1) Approach I: Sine wave fitting method - Sine Fit for the low frequency component. On the top, the sine fit is for the beginning of the spectrum while on the bottom, the sine fit is for the end of the spectrum . . . . .	26

4.27 Case (1) Approach I: Sine wave fitting method - Sine Fit for the high frequency component. On the top, the sine fit is for the beginning of the spectrum while on the bottom, the sine fit is for the end of the spectrum . . . . .	26
4.28 Case (1) Approach I: Sine wave fitting method - Sine Fit for the low frequency component . . . . .	27
4.29 Case (1) Approach I: Sine wave fitting method - Sine Fit for the high frequency component . . . . .	27
4.30 Case (1) Approach I: Sine wave fitting method - Sine Fit for the high frequency component Zoom . . . . .	27
4.31 Case (1) Approach I: Sine wave fitting method - Total Residuals from the sine fit for the High and low frequency components . . . . .	28
4.32 Case (1) Approach II: Sine wave fitting method - Sine Fit for the low frequency component. On the top, the sine fit is for the beginning of the spectrum while on the bottom, the sine fit is for the end of the spectrum . . . . .	29
4.33 Case (1) Approach II: Sine wave fitting method - Sine Fit for the low frequency component . . . . .	29
4.34 Case (1) Approach II: Sine wave fitting method - Sine Fit for the High frequency component. On the top, the sine fit is for the beginning of the spectrum while on the bottom, the sine fit is for the end of the spectrum . . . . .	29
4.35 Case (1) Approach II: Sine wave fitting method - Sine Fit for the high frequency component . . . . .	29
4.36 Case (1) Approach II: Sine wave fitting method - Residuals from the sine fit for the high frequency component, i.e. total residuals of the spectrum . . . . .	30
4.37 Case (1) Approach III: Sine wave fitting method - Sine Fit for the High frequency component. On the top, the sine fit is for the beginning of the spectrum while on the bottom, the sine fit is for the end of the spectrum . . . . .	31
4.38 Case (1) Approach III: Sine wave fitting method - Sine Fit for the high frequency component . . . . .	31
4.39 Case (1) Approach III: Sine wave fitting method - Sine Fit for the low frequency component. On the top, the sine fit is for the beginning of the spectrum while on the bottom, the sine fit is for the end of the spectrum . . . . .	32
4.40 Case (1) Approach III: Sine wave fitting method - Sine Fit for the low frequency component . . . . .	32
4.41 Case (1) Approach II: Sine wave fitting - Residuals from the sine fit for the low frequency component, i.e. total residuals of the spectrum . . . . .	33
4.42 Case (2) Approach I: Sine wave fitting method - Sine Fit for the low frequency component. On the top, the sine fit is for the beginning of the spectrum while on the bottom, the sine fit is for the end of the spectrum . . . . .	34
4.43 Case (2) Approach I: Sine wave fitting method - Sine Fit for the high frequency component. On the top, the sine fit is for the beginning of the spectrum while on the bottom, the sine fit is for the end of the spectrum . . . . .	34
4.44 Case (2) Approach I: Sine wave fitting method - Sine Fit for the low frequency component . . . . .	35
4.45 Case (2) Approach I: Sine wave fitting method - Sine Fit for the high frequency component . . . . .	35
4.46 Case (2) Approach I: Sine wave fitting method - Sine Fit for the high frequency component Zoom . . . . .	35
4.47 Case (2) Approach I: Sine wave fitting method - Total Residuals from the sine fit for the High and low frequency components . . . . .	36
4.48 Case (2) Approach II: Sine wave fitting method - Sine Fit for the low frequency component. On the top, the sine fit is for the beginning of the spectrum while on the bottom, the sine fit is for the end of the spectrum . . . . .	37
4.49 Case (2) Approach II: Sine wave fitting method - Sine Fit for the low frequency component . . . . .	37
4.50 Case (2) Approach II: Sine Fit for the High frequency component. On the top, the sine fit is for the beginning of the spectrum while on the bottom, the sine fit is for the end of the spectrum . . . . .	37
4.51 Case (2) Approach II: Sine wave fitting method - Sine Fit for the high frequency component . . . . .	37

4.52 Case (2) Approach II: Sine wave fitting method - Residuals from the sine fit for the high frequency component, i.e. total residuals of the spectrum . . . . .	38
4.53 Case (2) Approach III: Sine wave fitting method - Sine Fit for the High frequency component. On the top, the sine fit is for the beginning of the spectrum while on the bottom, the sine fit is for the end of the spectrum . . . . .	39
4.54 Case (2) Approach III: Sine wave fitting method - Sine Fit for the high frequency component . . . . .	39
4.55 Case (2) Approach III: Sine wave fitting method - Sine Fit for the low frequency component. On the top, the sine fit is for the beginning of the spectrum while on the bottom, the sine fit is for the end of the spectrum . . . . .	40
4.56 Case (2) Approach III: Sine wave fitting method - Sine Fit for the low frequency component . . . . .	40
4.57 Case (2) Approach II: Sine wave fitting method - Residuals from the sine fit for the low frequency component, i.e. total residuals of the spectrum . . . . .	41
4.58 Case (3) Approach I: Sine wave fitting method - Sine Fit for the low frequency component. On the top, the sine fit is for the beginning of the spectrum while on the bottom, the sine fit is for the end of the spectrum . . . . .	42
4.59 Case (3) Approach I: Sine wave fitting method - Sine Fit for the high frequency component. On the top, the sine fit is for the beginning of the spectrum while on the bottom, the sine fit is for the end of the spectrum . . . . .	42
4.60 Case (3) Approach I: Sine wave fitting method - Sine Fit for the low frequency component . . . . .	43
4.61 Case (3) Approach I: Sine wave fitting method - Sine Fit for the high frequency component . . . . .	43
4.62 Case (3) Approach I: Sine wave fitting method - Sine Fit for the high frequency component Zoom . . . . .	43
4.63 Case (3) Approach I: Sine wave fitting method - Total Residuals from the sine fit for the High and low frequency components . . . . .	44
4.64 Case (3) Approach II: Sine wave fitting method - Sine Fit for the low frequency component. On the top, the sine fit is for the beginning of the spectrum while on the bottom, the sine fit is for the end of the spectrum . . . . .	45
4.65 Case (3) Approach II: Sine wave fitting method - Sine Fit for the low frequency component . . . . .	45
4.66 Case (3) Approach II: Sine wave fitting method - Sine Fit for the High frequency component. On the top, the sine fit is for the beginning of the spectrum while on the bottom, the sine fit is for the end of the spectrum . . . . .	45
4.67 Case (3) Approach II: Sine wave fitting method - Sine Fit for the high frequency component . . . . .	45
4.68 Case (3) Approach II: Sine wave fitting method - Residuals from the sine fit for the high frequency component, i.e. total residuals of the spectrum . . . . .	46
4.69 Case (3) Approach III: Sine wave fitting method - Sine Fit for the High frequency component. On the top, the sine fit is for the beginning of the spectrum while on the bottom, the sine fit is for the end of the spectrum . . . . .	47
4.70 Case (3) Approach III: Sine wave fitting method - Sine Fit for the high frequency component . . . . .	47
4.71 Case (3) Approach III: Sine wave fitting method - Sine Fit for the low frequency component. On the top, the sine fit is for the beginning of the spectrum while on the bottom, the sine fit is for the end of the spectrum . . . . .	48
4.72 Case (3) Approach III: Sine wave fitting method - Sine Fit for the low frequency component . . . . .	48
4.73 Case (3) Approach III: Sine wave fitting method - Residuals from the sine fit for the low frequency component, i.e. total residuals of the spectrum . . . . .	49
4.74 All cases: Sine wave fitting method - Match of peaks flux of Region 1 and observed ones w.r.t. to Intrinsic Fluxes - Graphical Representation . . . . .	50

4.75 All cases: Sine wave fitting method - Match of peaks flux of Approach II and observed ones w.r.t. to Intrinsic Fluxes - Graphical Representation . . . . .	52
4.76 Case (1): multiplicative method - Spectrally flat source spectrum and its inverse . . . . .	53
4.77 Case (1): multiplicative method - Amplification Factors . . . . .	54
4.78 Case (1): multiplicative method - on the left: spectrum from the multiplicative method compared to the original spectral features spectrum. On the right: spectrum from the multiplicative method . . . . .	54
4.79 Case (2): multiplicative method - Spectrally flat source spectrum and its inverse . . . . .	55
4.80 Case (2): multiplicative method - Amplification Factors . . . . .	56
4.81 Case (2): multiplicative method - on the left: spectrum from the multiplicative method compared to the original spectral features spectrum. On the right: spectrum from the multiplicative method . . . . .	56
4.82 Case (3): multiplicative method - Spectrally flat source spectrum and its inverse . . . . .	57
4.83 Case (3): multiplicative method - Amplification Factors . . . . .	58
4.84 Case (3): multiplicative method - on the left: spectrum from the multiplicative method compared to the original spectral features spectrum. On the right: spectrum from the multiplicative method . . . . .	58
4.85 All Cases: multiplicative method - Match of line flux of the spectrum from the multiplicative method w.r.t. the observed one and the intrinsic spectrum - Graphical Representation . . . . .	60
4.86 All methods: Match of peaks flux w.r.t. to Intrinsic Fluxes - Graphical Representation . . . . .	63
4.87 Standard Deviation of line flux matches for all methods . . . . .	64
5.1 MRS - Channel Exposure . . . . .	66
5.2 FM MRS data - Channel 2B -Amplitude Fourier domain . . . . .	67
5.3 FM MRS data - Channel 2B -Amplitude Fourier domain of 2 regions to be filtered . . . . .	67
5.4 FM MRS data - Channel 2B - Amplitude Fourier domain of 2 regions to be filtered - zoom . . . . .	68
5.5 FM MRS data - Channel 2B - comparison among the original spectrum, filtered one and subtracted one for 2 different regions filtered . . . . .	68
5.6 FM MRS data - Channel 2B - Filtered spectrum for 2 different regions . . . . .	69
5.7 FM MRS data - Channel 2B - Filtered spectrum for Region 1 - zoom at interesting spectral feature location (not detected by Region 2) . . . . .	69
5.8 CV3 MRS data - Channel 1C -Amplitude Fourier domain . . . . .	70
5.9 CV3 MRS data - Channel 1C -Amplitude Fourier domain of 2 regions to be filtered . . . . .	70
5.10 CV3 MRS data - Channel 1C - Amplitude Fourier domain of 2 regions to be filtered - zoom . . . . .	71
5.11 CV3 MRS data - Channel 1C - comparison among the original spectrum, filtered one and subtracted one for 4 different regions filtered . . . . .	71
5.12 CV3 MRS data - Channel 1C- Filtered spectrum for 4 different regions . . . . .	72
5.13 CV3 MRS data - Channel 1C - Filtered spectrum for Regions 2 and 3 . . . . .	72
5.14 FM MRS data - Channel 2B - Sine wave fitting - Low and high frequencies components . . . . .	73
5.15 FM MRS data - Channel 2B - Sine wave fitting of low frequency component . . . . .	73
5.16 FM MRS data - Channel 2B - Sine wave fitting - Residuals of the low frequency component . . . . .	73
5.17 FM MRS data - Channel 2B - Sine wave fitting of high frequency component . . . . .	74
5.18 FM MRS data - Channel 2B - Sine wave fitting - Total Residuals of the spectrum . . . . .	74
5.19 CV3 MRS data - Channel 1C - Sine wave fitting - Low and high frequencies components . . . . .	74
5.20 CV3 MRS data - Channel 1C - Sine wave fitting of low frequency component . . . . .	75
5.21 CV3 MRS data - Channel 1C - Sine wave fitting - Residuals of the low frequency component . . . . .	75
5.22 CV3 MRS data - Channel 1C - Sine wave fitting of high frequency component . . . . .	75
5.23 CV3 MRS data - Channel 1C - Sine wave fitting - Total Residuals of the spectrum . . . . .	75

5.24 FM MRS data - Channel 2B - Multiplicative method - observed spectra with spectral features and spectrally flat source . . . . .	76
5.25 FM MRS data - Channel 2B - Multiplicative method - amplification factors . . . . .	76
5.26 FM MRS data - Channel 2B - Multiplicative method - on the right side: the final spectrum. On the left side: the final spectrum compared with the observed one . . . . .	77
5.27 CV3 MRS data - Channel 1C - Multiplicative method - observed spectra with spectral features and spectrally flat source . . . . .	77
5.28 CV3 MRS data - Channel 1C - Multiplicative method - amplification factors . . . . .	77
5.29 CV3 MRS data - Channel 1C - Multiplicative method - on the right side: the final spectrum. On the left side: the final spectrum compared with the observed one . . . . .	78
6.1 Case (1) - Combination 1 - Filtered Spectrum using the Fourier Filtering of Region 1 . . . . .	81
6.2 Case (1) - Combination 1 - Spectrally flat source spectrum . . . . .	81
6.3 Case (1) - Combination 1 - Amplification factors from the multiplicative method . . . . .	81
6.4 Case (1) - Combination 1 - multiplicative method spectrum . . . . .	81
6.5 Case (2) - Combination 1 - Filtered Spectrum using the Fourier Filtering of Region 1 . . . . .	82
6.6 Case (2) - Combination 1 - Spectrally flat source spectrum . . . . .	82
6.7 Case (2) - Combination 1 - Amplification factors from the multiplicative method . . . . .	83
6.8 Case (2) - Combination 1 - multiplicative method spectrum . . . . .	83
6.9 Case (3) - Combination 1 - Filtered Spectrum using the Fourier Filtering of Region 1 . . . . .	84
6.10 Case (3) - Combination 1 - Spectrally flat source spectrum . . . . .	84
6.11 Case (3) - Combination 1 - Amplification factors from the multiplicative method . . . . .	84
6.12 Case (3) - Combination 1 - multiplicative method spectrum . . . . .	84
6.13 Case (1) - Combination 2 - Total residuals set from sine wave fitting of high component (Approach II) .	86
6.14 Case (1) - Combination 2 - Spectrally flat source spectrum and its inverse compared to the residuals spectra ("original") from the sine wave fitting . . . . .	86
6.15 Case (1) - Combination 2 - Amplification Factors . . . . .	86
6.16 Case (1) - Combination 2 - multiplicative method spectrum . . . . .	86
6.17 Case (2) - Combination 2 - Total residuals set from sine wave fitting of high component (Approach II) .	87
6.18 Case (2) - Combination 2 - Spectrally flat source spectrum and its inverse compared to the residuals spectra ("original") from the sine wave fitting . . . . .	87
6.19 Case (2) - Combination 2 - Amplification Factors . . . . .	88
6.20 Case (2) - Combination 2 - multiplicative method spectrum . . . . .	88
6.21 Case (3) - Combination 2 - Total residuals set from sine wave fitting of high component (Approach II) .	88
6.22 Case (3) - Combination 2 - Spectrally flat source spectrum and its inverse compared to the residuals spectra ("original") from the sine wave fitting . . . . .	88
6.23 Case (3) - Combination 2 - Amplification Factors . . . . .	89
6.24 Case (3) - Combination 2 - multiplicative method spectrum . . . . .	89
7.1 Case (1) - Optimization Combination 1 - Filtered Spectrum using the Fourier Filtering of Region 1 . . .	92
7.2 Case (1) - Optimization Combination 1 - Spectrally flat source spectrum (i.e. "original"), its Fourier Filtered spectrum using Region 1 (i.e. "Filtered") and the subtracted spectrum resulting from the subtraction of the original flat source spectrum and the Fourier filtered one. . . . .	92
7.3 Case (1) - Optimization Combination 1 - Filtered spectrally flat source, its inverse and the residuals spectrum from method 1 . . . . .	92
7.4 Case (1) - Optimization Combination 1 - Amplification factors from the multiplicative method method	93
7.5 Case (1) - Optimization Combination 1 - spectrum from multiplicative method . . . . .	93

7.6	Case (2) - Optimization Combination 1 - Filtered Spectrum using the Fourier Filtering of Region 1 . . .	94
7.7	Case (2) - Optimization Combination 1 - Spectrally flat source spectrum (i.e. "original"), its Fourier Filtered spectrum using Region 1 (i.e. "Filtered") and the subtracted spectrum resulting from the subtraction of the original flat source spectrum and the Fourier filtered one. . . . .	94
7.8	Case (2) - Optimization Combination 1 - Filtered spectrally flat source, its inverse and the residuals spectrum from method 1 . . . . .	94
7.9	Case (2) - Optimization Combination 1 - Amplification factors from the multiplicative method method	95
7.10	Case (2) - Optimization Combination 1 - spectrum from multiplicative method . . . . .	95
7.11	Case (3) - Optimization Combination 1 - Filtered Spectrum using the Fourier Filtering of Region 1 . . .	96
7.12	Case (3) - Optimization Combination 1 - Spectrally flat source spectrum (i.e. "original"), its Fourier Filtered spectrum using Region 1 (i.e. "Filtered") and the subtracted spectrum resulting from the subtraction of the original flat source spectrum and the Fourier filtered one. . . . .	96
7.13	Case (3) - Optimization Combination 1 - Filtered spectrally flat source, its inverse and the residuals spectrum from the first method . . . . .	96
7.14	Case (3) - Optimization Combination 1 - Amplification factors from the multiplicative method method	97
7.15	Case (3) - Optimization Combination 1 - spectrum from multiplicative method . . . . .	97
7.16	Case (1) - Optimization Combination 2 - Filtered Spectrum using the Sine-wave Fitting Approach II . .	98
7.17	Case (1) - Optimization Combination 2 - Spectrally flat source spectrum using the Sine-wave Fitting Approach II . . . . .	98
7.18	Case (1) - Optimization Combination 2 - Spectrally flat source spectrum, its inverse, and the residuals	98
7.19	Case (1) - Optimization Combination 2 - Amplification factors from the multiplicative method method	99
7.20	Case (1) - Optimization Combination 2 - spectrum from multiplicative method . . . . .	99
7.21	Case (2) - Optimization Combination 2 - Filtered Spectrum using the Sine-wave Fitting Approach II . .	100
7.22	Case (2) - Optimization Combination 2 - Spectrally Flat source spectrum using Sine-wave Fitting Approach II . . . . .	100
7.23	Case (2) - Optimization Combination 2 -Spectrally flat source spectrum, its inverse and the residuals .	100
7.24	Case (2) - Optimization Combination 2 - Amplification factors from the multiplicative method method	101
7.25	Case (2) - Optimization Combination 2 - spectrum from multiplicative method . . . . .	101
7.26	Case (3) - Optimization Combination 2 - Filtered Spectrum using the Sine-wave Fitting Approach II . .	101
7.27	Case (3) - Optimization Combination 2 - Spectrally flat source spectrum using the Sine-wave fitting Approach II . . . . .	101
7.28	Case (3) - Optimization Combination 2 - Spectrally flat source spectrum, its inverse and the residuals .	102
7.29	Case (3) - Optimization Combination 2 - Amplification factors from the multiplicative method method	102
7.30	Case (3) - Optimization Combination 2 - spectrum from multiplicative method . . . . .	102
7.31	All Optimized Combinations: Match of peaks flux w.r.t. to Intrinsic Fluxes - Graphical Representation .	104
7.32	All methods investigated at this stage: Match of peaks flux w.r.t. to Intrinsic Fluxes - Graphical Representation . . . . .	105
7.33	Case (1) - Optimization 3 - Sine wave fitting for the low frequency component . . . . .	107
7.34	Case (1) - Optimization 3 - Sine wave fitting for the high frequency component - zoom . . . . .	107
7.35	Case (1) - Optimization 3 - final spectrum . . . . .	107
7.36	Case (2) - Optimization 3 - Sine wave fitting for the low frequency component . . . . .	108
7.37	Case (2) - Optimization 3 - Sine wave fitting for the high frequency component - zoom . . . . .	108
7.38	Case (2) - Optimization 3 - final spectrum . . . . .	109
7.39	Case (3) - Optimization 3 - Sine wave fitting for the low frequency component . . . . .	110
7.40	Case (3) - Optimization 3 - Sine wave fitting for the high frequency component - zoom . . . . .	110
7.41	Case (3) - Optimization 3 - final spectrum . . . . .	110

7.42 Case (1) - Optimization 4 - observed spectrum and Spectrally flat source spectrum with extra noise included. . . . .	112
7.43 Case (1) - Optimization 4 - final spectrum . . . . .	112
7.44 Case (2) - Optimization 4 - observed spectrum and Spectrally flat source spectrum with extra noise included. . . . .	113
7.45 Case (2) - Optimization 4 - final spectrum . . . . .	113
7.46 Case (3) - Optimization 4 - observed spectrum and Spectrally flat source spectrum with extra noise included. . . . .	114
7.47 Case (3) - Optimization 4 - final spectrum . . . . .	114
7.48 All Optimized single methods: Match of peaks flux w.r.t. to Intrinsic Fluxes - Graphical Representation	116
7.49 All traditional and Optimized single methods investigated at this stage: Match of peaks flux w.r.t. to Intrinsic Fluxes - Graphical Representation . . . . .	117
7.50 All Optimized methods (single and combinations): Match of peaks flux w.r.t. to Intrinsic Fluxes - Graphical Representation . . . . .	120
7.51 All Optimized and non-optimized methods (single and combinations): Match of peaks flux w.r.t. to Intrinsic Fluxes - Graphical Representation . . . . .	121
8.1 FM MRS data - Channel 2B - Optimization 1 - Fourier filtering (Region 1) of observed spectrum . . . . .	122
8.2 FM MRS data - Channel 2B - Optimization 1 - Fourier filtering (Region 1) of spectrally flat source spectrum . . . . .	122
8.3 FM MRS data - Channel 2B - Optimization 1 - Fourier filtered spectra of spectrally flat source and observed spectrum . . . . .	123
8.4 FM MRS data - Channel 2B - Optimization 1 - on the left: final spectrum and original observed spectrum after Fourier filtering. On the right: final spectrum . . . . .	123
8.5 CV3 MRS data - Channel 1C - Optimization 1 - Fourier filtering (Region 1) of observed spectrum . . . . .	124
8.6 CV3 MRS data - Channel 1C - Optimization 1 - Fourier filtering (Region 1) of spectrally flat source spectrum . . . . .	124
8.7 CV3 MRS data - Channel 1C - Optimization 1 - Fourier filtered spectra of spectrally flat source and observed spectrum . . . . .	124
8.8 CV3 MRS data - Channel 1C - Optimization 1 - on the left: final spectrum and original observed spectrum after Fourier filtering. On the right: final spectrum . . . . .	125
8.9 FM MRS data - Channel 2B - Optimization 2 - Sine wave fitting of observed spectrum . . . . .	126
8.10 FM MRS data - Channel 2B - Optimization 2 - Sine wave fitting of spectrally flat source spectrum . . . . .	126
8.11 FM MRS data - Channel 2B - Optimization 2 - Sine wave fitting of spectrally flat source and observed spectrum . . . . .	126
8.12 FM MRS data - Channel 2B - Optimization 2 - on the left: final spectrum and original observed spectrum after sine wave fitting. On the right: final spectrum . . . . .	127
8.13 CV3 MRS data - Channel 1C - Optimization 2 - Sine wave fitting of observed spectrum . . . . .	127
8.14 CV3 MRS data - Channel 1C - Optimization 2 - Sine wave fitting of spectrally flat source spectrum . . . . .	127
8.15 CV3 MRS data - Channel 1C - Optimization 2 - Sine wave fitting of spectrally flat source and observed spectrum . . . . .	128
8.16 CV3 MRS data - Channel 1C - Optimization 2 - on the left: final spectrum and original observed spectrum after sine wave fitting. On the right: final spectrum . . . . .	128
8.17 FM MRS data - Channel 2B - Optimization 3 - Sine wave fitting - Residuals of the low frequency component . . . . .	129

8.18 FM MRS data - Channel 2B - Optimization 3 - Sine wave fitting - Total Residuals of the spectrum (Approach II) . . . . .	129
8.19 FM MRS data - Channel 2B - Optimization 3 - final Spectrum . . . . .	130
8.20 CV3 MRS data - Channel 1C - Optimization 3 -Sine wave fitting - Residuals of the low frequency component . . . . .	130
8.21 CV3 MRS data - Channel 1C - Optimization 3 - Sine wave fitting - Total Residuals of the spectrum (Approach II) . . . . .	130
8.22 CV3 MRS data - Channel 1C - Optimization 3 - final Spectrum . . . . .	131
8.23 FM MRS data - Channel 2B - Optimization 4 - observed and spectrally flat source spectra . . . . .	131
8.24 FM MRS data - Channel 2B - Optimization 4 - final spectrum . . . . .	132
8.25 CV3 MRS data - Channel 1C - Optimization 4 - observed and spectrally flat source spectra . . . . .	132
8.26 CV3 MRS data - Channel 1C - Optimization 4 - final spectrum . . . . .	133
A.1 Architecture of the coding files for this study . . . . .	140
A.2 Main.py file layout- input data for the user- detailed version . . . . .	141
B.1 Schematic description of CALSPEC2 . . . . .	143
B.2 Schematic description of CALSPEC3 . . . . .	145

# List of Tables

4.1	Spectrum Features	10
4.2	All cases: Fourier Filtering method - Match of peaks flux w.r.t. to observed Fluxes - Best Matches are shown in blue	19
4.3	All cases: Fourier Filtering method - Match of peaks flux w.r.t. to Intrinsic Fluxes - Best Matches are shown in blue	20
4.4	All cases: Fourier Filtering method : Signal to Noise Ratio - In Red: poor detection, In black : acceptable detection, In blue : excellent detection	22
4.5	All cases: Fourier Filtering method - Match of peaks flux of Region 1 and observed ones w.r.t. to Intrinsic Fluxes - Best Matches are shown in blue	22
4.6	Case (1) Approach I: Sine wave fitting method - Parameters of the sine Equation (4.7), estimated for the beginning, end of the spectrum and for entire spectrum	26
4.7	Case (1) Approach I: Sine wave fitting method - Match of peaks flux w.r.t. to observed and Intrinsic Fluxes	28
4.8	Case (1) Approach II: Sine wave fitting method - Parameters of the sine Equation (4.7), estimated for the beginning, end of the spectrum and for entire spectrum	30
4.9	Case (1) Approach II: Sine wave fitting method - Match of peaks flux w.r.t. to observed and Intrinsic Fluxes	31
4.10	Case (1) Approach III: Sine wave fitting method - Parameters of the sine Equation (4.7), estimated for the beginning, end of the spectrum and for entire spectrum	32
4.11	Case (1) Approach III: Sine wave fitting method - Match of peaks flux w.r.t. to observed and Intrinsic Fluxes	33
4.12	Case (2) Approach I: Sine wave fitting method - Parameters of the sine Equation (4.7), estimated for the beginning, end of the spectrum and for entire spectrum	34
4.13	Case (2) Approach I: Sine wave fitting method - Match of peaks flux w.r.t. to observed and Intrinsic Fluxes	36
4.14	Case (2) Approach II: Sine wave fitting method - Parameters of the sine Equation (4.7), estimated for the beginning, end of the spectrum and for entire spectrum	38
4.15	Case (2) Approach II: Sine wave fitting method - Match of peaks flux w.r.t. to observed and Intrinsic Fluxes	39
4.16	Case (2) Approach III: Sine wave fitting method - Parameters of the sine Equation (4.7), estimated for the beginning, end of the spectrum and for entire spectrum	40
4.17	Case (2) Approach III: Sine wave fitting method - Match of peaks flux w.r.t. to observed and Intrinsic Fluxes	41
4.18	Case (3) Approach I: Sine wave fitting method - Parameters of the sine Equation (4.7), estimated for the beginning, end of the spectrum and for entire spectrum	42
4.19	Case (3) Approach I: Sine wave fitting method - Match of peaks flux w.r.t. to observed and Intrinsic Fluxes	44
4.20	Case (3) Approach II: Sine wave fitting method - Parameters of the sine Equation (4.7), estimated for the beginning, end of the spectrum and for entire spectrum	46
4.21	Case (3) Approach II: Sine wave fitting method - Match of peaks flux w.r.t. to observed and Intrinsic Fluxes	47

4.22 Case (3) Approach III: Sine wave fitting method - Parameters of the sine Equation (4.7), estimated for the beginning, end of the spectrum and for entire spectrum . . . . .	48
4.23 Case (3) Approach III: Sine wave fitting method - Match of peaks flux w.r.t. to observed and Intrinsic Fluxes . . . . .	49
4.24 All cases: Match of peaks flux w.r.t. to Intrinsic Fluxes from Sine wave fitting method- The best matches are shown in blue . . . . .	50
4.25 All cases and all Approaches: Signal to Noise Ratio for Sine Wave fitting - In red: poor detection, In black: acceptable detection, In blue: excellent detection . . . . .	51
4.26 All cases: Sine wave fitting method - Match of peaks flux of Approach II and observed ones w.r.t. to Intrinsic Fluxes - Best matches are shown in blue . . . . .	51
4.27 Case (1): multiplicative method - Match of line flux of (1) the observed spectrum w.r.t. the intrinsic spectrum and of the spectrum from the multiplicative method w.r.t. (2) the observed one and (3) the intrinsic spectrum. . . . .	55
4.28 Case (2): multiplicative method - Match of line flux of (1) the observed spectrum w.r.t. the intrinsic spectrum and of the spectrum from the multiplicative method w.r.t. (2) the observed one and (3) the intrinsic spectrum. . . . .	57
4.29 Case (3): multiplicative method - Match of line flux of (1) the observed spectrum w.r.t. the intrinsic spectrum and of the spectrum from the multiplicative method w.r.t. (2) the observed one and (3) the intrinsic spectrum. . . . .	59
4.30 All Cases: multiplicative method - Match of line flux of (1) the observed spectrum w.r.t. the intrinsic spectrum and of the spectrum from the multiplicative method w.r.t. (2) the observed one and (3) the intrinsic spectrum - The best matches are shown in blue . . . . .	59
4.31 All cases : Signal to Noise Ratio for Multiplicative method - In blue: excellent detection, In black: acceptable detection . . . . .	60
4.32 Location Comparison for all single methods for Case (1) . . . . .	61
4.33 Location Comparison for all single methods for Case (2) . . . . .	61
4.34 Location Comparison for all single methods for Case (3) . . . . .	61
4.35 All cases- All methods : Signal to Noise Ratio . . . . .	62
4.36 All methods: Match of peaks flux w.r.t. to Intrinsic Fluxes - The best matches are shown in Blue . . . .	63
6.1 Method Combination 1- Case (1): Match of peaks flux w.r.t. to Intrinsic Fluxes - The best matches are shown in blue . . . . .	82
6.2 Method Combination 1- Case (2): Match of peaks flux w.r.t. to Intrinsic Fluxes - The best matches are shown in blue . . . . .	83
6.3 Method Combination 1- Case (3): Match of peaks flux w.r.t. to Intrinsic Fluxes - The best matches are shown in blue . . . . .	85
7.1 Optimization of Methods Combination 1- Case (1): Match of peaks flux w.r.t. to Intrinsic Fluxes - The best matches are shown in blue . . . . .	93
7.2 Optimization of Methods Combination 1- Case (2): Match of peaks flux w.r.t. to Intrinsic Fluxes - The best matches are shown in blue . . . . .	95
7.3 Optimization of Methods Combination 1- Case (3): Match of peaks flux w.r.t. to Intrinsic Fluxes - The best matches are shown in blue . . . . .	97
7.4 Optimization of Methods Combination 2- Case (1): Match of peaks flux w.r.t. to Intrinsic Fluxes - The best matches are shown in blue . . . . .	99
7.5 Optimization of Methods Combination 2- Case (2): Match of peaks flux w.r.t. to Intrinsic Fluxes - The best matches are shown in blue . . . . .	101

7.6 Optimization of Methods Combination 2- Case (3): Match of peaks flux w.r.t. to Intrinsic Fluxes - The best matches are shown in blue . . . . .	103
7.7 All cases- All single methods and optimized combinations : Signal to Noise Ratio - In red: poor detection, In black: acceptable detection and In Blue: excellent detection . . . . .	103
7.8 All Optimized Combinations: Match of peaks flux w.r.t. to Intrinsic Fluxes - The best matches are shown in blue and values close by 1% to the best matches are shown in green . . . . .	104
7.9 All Optimized Combinations: Standard Deviation and Average of offset values for all Cases . . . . .	105
7.10 Optimization 3 - Case (1): Match of peaks flux w.r.t. to Intrinsic Fluxes - The best matches are shown in blue . . . . .	108
7.11 Optimization 3 - Case (2): Match of peaks flux w.r.t. to Intrinsic Fluxes - The best matches are shown in blue . . . . .	109
7.12 Optimization 3- Case (3): Match of peaks flux w.r.t. to Intrinsic Fluxes - The best matches are shown in blue . . . . .	111
7.13 Optimization 4 - Case (1): Match of peaks flux w.r.t. to Intrinsic Fluxes - The best matches are shown in blue . . . . .	112
7.14 Optimization 4 - Case (2): Match of peaks flux w.r.t. to Intrinsic Fluxes - The best matches are shown in blue . . . . .	113
7.15 Optimization 3- Case (3): Match of peaks flux w.r.t. to Intrinsic Fluxes - The best matches are shown in blue . . . . .	115
7.16 All cases- All single methods and optimized combinations : Signal to Noise Ratio - In red: poor detection, In black: acceptable detection and In Blue: excellent detection . . . . .	115
7.17 Optimized and non-optimized single methods : Match of peaks flux w.r.t. to Intrinsic Fluxes - The best matches are shown in blue and values close by 1% to the best matches are shown in green . . . . .	116
7.18 Location Comparison for all single methods and optimizations for Case (1) . . . . .	118
7.19 Location Comparison for all single methods and optimizations for Case (2) . . . . .	118
7.20 Location Comparison for all single methods and optimizations for Case (3) . . . . .	118
7.21 All cases- All single and optimized methods : Signal to Noise Ratio . . . . .	119
7.22 All Optimized and non-optimized methods (single and combinations): Match of peaks flux w.r.t. to Intrinsic Fluxes . . . . .	120
7.23 All Optimized and non optimized methods: Standard Deviation of offset values for all Cases . . . . .	120
B.1 Functionalities of CALDETECTOR1 for MIRI . . . . .	143
B.2 Sub-steps for MRS and Imager in stage 2 . . . . .	143
B.3 Sub-steps for stage 3 . . . . .	144

# Nomenclature

## ABBREVIATIONS

Combi.	Combination
CV	Cryo-vacuum
FaF	Flat fielding
FF	Fourier Filtering
FGS	Fine Guidance Sensor
FM	Flight model
HST	Hubble Space Telescope
HIFI	Heterodyne Instrument for the Far-Infrared
IMA	Imager
inf	Infinity
JWST	James Webb Space Telescope
L1, L2, L3	Lagrange Point 1, 2, 3
LRS	Low-Resolution Spectrometer
LWS	Long Wavelength Spectrometer
MIRI	Mid-Infrared Instrument
MRS	Medium-Resolution Spectrometer
Mult.	Multiplicative method
NIRCam	Near-Infrared Camera
NIRISS	Near-Infrared Imager & Slitless Spectrograph
NIRSpec	Near-Infrared Spectrometer
Obs	Observed spectrum
Opti.	Optimization
POP	Primary Optical Path
PSF	Point Spread Function
RSRF	Relative Spectral Response Function
S/N	Signal-to-Noise ratio
SMO	spectrometer main optics
SNR	Signal-to-Noise ratio
SPO	spectrometer pre-optics
SRON	Netherlands Institute for Space Research
STIS	Space Telescope Imaging Spectrograph
SW	Sine wave fitting
SWS	Short Wavelength Spectrometer
TU Delft	Delft University of Technology
w.r.t.	with respect to

## GREEK SYMBOLS

$\alpha_i$	Incident angle
$\alpha_i$	Refractive angle
$\lambda$	Wavelength

## LATIN SYMBOLS

$a_0, a_m, a_k$	Fourier coefficients
$A_i$	Amplification factor at wavelength $i$
$F$	Fourier Serie
$F_c$	Corrected line flux
$F_{fringe_i}$	Intensity of the spectrally flat source at wavelength $i$
$F_{intri}$	Intrinsic flux line
$F_{obs}$	Observed flux line
$F_{obs_i}$	Observed flux intensity at wavelength $i$
$n_i$	Incident index
$n_r$	Refractive index
$T$	Time
$y_i$	Flux intensity at wavelength $i$
$\bar{y}_i$	Mean of the corresponding total sinusoidal function



# Introduction

Understanding and conquering space have always been primary goals for the mankind. Observing the sky by telescopes allowed previous generations to better understand the universe surrounding the Earth. As the effect of the Earth's atmosphere is not optimizing the observations, since the XXth century, scientific instruments have been sent directly into space, allowing the development of a new generation of telescopes.

One main feature of these telescopes is to describe the components of the observed entities (i.e. stars, planets, etc.) by the means of spectrometers. Throughout the years, the scientists discovered that the results were corrupted by a physical phenomenon occurring within the instrumentation. This phenomenon originating from the Fabry-Pérot principle modifies the original spectrum by the amplitude (de-)amplification of the original spectral features and additional artifacts. However, specific methods for entirely correcting this phenomenon have not been developed so far. Therefore, the purpose of this report is to better understand the impact of defringing methods on this phenomenon and define an algorithm removing this effect.

These types of fringes appeared to be present in many space telescope instruments as depicted by [13, 18]; such as the space telescope imaging spectrograph (STIS), long and short wavelength spectrometer (LWS/SWS), Spitzer infrared spectrometer and the heterodyne instrument for the far-infrared (HIFI). Therefore, the need to develop reliable solutions for correcting these fringes has been a critical requirement in the astronomical society; notably for the data analysis and for the development of future spectrometers & detectors. The outcome of this study will not only revolutionize the studies of space exploration, but will also be directly applicable to the spectrometers and detectors aboard the James Webb Space Telescope in 2019, the highly anticipated successor of the Hubble Space Telescope (HST).

Several methods have been developed throughout the years for correcting these fringes, as discussed by [8, 15]. However, each fringe pattern is unique due to its light characteristics, therefore applying a single algorithm to all the spectra was not possible. These have to be modeled on the spectrum to be treated, in order to deliver reliable results. The current defringing method used by most scientists is the combination of the pixel flat-fielding and sine-wave fitting on 1d spectrum. This algorithm presently appears as the most robust combination for processing the data, despite its flaws. However, no current study compares all the possible defringing methods. Therefore, the goal of this project is to consider a large range of algorithmic combinations of the existing and new defringing methods on the 1d spectrum, for quantifying their impact on the line fluxes. In this way, it would be possible to determine if

the line fluxes damaged by the fringes can be corrected, and if yes, how well. Each algorithm will be tested in two phases: first, theoretically, namely based on a created data set. Then, the algorithms will be applied to the real MIRI data set. These MIRI data set are laboratory data from the medium resolution spectrometer of the JWST used as the application subject.

This report will be conducted in nine parts. First, Chapter 2 will explain the problem definition of this study as well as the assessment criteria used. In Chapter 3, the physical description of the fringes and their impact will be discussed. Then, Chapter 4 will discuss the application of the three main defringing methods on a created data set and their comparison. In Chapter 5, the single defringing methods developed in Chapter 4 will be applied to the MIRI data set, and comparisons will be made between the theoretical data outcome and the one from MIRI. Chapter 6 will discuss some combinations of the single defringing methods from Chapter 4, while Chapter 7 will further investigate possible optimization's of the discussed combinations and single methods by applying these optimized versions to the created data set. The application of these improved algorithms will be tested on MIRI data in Chapter 8. Finally, the conclusion of this report will be made in Chapter 9.

# 2

## Problem Definition

Before diving into the study, it is important to define the detailed goals of the study as well as the assessment criteria. Throughout this Chapter, first, the aim of the report will be explained. Then, the different criteria on which the reliability assessment of each method is based, will be described.

### 2.1. Aim of the study

The purpose of this MSc thesis is the development of methods allowing the improvement of astronomical line fluxes, which are applicable on astronomical instruments suffering from the fringes in their spectra, more specifically fringes resulting from the Fabry-Pérot optical scheme. Such discoveries would positively influence data analysis in the scientific domain notably in the astronomical field.

This study will consist of developing several methods for improving the astronomical line fluxes quality. The qualification of each algorithm is based on two primary criteria. On one side, the spectral features detectability shall be improved, allowing to easier point out the spectral features from the remaining noise. This is verified qualitatively by means of the final graphical representation of the spectrum and quantitatively by the means of the signal to noise ratio. On the other side, the spectral photometric accuracy shall also be ameliorated by compensating the line fluxes from the fringe effect. It is important to underline that these two goals are not positively correlated and are thus distinct.

At the end of the thesis, the user will be able to determine which algorithm of the defringing methods would optimize the detectability and photometric accuracy of the line fluxes from data from the spectrometer & focal plane detector spectra suffering from this type of instrumental fringes. This study will not only give insight on the most reliable algorithm but, shall also consider the quality of the data after applying such algorithms; assuring that these have not included more artifacts in the spectra which would lead to a wrong and/or worst interpretation of the line fluxes result than analyzing the original spectrum (i.e. a possible solution would be to not modify the spectrum).

As specified throughout the literature survey [1], this study will use an application subject, the spectrometer and associated Focal Plane Module (i.e. detectors) of MIRI, one scientific instrument of the James Webb Space telescope. The aim of this thesis will therefore also concern this instrument specifically and hopefully provide a reliable solution for quantitatively estimating the fringing impact on the line fluxes and determine if it can be corrected.

## 2.2. Assessment criteria

As explained previously, two main criteria will be considered for comparing the outcome of each defringing method: detectability and photometric accuracy.

### 2.2.1. Detectability

This criterion will be treated qualitatively and quantitatively throughout this study. Indeed, when analyzing the final corrected spectrum, the user can instinctively determine if the spectrum has been improved from the original one. This instinctive analysis is based on several criteria which have been summarized below:

- **CRITERION 1:** Visibility of the weak spectral features
- **CRITERION 2:** Visibility of the strong spectral features
- **CRITERION 3:** Width of the spectrum continuum → the left residuals
- **CRITERION 4:** Presence of a frequency component left
- **CRITERION 5:** Flatness of the continuum

Therefore, the qualitative method for analyzing the final spectrum will be the development of a trade-off matrix based on these five criteria, using a grading on a scale of three components:

- **Good** or [G] as **Green**: shows reliable results
- **Mitigated** or [M] as **Yellow**: does not provide the best results but, the outcome is acceptable
- **Bad** or [B] as **Red**: does not provide reliable results nor acceptable ones

However, this qualification method might still be considered as subjective. Consequently, the signal-to-noise ratio was determined and compared to the one from the initial spectrum. This later analysis will allow the quantification of the qualitative analysis.

As its name indicates, the signal-to-noise ratio allows one to determine if the spectral features can clearly distinguish themselves from the continuum, especially when noise is present. The overall goal when applying the defringing would be to improve this ratio, as often in the simulated spectra (also called the observed spectra), the noise (including the fringes) is so important that spectral features are undetectable.

Several ratios are used by scientists for quantifying the signal quality. Usually, values below 2-3 are considered poor signal and values between 7-10, therefore it was decided for this study to take the extreme values as indication for the signal quality:[7]

- $2 < S/N < 10$  : acceptable signal quality
- $S/N \leq 2$  : bad signal quality
- $S/N \geq 10$  : excellent signal quality

The noise not being a constant value over the wavelength range, for this study it was decided to consider a part of the spectrum before and after the studied line flux and then take its standard deviation.

Nevertheless, for some data sets, it will not be possible to determine the S/N ratio as the location of the spectral features are unknown or as there are no spectral features. In these cases, the averaged fringe amplitude of the simulated spectrum will be compared to the one of the defringed spectrum.

### 2.2.2. Photometric accuracy

The second goal of the defringed data quality is the optimization of the photometric accuracy. In other words, the line flux amplitude should be improved w.r.t. the simulated one. For this, for each new defringed spectrum, the line flux amplitude of the spectral features will be measured and compared to the intrinsic values. The same will be realized with the simulated spectrum in order to compare the line flux amplitude match of the simulated spectrum and the new one. Furthermore, in order to be as objective as possible, the conclusion on the photometric accuracy of each method will not only be based on the highest number of best matches, but also on their standard deviation. Indeed, this last criterion will allow to determine the constancy of the method.

# 3

## Spectral Fringes

Fringes present in astronomical spectra are frequently caused by spectrometers and associated detectors. Even though, the origin is often known, several methods are considered to correct the effect but an effective universal correction has not yet been developed. In this Chapter, first, a summary of the fringes physical concept will be discussed. Then, the second section will be dedicated to the spectral fringes within MIRI. For deeper explanation of the physical phenomenon behind the fringes, the reader is advised to read the literature study of this report [1].

### 3.1. Origin of the spectral fringe pattern

The fringes are interference that can be depicted in flux spectrum. Due to the internal configuration of the instrumentation (spectrometer and associated detector), artifacts are introduced into the spectra. This internal configuration induces the so-called Fabry-Pérot effect, which is the application of multibeam interference. As explained by [14], this last optical scheme uses the reflection principle between closely separated mirrors/reflecting flat surfaces. The incoming flux is therefore split into two entities, following the Snell's law (Equation (3.1)), leading to path differences.

$$n_i \sin(\alpha_i) = n_r \sin(\alpha_r) \quad (3.1)$$

in which,

- $n_i$  is the incident index
- $\alpha_i$  is the incident angle
- $n_r$  is the refractive index
- $\alpha_r$  is the refractive angle

The smallest amplitude is transmitted through the second flat surface while the largest amplitude is reflected back to the first flat surface. This process is repeated multiple times, splitting away each time the incident light amplitude into two. At this splitting location, there is a phase of change of  $\lambda/2$  ( $\lambda$  being the corresponding wavelength), due to the incident wave reflecting of a denser optical medium than the one it has been travelling through. If this phase change is a multiple of  $\pi$ , then constructive interference (i.e. the two waves summed up when they reach the screen leading to a maximum) will occur; the opposite will lead to a destructive interference (i.e. the two waves summed up and produce zero amplitude when they reach the screen leading to a minimum).

The multiple transmissions from the second flat surface (cf. multibeam interferometer) are focused through a lens onto a screen where they can interfere. The amplitudes and their corresponding positions at each point into space of the waves are combined into single resultant wave; resulting to an interference pattern on the screen, which consists of bright and dark bands, describing constructive and destructive interference's respectively. The Figure 3.1 gives an overview the Fabry-Pérot principle.

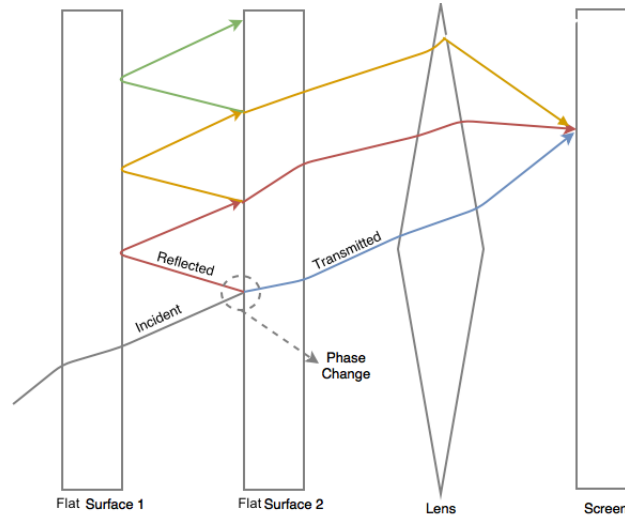


Figure 3.1: Scheme of Fabry-Pérot principle

The Fabry-Pérot interferometer configuration can be the source of the interferences (i.e. fringes) in the astronomical spectra. This type of optical interference might be present within the filter, flat mirror or (more often) the detector surfaces themselves.[6] These interferences have diverse and non negligible effects on the scientific results, such as:

- Additional noise to the spectra
  - Complicating the detection of weak elements in the spectra
- Variation in the spectral response
  - Shifting the main wavelength of a spectral feature
- Modification of the detected line flux
  - It is amplified/reduced if the spectral line is on top of a fringe maximum/minimum.

The difficulty to model a defringing method applicable to most of the spectra is due to the irregularities of the fringes pattern. Indeed, the fringes are strongly dependent on several elements such as:[9]

- Wavelength Calibration:
 

Relatively small variations from the perfect wavelength calibration might lead to non-negligible effects (i.e. fringe amplitude and frequency variations) on the observed fringes and thus on the RSRE
- Aperture orientation:
 

The observed fringes also differ from the expected ones, when the source of the signal is not placed at the aperture center. This might affect the amplitudes and other characteristics of the fringes, resulting in a complex fringe pattern.
- Source features:
 

The source features such as its structure and spatial extent influence the fringes, by reducing their resolution and affecting their characteristics.
- Optical properties of the instrumentation (detector, spectrometer)

These external elements emphasize that each fringe pattern is unique (i.e. different fringes peaks position and spacing) and therefore the expected RSRE is limited in the simulation of the real data.[12] Accordingly, defringing meth-

ods are mandatory for analyzing the real observations. Nevertheless, the uniqueness of the fringes does not allow the development of a specific method for resolving the fringing pattern.[5]

### 3.2. Instrumental fringes within MIRI

Throughout the laboratory experiments realized on MIRI, fringes were depicted in the different spectrometers, more specifically in low resolution spectrometer (LRS) and the medium one (MRS), through mainly the filters and associated detectors.

Although the fringes from the MRS with a medium to high modulation depth appeared to be partially resolved as mentioned by [2], the fringes from the LRS are still unsolved and can be depicted in the spectral response function (SRF). Indeed, from [3], it appeared that the particular layout design of MIRI's detectors lead to two different detector fringes at the resolution in the full wavelength spectrum, i.e. 5  $\mu\text{m}$  to 28.5  $\mu\text{m}$ . However, the optical features of the LRS detector being analogous to the ones of the MRS, the current defringing approach for the LRS detector is based on the predictions of the MRS one. Therefore, this study will be focused on the MRS principally.

Before further discussing the fringes within the MRS, it is important to briefly explain the design of this instrument. The MRS is composed of two main subsystems; the spectrometer main optics (SMO) and the spectrometer pre-optics (SPO). Moreover, due to electrical and thermal constraints, two detectors have been associated with the MRS. The spectrometer design is thus divided into two sets of optics, short and long wavelength arms, respectively. The light spectrum coming from the relay optics is sent to SPO, where it is split in four; as the SPO consists of four simultaneous spectral channels (two for the short wavelengths and two for the long ones). The SPO is principally made of dichroics which select the required reflection band from the spectrum and send it to its corresponding filters.

Several features were identified on the experimental data such as pointing offsets, as discussed by [10]. Having pointing offsets (even really small ones) leads to a wavelength shift and thus can be seen in the fringe pattern; notwithstanding, the variation is often in the order of  $10\text{E}4$ . Therefore, for nominal operations, these small fluctuations will not be an important issue and the fringe pattern will be easily distinguished from the correct SRF. However, for important S/N observations such as the exoplanet spectroscopy, pointing jitter and drifts, it might lead to extreme additional noise if the observations are not correctly adjusted by defringing methods, such as "modeling framework correlated with targeted in-orbit calibration observations" as stated by [3].

As specified by [2] and [11], the physical phenomenon at the origin of these fringes, i.e. Fabry-Pérot principle, occurs in the spectrometer within the spectral filters of its dichroics, leading to so-called "dichroic fringes". Furthermore, due to their different optical thickness, each filter causes a specific fringe pattern. A second source of fringe is the substrate of the detectors, which is a thick passive layer composing the detector. This layer is highly reflective, thus conducive to the Fabry-Pérot effect. The detector fringes are characterized by a lower frequency than the one of the dichroic fringes. Moreover, fringe fluctuations seen in the spectra from these two fringe origins are caused by the substrate layered composition and the optical differences among the dichroic filters. As pointed by [2], the third origin of the fringes is not associated with specific surfaces, as the other fringe sources. Indeed, its fringes arise from the beating among primary fringe elements.

# 4

## Traditional Defringing methods - Theoretical Model

Over the years, three main defringing methods have been considered for correcting the data, but have never been analyzed through an extensive report. Therefore, in this study, each of these methods has been analyzed and compared in order to quantify their impact on the data.

### 4.1. Flux Spectra

For quantifying the performance of each method, test cases were necessary. As a first step, 'fake' cases have been considered; in these, fringe patterns of different frequencies were simulated and peaks were introduced in the spectrum at specific locations. In this way, after applying the defringing correction, the output could be compared to the correct one (i.e. spectrum without fringe pattern included). Once conclusion are made on the best correcting methods, the second step, detailed in Chapter 5, will consist of applying these methods to the real test case (i.e. the Medium Resolution Spectrometer of MIRI) and analyzing the output.

For each case, a wavelength range between 7.4 and 8.8  $\mu\text{m}$  has been considered, which corresponds to the wavelength range of channel 2A in MIRI (this will be later discussed in Chapter 5). Each case is a combination of different sinusoidal shapes and a peaks spectrum. This last is the same for each case and is composed of four spectral features (i.e. line fluxes), two strong and two weak, as summarized in Table 4.1, while Figure 4.1 provides an overview of the non-defringed spectrum. Introducing the peaks in the spectrum would allow to quantify the different methods by analyzing not only their position on the defringed data set, but also the peak's amplitudes. It is important to underline that for these data sets two main simplifications have been considered:

1. Constant frequency for the fringes components
2. Delta function modelling the lines fluxes:

This has been considered for simplicity because as long as the line width is much smaller than the fringe period, modelling the spectral feature as a delta function or not, does not influence the outcome.

The goal of these fake data sets was to be as similar as possible to the real MIRI data. It is known that the fringe amplitude varies between -30% up to 30% in general. Therefore, the variations of amplitude between the maximum of wave and its mean have not been considered more than this range. Moreover, in MIRI, the fringe components being known to come from two sources: the detector and the dichroics ([2]) only two sinusoidal components have

been introduced in the fake data. Furthermore, unfortunately, the real data does not contain only fringes as artifacts but also some extra noise might be included in the spectrum. Some noise was thus included in the third spectrum Case. For defining the sinusoidal components of the cases, the Equation (4.1) has been used in which the parameters have been modified.

$$y = A \cdot \sin(B \cdot x + D) + C \quad (4.1)$$

where,

- A is the amplitude parameter of the wave
- B is the frequency parameter of the wave
- C represents the vertical shift parameter of the wave
- D represents the horizontal shift (phase shift) parameter of the wave
- x is the wavelength

Flux Intensity [Jy]	Wavelength [μm]
150	7.7350831
100	8.1908331
15	8.4413214
7.6	8.5468512

Table 4.1: Spectrum Features

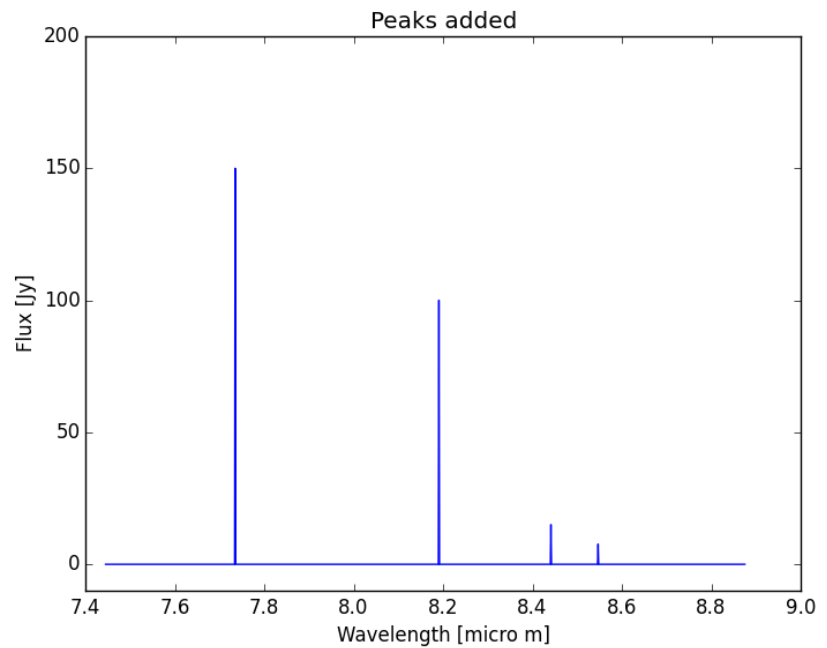


Figure 4.1: Four Peaks introduced in the spectrum

This peaks spectrum represents the so-called intrinsic peaks; these are the real intensity values to be seen by the user, before fringes occur. Although the sinusoidal components representing the fringes can be added together, it is unfortunately not the case for the intrinsic peaks. Their values are affected by the fringes leading to observed values. The goal of these fake cases is to approximate the best reality, therefore, the lines flux have not been simply added to the spectrum but, have been '*de-amplified*' by the fringes components, as described by set of Equations (4.2).

$$F_{obs} = F_{intri} \cdot (FringeAmplification) \quad (4.2a)$$

$$F_{obs} = F_{intri} \cdot (y_i / \bar{y}_i) \quad (4.2b)$$

In which,

- $F_{intri}$  is the intrinsic line flux
- $F_{obs}$  is the observed line flux
- $i$  is the wavelength location where the peak is introduced
- $y_i$  is the flux intensity at wavelength  $i$  of the total sinusoidal function from the fringe components (cf. Equation (4.1))
- $\bar{y}_i$  is the mean of the corresponding total sinusoidal function

## Case (1)

It is made of three components described below and shown in Figure 4.2.

- Component 1:

Equation (4.1), with

$$\begin{aligned} A &= 16.5 \\ B &= 9.1 \\ C &= 120 \\ D &= 451.5 \end{aligned}$$

- Component 2:

Equation (4.1), with

$$\begin{aligned} A &= 5 \\ B &= 1407 \\ C &= 26 \\ D &= 0.34 \end{aligned}$$

- Four peaks introduced in the spectrum

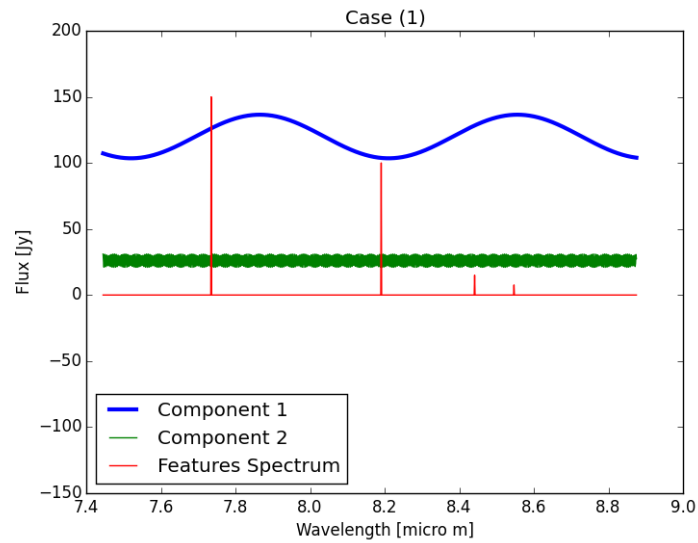


Figure 4.2: Different components of spectrum for Case (1)

## Case (2)

It is also made of three components described below and shown in Figure 4.3.

- Component 1:

Equation (4.1), with

$$\begin{aligned} A &= 15 \\ B &= 20.07 \\ C &= 68.3 \\ D &= 821.5 \end{aligned}$$

- Component 2:

Equation (4.1), with

$$\begin{aligned} A &= 20.5 \\ B &= 90.07 \\ C &= 451.5 \\ D &= 40.3 \end{aligned}$$

- Four peaks introduced in the spectrum

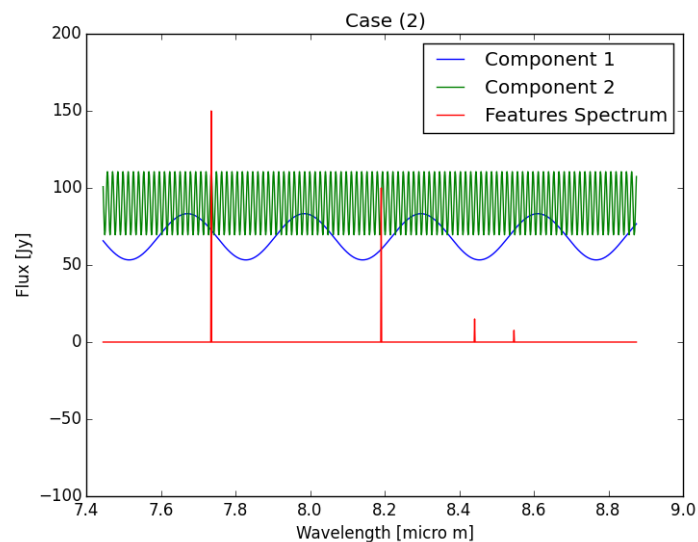


Figure 4.3: Different components of spectrum for Case (2)

### Case (3)

It is made of two components described below and shown in Figure 4.4.

- Component 1:

Equation (4.1), with

$$\begin{aligned} A &= 12 \\ B &= 1407 \\ C &= 40 \\ D &= 2.34 \end{aligned}$$

- Component 2:

Equation (4.1), with

$$\begin{aligned} A &= 8.5 \\ B &= 21.5 \\ C &= 150.1 \\ D &= 7.34 \end{aligned}$$

- Four peaks introduced in the spectrum

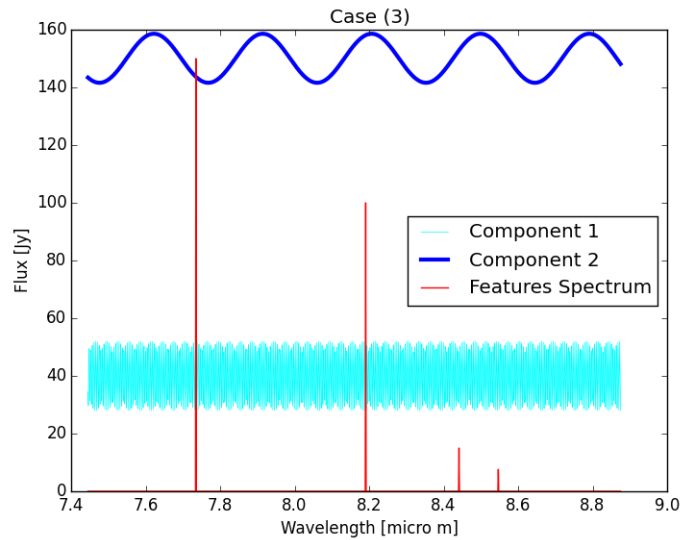


Figure 4.4: Different components of spectrum for Case (3)

Summing the sinusoidal components of each case and adding some noise in the third case only, while specifying definite flux at certain wavelengths (cf. peaks introduced in the spectrum) lead to the final spectra cases, shown in Figure 4.5.

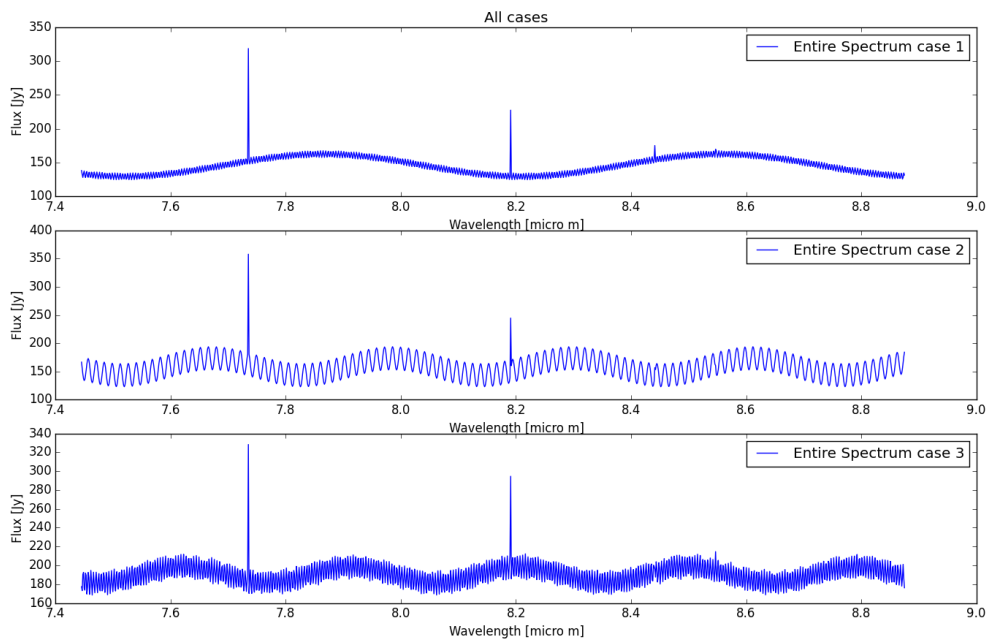


Figure 4.5: All cases spectra

## 4.2. Method 1: Fourier Filtering

The Fourier Filtering is the first method to be investigated. It consists of three main steps. First, as its name indicates, the data set is transformed into the Fourier domain. Then, the filter is applied on a selected region, i.e. the amplitude in this region is set to zero. Finally, the new data set is converted back to the original domain and is said "filtered".

For this study, the width of the region to be set to zero has been varied. The results have been compared to the original ones, in order to quantify the effect of this method.

### 4.2.1. Theoretical Background

The Fourier series splits a periodic function into its sinusoidal components. In the fringes analysis perspective, the sinusoidal components refer to fringes which have different frequencies based on the origin; i.e. from the detector or from the spectrometer.

The Fourier series can be described, as stated previously, by the sum of sine and cosine elements, cf. Equation (4.3).

$$F = a_0 + \sum_{m=1}^{\infty} a_m \cdot \cos\left(\frac{2\pi m \cdot t}{T}\right) + \sum_{k=1}^{\infty} a_k \cdot \sin\left(\frac{2\pi k \cdot t}{T}\right) \quad (4.3)$$

In which,

$$a_0 = \frac{1}{T} \int_0^T f(t) dt \quad (4.4a)$$

$$a_m = \frac{2}{T} \int_0^T f(t) \cdot \cos\left(\frac{2\pi m \cdot t}{T}\right) dt \quad (4.4b)$$

$$b_k = \frac{2}{T} \int_0^T f(t) \cdot \sin\left(\frac{2\pi k \cdot t}{T}\right) dt \quad (4.4c)$$

where,  $f(t)$  is the original function.

Equations (4.3)- (4.4) are valid only for real data. However, it might be possible that the set of data leads to complex values, in the later case, another function approximation will be used.

$$F = \sum_{l=-\infty}^{\infty} c_l e^{i \cdot 2\pi l \cdot t \cdot T^{-1}} \quad (4.5)$$

In which,

$$e^{it} = \cos(t) + i \sin(t) \quad (4.6a)$$

$$c_l = \frac{1}{T} \int_0^T f(t) e^{i \cdot -2\pi l \cdot t \cdot T^{-1}} dt \quad (4.6b)$$

### 4.2.2. All Cases

In this Subsection, all the cases simulated in Section 4.1 will be tested with the Fourier Filtering method. The first step has been to determine the region to filter based on the amplitude graph from the Fourier domain.

As expected and shown in Figures 4.6, 4.7 and 4.8, two main peaks regions (i.e. a central peak and a pair of same amplitude peaks) can be depicted, which correspond to the two sinusoidal functions introduced to the spectrum (dominant frequency and second harmonics). The same scheme can be seen for the three cases as two frequency

components were simulated for each case.

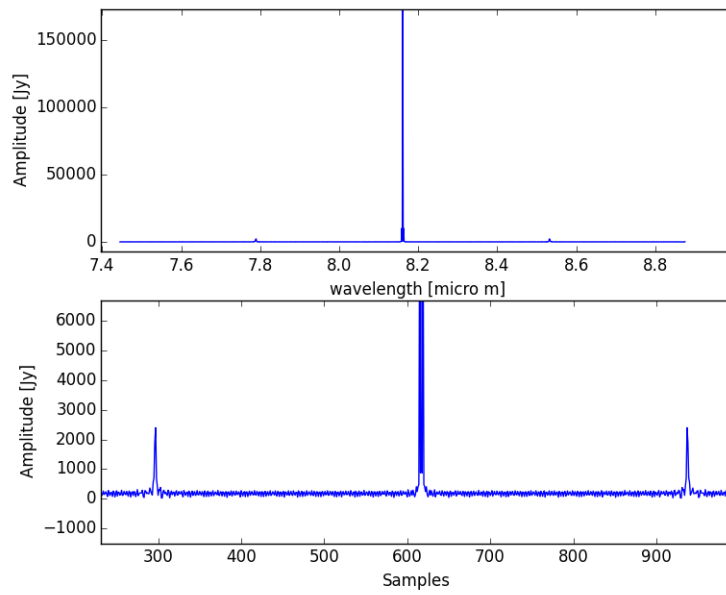


Figure 4.6: Case (1): Fourier Filtering method - Amplitude Fourier Applied. On top: entire wavelengths range, on the bottom: zoom of the central region

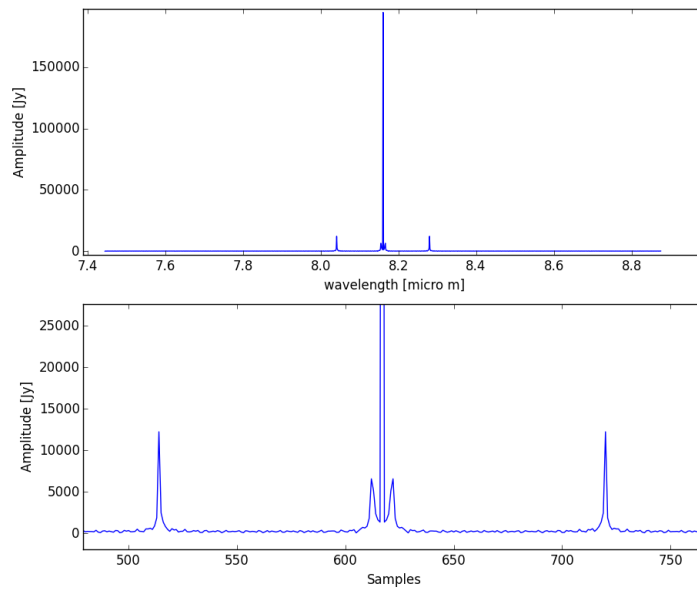


Figure 4.7: Case (2): Fourier Filtering - Amplitude Fourier Applied. On top: entire wavelengths range, on the bottom: zoom of the central region

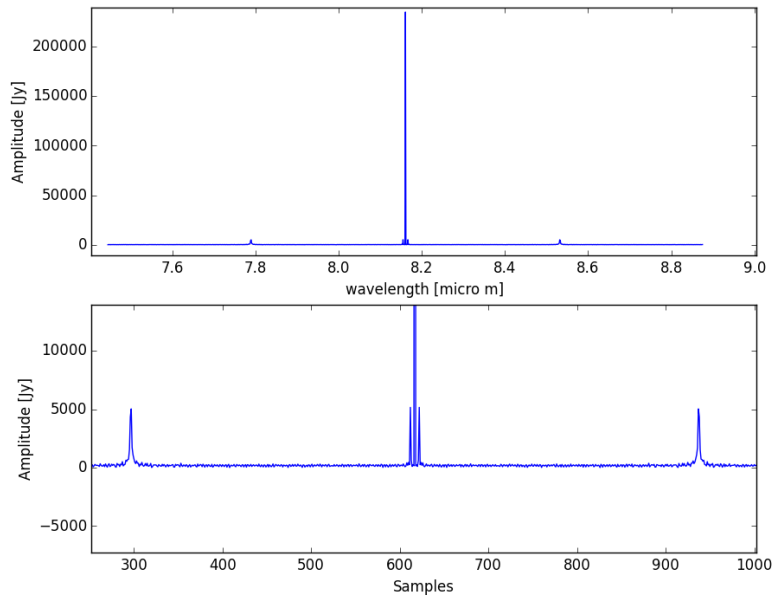


Figure 4.8: Case (3): Fourier Filtering method - Amplitude Fourier Applied. On top: entire wavelengths range, on the bottom: zoom of the central region

The region width to filter has then been varied in order to determine its effect on the data; in this study two regions, corresponding to the peaks regions, have been considered. This can be seen in Figures 4.9- 4.14, in which the colored regions correspond to the regions to filter (i.e. which will be set to zero).

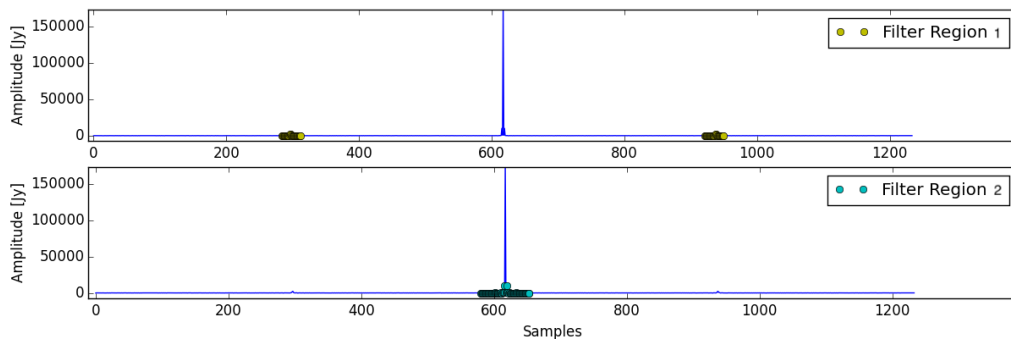


Figure 4.9: Case (1): Fourier Filtering method - Amplitude Fourier Applied with 4 regions- Entire spectrum

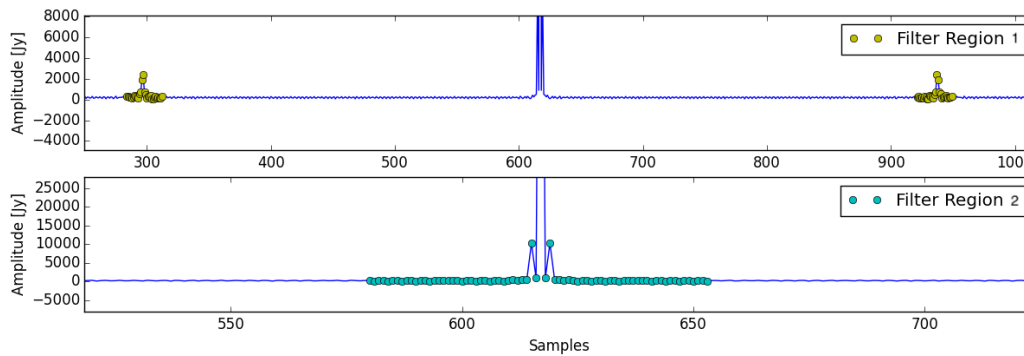


Figure 4.10: Case (1): Fourier Filtering method - Amplitude Fourier Applied with 4 regions- Zoom of filtered regions

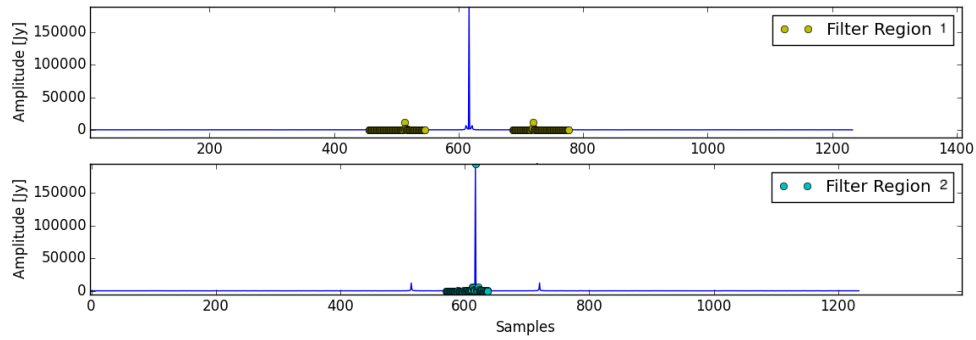


Figure 4.11: Case (2): Fourier Filtering method - Amplitude Fourier Applied with 4 regions- Entire spectrum

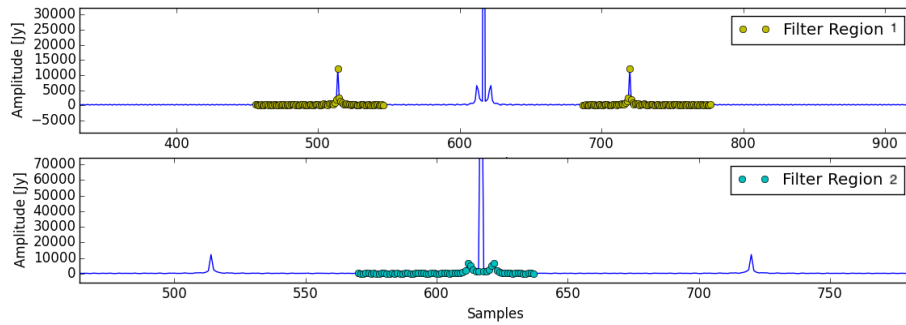


Figure 4.12: Case (2): Fourier Filtering method - Amplitude Fourier Applied with 4 regions- Zoom of filtered regions

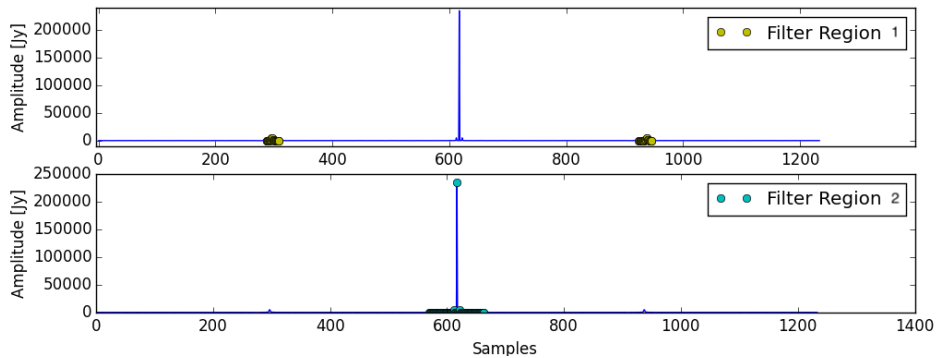


Figure 4.13: Case (3): Fourier Filtering method - Amplitude Fourier Applied with 4 regions- Entire spectrum

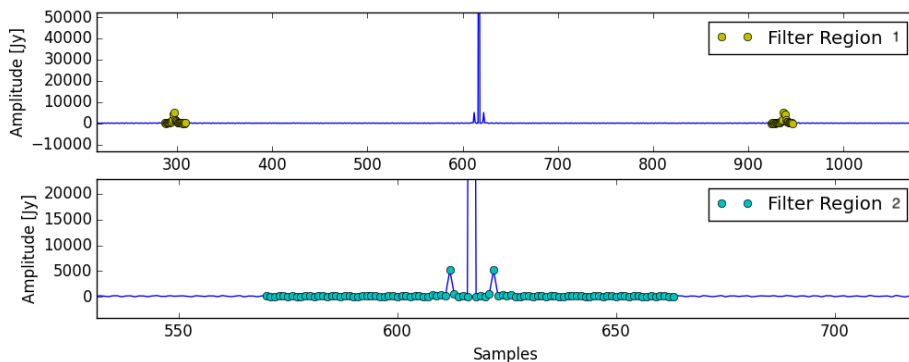


Figure 4.14: Case (3): Fourier Filtering method - Amplitude Fourier Applied with 4 regions- Zoom of filtered regions

Now that the regions to filter have been determined, the filter was applied in these areas by simply setting the amplitude to zero. And the inverse of the Fourier Transform was applied to the new data set (called the filtered data) for

having them in the original domain (i.e. Flux [Jy] vs. wavelength [micron]).

On Figures 4.15, 4.16 and 4.17, three data sets are plotted: the original data, the filtered and the subtracted ones. The subtracted spectrum, as its name indicates, results from the subtraction of the filtered spectrum from the original spectrum. It should thus represent the sinusoidal component corresponding to the peak region taken out from Fourier amplitude data.

It can be clearly seen from these Figures that filtering the peaks allows to remove the corresponding sinusoidal components introduced in the spectrum. Therefore, the output data are still affected by a sinusoidal component; for the Region 1, the high frequency component is left while for Region 2, the low one is left.

From a graphical analysis Region 1 provides the overall best results as all the spectral features can be depicted and major part of the noise is removed. While, in Region 2, the weakest spectral features are often hardly distinguishable, underlining the poor detectability from this region filtering. Indeed, in this Region 2, the weak spectral features (especially peak 4) seem to be absorbed by the high frequency component left in the spectrum. Furthermore, the reader might have noticed that the detectability of the weak spectral features for Case (3) is worse than for the other Cases. It can be explained by the extra noise added in the simulated spectrum. This introduced noise seems to have absorbed the weak spectral features, making it difficult for any reader to find all the spectral signatures of such signal. Therefore, aesthetically speaking, Region 1 seems at first sight to provide the best spectrum.

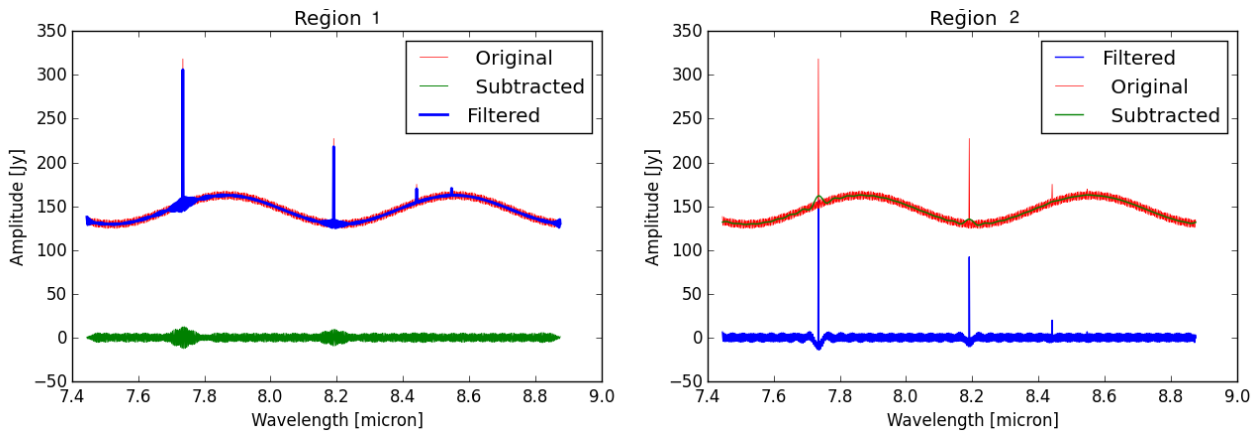


Figure 4.15: Case (1): Fourier Filtering method - Comparison among original spectrum, filtered one and subtracted one

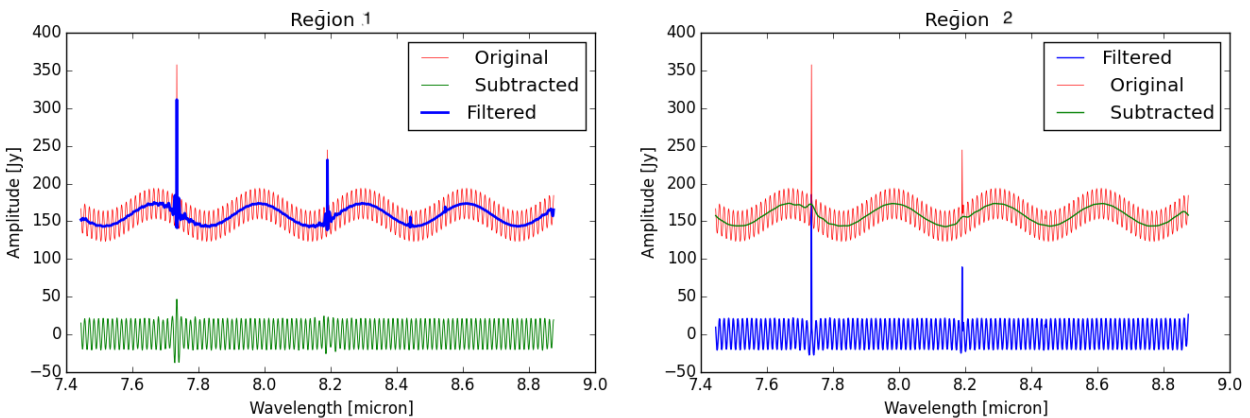


Figure 4.16: Case (2): Fourier Filtering method - Comparison among original spectrum, filtered one and subtracted one

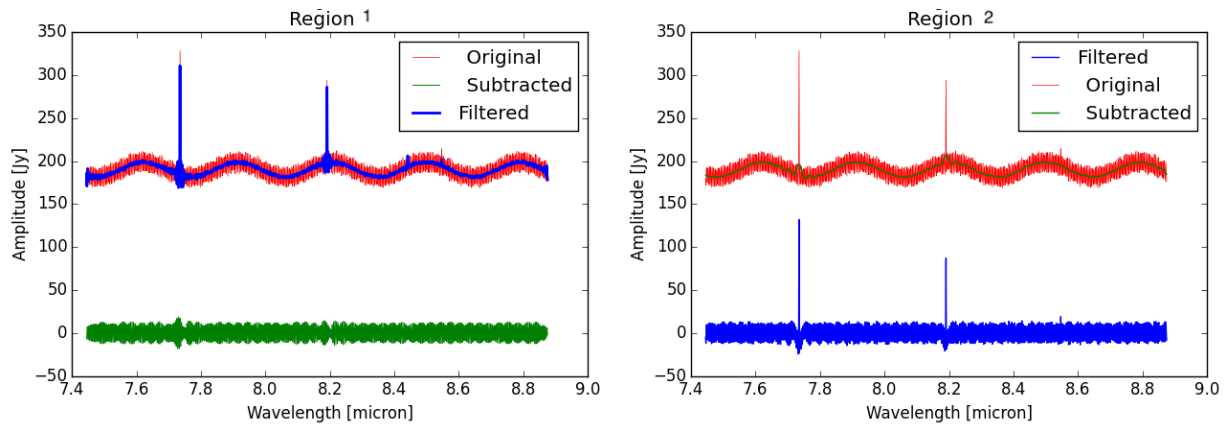


Figure 4.17: Case (3): Fourier Filtering method - Comparison among original spectrum, filtered one and subtracted one

In the previous analysis, it was pointed out if the spectral features were observable by the user. The next step of the analysis would be to verify if the spectral features observed are matching the expected ones (i.e. observed from the noisy spectrum and intrinsic values). The analysis will therefore be carried in two parts:

- Comparison filtered data to observed data
- Comparison filtered data to intrinsic data

#### COMPARISON FILTERED DATA TO OBSERVED DATA

As explained in Section 4.1, the intrinsic peak amplitudes are affected by the sinusoidal components simulating the fringes components, leading to the so-called observed peaks. Even-though, the goal of applying this method is to correct the fringes effect on the spectral lines, thus to study the compare the filtered data to the intrinsic ones; it is interesting to see how this method influences the data affected by the fringes (i.e. the observed peaks).

Table 4.2 summarizes the match among the peaks in % and Figures 4.18, 4.19 and 4.20 provide a graphical overview of the data from Table 4.2.

Region 1 was considered as a good filter in the graphical analysis as all the spectral features were clearly distinguishable even-though a fringe component was left in the spectrum. When analyzing Table 4.2, the amplitude of the peaks are slightly shifted from the observed ones for the strong spectral features and more shifted for the weak ones (especially for the Peak 4 of Case (3)). These shifts translate the effect of this filter on the data. Indeed, if the matches from Table 4.2 are not perfect (i.e. close to 100 %), it means that the flux is not similar to the observed ones and thus it has been corrected by the method. Therefore, better fluxes corrections are expected for large deviations w.r.t. the observed values.

It is clear that Region 2 has the best matches with the observed values for all peaks, although its poor graphical visualization. The person analyzing the spectrum might therefore miss the weak spectral characteristics. However, the strong matches with the observed values underlines the poor effect of the low frequency component on the data and, therefore the flux modification. It would be interesting to see if this correlation is also valid for the intrinsic peaks values. Applying this model to the data would therefore allow the reader to only clearly determine the location of the spectral features but will not provide the most reliable information (i.e. fluxes) of these features compared to the ones from the observed spectrum.

# Region	Filtered Value/ observed Value[%]											
	Case (1)				Case (2)				Case (3)			
	Peak 1	Peak 2	Peak 3	Peak 4	Peak 1	Peak 2	Peak 3	Peak 4	Peak 1	Peak 2	Peak 3	Peak 4
Region 1	92.20	89.82	73.98	113.75	95.90	97.48	97.99	118.25	74.31	76.83	95.56	36.38
Region 2	99.96	99.97	99.97	99.94	99.95	99.95	99.96	99.97	96.98	97.97	98.51	101.97

Table 4.2: All cases: Fourier Filtering method - Match of peaks flux w.r.t. to observed Fluxes - Best Matches are shown in blue

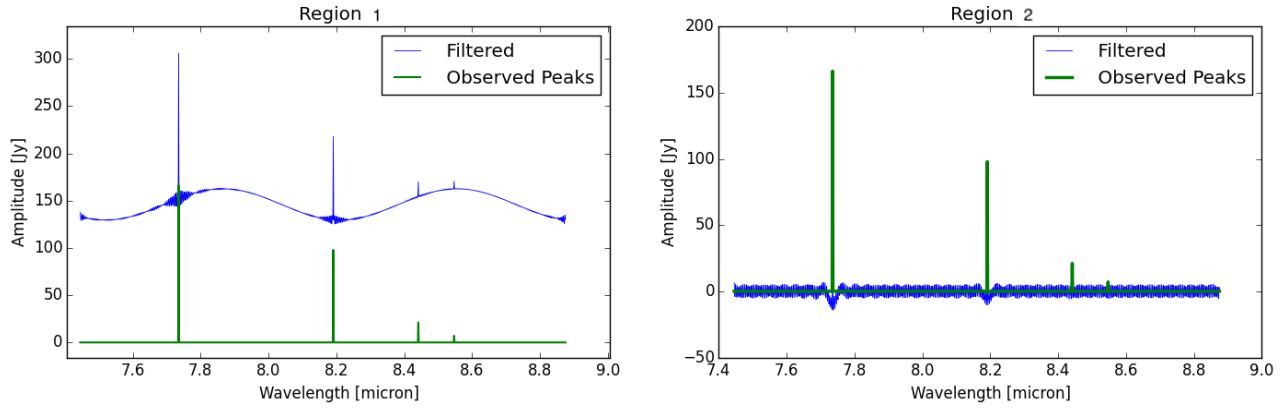


Figure 4.18: Case (1): Fourier Filtering method - Comparison among observed peaks spectrum and the filtered one

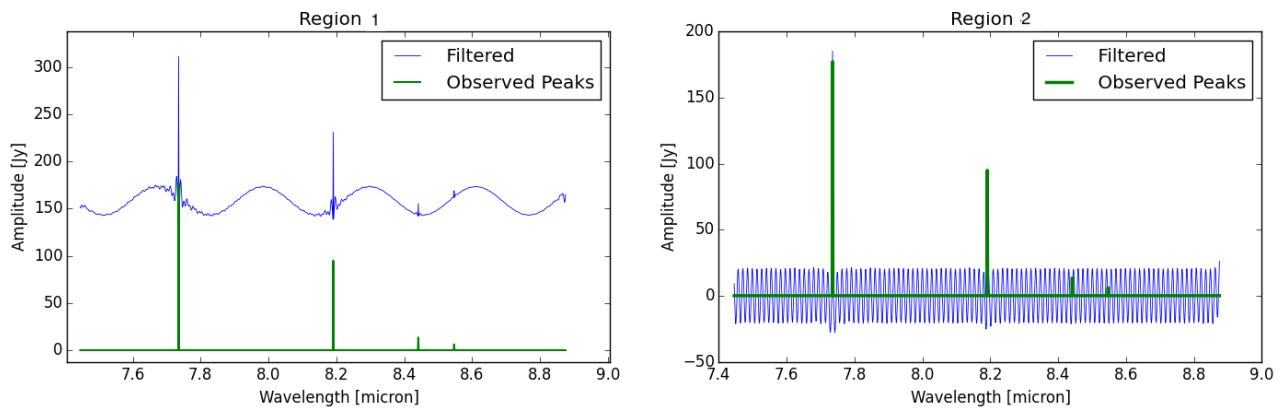


Figure 4.19: Case (2): Fourier Filtering method - Comparison among observed peaks spectrum and the filtered one

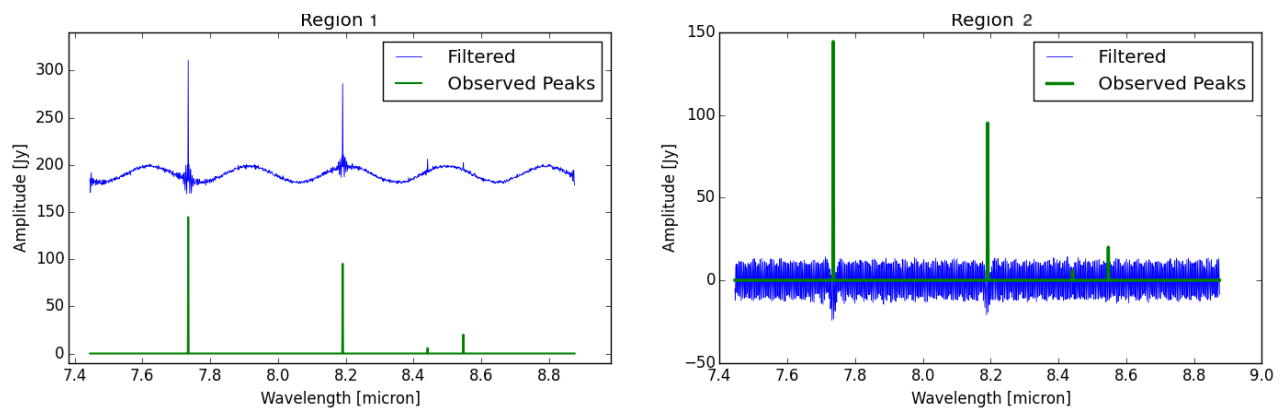


Figure 4.20: Case (3): Fourier Filtering method - Comparison among observed peaks spectrum and the filtered one

COMPARISON FILTERED DATA TO INTRINSIC DATA

A similar scheme as for the comparison with the observed data was realized. As can be seen in Table 4.3 and Figures 4.21, 4.22 and 4.23, in Regions 1 & 2, the opposite analysis than for the observed values holds for Cases (1) and (2). Namely, the matches are in general stronger for Region 1 than 2. This could have been predicted as the line fluxes were similar to the observed ones which were already influenced by the fringes. The results from this Region represent thus the lines flux variation if no method was applied to the data. One can conclude for these Cases, that applying the Fourier Filtering method by filtering the high frequency component only (i.e. Region 1 filter) allows to clearly distinguish the spectral characteristics and to achieve good line flux approximations.

However, a different pattern has been noticed for the Case (3), namely the matches were better with the Region 2 than with Region 1. It is important to remember that the case studied here includes an additional noise component, and the poor match with all the weakest components might be explained by the strong effect of the noise on the weakest spectral features; indeed, their line flux being smaller, a noise component might have a greater effect on them than simple fringing. The method does not seem to also correct the noise included in the spectrum. The Region 1 was also considered as the best for this Case, as it did not only provide acceptable photometric accuracy for, in general, all spectral features, but also a better graphical detectability.

# Region	Filtered Value/ Intrinsic Value[%]											
	Case (1)				Case (2)				Case (3)			
	Peak 1	Peak 2	Peak 3	Peak 4	Peak 1	Peak 2	Peak 3	Peak 4	Peak 1	Peak 2	Peak 3	Peak 4
Region 1	102.24	87.93	103.82	105.83	113.37	92.54	88.43	95.05	81.80	84.48	101.16	60.01
Region 2	110.86	97.86	140.29	92.99	118.17	94.89	90.21	80.36	90.60	90.92	104.29	168.21

Table 4.3: All cases: Fourier Filtering method - Match of peaks flux w.r.t. to Intrinsic Fluxes - Best Matches are shown in blue

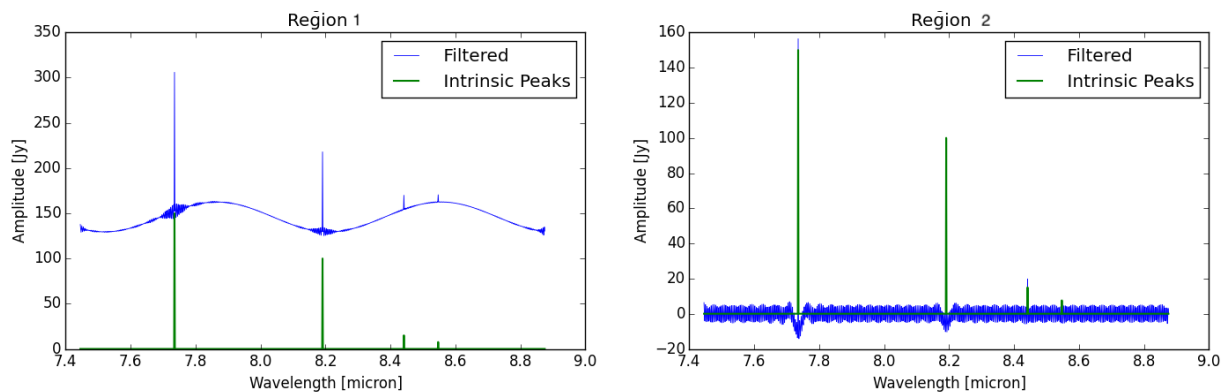


Figure 4.21: Case (1): Comparison among Intrinsic peaks spectrum and the filtered one

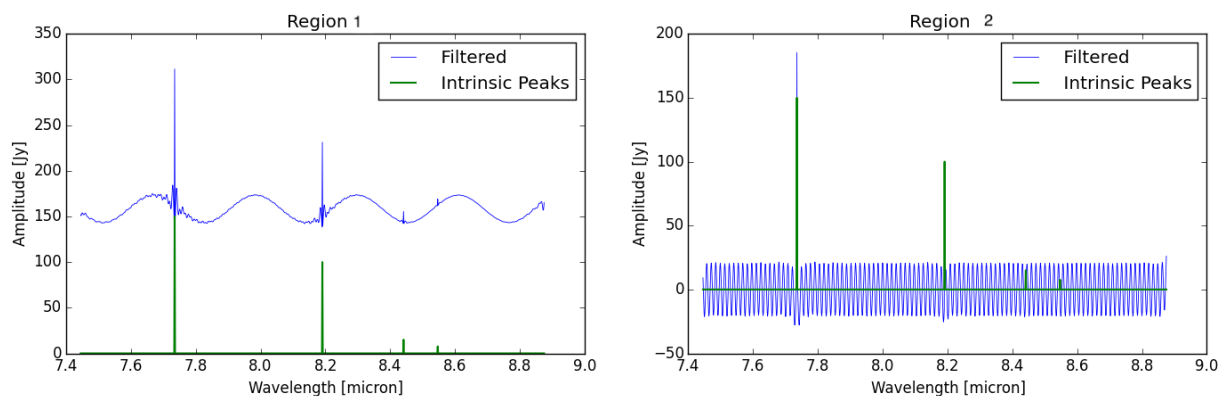


Figure 4.22: Case (2): Fourier Filtering method - Comparison among Intrinsic peaks spectrum and the filtered one

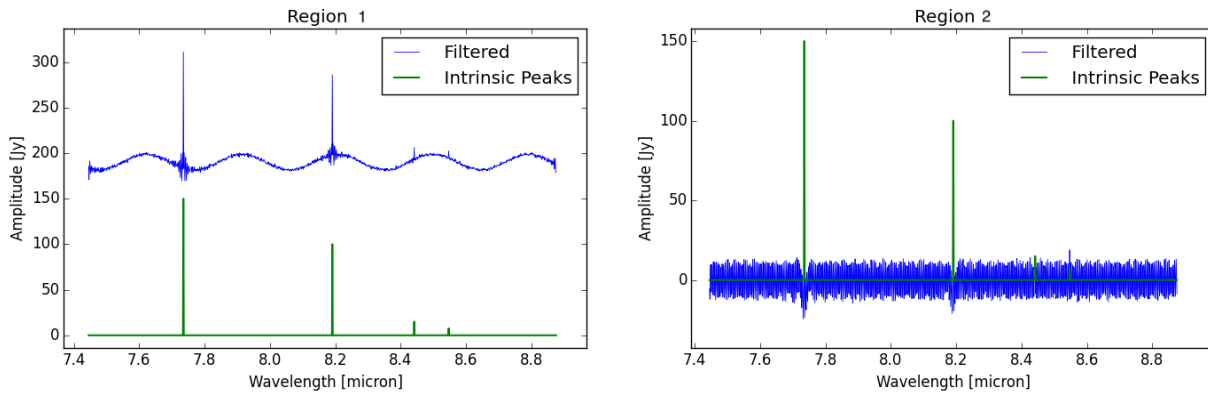


Figure 4.23: Case (3): Fourier Filtering method - Comparison among Intrinsic peaks spectrum and the filtered one

### 4.2.3. Conclusion

The Fourier Filtering method is simple and straight-forward to apply to any spectra. However, throughout its application to the three cases, some weaknesses of this method have been underlined. It is important to draw a conclusion based on the three cases and not a single one, as in reality, the fringes components are not the same and if a similar pattern appears in the three cases, it might likely occur in reality.

The output from each cases, already summarized by Tables 4.2 and 4.3, have been represented graphically by Figure 4.24.

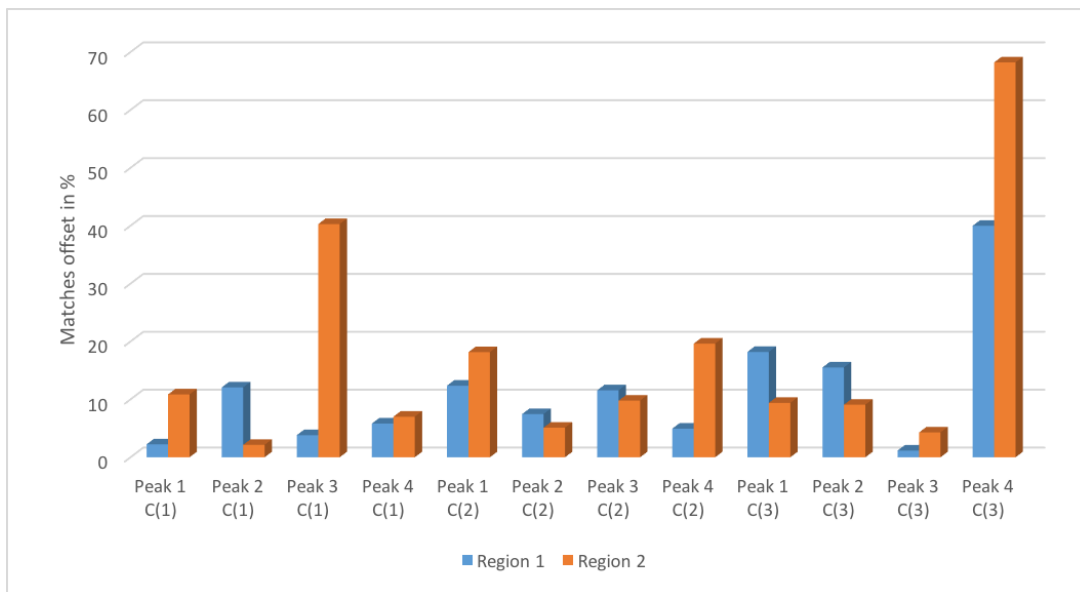


Figure 4.24: All cases: Fourier Filtering method - Match of peaks flux w.r.t. to Intrinsic Fluxes - Graphical Representation

For each case, in general, Region 1 provides the best line flux matches for most of the spectral features, w.r.t. the intrinsic values, while Region 2 line flux values are similar to the observed ones. As explained previously, the similarity of the results of Region 2 with the observed ones mean that this Region does not correct the fringe effect but allows only to provide a cleaner spectrum by removing the low frequency component. This also underlines the poor effect of the low frequency component fringe on the line fluxes. Therefore, for the quantitative analysis of this method, only Region 1 data will be considered.

In this Region, the two dominant amplitude peaks (excluded the central peak) in the Fourier domain have been fil-

tered by setting the data in this range to zero. For the ideal cases (i.e. fringe components without noise), all the spectral features are well approximated, although the match is not perfect; indeed the variations rank between 2 and 13 %. While for the third Case which represents most the reality due to its additional noise component, the variations are recorded between 1 and 40 %. Furthermore, for all Cases, the Region 1 did not provide the best graphical results as the low frequency component was still clearly visible in the filtered spectrum, but this left component did not absorb the spectral features, especially the weak ones as it was the case for Region 2. This is illustrated by Table 4.4, in which Region 1 provides better SNR for peaks 3 & 4 than Region 2. However, it is important to point out that the SNR for weak spectral features are still low and therefore their detectability can be considered as poor.

# Region	SNR [-]											
	Case (1)				Case (2)				Case (3)			
	Peak 1	Peak 2	Peak 3	Peak 4	Peak 1	Peak 2	Peak 3	Peak 4	Peak 1	Peak 2	Peak 3	Peak 4
Region 1	12.03	9.77	2.13	1.98	7.34	4.90	1.41	1.25	11.07	7.77	1.71	1.30
Region 2	20.01	11.54	2.77	1.32	5.08	2.39	0.43	0.43	7.60	5.06	0.59	1.50

Table 4.4: All cases: Fourier Filtering method : Signal to Noise Ratio - In Red: poor detection, In black : acceptable detection, In blue : excellent detection

We might have concluded that none of the regions provides individually perfect results, as the effect of the fringes (i.e. sinusoidal components) are not entirely removed. It was seen that removing the central peak from the Fourier amplitude domain did not correct the fringes effect, but only smooth the spectrum. While, removing the other pair of peaks (not central one) allowed to correct the fringe effect and to remove the high frequency component from the data, providing a cleaner spectrum for pointing out the spectral signature.

Now that the best Region has been defined, the reader might wonder at this point if using the Fourier Filtering improves the data or if it would be better to leave the data set with fringes included. Let's therefore have a look at Table 4.5, in which the match of the observed data with respect to the intrinsic ones is measured and the best matching values have been spotlighted by the blue color.

When comparing the results from Table 4.5 and Figure 4.25, it can clearly be seen that the application of this filter does not lead to better results for each spectral features of each case. Although, for Case (1), applying the filter would be advised as it provides in general the best approximations; for Cases (2) and (3), the distinction is less evident. For Case (2), the difference of Peaks 2 and 3 w.r.t. the observed values is relatively small (i.e. 2%) and thus, this method would still be a good choice to apply to the data set. For the Case (3), it was already underlined that the noise introduced in the data had a bigger effect on the weak spectral features than on the strong ones, explaining the poor correspondence of peak 4. However, the filter appears to better estimate the weak spectral features than the observed values. But, for the strong spectral features, the filter strongly worsens the results (i.e. the difference between the observed values match and the filtered ones being between 10-14 %), while its difference for the weak spectral features varies between (4-24 %). Therefore, for the Case (3), it would be advised to only use the filter for correctly positioning the spectral characteristics and use the observed intensity graph for determining their lines flux.

#	Observed or Filtered Value/ Intrinsic Value[%]											
	Case (1)				Case (2)				Case (3)			
	Peak 1	Peak 2	Peak 3	Peak 4	Peak 1	Peak 2	Peak 3	Peak 4	Peak 1	Peak 2	Peak 3	Peak 4
observed	110.9	97.9	140.3	93.04	118.21	94.93	90.24	80.38	96.41	95.28	105.86	164.95
Region 1	102.24	87.93	103.82	105.83	113.37	92.54	88.43	95.05	81.80	84.48	101.16	60.01

Table 4.5: All cases: Fourier Filtering method - Match of peaks flux of Region 1 and observed ones w.r.t. to Intrinsic Fluxes - Best Matches are shown in blue

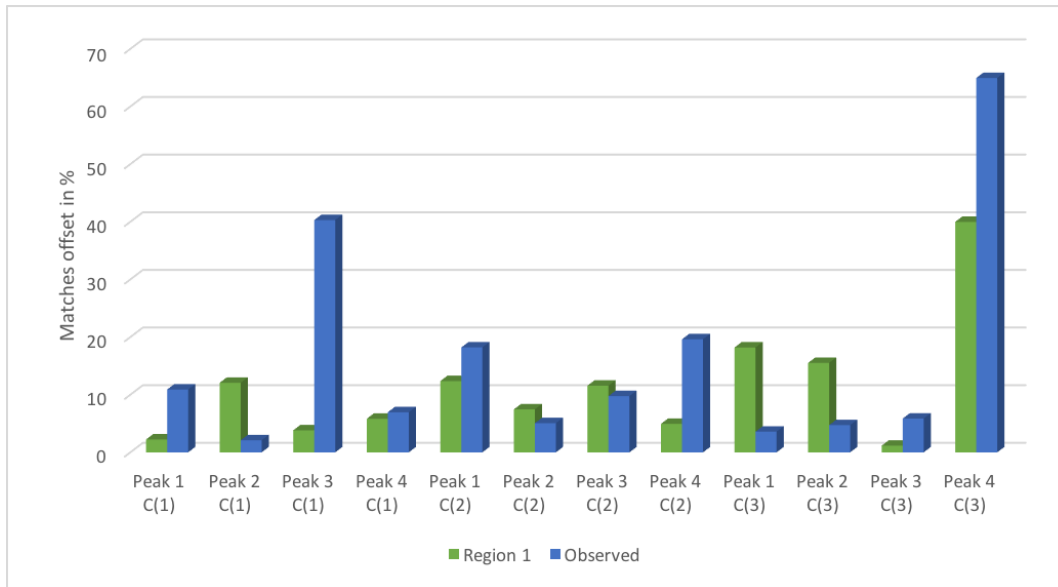


Figure 4.25: All cases: Fourier Filtering method - Match of peaks flux of Region 1 and observed ones w.r.t. to Intrinsic Fluxes - Graphical Representation

In conclusion, for general interpretation of the data, using the Fourier Filtering method would not be advised for an accurate study of the spectrum. For the ideal spectral cases (i.e. only fringes component included), this method and more specifically Region 1 would be recommended as it provides not only a cleaner spectrum, but also good approximations of the lines flux. However, Case (3) represents better the reality due to its additional noise component. Although, it provides the best approximations for the weak spectral features and a cleaner spectrum than the original, its approximations for the strong spectral features are too deviant compared to the observed ones, and would lead to an inaccurate interpretation of the data.

### 4.3. Method 2 : Sine Wave Fitting

The second method for removing fringes is the Sine Wave Fitting. It is currently considered by scientists as the most robust method in combination with the pixel flat fielding for correcting fringes.

This method consists of fitting a sine wave within the set of data and then extracting this sine wave. The ideal residuals should therefore be the spectral features.

#### 4.3.1. Theoretical Background

Theoretically, fitting a sine wave of the form of Equation (4.7) to the spectrum is straight-forward.

$$y = A \cdot \sin(B \cdot x + D) + C \quad (4.7)$$

In which,

- A is the amplitude of the wave
- B is the frequency of the wave
- C is the offset of the wave
- D is the phase of the wave

But its application to the 'normal' spectrum includes some prerequisites. Indeed, an actual spectrum comprises several components with usually a main low & high frequency and fitting a sine wave to the entire spectrum in one

step might not converge. Therefore, the first step is to separate the different frequencies.

A simple way would be to use the Fourier Transform and filter the central peak only in the Fourier domain, then convert the data back to the original domain and subtract it from the original spectrum. It allows to separate the high frequency component to the low one. It is important to underline that the data reduction occurring due to the Fourier Filtering, which have demonstrated in the previous Section, are not applicable here. Indeed, in this method, the Fourier Filtering is used only for separating the two frequency components, which will both be used, and therefore, no part of the spectrum will be neglected.

Now that the signal has been split, the sine wave fitting can be applied to each signal. Once again, several approaches for fitting a sine wave are possible and were tested.

The first Approach investigated was to take from 1 up to 5 peaks in the beginning of the spectrum then the Equation 4.7 was fitted, thus parameters A,B,C and D were determined. Then, the operation was re-done for 1 up to 5 peaks at the end of the spectrum.

Based on both sine fitted curves, a new sine wave fitting could be approximated to the entire spectrum. For this, parameters A,C and D were taken as the average from the previous two sine curves found; thus:

$$A_{new} = \frac{A_{end} - A_{begin}}{2} \quad (4.8a)$$

$$C_{new} = \frac{C_{end} - C_{begin}}{2} \quad (4.8b)$$

$$D_{new} = \frac{D_{end} - D_{begin}}{2} \quad (4.8c)$$

From the literature, it is known that fringes affect only the frequencies of the sinusoidal components, therefore, this parameter has not been averaged as the other ones, but a has been considered as a varying parameter (linear variation).

However, this estimation of the parameters for the new sine wave did not converge to the right spectrum. Although, the amplitude was correct, the vertical shift was slightly off and the phase and the frequency were completely different. The resulting sine wave had clear offsets in frequency and phase from the expected wave. Therefore, it was decided not to use this approach for this method. The averaged amplitude (parameter A from Equation (4.8a)) being already a good estimate of the expected initial amplitude, it was decided to keep this value. But, taking the average of the other parameters did not converge to the desired spectrum. Therefore, an optimizing algorithm has been defined which starts with initial values based on the averaged ones.

These averaged values have been used as range boundaries for parameters B, C and D in the form [-Averaged value until Averaged value] and all combinations of these parameters were tested. These boundaries were considered as the averaged values already provide a good estimate of the expected values and allow to reduce the computational load (i.e. if the user wants to run the sine fitting, it will take maximum 20-40 min to run, instead of hours if considering larger range).

In other words, for each combination of B,C and D, the corresponding sine wave has been estimated over the wavelength range. Then, the residuals of this function with respect to the observed values (i.e. frequency extracted from the Fourier Filtering) have been determined and the corresponding standard deviation was calculated (cf. Equation (4.9)). In order to select the best parameters approximation, the smallest standard deviation from all the combina-

tions was selected.

$$\text{Standard - Deviation} = \sqrt{\frac{\sum_{n=1}^j (x_n - \bar{x})^2}{j - 1}} \quad (4.9)$$

in which,

$\bar{x}$  represents the mean of x

The new sine wave being approximated, the last step of this method can be applied, namely subtracting the wave from the signal and analyzing the residuals. Once again, different approaches possible were investigated:

- Approach I:
  - Step 1: Determining the sine wave of the low frequency component
  - Step 2: Calculating the residuals of this sine wave based on the low frequency component
  - Step 3: Perform Steps 1 & 2 to the high frequency component
  - Step 4: Add the residuals together
  
- Approach II:
  - Step 1: Determining the sine wave of the low frequency component
  - Step 2: Calculating the residuals of this sine wave based on the low frequency component
  - Step 3: Add the residuals from the low frequency to high frequency data set
  - Step 4: Determine the sine wave of the new high frequency component
  - Step 5: Calculate the residuals of this sine wave based on the original high frequency component
  
- Approach III:
  - Step 1: Determining the sine wave of the high frequency component
  - Step 2: Calculating the residuals of this sine wave based on the high frequency component
  - Step 3: Add the residuals from the high frequency to low frequency data set
  - Step 4: Determine the sine wave of the new low frequency component
  - Step 5: Calculate the residuals of this sine wave based on the original low frequency component

#### 4.3.2. Case (1)

As explained previously, the first step is to separate the different frequency components forming the total spectrum. This has been done using the Fourier filtering method of the central peak, described in Section 4.2.

##### APPROACH I

Now that the main components in the signal have been separated, peaks have been selected in the beginning and end of the spectrum, as can be seen in Figures 4.26 and 4.27, which show the peak regions to be fitted for the low and high frequency components, respectively.

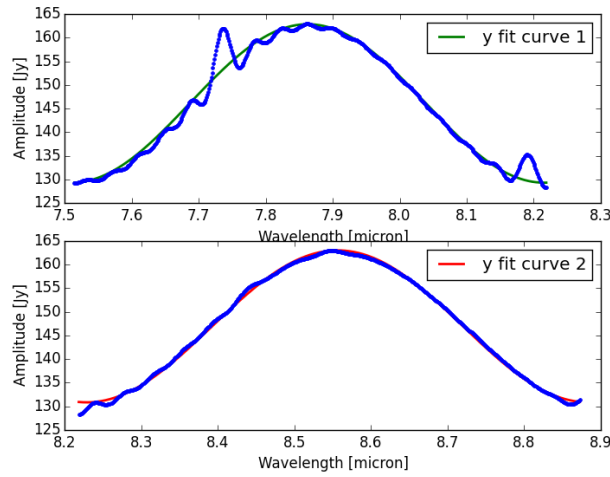


Figure 4.26: Case (1) Approach I: Sine wave fitting method - Sine Fit for the low frequency component. On the top, the sine fit is for the beginning of the spectrum while on the bottom, the sine fit is for the end of the spectrum

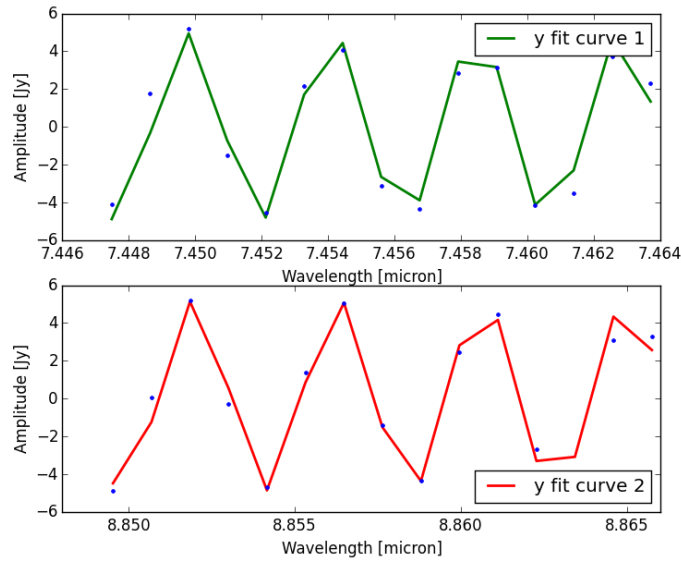


Figure 4.27: Case (1) Approach I: Sine wave fitting method - Sine Fit for the high frequency component. On the top, the sine fit is for the beginning of the spectrum while on the bottom, the sine fit is for the end of the spectrum

For each part (beginning and end) of the signal, a sine wave has been fitted, and thus the parameters A, B, C and D could be estimated as follow:

Component	Parameter	Beginning Spectrum	End Spectrum	Sine Fit	Expected value
Low Frequency	A	16.76	16.07	16.41	16.5
	B	8.91	9.58	8.69	9.1
	D	6.9	1.2	-3.75	451.5
	C	146.07	146.92	145.1	120
High Frequency	A	4.95	5.04	5.00	5
	B	1444.82	1444.82	1407.02	1407
	D	19.9	4.6	0.55	0.34
	C	-0.0051	0.172	0.02	26

Table 4.6: Case (1) Approach I: Sine wave fitting method - Parameters of the sine Equation (4.7), estimated for the beginning, end of the spectrum and for entire spectrum

Following the method developed in Subsection 4.3.1, a new sine wave has been derived for the low and high frequency component separately: these can be seen in Figures 4.28 - 4.30. From these figures, it can be clearly seen that the sine waves derived are matching the original data with a negligible offset for the low frequency, but for the high one, the match seems close to perfect.

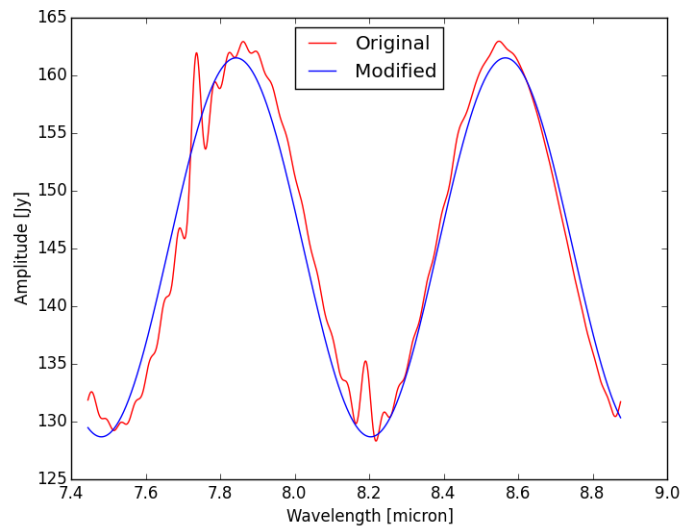


Figure 4.28: Case (1) Approach I: Sine wave fitting method - Sine Fit for the low frequency component

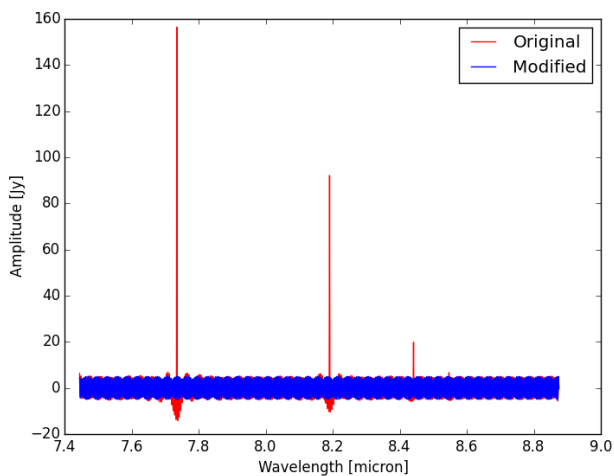


Figure 4.29: Case (1) Approach I: Sine wave fitting method - Sine Fit for the high frequency component

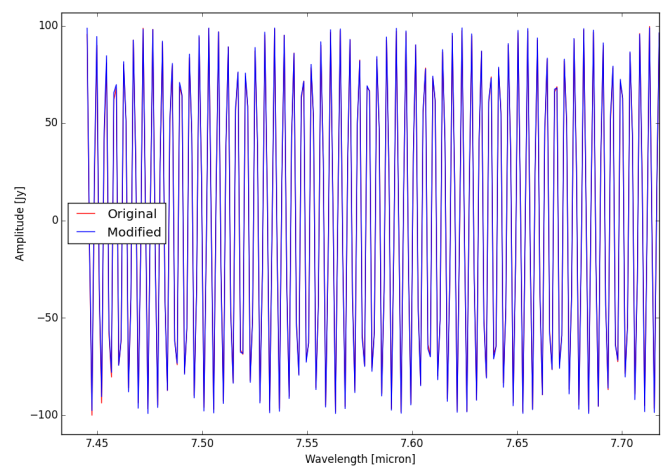


Figure 4.30: Case (1) Approach I: Sine wave fitting method - Sine Fit for the high frequency component Zoom

As explained previously, this approach consists of determining the residuals of each frequency component and adding them together as the final corrected spectrum, which leads to Figure 4.31.

From this graph, it is possible to determine the location of the spectral features. However, let's have a closer look at the peaks comparison; as realized for the Fourier Filtering analysis, the peaks amplitudes are compared to the observed ones and to the intrinsic ones.

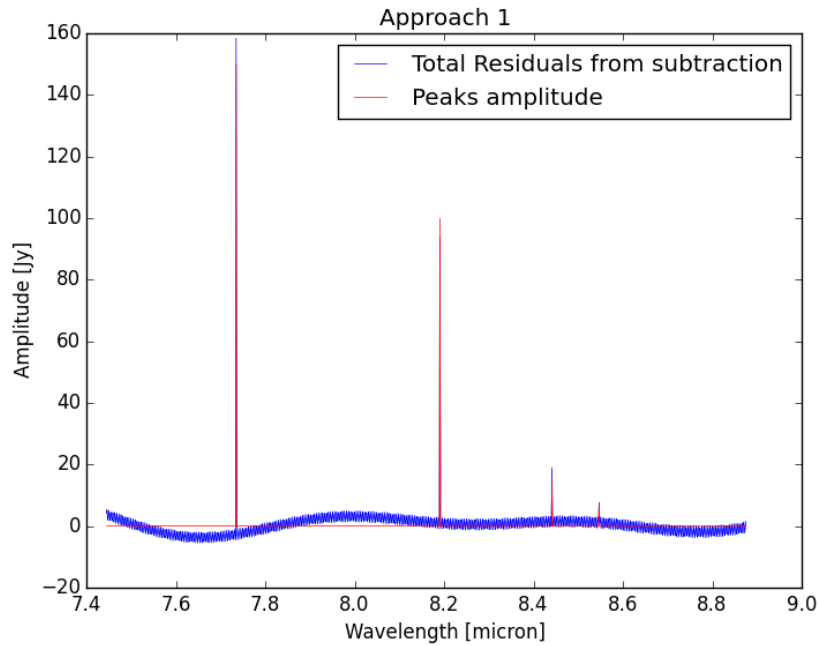


Figure 4.31: Case (1) Approach I: Sine wave fitting method - Total Residuals from the sine fit for the High and low frequency components

When comparing the peaks amplitudes, the same outcome as from the graphical analysis holds; namely, the spectral features are clearly distinguishable although some residuals are still left in the spectrum. The peak amplitude matches for the strong spectral features are not reliable as they provide worse estimates of the intrinsic values (deviation of 7-8 %) than the ones from the observed spectrum (deviation of 4-6 %), shown in Table 4.7. For the weak spectral features, also in this case, the lines flux match is more divergent as the deviation from the intrinsic expected values are in the order of 16-17 %. It would therefore not be advisable to use this method and the specific residuals approach for studying the weak spectral features.

X Value	Reduced Value/ X Value[%]			
	Case (1)			
	Peak 1	Peak 2	Peak 3	Peak 4
observed	96.82	94.79	83.68	90.71
Intrinsic	107.37	92.80	117.44	84.46

Table 4.7: Case (1) Approach I: Sine wave fitting method - Match of peaks flux w.r.t. to observed and Intrinsic Fluxes

## APPROACH II

In the second approach, the low frequency component is first studied. Therefore, some peaks are selected in the beginning and end of the spectrum; and for each part a sine wave has been fitted, as shown in Figure 4.32. Once the sine waves parameters have been defined, the new sine wave for the entire low frequency spectrum could be derived (cf. Figure 4.33) and the residuals deducted from it.

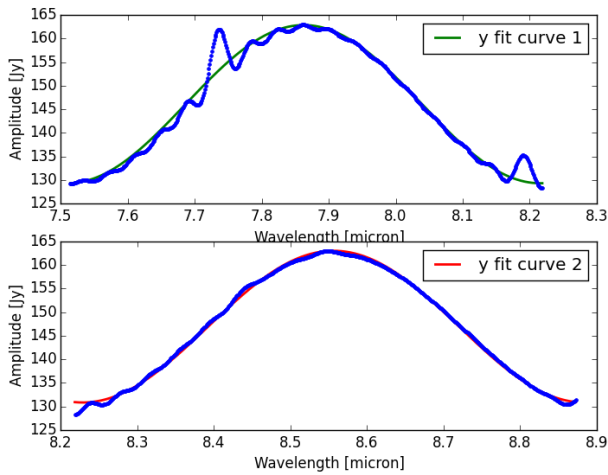


Figure 4.32: Case (1) Approach II: Sine wave fitting method - Sine Fit for the low frequency component. On the top, the sine fit is for the beginning of the spectrum while on the bottom, the sine fit is for the end of the spectrum

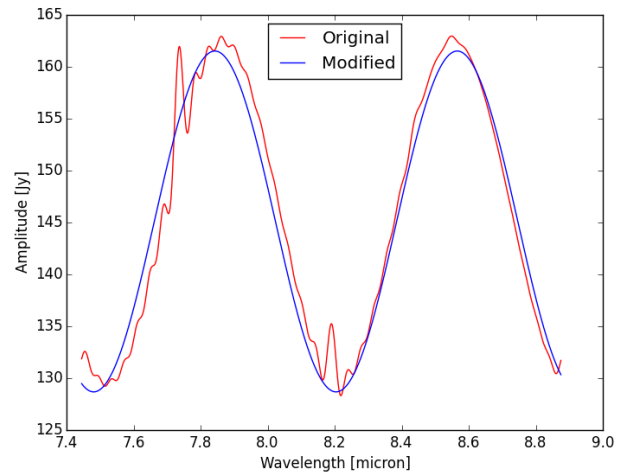


Figure 4.33: Case (1) Approach II: Sine wave fitting method - Sine Fit for the low frequency component

As expected, the results are similar to the ones of Approach I, but now that the residuals have been determined, these are added to the high frequency component extracted from the signal with the Fourier filtering method. The same steps are then applied to this new set of data for the high frequency component (cf. Figure 4.34). Table 4.8 summarizes all the sine parameters used in this simulation. When comparing this table with the one from Approach I (i.e. Table 4.6), it can be clearly seen that although the residuals from the low frequency component are small, they strongly affect the new sine wave fit of the high frequency component.

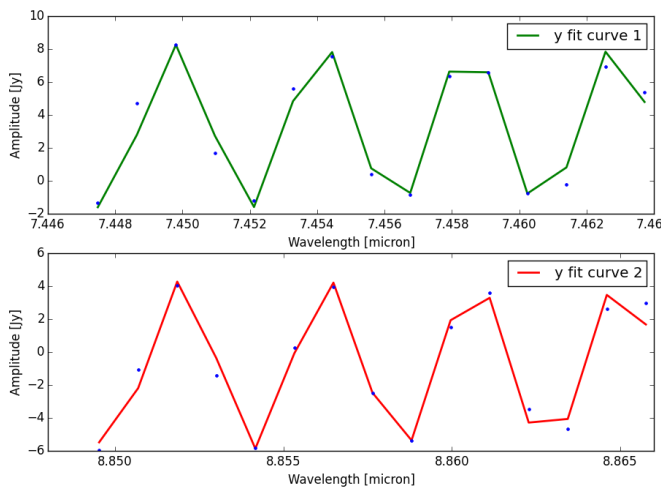


Figure 4.34: Case (1) Approach II: Sine wave fitting method - Sine Fit for the High frequency component. On the top, the sine fit is for the beginning of the spectrum while on the bottom, the sine fit is for the end of the spectrum

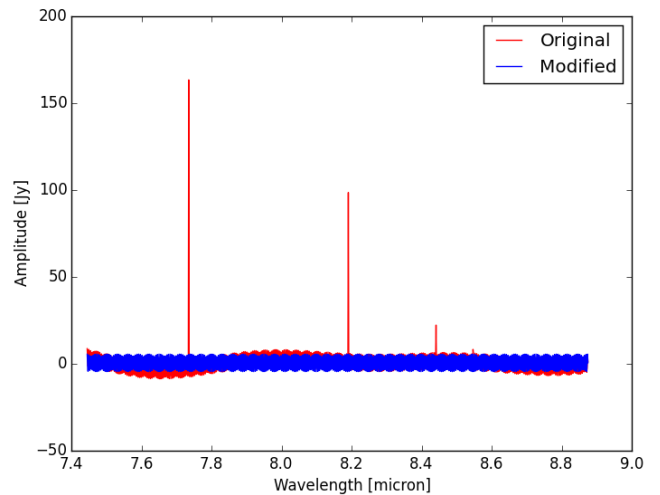


Figure 4.35: Case (1) Approach II: Sine wave fitting method - Sine Fit for the high frequency component

Component	Parameter	Beginning Spectrum	End Spectrum	Sine Fit	Expected value
Low Frequency	A	16.76	16.07	16.41	16.5
	B	8.91	9.58	8.69	9.1
	D	6.9	1.2	-3.75	451.5
	C	146.07	146.92	145.1	120
-----					
High Frequency	A	4.98	5.11	5.04	5
	B	1444.82	1444.82	1407.12	1407
	D	7.3	4.6	5.85	0.34
	C	3.26	-0.76	0.55	26

Table 4.8: Case (1) Approach II: Sine wave fitting method - Parameters of the sine Equation (4.7), estimated for the beginning, end of the spectrum and for entire spectrum

Once a sine wave was fitted to the modified high frequency data set, the residuals were calculated, as shown in Figure 4.36. At first sight, the overall shape seems similar the one found with Approach I (Figure 4.31). Namely, all the spectral features are strongly distinguishable, but residuals are still present in the spectrum, especially the ones from the low frequency component. If the reader compares carefully this graph with the results of Approach I, he will notice that the residuals are more dominant in this Approach than the previous one. This can be seen in the spectrum at wavelengths 7.5 and 7.7 [micron].

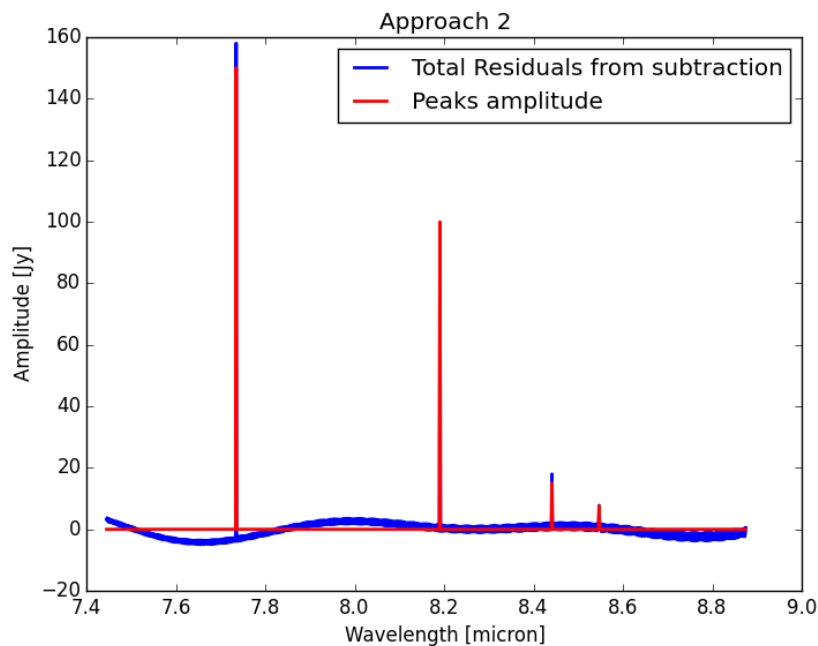


Figure 4.36: Case (1) Approach II: Sine wave fitting method - Residuals from the sine fit for the high frequency component, i.e. total residuals of the spectrum

Graphically, this approach leads to more residuals than the previous one. Therefore, one could look at the peaks amplitude in order to classify quantitatively the approach. The results displayed in Table 4.9 show a contradictory conclusion than the graph; same match range for the strong spectral features (i.e. deviations between 7-8 %) and a better match range for the weak ones (i.e. deviations between 7-13 %). Graphically, this approach leads to less satisfactory graph but, it provides better lines flux approximations than the previous Approach.

X Value	Reduced Value/ X Value[%]			
	Case (1)			
	Peak 1	Peak 2	Peak 3	Peak 4
observed	96.918	94.56	81.00	100.34
Intrinsic	107.47	92.57	113.67	93.36

Table 4.9: Case (1) Approach II: Sine wave fitting method - Match of peaks flux w.r.t. to observed and Intrinsic Fluxes

APPROACH III

The third Approach is exactly the opposite of the Approach II. Therefore, first the high frequency component extracted from the Fourier filtering method is studied, as shown in Figures 4.37 and 4.38. In these figures, the fit for the beginning and end of the extracted high frequency spectrum and the fit for the entire extract frequency spectrum are respectively shown.

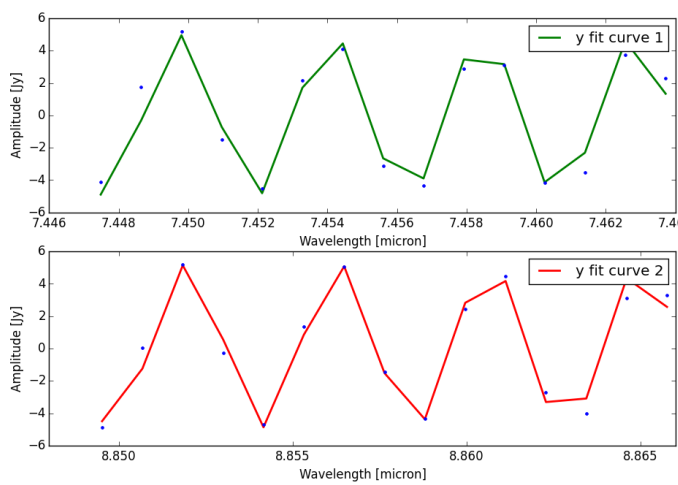


Figure 4.37: Case (1) Approach III: Sine wave fitting method - Sine Fit for the High frequency component. On the top, the sine fit is for the beginning of the spectrum while on the bottom, the sine fit is for the end of the spectrum

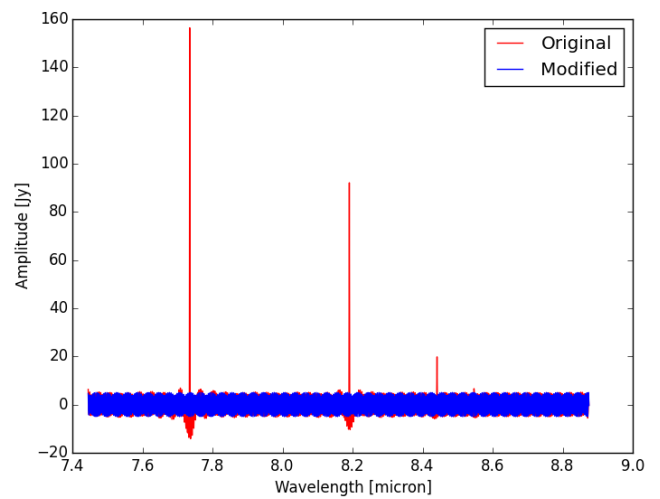


Figure 4.38: Case (1) Approach III: Sine wave fitting method - Sine Fit for the high frequency component

Once the residuals have been determined, these can be added to the extracted low frequency spectrum and the same analysis as usual can be carried out, namely, fitting the beginning and end of the spectrum (Figure 4.39) and then fitting the entire spectrum (Figure 4.40).

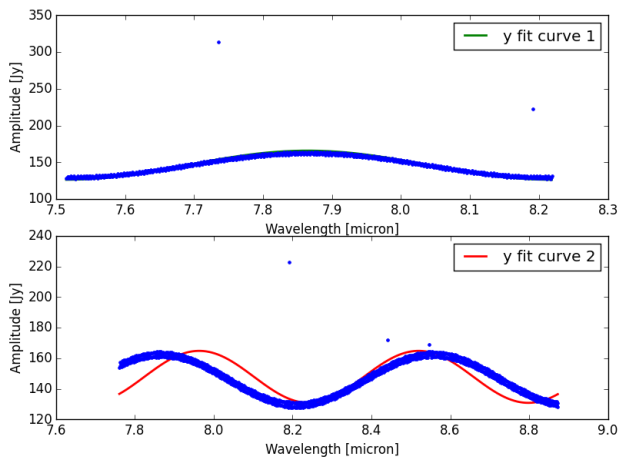


Figure 4.39: Case (1) Approach III: Sine wave fitting method - Sine Fit for the low frequency component. On the top, the sine fit is for the beginning of the spectrum while on the bottom, the sine fit is for the end of the spectrum

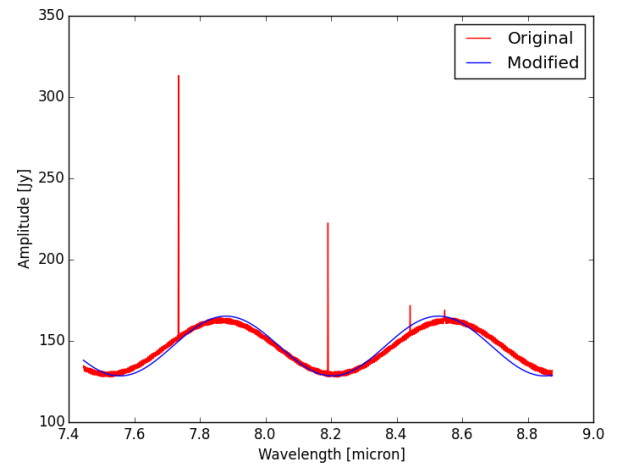


Figure 4.40: Case (1) Approach III: Sine wave fitting method - Sine Fit for the low frequency component

Let's have a look at the final sine wave parameters for each of the frequency components from Table 4.10. As with the two previous approaches, the parameters are nearly similar to the expected ones (amplitude and frequency), although the vertical and horizontal shift parameters (i.e. C and D) are different, their estimated values provide small graphical shifts compared to the initial ones.

Component	Parameter	Beginning Spectrum	End Spectrum	Sine Fit	Expected value
Low Frequency	A	19.78	16.98	18.38	16.5
	B	8.911	11.28	9.7	9.1
	D	0.6	18.5	-5.75	451.5
	C	146.05	147.84	146.85	120
High Frequency	A	4.95	5.044	5.00	5
	B	1444.82	1444.82	1407.02	1407
	D	19.9	4.6	0.55	0.34
	C	-0.0051	0.172	0.02	26

Table 4.10: Case (1) Approach III: Sine wave fitting method - Parameters of the sine Equation (4.7), estimated for the beginning, end of the spectrum and for entire spectrum

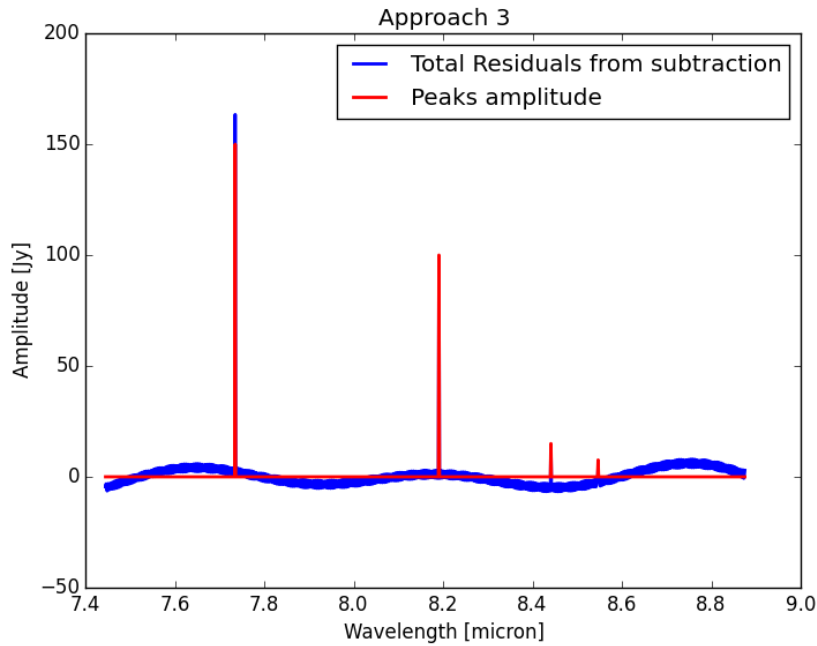


Figure 4.41: Case (1) Approach II: Sine wave fitting - Residuals from the sine fit for the low frequency component, i.e. total residuals of the spectrum

The total residuals which are the ones calculated from the new low frequency data set are shown in Figure 4.41. Graphically, this approach leads to a different residuals spectrum than the two previous approaches (cf. Figures 4.31 and 4.36), indeed the final overall shape is slightly different from the others (i.e. inverse fluctuation pattern in the first part of the spectrum, but more fluctuations in the second part). It appears like a left low frequency component in the data and therefore, the spectrum looks less clean than previously as its continuum is not flat. Although, the spectral features are clearly distinguishable, the previous Approaches provided a better graphical representation.

The line flux study sustains the graphical analysis. As shown in Table 4.11, this approach does not improve the lines flux approximations of the peaks. It actually provides the same results as Approach I, but its graph is less optimal. For this Case, Approach III will therefore not be advised. However, for a first general analysis, this method would be considered as reliable for the strong spectral features.

X Value	Reduced Value/ X Value[%]			
	Case (1)			
	Peak 1	Peak 2	Peak 3	Peak 4
observed	96.82	94.79	83.68	90.71
Intrinsic	107.37	92.80	117.43	84.40

Table 4.11: Case (1) Approach III: Sine wave fitting method - Match of peaks flux w.r.t. to observed and Intrinsic Fluxes

### 4.3.3. Case (2)

The first step is to separate the different frequency components forming the total spectrum. This has been done using the Fourier filtering method of the central peak, described in Section 4.2.

#### APPROACH I

The main components in the signal being separated, some peaks can be selected at the beginning and end of the

spectrum, as shown in Figures 4.42 and 4.43, which display the fitted peaks for the low and high frequency component, respectively.

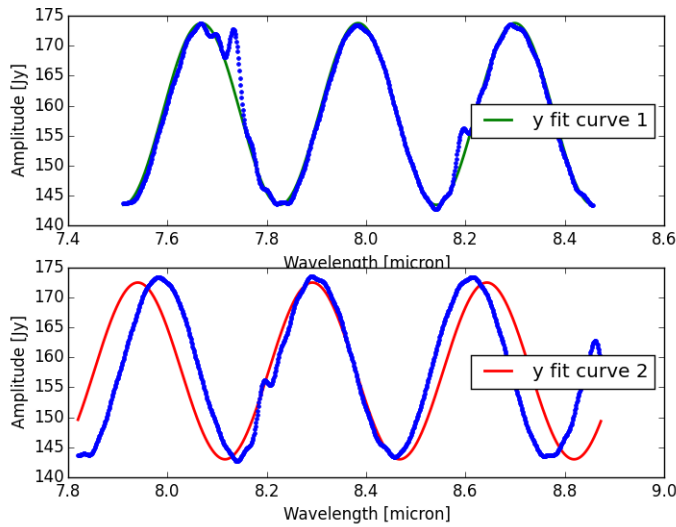


Figure 4.42: Case (2) Approach I: Sine wave fitting method - Sine Fit for the low frequency component. On the top, the sine fit is for the beginning of the spectrum while on the bottom, the sine fit is for the end of the spectrum

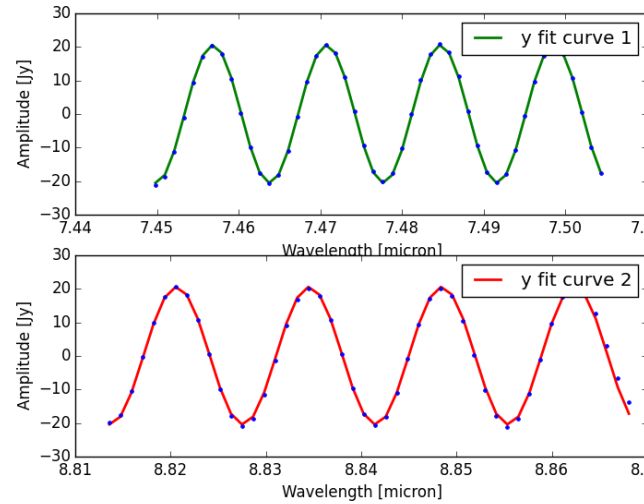


Figure 4.43: Case (2) Approach I: Sine wave fitting method - Sine Fit for the high frequency component. On the top, the sine fit is for the beginning of the spectrum while on the bottom, the sine fit is for the end of the spectrum

For each part (beginning and end) of the signal, a sine wave has been fitted, thus the parameters A, B, C and D have been estimated, listed in Table 4.12. As it was pointed out for Case (1), the amplitude and frequency parameters are quite similar to the expected ones, which is not the case for the phase and vertical offset parameters, but graphically these generate negligible shifts in the spectrum.

Component	Parameter	Beginning Spectrum	End Spectrum	Sine Fit	Expected value
Low Frequency	A	15.15	14.55	14.85	15
	B	19.92	17.11	18.2	20.07
	D	5.9	4.7	-5.1	821.5
	C	158.60	157.61	156.89	68.3
High Frequency	A	20.54	20.49	20.52	20.5
	B	451.50	451.50	451.33	451.5
	D	15.1	15.1	-14.9	40.3
	C	0.047	0.06	-0.05	90.07

Table 4.12: Case (2) Approach I: Sine wave fitting method - Parameters of the sine Equation (4.7), estimated for the beginning, end of the spectrum and for entire spectrum

Following the method developed in Subsection 4.3.1, a new sine wave has been derived for the low and high frequency component separately, using the parameters shown in the column 'sine fit' in Table 4.12; these can be seen in Figures 4.44 - 4.46. From these figures, it can be clearly shown that the sine waves derived match the original data with a negligible offset for the low frequency, but for the high one the match seems close to perfect.

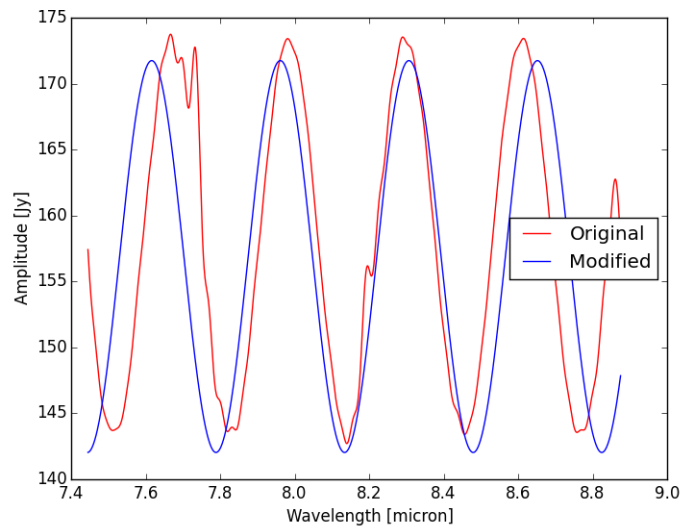


Figure 4.44: Case (2) Approach I: Sine wave fitting method - Sine Fit for the low frequency component

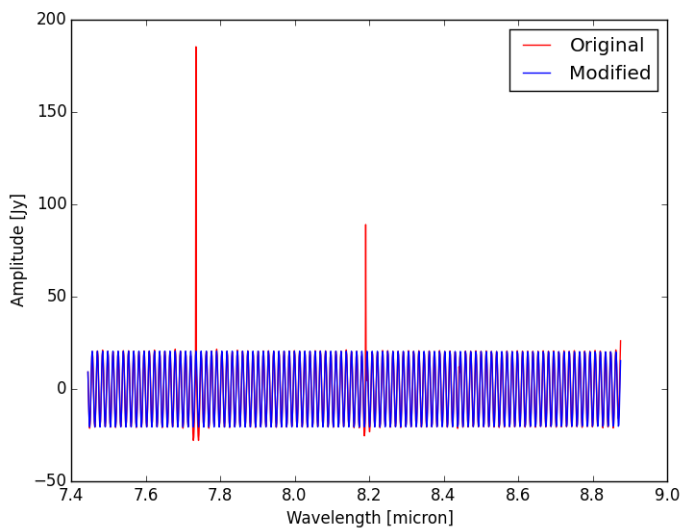


Figure 4.45: Case (2) Approach I: Sine wave fitting method - Sine Fit for the high frequency component

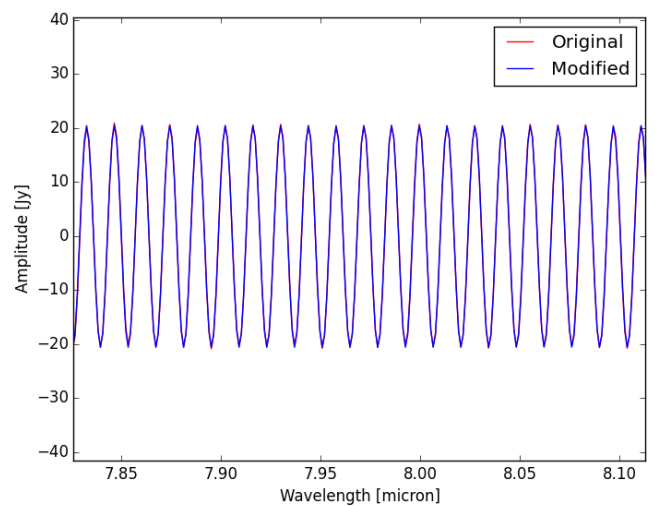


Figure 4.46: Case (2) Approach I: Sine wave fitting method - Sine Fit for the high frequency component Zoom

This approach consists of determining the residuals of each frequency component and adding them together as the final corrected spectrum, displayed in Figure 4.47. The final spectrum shows a similar shape than the residuals from the low frequency component which were more dominant than the high frequency residuals. From this graph, it is possible to determine the location of the strong spectral features easily because the weak ones seem to have been absorbed by the low frequency residuals.

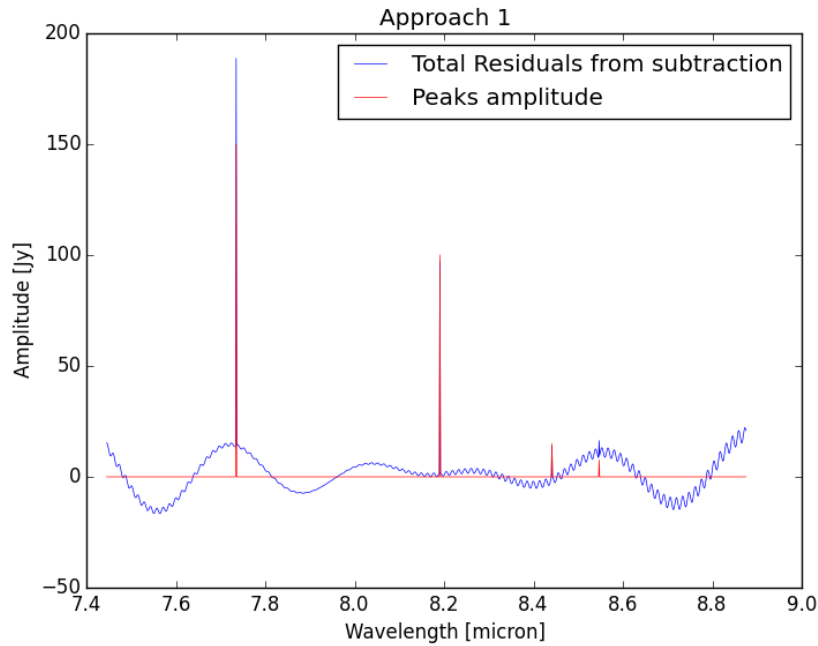


Figure 4.47: Case (2) Approach I: Sine wave fitting method - Total Residuals from the sine fit for the High and low frequency components

When analyzing the peaks amplitudes comparison, it is surprising to see that the best matches are for the weak spectral features, while the strong features show deviation up to 16 % for the first peak and of 5 % for the second. However, it can also be noticed that for three peaks out of the four, this method seems to have not really corrected the lines flux as the matches with the observed values is close to 100 %. Therefore, this method does not provide an excellent graphical representation and does not correct the lines flux.

X Value	Reduced Value/ X Value[%]			
	Case (2)			
	Peak 1	Peak 2	Peak 3	Peak 4
observed	98.45	100.22	102.49	116.80
Intrinsic	116.38	95.15	92.49	93.88

Table 4.13: Case (2) Approach I: Sine wave fitting method - Match of peaks flux w.r.t. to observed and Intrinsic Fluxes

## APPROACH II

In the second approach, the low frequency component is first studied. Again, some peaks are selected at the beginning and end of the spectrum; and for each part a sine wave has been fitted, as shown in Figure 4.48. Once the sine waves parameters have been defined, the new sine wave for the entire low frequency spectrum can be derived (cf. Figure 4.49) and the residuals deducted from it.

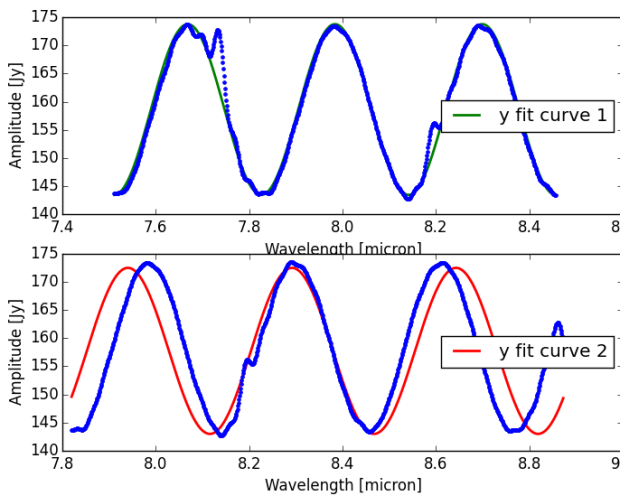


Figure 4.48: Case (2) Approach II: Sine wave fitting method - Sine Fit for the low frequency component. On the top, the sine fit is for the beginning of the spectrum while on the bottom, the sine fit is for the end of the spectrum

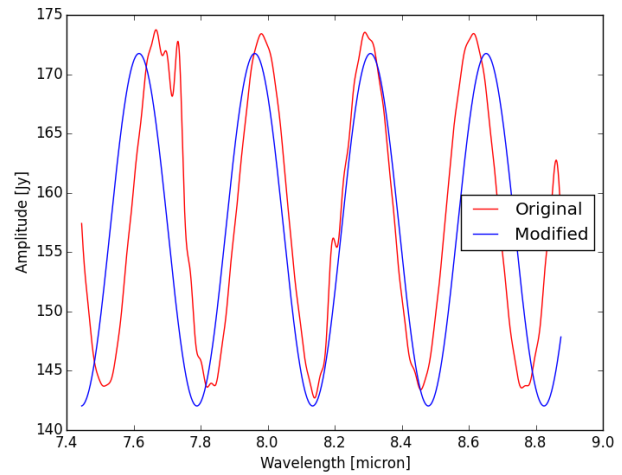


Figure 4.49: Case (2) Approach II: Sine wave fitting method - Sine Fit for the low frequency component

As expected, the results for the low frequency component are similar to Approach I. The residuals being determined, these are added to the high frequency component extracted from the signal by the Fourier filtering method. The same steps are then applied to this new data set of the high frequency component (cf. Figures 4.50-4.51). Table 4.14 summarizes all the sine parameters used in this simulation. The effect of the low frequency residuals on the sine fitting for the new high frequency component can clearly be seen, notably in the amplitude parameter. Its new value of 21.48 [-] is slightly off compared to the one estimated in approach I (i.e. 20.5 [-]), thus it is expected to induce more amplitude residuals than in the previous Approach.

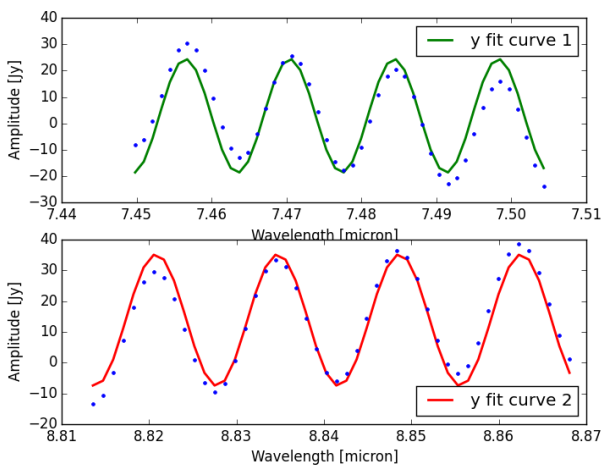


Figure 4.50: Case (2) Approach II: Sine Fit for the High frequency component. On the top, the sine fit is for the beginning of the spectrum while on the bottom, the sine fit is for the end of the spectrum

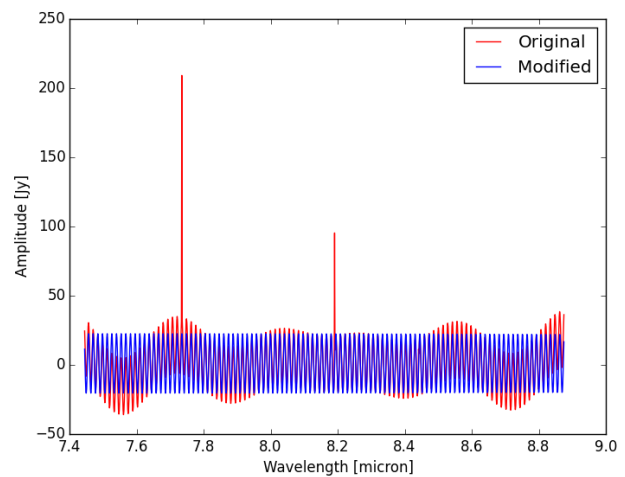


Figure 4.51: Case (2) Approach II: Sine wave fitting method - Sine Fit for the high frequency component

Component	Parameter	Beginning Spectrum	End Spectrum	Sine Fit	Expected value
Low Frequency	A	15.15	14.55	14.85	15
	B	19.91	17.11	18.2	20.07
	D	5.9	4.7	-5.1	821.5
	C	158.60	157.61	156.89	68.3
High Frequency	A	21.57	21.38	21.48	20.5
	B	451.50	451.50	451.33	451.5
	D	2.7	15.0	-8.65	40.3
	C	2.84	13.80	1.08	90.07

Table 4.14: Case (2) Approach II: Sine wave fitting method - Parameters of the sine Equation (4.7), estimated for the beginning, end of the spectrum and for entire spectrum

Once a sine wave was fitted to the modified high frequency data set, the residuals were calculated, as shown in Figure 4.52. At first sight, the overall shape seems similar the one found with Approach I (Figure 4.47), but the spectrum width of approach II is larger, which might be explained by the offset of the high frequency amplitude parameter. Moreover, only the strong spectral features are clearly distinguishable, as was the case in approach I. However, for this Approach, the weak spectral features seem even more absorbed by the spectrum due to the important residuals left from the low frequency fit.

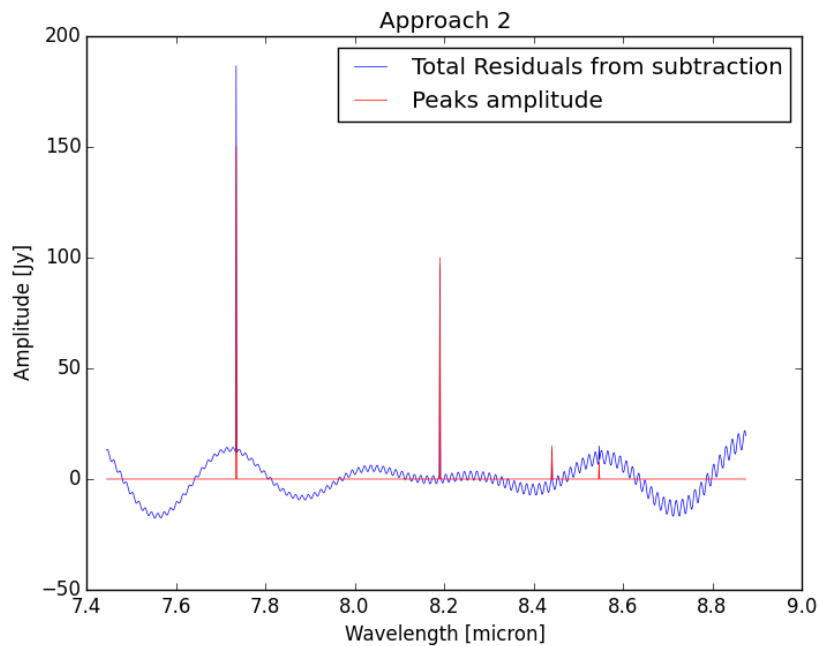


Figure 4.52: Case (2) Approach II: Sine wave fitting method - Residuals from the sine fit for the high frequency component, i.e. total residuals of the spectrum

Graphically, this approach leads to more residuals than the previous one and is therefore less satisfying. However, one could look at the peaks amplitude in order to classify quantitatively the approach. The results displayed in Table 4.15 show the same conclusion as for the Approach I. Indeed, the peak deviations are similar for all the peaks. As mentioned for the previous method, the reader might point their attention to the match with the observed values. These are nearly perfect for 75% of the spectral features, which can be translated by a non-correction of the fringes effect on the lines flux. This approach would therefore not be advised as it worsens the graphical spectral representation and does not provide lines flux correction.

X Value	Reduced Value/ X Value[%]			
	Case (2)			
	Peak 1	Peak 2	Peak 3	Peak 4
observed	98.38	100.33	103.30	116.12
Intrinsic	116.29	95.25	93.23	93.34

Table 4.15: Case (2) Approach II: Sine wave fitting method - Match of peaks flux w.r.t. to observed and Intrinsic Fluxes

APPROACH III

The first step of the third approach consists of studying the extracted high frequency component extracted from the Fourier filtering method, as shown in Figures 4.53 and 4.54. In the previous figures, the fit for the beginning and end of the extracted high frequency spectrum and the fit for the entire extract frequency spectrum are respectively shown.

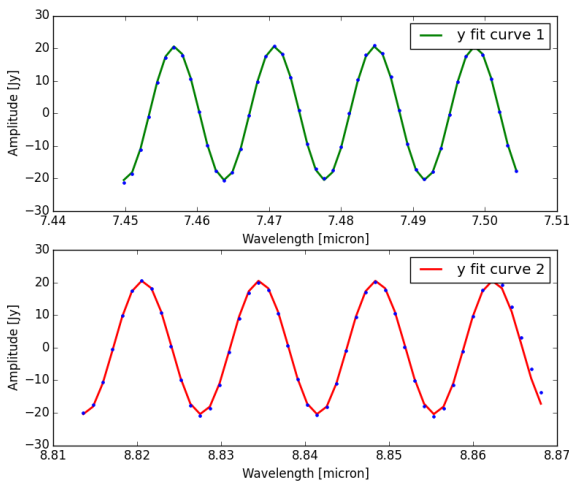


Figure 4.53: Case (2) Approach III: Sine wave fitting method - Sine Fit for the High frequency component. On the top, the sine fit is for the beginning of the spectrum while on the bottom, the sine fit is for the end of the spectrum

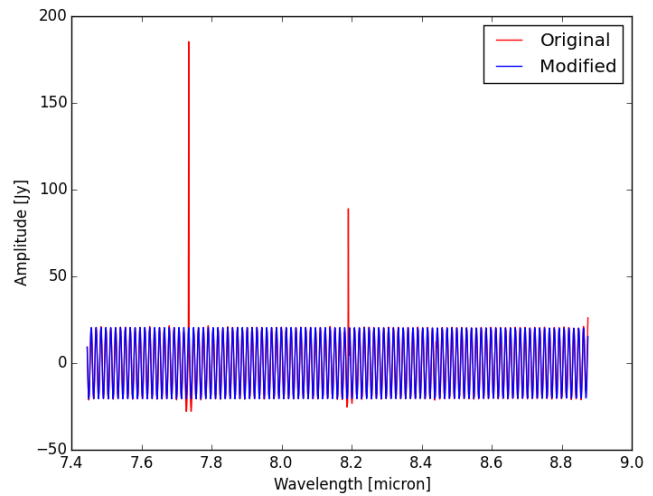


Figure 4.54: Case (2) Approach III: Sine wave fitting method - Sine Fit for the high frequency component

Once the residuals have been determined, these can be added to the extracted low frequency spectrum and the same analysis as usual can be carried out, namely, fitting the beginning and end of spectrum (Figure 4.55) and then fitting the entire spectrum (Figure 4.56).

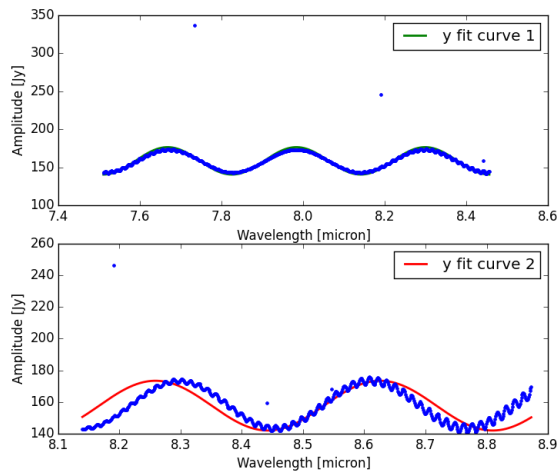


Figure 4.55: Case (2) Approach III: Sine wave fitting method - Sine Fit for the low frequency component. On the top, the sine fit is for the beginning of the spectrum while on the bottom, the sine fit is for the end of the spectrum

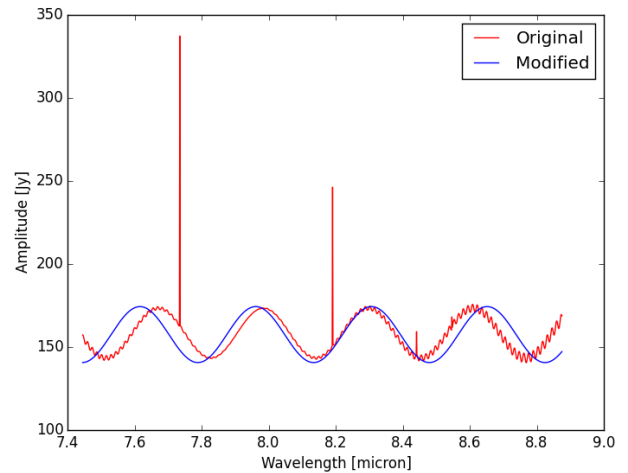


Figure 4.56: Case (2) Approach III: Sine wave fitting method - Sine Fit for the low frequency component

In Table 4.16, the final sine wave parameters for each of the frequency components have been summarized. As with the two previous approaches, the amplitude and frequency parameters are nearly similar to the expected ones, although the vertical and horizontal shift parameters (i.e. C and D) are different, their estimated values provide small graphical shifts compared to the initial ones.

Component	Parameter	Beginning Spectrum	End Spectrum	Sine Fit	Expected value
Low Frequency	A	17.99	15.69	16.84	15
	B	19.91	17.11	18.2	20.07
	D	5.9	4.7	-5.1	821.5
	C	158.65	157.70	157.52	68.3
High Frequency	A	20.54	20.49	20.52	20.5
	B	451.50	451.50	451.33	451.5
	D	15.1	15.1	-14.9	40.3
	C	0.047	0.060	-0.05	90.07

Table 4.16: Case (2) Approach III: Sine wave fitting method - Parameters of the sine Equation (4.7), estimated for the beginning, end of the spectrum and for entire spectrum

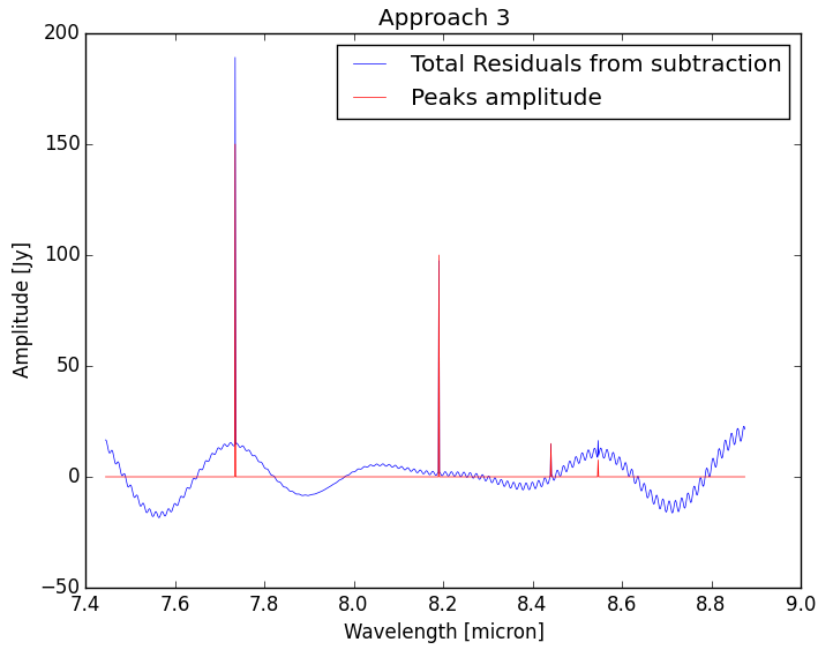


Figure 4.57: Case (2) Approach II: Sine wave fitting method - Residuals from the sine fit for the low frequency component, i.e. total residuals of the spectrum

The total residuals which are the ones calculated from the new low frequency data set are shown in Figure 4.57. Graphically, the overall shape of this approach is similar to the previous approaches. However, the width of the spectrum over the all wavelength range is smaller than the one from approach II. This approach is thus expected to provide better results than approach II as the residuals amplitude are smaller. When comparing this approach with approach I, the same graphical conclusions can be drawn, namely only the strong spectral features can be depicted and the residuals of the low frequency component are dominant in the final residual spectrum. Moreover, from the comparison of the peaks amplitude, Approach III leads to the same results as Approach I. For this Case, a differentiation between Approach I and III is not possible.

One might conclude that this method does not allow to clearly point out all the spectral features, and is not optimal for determining their amplitudes. However, for a first general analysis, this method would be considered as reliable for providing a cleaner spectrum, but will not give any relevant information on the lines flux. The Approach I and III would be considered as the best.

X Value	Reduced Value/ X Value[%]			
	Peak 1	Peak 2	Peak 3	Peak 4
observed	98.45	100.22	102.49	116.90
Intrinsic	116.38.45	95.16	92.49	93.80

Table 4.17: Case (2) Approach III: Sine wave fitting method - Match of peaks flux w.r.t. to observed and Intrinsic Fluxes

#### 4.3.4. Case (3)

The third case differs from the two previous ones as it includes two fringes components and noise. In the matter of consistency, the same approaches as realized before will be done for this case. The goal of analyzing this case is to determine the efficiency of the algorithm if the spectrum does not represent ideal fringe effect and therefore, includes some noise.

The first step is to separate the main different frequency components forming the total spectrum. This has been done using the Fourier filtering method of the central peak, described in Section 4.2.

#### APPROACH I

The main frequency components in the signal being separated, some peaks can be selected at the beginning and end of the spectrum, as shown in Figures 4.58 and 4.59, which display the fitted peaks for the low and high frequency component, respectively.

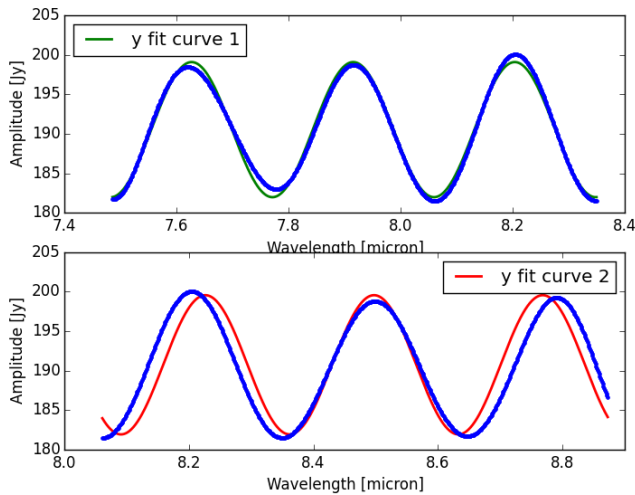


Figure 4.58: Case (3) Approach I: Sine wave fitting method - Sine Fit for the low frequency component. On the top, the sine fit is for the beginning of the spectrum while on the bottom, the sine fit is for the end of the spectrum

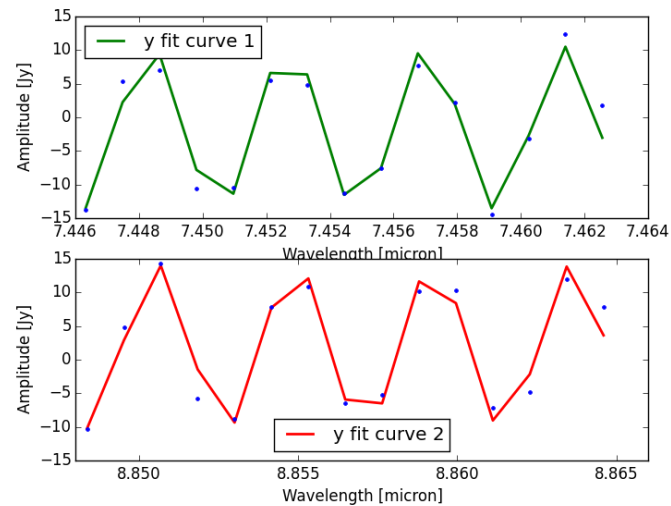


Figure 4.59: Case (3) Approach I: Sine wave fitting method - Sine Fit for the high frequency component. On the top, the sine fit is for the beginning of the spectrum while on the bottom, the sine fit is for the end of the spectrum

For the beginning and end of the signal, a sine wave was fitted, by determining the parameters A, B, C and D from Equation (4.7), listed in Table 4.18. As it was pointed for Cases (1) and (2), the amplitude and frequency parameters are quite similar to the expected ones, which is not the case for the phase and vertical offset parameters, but graphically these last generate negligible shifts in the spectrum.

Component	Parameter	Beginning Spectrum	End Spectrum	Sine Fit	Expected value
Low Frequency	A	8.45	8.72	8.58	8.5
	B	21.73	23.18	21.41	21.5
	D	5.5	5.6	-4.45	7.34
	C	190.53	190.75	190.55	150.1
High Frequency	A	12.63	12.37	12.50	12
	B	1444.82	1444.82	1407.04	1407
	D	15.6	19.2	-10.8	2.34
	C	-1.19	1.53	0.13	40

Table 4.18: Case (3) Approach I: Sine wave fitting method - Parameters of the sine Equation (4.7), estimated for the beginning, end of the spectrum and for entire spectrum

Following the method developed in Subsection 4.3.1, a new sine wave has been derived for the low and high frequency component separately, using the parameters shown in the column 'sine fit' in Table 4.18. Graphs in Figures 4.44 - 4.46 display the sine wave fits. From these figures, it can be clearly seen that the sine waves derived are matching the original data, for the high and low frequency components.

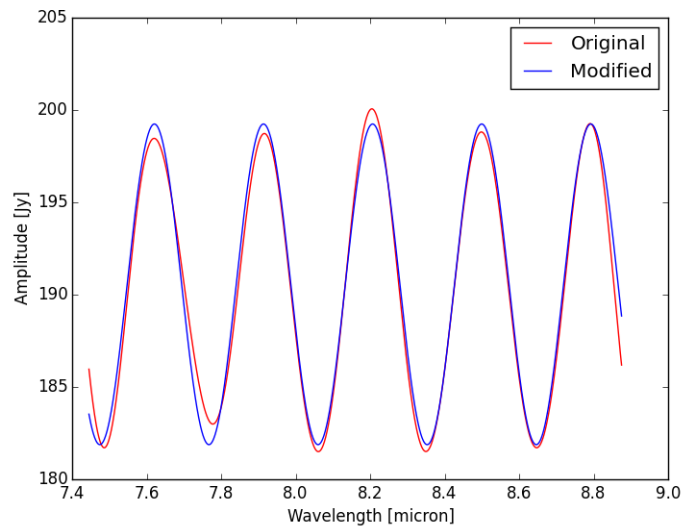


Figure 4.60: Case (3) Approach I: Sine wave fitting method - Sine Fit for the low frequency component

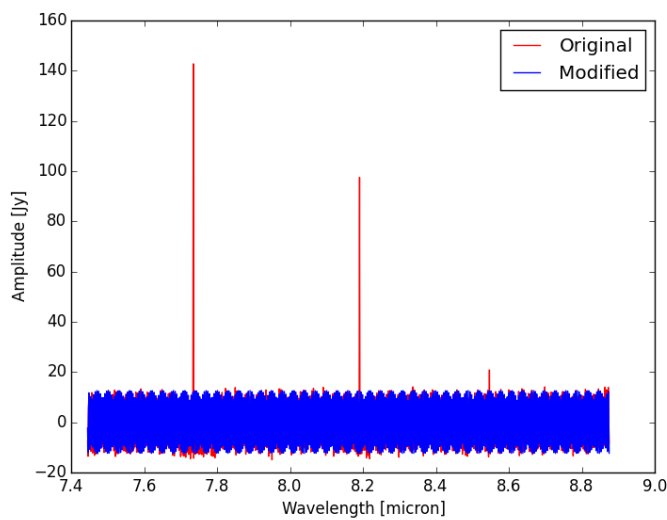


Figure 4.61: Case (3) Approach I: Sine wave fitting method - Sine Fit for the high frequency component

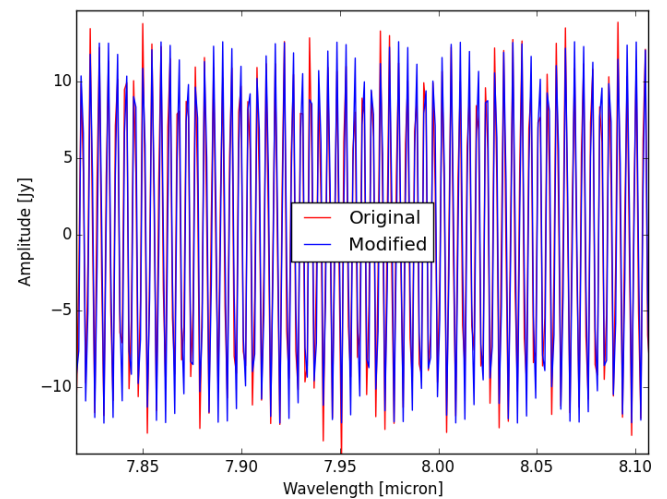


Figure 4.62: Case (3) Approach I: Sine wave fitting method - Sine Fit for the high frequency component Zoom

Adding the residuals together leads to Figure 4.63, which does not show all the weak spectral features. From this graph, it is clear that the method does not clean the noise and the left artifacts do not improve the graphical quality of the spectrum.

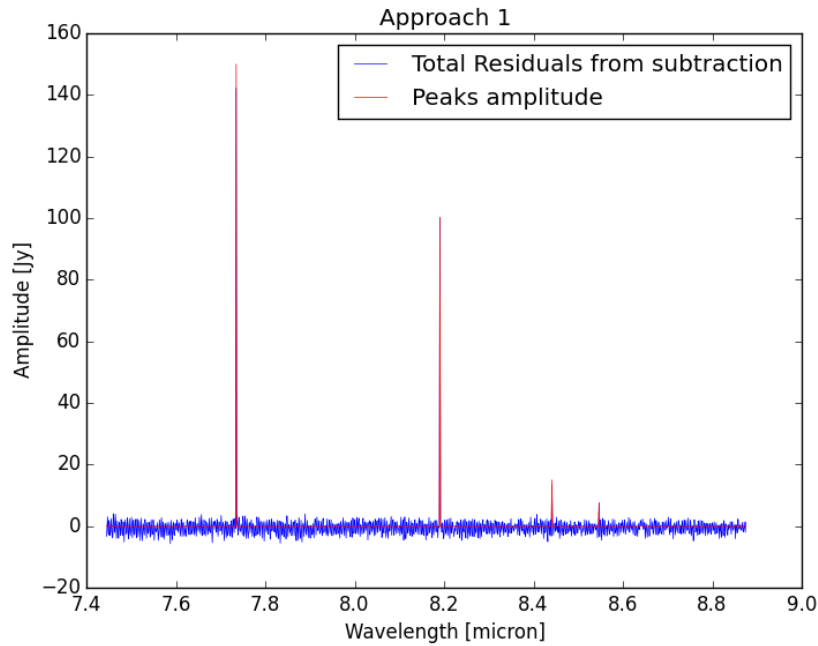


Figure 4.63: Case (3) Approach I: Sine wave fitting method - Total Residuals from the sine fit for the High and low frequency components

When analyzing the exact peaks amplitudes, some conclusions can be drawn. As expected, it appears that the noise has a stronger effect on the weak spectral features than on the strong ones. The lines flux matches for the strong peaks are nearly similar to the observed ones, therefore this approach is not expected to correct the fringe effect on these peaks. However, when looking at the matches with the intrinsic values, the results obtained are excellent, which means that in this Case, these two peaks have initially not been highly amplified by the fringes (in other words, these peaks might have fallen in a spectrum region near the fringes mean) or the artifacts have de-amplified the effect of the fringes.

Concerning the weak spectral features, the opposite holds. Namely, the small match with the observed values would have suggested either an excellent match or a poor one with the intrinsic values. However, the results obtained are "in the average" (i.e. a deviation w.r.t. the expected intrinsic value between 12-23 %). It would therefore not be advised to use this method and this specific residuals approach for studying the signal, especially for the weak spectral features.

X Value	Reduced Value/ X Value[%]			
	Case (3)			
	Peak 1	Peak 2	Peak 3	Peak 4
observed	97.45	101.23	267.24	41.55
Intrinsic	93.99	100.56	88.99	123.92

Table 4.19: Case (3) Approach I: Sine wave fitting method - Match of peaks flux w.r.t. to observed and Intrinsic Fluxes

## APPROACH II

In the second approach, the low frequency component is first studied. Again, some peaks are selected at the beginning and end of the spectrum; and for each part a sine wave has been fitted, as shown in Figure 4.64. The sine wave parameters being defined, the new sine wave for the entire low frequency spectrum can be derived, which can be seen in Figure 4.65, and the residuals deducted from it.

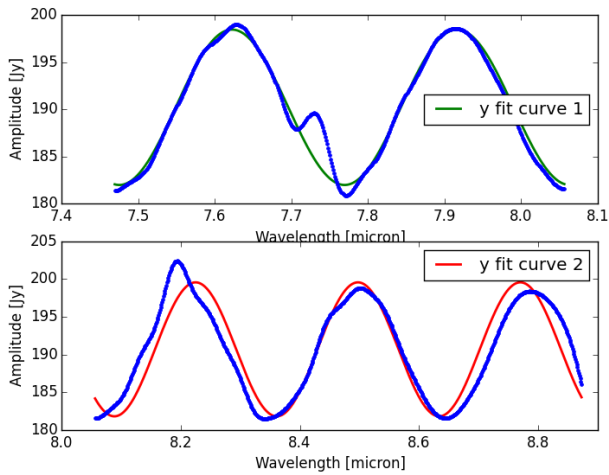


Figure 4.64: Case (3) Approach II: Sine wave fitting method - Sine Fit for the low frequency component. On the top, the sine fit is for the beginning of the spectrum while on the bottom, the sine fit is for the end of the spectrum

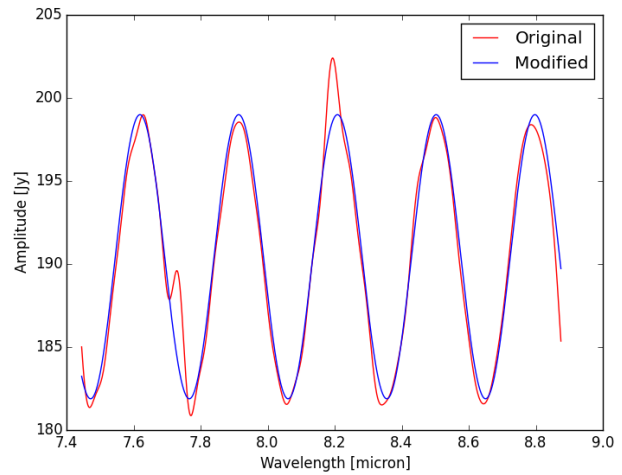


Figure 4.65: Case (3) Approach II: Sine wave fitting method - Sine Fit for the low frequency component

The results for the low frequency component are similar to ones found in Approach I. The residuals being determined, these are added to the high frequency component extracted from the signal by the Fourier filtering method. The same steps are then applied to this new data set of the high frequency component (cf. Figures 4.66-4.67). And Table 4.20 summarizes all the sine parameters used in this simulation. The addition of the low frequency residuals on the sine fitting to the high frequency component does not highly influence the data. Indeed, it did not affect the frequency parameter, but improved the amplitude; indeed, the new parameter value estimated (i.e.  $A = 12.15$ ) is closer to the expected one ( $A = 12.00$ ).

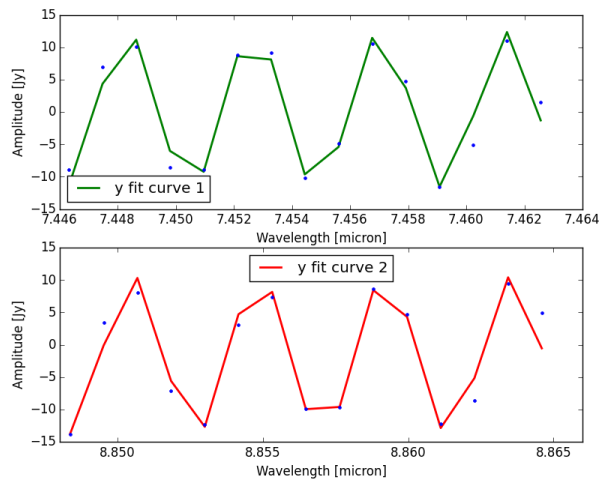


Figure 4.66: Case (3) Approach II: Sine wave fitting method - Sine Fit for the High frequency component. On the top, the sine fit is for the beginning of the spectrum while on the bottom, the sine fit is for the end of the spectrum

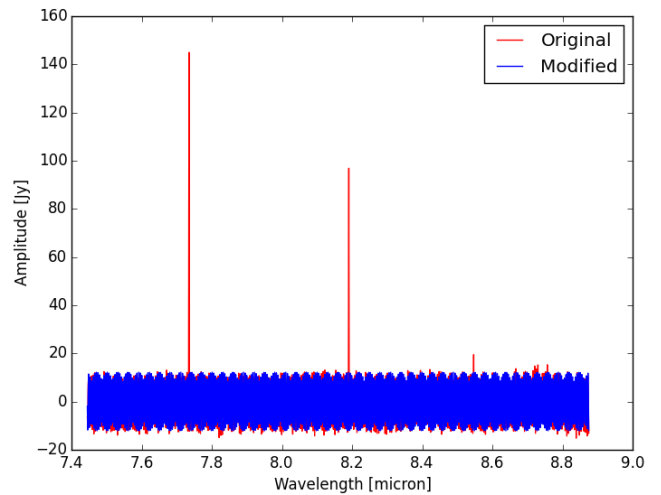


Figure 4.67: Case (3) Approach II: Sine wave fitting method - Sine Fit for the high frequency component

Component	Parameter	Beginning Spectrum	End Spectrum	Sine Fit	Expected value
Low Frequency	A	8.23	8.87	8.55	8.5
	B	21.37	23.05	21.33	21.5
	D	8.3	13.0	-10.15	7.34
	C	190.21	190.69	190.44	150.1
High Frequency	A	12.06	12.24	12.15	12
	B	1444.82	1444.82	1407.04	1407
	D	15.7	0.4	-4.55	2.34
	C	0.31	-1.60	0.06	40

Table 4.20: Case (3) Approach II: Sine wave fitting method - Parameters of the sine Equation (4.7), estimated for the beginning, end of the spectrum and for entire spectrum

The new residuals of the modified high frequency data can be seen in Figure 4.68. The results are quite similar to the ones found in approach I, indeed the graph has the same overall shape and the second weak spectral feature is not distinguishable. Furthermore, the noise is clearly present in the spectrum. Nevertheless, when comparing the spectrum with the one of approach I, it can be noticed that the width of the continuum is less large than the one of approach I. The artifacts are therefore more visible in this approach making it more difficult to detect the weak spectral features.

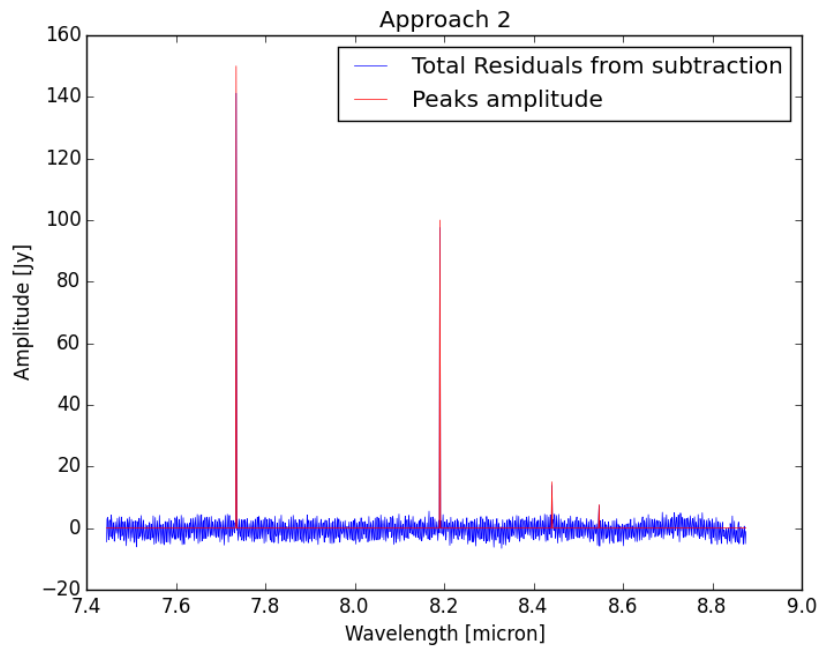


Figure 4.68: Case (3) Approach II: Sine wave fitting method - Residuals from the sine fit for the high frequency component, i.e. total residuals of the spectrum

Let's look at the peaks amplitude for studying quantitatively this approach. The results displayed in Table 4.21 show the same conclusion than in approach I; the strong match with the observed and intrinsic values for the strong spectral features and the strong match with the weak spectral features only with the intrinsic values. It is clear that this approach is beneficial for the determination of the weak spectral lines. Furthermore, it provides in general better estimates of the intrinsic values than with Approach I, contrary to their graphical comparison. However, this method will not be advised for an accurate study due to the poor visibility of the weak spectral features and the difference of line flux match for the weak spectral features which is still non negligible (i.e. 11 %).

X Value	Reduced Value/ X Value[%]			
	Peak 1	Peak 2	Peak 3	Peak 4
observed	97.25	100.78	214.06	39.73
Intrinsic	94.09	98.28	97.41	111.42

Table 4.21: Case (3) Approach II: Sine wave fitting method - Match of peaks flux w.r.t. to observed and Intrinsic Fluxes

APPROACH III

The first step of the third approach consists of studying the high frequency component extracted from the Fourier filtering method, as shown in Figures 4.69 and 4.70. In these figures, the fit for the beginning and end of the extracted high frequency spectrum and the fit for the entire extract frequency spectrum are shown, respectively.

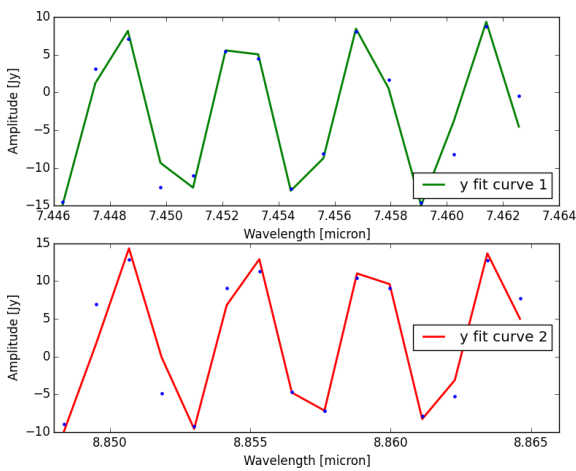


Figure 4.69: Case (3) Approach III: Sine wave fitting method - Sine Fit for the High frequency component. On the top, the sine fit is for the beginning of the spectrum while on the bottom, the sine fit is for the end of the spectrum

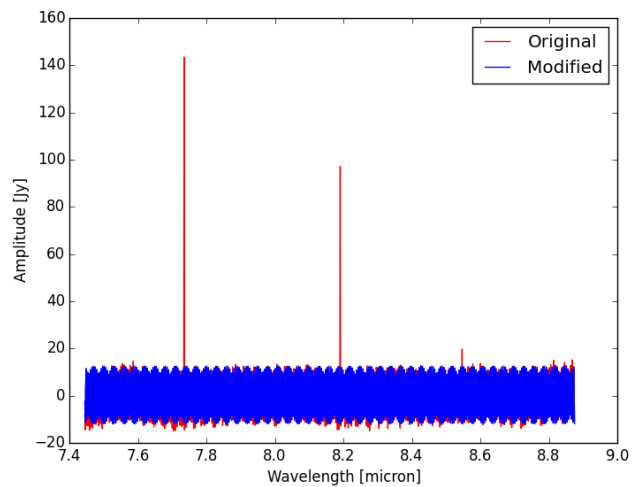


Figure 4.70: Case (3) Approach III: Sine wave fitting method - Sine Fit for the high frequency component

Once the residuals have been determined, these can be added to the extracted low frequency spectrum and the same analysis as usual can be carried out, namely, fitting the beginning & end of spectrum (Figure 4.71) and then fitting the entire spectrum (Figure 4.72).

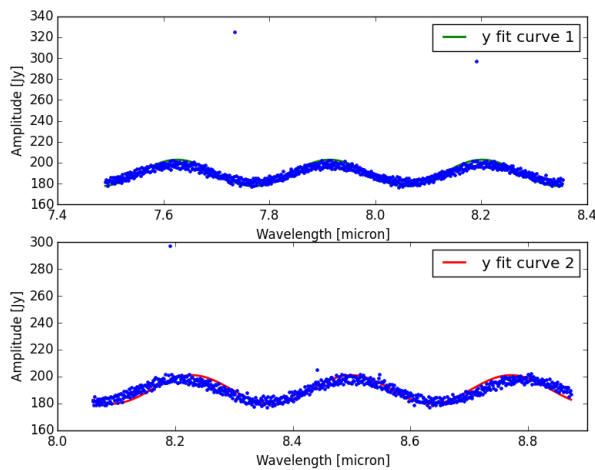


Figure 4.71: Case (3) Approach III: Sine wave fitting method - Sine Fit for the low frequency component. On the top, the sine fit is for the beginning of the spectrum while on the bottom, the sine fit is for the end of the spectrum

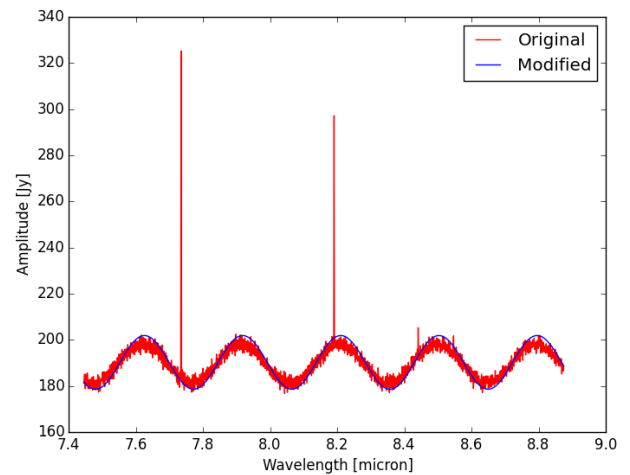


Figure 4.72: Case (3) Approach III: Sine wave fitting method - Sine Fit for the low frequency component

In Table 4.22, the final sine wave parameters for each of the frequency components have been summarized. As for the two previous approaches, the amplitude and frequency parameters are nearly similar to the expected ones, although the vertical and horizontal shift parameters (i.e. C and D) are different, their estimated values provide small graphical shifts compared to the initial ones.

Component	Parameter	Beginning Spectrum	End Spectrum	Sine Fit	Expected value
Low Frequency	A	12.63	10.63	11.63	12
	B	21.81	23.15	21.49	21.5
	D	17.4	18.4	-17.8	7.34
	C	190.19	190.36	190.22	150.1
High Frequency	A	12.26	12.22	12.24	12.00
	B	1444.82	1444.82	1407.03	1407
	D	15.7	19.1	-10.7	2.34
	C	-2.9	2.15	0.32	40

Table 4.22: Case (3) Approach III: Sine wave fitting method - Parameters of the sine Equation (4.7), estimated for the beginning, end of the spectrum and for entire spectrum

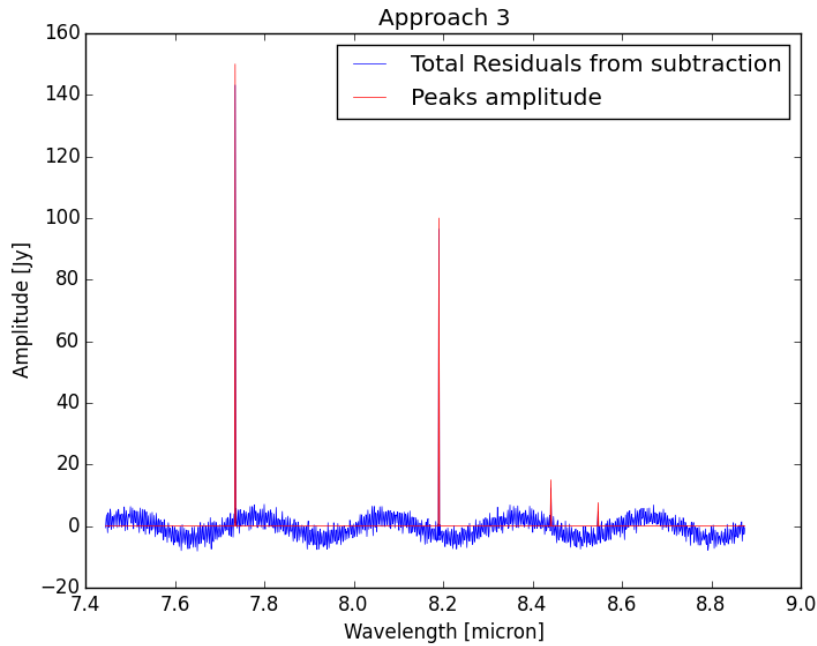


Figure 4.73: Case (3) Approach III: Sine wave fitting method - Residuals from the sine fit for the low frequency component, i.e. total residuals of the spectrum

The total residuals which are the ones calculated from the new low frequency data set are shown in Figure 4.73. Graphically, the overall shape of this approach is not similar to the total residuals graphs from the previous approaches. Indeed, it seems that a low frequency component is still present in the data. This in combination with the remaining noise makes it impossible to detect the small spectral features. From all approaches of this Case, this one leads to the worst graphical representation. This approach is thus expected to provide the worst results. Indeed, the results from Table 4.23 emphasizes this conclusion, as the results from this Approach are not the best, especially for the weak spectral features (deviation between 19-21 %)

For this case, one might conclude that this method does not allow to clearly point all the spectral features and is not optimal for determining their amplitudes.

X Value	Reduced Value/ X Value[%]			
	Case (3)			
	Peak 1	Peak 2	Peak 3	Peak 4
observed	97.72	101.45	334.11	32.24
Intrinsic	94.99	100.14	79.31	81.24

Table 4.23: Case (3) Approach III: Sine wave fitting method - Match of peaks flux w.r.t. to observed and Intrinsic Fluxes

#### 4.3.5. Conclusion

Sine wave fitting is the second fringe correction method studied in this report. For this method, three ways of defining the final residuals have been investigated. Throughout the different cases studied, it was clear that this method cleans considerably the spectrum and allows to identify most of the spectral features.

Let's summarize the peaks amplitude comparison for all the cases in Table 4.24, graphically represented by Figure 4.74.

#	SNR [-]											
	Case (1)				Case (2)				Case (3)			
Approach	Peak 1	Peak 2	Peak 3	Peak 4	Peak 1	Peak 2	Peak 3	Peak 4	Peak 1	Peak 2	Peak 3	Peak 4
I	107.37	92.80	117.44	84.46	116.38	95.15	92.49	93.88	93.99	100.56	88.99	123.92
II	107.47	92.57	113.67	93.36	116.29	95.25	93.23	93.34	94.09	98.28	97.41	111.42
III	107.37	92.80	117.43	84.40	116.38	95.16	92.49	93.80	94.99	100.14	79.31	81.24

Table 4.24: All cases: Match of peaks flux w.r.t. to Intrinsic Fluxes from Sine wave fitting method- The best matches are shown in blue

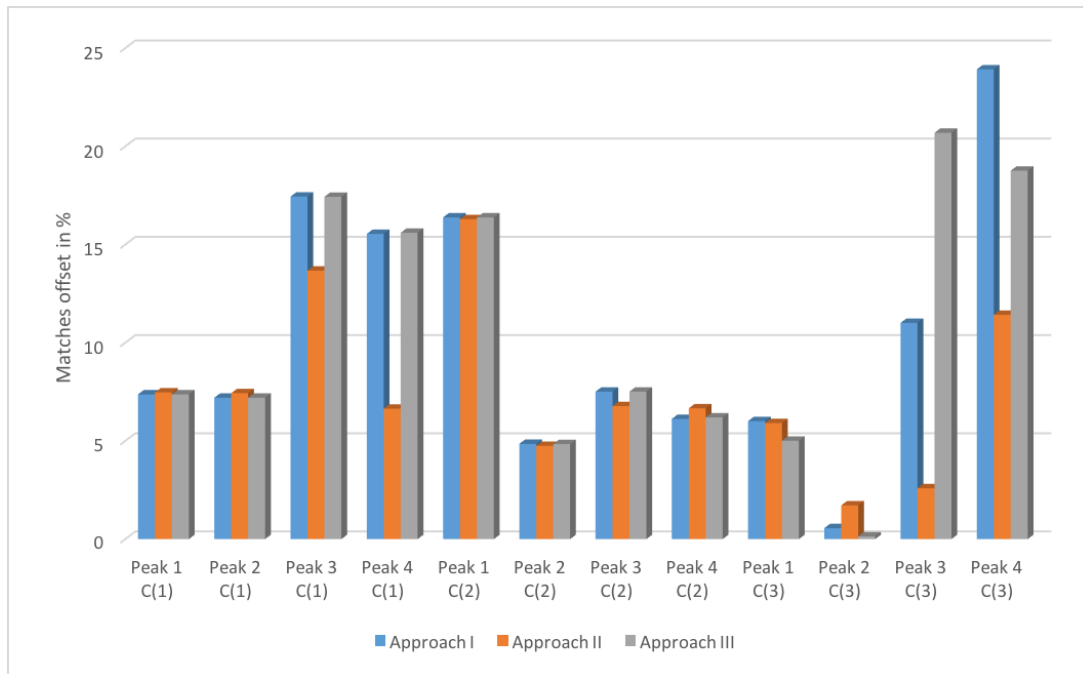


Figure 4.74: All cases: Sine wave fitting method - Match of peaks flux of Region 1 and observed ones w.r.t. to Intrinsic Fluxes - Graphical Representation

For all cases, none of the approaches strongly differentiates itself. It is interesting to see that the outcome from the different approaches are quite similar for Approach I and II. Moreover, in general Approach II provides better lines flux results for the weak spectral features while the other two Approaches are more optimal for the strong features. However, the difference in line flux match between Approach II and the other two is in the order of maximum 2 %, while the difference for the weak spectral feature is of maximum 17 %. Therefore, from a lines flux analysis, Approach II seems the most reliable one out of the three.

Concerning Cases (1) and (2), it is important to underline that although none of the approaches are optimal for all the peaks, they all provide good estimates of the spectral features at the same level of accuracy which was achieved with only the Fourier Filtering method (cf. Subsection 4.2.3). Although the best Approach for dealing with the residuals provides acceptable results, their level of accuracy is still too low for considering this method as reliable, indeed the deviation from the intrinsic values can reach up to 16 %. When analyzing each case, not only the peak amplitude was considered but also the aesthetics of the cleaned spectrum, as before determining the amplitude of the spectral features, it is important to identify them in the signal. For both cases, the final spectrum seemed at first sight cleaned from major fringe components and the spectral features were easily detected. It was shown that the overall shape of the graphs from Approach I and II were similar, while the one from Approach III shows some left low frequency component in the data and provides the lowest SNR in average. However, it was seen especially in Case (2) that the residuals of Approach II seemed more important than the one of Approach I due to the larger width of the spectrum, which made harder the distinction of the weak spectral features. Graphically speaking, Approach II provided the flatter continuum for these 2 Cases. Indeed, from Table 4.25, it is clear that the best SNR are obtained more often

by this Approach, which means that the spectral features are more easily distinguished from the continuum than by using the other Approaches.

The outcome from Case (3) is quite different from the ones of Case (1) and (2). This is due to the noise component added to the spectrum. This method is tailored for ideal fringes components added to the original signal, but this Case represents most of the real situations. It was interesting to see how this method if developed would deal with this noise component case. All the results showed a similar pattern as for the previous Cases, namely the matches are acceptable for some peaks, but for other peaks, deviations from the intrinsic values are non negligible. Furthermore, Approach II gives the best overall results. Contrarily to the previous Cases, all the strong spectral features have a strong match (high photometric accuracy); this might be due to the larger effect of the noise on the small spectral features. Concerning the graphical analysis, the same conclusion as for Cases (1) and (2) holds, namely the left frequency residuals in the Approach III graph excludes its reliability. And the graphical quality of Approach I and II are similar for the weak spectral features, but Approach II is better for the strong spectral signatures. This is pointed out by the SNR from Table 4.25, in which it is clear that these two Approaches allow in overall better spectral features detectability for Case (3) and Approach II differentiates itself from Approach I by its better detectability of the strong features.

#	SNR [-]											
	Case (1)				Case (2)				Case (3)			
Approach	Peak 1	Peak 2	Peak 3	Peak 4	Peak 1	Peak 2	Peak 3	Peak 4	Peak 1	Peak 2	Peak 3	Peak 4
App.I	51.77	31.38	5.85	2.94	113.06	65.06	10.53	3.88	56.03	30.41	4.20	2.09
App. II	111.17	34.7	6.36	2.44	84.55	13.71	1.44	2.16	110.76	31.29	5.74	2.60
App. III	23.99	16.34	2.38	2.26	24.66	17.35	2.82	1.79	60.04	56.11	1.22	0.79

Table 4.25: All cases and all Approaches: Signal to Noise Ratio for Sine Wave fitting - In red: poor detection, In black: acceptable detection, In blue: excellent detection

The last step of this conclusion is to determine whether applying the sine wave fitting method improve the data quality or not. For this, the best Approach outcome has been compared to the match of the observed data w.r.t. the intrinsic ones, in Table 4.26 and Figure 4.75. The conclusion is quite obvious. It is clear that applying this method improves the lines flux approximation and therefore corrects for the fringes effect. However, the reader might notice that this method does not improve all the spectral features and for some Cases, it actually worsen them (up to 5 %). Furthermore, the improvement is not optimal as it is in general in the range of 2-4 %.

#	Observed or Reduced Value/ Intrinsic Value[%]											
	Case (1)				Case (2)				Case (3)			
	Peak 1	Peak 2	Peak 3	Peak 4	Peak 1	Peak 2	Peak 3	Peak 4	Peak 1	Peak 2	Peak 3	Peak 4
App. II	107.47	92.57	113.67	93.36	116.29	95.25	93.23	93.34	94.09	98.28	97.41	111.42
observed	110.9	97.9	140.3	93.04	118.21	94.93	90.24	80.38	96.41	95.28	105.86	164.95

Table 4.26: All cases: Sine wave fitting method - Match of peaks flux of Approach II and observed ones w.r.t. to Intrinsic Fluxes - Best matches are shown in blue

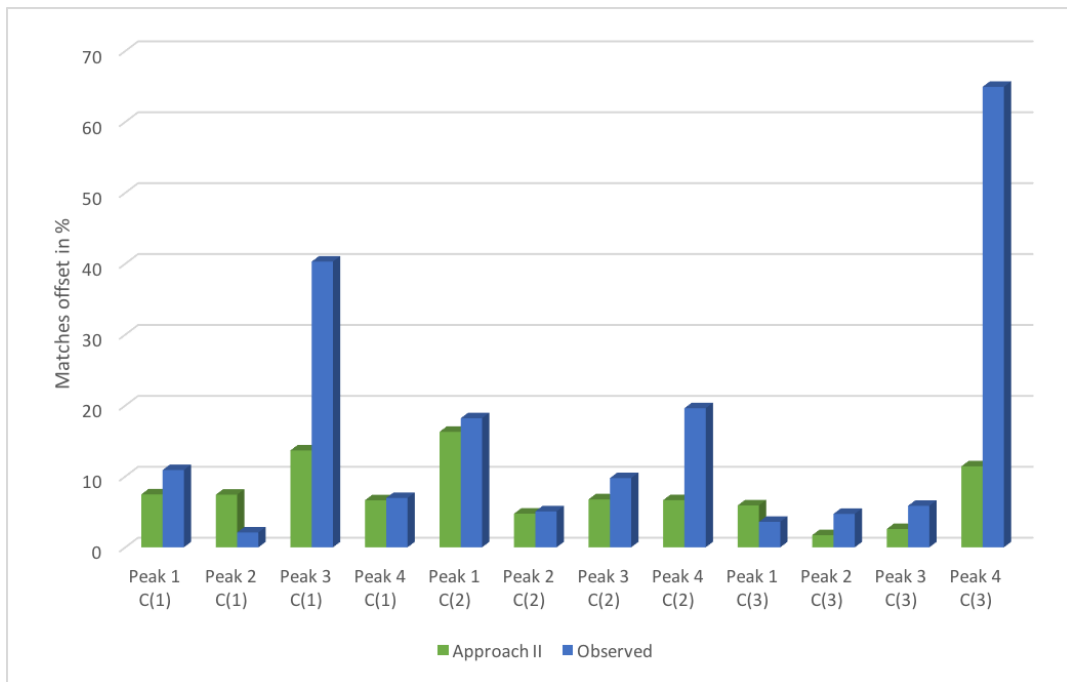


Figure 4.75: All cases: Sine wave fitting method - Match of peaks flux of Approach II and observed ones w.r.t. to Intrinsic Fluxes - Graphical Representation

In conclusion, this method has not proved to be reliable in all cases, but provides in general better results than with the Fourier Filtering method only. It also gives cleaned spectra which are aesthetically acceptable, but the subtraction of the sine wave fringes deducted also important spectral information which explains some disparities in the peaks amplitude comparison. This method is thus acceptable for providing a general picture of the signal signatures mostly for strong spectral features, but is not recommended as optimal for a deep study of the signal.

#### 4.4. Method 3 : Multiplicative method

The Multiplicative method is the third method to be investigated for removing the artifacts from the spectrum and is often used in combination with the sine wave fitting for correcting the fringes.

This method corrects the pixel to pixel variations by defining the value which will divide the initial flux value for correcting the undesired artifacts.

##### 4.4.1. Theoretical Background

This method is model independent therefore, its application is more straight-forward than the previous methods studied, as no prerequisites are needed.

For applying this method, the user will need not only the data set to analyze but also a data set of a spectrally flat source (i.e. a constant uniform illumination).

The observed spectrum of this flat source will ideally provide the fringes components. The first step of this method consists of taking the inverse of this observed spectrum and then dividing the initial observed spectrum (i.e. including the spectral features) by this inverse spectrum (cf. Equation (4.10)). This division will provide the amplification factors, which are the factors by which the values have been modified due to the fringes. The amplification factors describe therefore how much the signal has been amplified or de-amplified at each wavelength.

$$A_i = \frac{F_{obs_i}}{F_{fringe_i}} \quad (4.10)$$

in which,

$F_{fringe_i}$  is the intensity of the spectrally flat source at wavelength  $i$   
 $F_{obs_i}$  is the observed flux intensity at wavelength  $i$   
 $A_i$  is the amplification factor at wavelength  $i$

Now that the amplification factors have been determined, the amplification could be determined by subtracting 1 from the amplification factors. Indeed, if the observed spectrum at wavelength  $Y$  is 1.2 times the fringe spectrum at wavelength  $Y$ , then the amplification is of 20 % so  $(1.2 - 1 = 0.2)$ . The last step of this method is to correct the spectrum by correcting the flux of each wavelength of the entire spectrum, as shown in Equation (4.11).

$$F_c = F_{obs_i} \cdot \left(1 - \frac{1}{A_i}\right) \quad (4.11)$$

in which,

$F_c$  is the corrected line flux

#### 4.4.2. Case (1)

For determining the spectrally flat source of Case (1), the original spectrum without the spectral features (i.e. four peaks) has been considered, which thus consists only of the fringes components. This spectrum and its inverse can be seen in Figure 4.76.

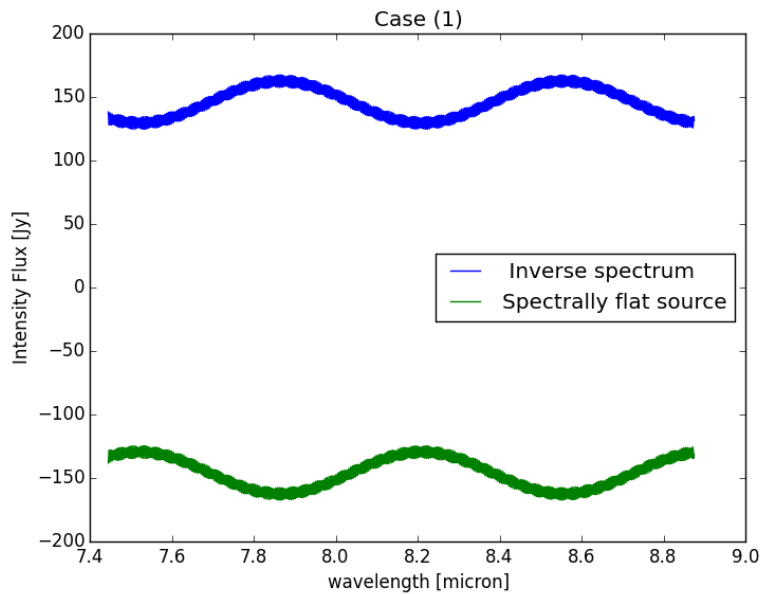


Figure 4.76: Case (1): multiplicative method - Spectrally flat source spectrum and its inverse

The inverse of the spectrally flat source being determined, the amplification factors were calculated using Equation (4.10). From Figure 4.77, it is clear that this method allows to remove the fringe artifacts as its amplification factors spectrum has a similar shape than the expected one. Figure 4.78 displays the final spectrum from the multiplicative method (i.e. with the corrected line fluxes). It has the same graphical pattern than the amplification factor spectrum; therefore it can be said that graphically this method is optimal. Indeed, when comparing the observed spectrum with

the multiplicative method one, the fringes components are removed and the spectral features are clearly distinguishable and at their expected locations.

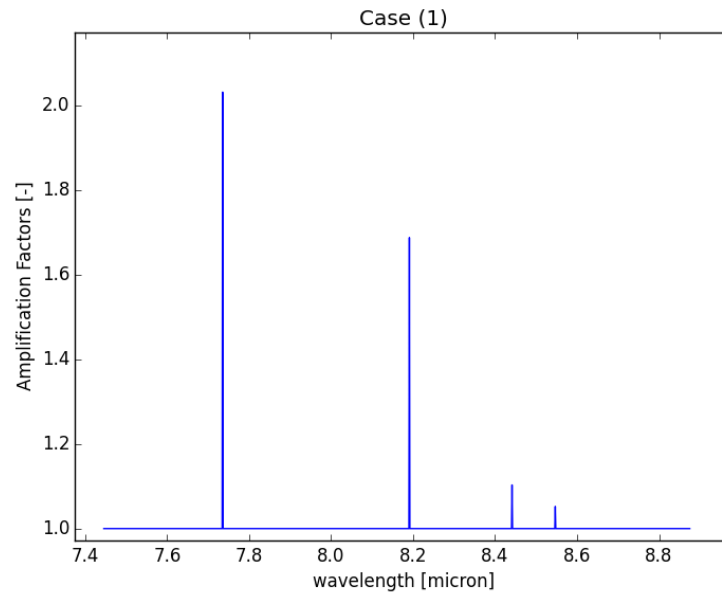


Figure 4.77: Case (1): multiplicative method - Amplification Factors

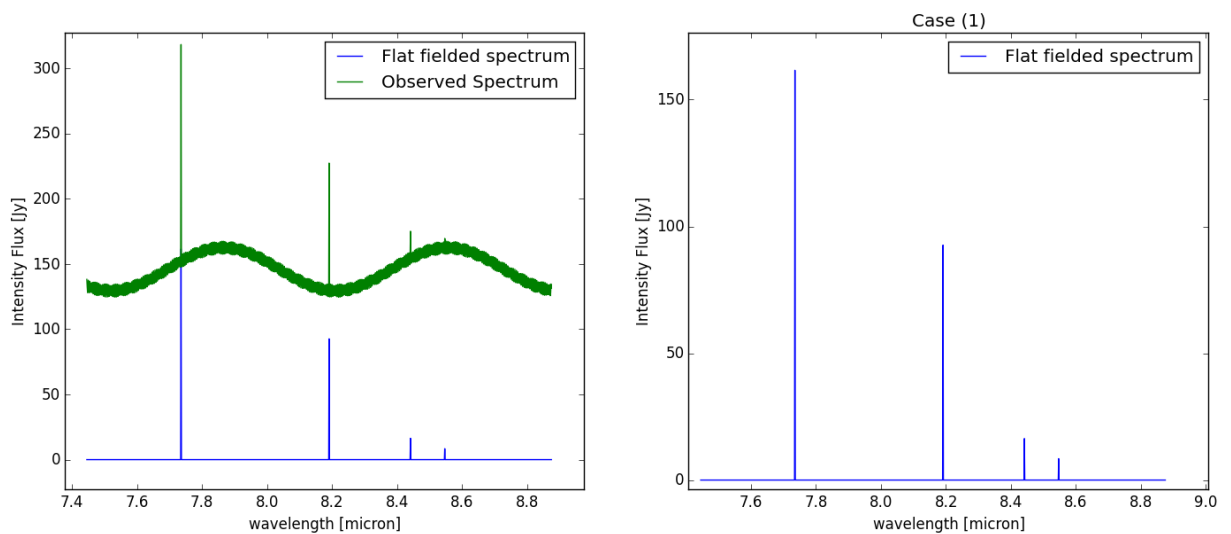


Figure 4.78: Case (1): multiplicative method - on the left: spectrum from the multiplicative method compared to the original spectral features spectrum. On the right: spectrum from the multiplicative method

Graphically this method allows to achieve the best results compared to the methods developed earlier, but one might wonder how accurately the line fluxes have been corrected. Therefore, the line fluxes of the spectrum from the multiplicative method at the four peaks locations have been studied with respect to the observed spectrum and the intrinsic values.

Case (1)				
Mult. method or Obs. Value/ observed of Intrinsic Value [%]	Value/ observed of Intrinsic Value [%]			
	Peak 1	Peak 2	Peak 3	Peak 4
Mult. / Obs	97.12	94.60	77.74	119.05
Mult. / Intri	107.70	92.61	109.10	110.77
Obs / Intri	110.89	97.89	140.33	93.044

Table 4.27: Case (1): multiplicative method - Match of line flux of (1) the observed spectrum w.r.t. the intrinsic spectrum and of the spectrum from the multiplicative method w.r.t. (2) the observed one and (3) the intrinsic spectrum.

From Table 4.27, several conclusions can be drawn. First, the matching values with the observed spectrum are not perfect, which means that this method affects the line fluxes and thus modifies the fringe effect on them. The reader might notice that the poor match w.r.t. the observed values are seen mostly for the weak spectral features, which can be translated by a strongest effect of this method on weak spectral features.

The comparison with the intrinsic values shows a positive effect on the data. Indeed, when compared with the observed value w.r.t. the intrinsic ones, applying this method allows a smaller standard deviation of the matches. In other words, in general the Multiplicative method value varies less to the intrinsic values than the observed ones as the variation comprises between 7 and 10 %, while for the observed spectrum it is between 3 and 40 %. This method will therefore be reliable for cleaning the spectrum and it provides good estimates of the lines flux, but it will not be advised for an accurate study of the line fluxes as the variations are still non negligible and in some cases (e.g. Peaks 2 and 4), it introduces artifacts which worsen the results.

#### 4.4.3. Case (2)

As realized for Case (1), the original spectrum of this Case without the spectral features has been considered as the spectrally flat source and its inverse has been taken as shown in Figure 4.79.

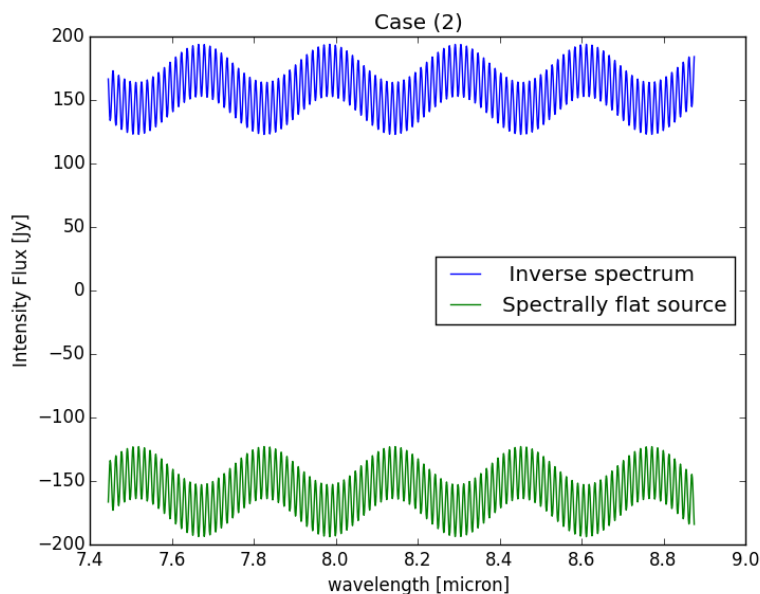


Figure 4.79: Case (2): multiplicative method - Spectrally flat source spectrum and its inverse

The second step consists of determining the amplification factors using Equation (4.10). For this case also, the overall shape of the spectrum is similar to the expected one as can be seen in Figure 4.81. Furthermore, it is interesting to notice that the amplification factors are in a similar range than for Case (1), namely between 1.95 and 1.05 [-] (cf. Figure 4.80). This similar range can be explained by the fringes amplitude which does not vary more than [-

20%;20%], as explained in Section 4.1. Consequently, in a real application, the amplification factors are expected to be in the same range for an ideal case, namely when only fringes are the artifacts of the signal.

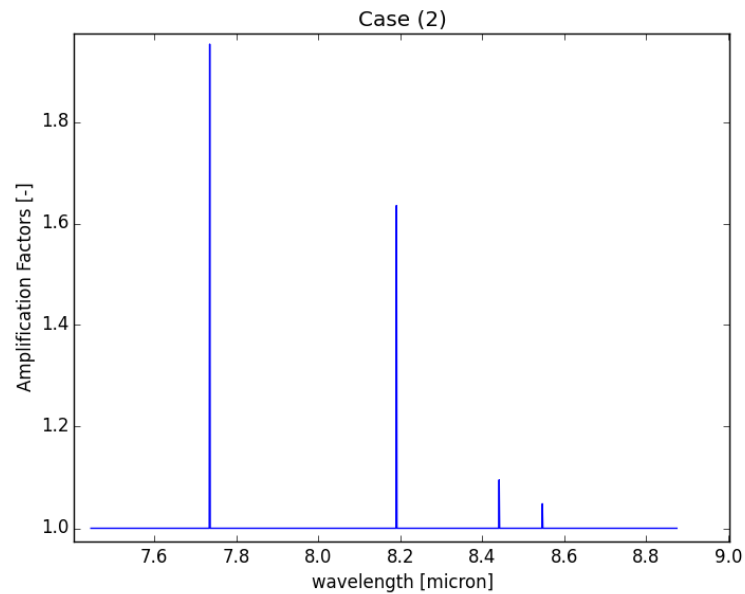


Figure 4.80: Case (2): multiplicative method - Amplification Factors

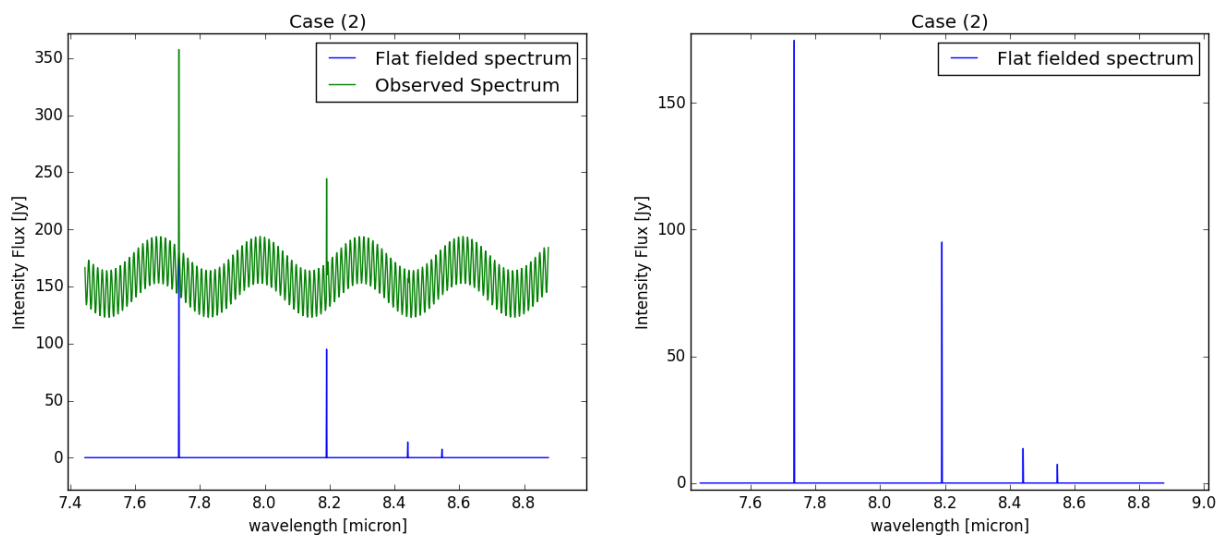


Figure 4.81: Case (2): multiplicative method - on the left: spectrum from the multiplicative method compared to the original spectral features spectrum. On the right: spectrum from the multiplicative method

Graphically this method provides an extremely clean spectrum similar to the expected one, in which the spectral features are easily distinguishable. Let's have a look at the line fluxes in order to quantify the impact of this method on the signal characteristics. As previously, the line fluxes of the spectrum from the multiplicative method at the four peaks locations have been studied with respect to the observed spectrum and the intrinsic values.

Case (2)				
Mult. method or Obs. Value/ observed of Intrinsic Value [%]	Peak 1	Peak 2	Peak 3	Peak 4
	Mult. / Obs	98.45	100.10	100.75
Mult. / Intri	116.38	95.03	90.92	97.27
Obs / Intri	118.21	94.93	90.24	80.38

Table 4.28: Case (2): multiplicative method - Match of line flux of (1) the observed spectrum w.r.t. the intrinsic spectrum and of the spectrum from the multiplicative method w.r.t. (2) the observed one and (3) the intrinsic spectrum.

When analyzing the results of Table 4.28, a different outcome than from the previous case appears. Indeed, previously, the correspondence with the observed values was not optimal, especially for the weak spectral features. However, for this Case, the match with the observed spectrum is strong for three spectral features out of four, which means that this method did not correct the fringe effect.

The match with the observed values being high, a strong improvement of the value from the multiplicative method compared to the intrinsic one is not expected. Indeed, although all the lines flux have been improved and are thus more similar to the intrinsic ones, this improvement is meager (i.e. at most 2 % improvement compared to the observed values w.r.t. intrinsic ones). The only peak which has been considerably improved, is the weakest spectral feature (i.e. Peak 4), which has a deviation of the expected value of 2.8%. To conclude, this method provides a clean spectrum which allows the user to directly determine the signal signatures, but it does not improve considerably the lines flux especially for the strong spectral features; therefore the user will not learn more about their amplitude than when using the observed spectrum.

#### 4.4.4. Case (3)

The Case (3) is slightly different from the previous two as it includes also noise. For its spectrally flat source, the noise has also been present, as when the instrument will observe a flat source (i.e. constant intensity source), the noise will also be included in the observed spectrum. As has been realized previously, the inverse of this spectrally flat source spectrum has been considered (cf. Figure 4.79).

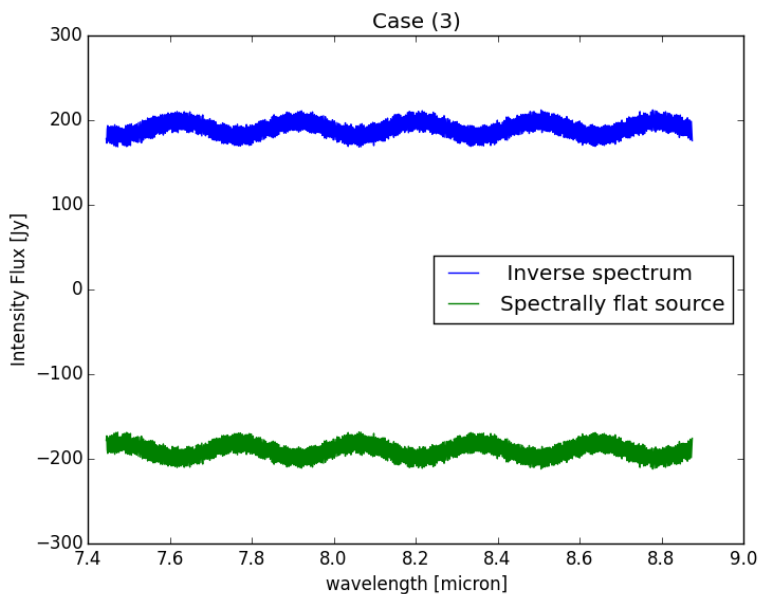


Figure 4.82: Case (3): multiplicative method - Spectrally flat source spectrum and its inverse

The inverse of the spectrally flat source being determined, the amplification factors can be calculated, as can be seen

in Figure 4.83. The overall shape of this spectrum is less similar to the previous one, as the effect of the extra noise can clearly be distinguished. In Figure 4.84, the real amplitude graph can be seen. As expected from the amplification factors, the spectrum shows still some residuals, but is cleaner than the observed one. The spectral features can still be positioned correctly. However, it is important to notice that the weakest spectral feature is less graphically dominant than it was seen in the two previous Cases. Therefore, if the noise was more important (amplitude-wise), it is expected to absorb graphically the weak spectral features, and the graph from the multiplicative method will not be as optimal as currently.

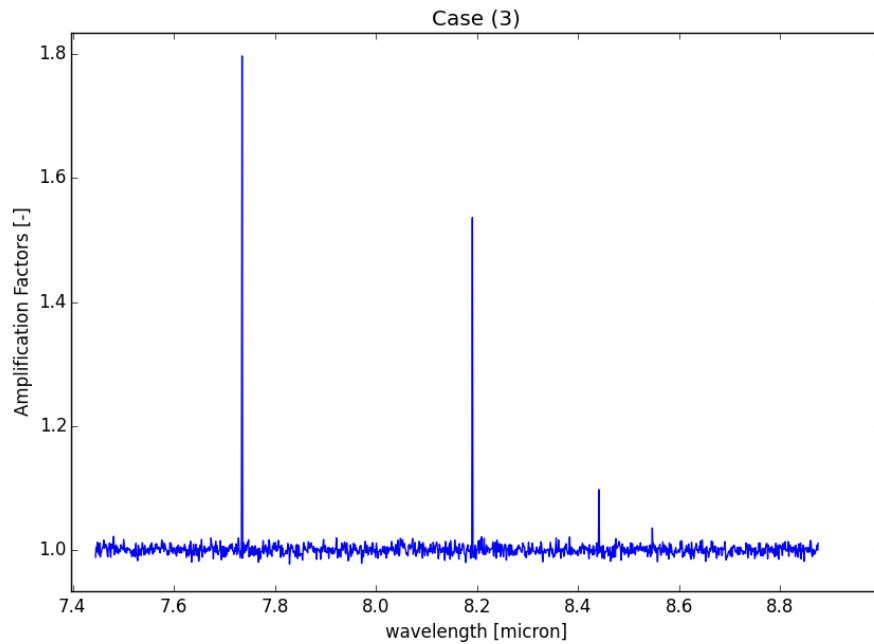


Figure 4.83: Case (3): multiplicative method - Amplification Factors

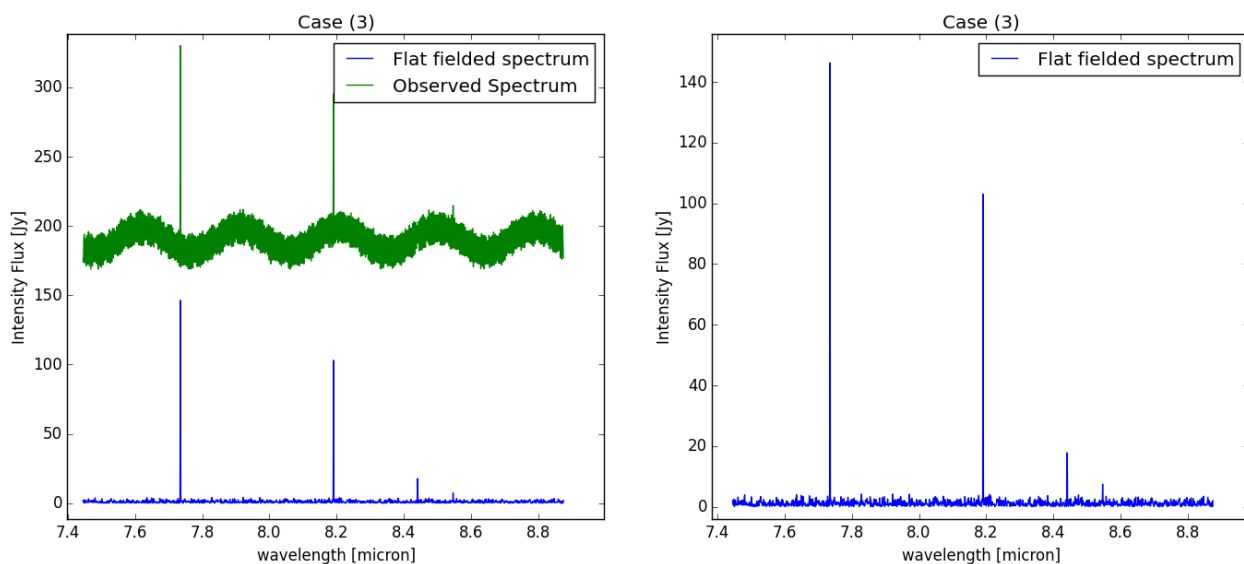


Figure 4.84: Case (3): multiplicative method - on the left: spectrum from the multiplicative method compared to the original spectral features spectrum. On the right: spectrum from the multiplicative method

Graphically, this method has shown a lower quality level for a more realistic spectrum, but still allows to clean considerably the spectrum from the fringe components. The next step would be to analyze the spectral lines flux to

quantify this method accuracy.

Case (3)				
	Mult. method or Obs. Value/ observed of Intrinsic Value [%]			
	Peak 1	Peak 2	Peak 3	Peak 4
Mult. / Obs	98.16	104.52	123.21	41.11
Mult. / Intri	96.75	101.34	109.06	81.07
Obs / Intri	98.56	96.95	88.51	197.17

Table 4.29: Case (3): multiplicative method - Match of line flux of (1) the observed spectrum w.r.t. the intrinsic spectrum and of the spectrum from the multiplicative method w.r.t. (2) the observed one and (3) the intrinsic spectrum.

Table 4.29 summarizes all the lines flux comparison. The match with the observed values is not perfect, which means that this method has not only provided a cleaner graph, but has also modified the lines flux. This is particularly visible with the Peak 4.

The comparison with the intrinsic values is quite interesting as this method has in general improved the values, although there is noise effect in the data. It actually gives a better match than for Case (2). This method improves considerably the accuracy from 3 up to 78 % compared to the observed values, except for the strong spectral feature with reduces its accuracy of 2%. However, the deviation with respect to the expected intrinsic values are still non negligible, with a deviation from 1 up to 19 %. One might conclude for this Case that this method cleans the graph, but if the noise has a larger amplitude, some weak spectral features might be missed by the user. Moreover, it also considerably improves the lines flux in general, but is not optimal and an accurate study of the signal will not be possible with this method.

#### 4.4.5. Conclusion

All the Cases have been tested with the multiplicative method and individual conclusions have been drawn for each. The purpose of this Subsection is to summarize all of the Cases conclusion in order to quantify generally this method and define whether or not, it is preferable to use it or to work with the observed spectrum only. All the spectral features match have been summarizes in Table 4.30, in which the best match for each peak of each case has been underlined in blue. Furthermore, a graphical representation of the data listed in Table 4.30 is given by Figure 4.85.

#	Multiplicative method or observed Value/ observed of Intrinsic Value [%]											
	Case (1)				Case (2)				Case (3)			
	Peak 1	Peak 2	Peak 3	Peak 4	Peak 1	Peak 2	Peak 3	Peak 4	Peak 1	Peak 2	Peak 3	Peak 4
Mult. / Obs	97.12	94.60	77.74	119.05	98.45	100.10	100.75	121.0	198.16	104.52	123.21	41.11
Mult. / Intri	<u>107.70</u>	92.61	<u>109.10</u>	110.77	<u>116.38</u>	<u>95.03</u>	<u>90.92</u>	<u>97.27</u>	<u>96.75</u>	<u>101.34</u>	109.06	<u>81.07</u>
Obs / Intri	110.89	<u>97.89</u>	140.33	<u>93.04</u>	118.21	94.93	90.24	80.38	96.41	95.28	<u>105.86</u>	164.95

Table 4.30: All Cases: multiplicative method - Match of line flux of (1) the observed spectrum w.r.t. the intrinsic spectrum and of the spectrum from the multiplicative method w.r.t. (2) the observed one and (3) the intrinsic spectrum - The best matches are shown in blue

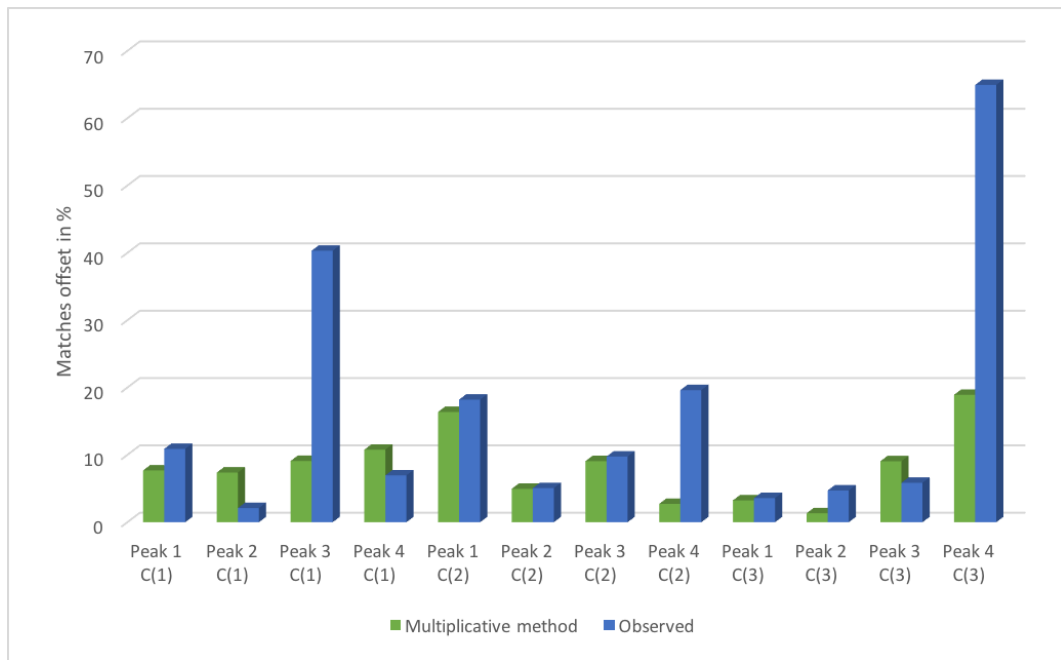


Figure 4.85: All Cases: multiplicative method - Match of line flux of the spectrum from the multiplicative method w.r.t. the observed one and the intrinsic spectrum - Graphical Representation

It was concluded for all Cases that this method considerably improves graphically the spectrum allowing to clearly determine the spectral feature positions. This is illustrated by the SNR of Table 4.31, which provide "infinity" value for Cases (1) and (2), which means that the noise is close to zero contrarily to the signal. However, for the third case, the extra noise has generated some artifacts in the spectrum from the multiplicative method which might absorb the weak spectral features and thus worsen the graphical quality. But, the SNR values found for this Case are still excellent, allowing to clearly point the spectral features from the continuum.

Method	SNR [-]											
	Case (1)				Case (2)				Case (3)			
	Peak 1	Peak 2	Peak 3	Peak 4	Peak 1	Peak 2	Peak 3	Peak 4	Peak 1	Peak 2	Peak 3	Peak 4
Mult.	inf.	inf.	inf.	inf.	inf.	inf.	inf.	inf.	174.17	95.30	11.02	6.10

Table 4.31: All cases : Signal to Noise Ratio for Multiplicative method - In blue: excellent detection, In black: acceptable detection

Concerning the lines flux, in general this method improves them and when it is not the case (cf. second and third lines of Table 4.30), the difference in accuracy is at most 3 %, compared to the observed values. However, even after the multiplicative method, the results are sometimes not optimal; indeed, variations up to 19 % are still depicted. In conclusion, this method can not be entirely reliable as the photometric accuracy is not perfect nor constant (i.e. the lines flux show still important match deviation compared to the expected intrinsic values) although its graphical analysis is reliable (i.e. excellent SNR) This method would be advised for a general study of the signal but, not for an accurate one.

## 4.5. Conclusion: Method's Comparison

Throughout this Chapter, three methods for defringing have been tested. For the first two methods developed, several combinations were considered and conclusions were drawn on the results.

To summarize all the results, comparison will be made on two points namely the locations of the spectral features and the their amplitude match.

LOCATION

The graphical analysis of the spectrum is an important point for selecting a defringing method. Indeed, the fringes affect the spectrum such as it becomes difficult to distinguish the spectral elements directly from the observed spectrum. For determining which method provides the best spectrum a trade-off matrix was realized based on several criteria:

- **CRITERION 1:** Visibility of the weak spectral features
- **CRITERION 2:** Visibility of the strong spectral features
- **CRITERION 3:** Width of the spectrum continuum → the left residuals
- **CRITERION 4:** Presence of a frequency component left
- **CRITERION 5:** Flatness of the continuum

For each Case, the best configuration of each method (i.e. Region 1 and Approach II) was selected for the graphical comparison. The grading is made on a scale of three components:

- **Good** or [G] as **Green**: shows reliable results
- **Mitigated** or [M] as **Yellow**: does not provide the best results but the outcome is acceptable
- **Bad** or [B] as **Red**: does not provide reliable results nor acceptable ones

CASE (1)					
# Method	Criterion				
	1	2	3	4	5
Fourier Filtering	[G]	[G]	[G]	[B]	[B]
Sine Wave Fitting	[G]	[M]	[B]	[M]	[M]
multiplicative method	[G]	[G]	[G]	[G]	[G]

Table 4.32: Location Comparison for all single methods for Case (1)

CASE (2)					
# Method	Criterion				
	1	2	3	4	5
Fourier Filtering	[G]	[M]	[M]	[M]	[B]
Sine Wave Fitting	[G]	[B]	[B]	[B]	[B]
multiplicative method	[G]	[G]	[G]	[G]	[G]

Table 4.33: Location Comparison for all single methods for Case (2)

CASE (3)					
# Method	Criterion				
	1	2	3	4	5
Fourier Filtering	[G]	[M]	[G]	[B]	[B]
Sine Wave Fitting	[G]	[B]	[B]	[G]	[G]
multiplicative method	[G]	[B]	[M]	[G]	[G]

Table 4.34: Location Comparison for all single methods for Case (3)

It can clearly be seen that the Multiplicative method provides the best graphical results for all Cases, while the sine wave fitting provides the less accurate graphical interpretation of the spectrum. Moreover, the multiplicative method scores excellent results for Cases (1) and (2), as these are free of extra noise. While, for the third Case, the distinction of the weak spectral features is non reliable. It would therefore be advised to clean the spectra from all external noise

first (e.g. remaining noise for data pre-processing such as straylight correction, etc.) before applying the defringing process. However, it is important to underline that each method cleans considerably the graphs compared to the observed spectrum, allowing to point out most spectral features.

When analyzing the signal-to-noise ratios, in Table 4.35, the same conclusion from the trade-off matrices is applicable. Indeed, the multiplicative method provides the best detectability of the spectral features for all cases. However, contrary to the qualitative analysis performed above, the sine-wave fitting method provides a better detectability of the spectral features than the Fourier filtering, especially for the weak spectral characteristics, as shown in Table 4.35, in which the assessment criteria is based on the following:

- $2 < S/N < 10$  : acceptable signal quality → Black data
- $S/N \leq 2$  : bad signal quality → Red data
- $S/N \geq 10$  : excellent signal quality → Blue data

This difference in the graphical conclusion from the matrices and SNR for these two methods might be due to the left frequency of Region 1 which de-amplified the visual effect of the fringes on the continuum (that would explain why the weak spectral features detection is considered as medium for the Fourier Filtering and Bad for the Sine-wave fitting).

Therefore, from an aesthetics point of view, applying the methods described above allows to obtain a spectrum more compliant to the real one than the observed one and to improve the detectability of the spectral features. Indeed, whatever the method used, the SNR are in general better than the ones from the observed spectrum. Moreover, it is important to underline that although fringes modify the original data, applying the method to the data might also lead to misleading interpretation of the results. Indeed, in some cases, the weak lines are indistinguishable and for the Fourier method, some artifacts are introduced near the real spectral features.

#	SNR [-]											
	Case (1)				Case (2)				Case (3)			
Method	Peak 1	Peak 2	Peak 3	Peak 4	Peak 1	Peak 2	Peak 3	Peak 4	Peak 1	Peak 2	Peak 3	Peak 4
FF	12.03	9.77	2.13	1.98	7.34	4.90	1.41	1.25	11.07	7.77	1.71	1.30
SW	111.17	34.7	6.36	2.44	84.55	13.71	1.44	2.16	110.76	31.29	5.74	2.60
Mult.	inf.	inf.	inf.	inf.	inf.	inf.	inf.	inf.	174.17	95.30	11.02	6.10
Obs.	20.00	9.01	2.13	1.14	5.25	2.67	0.49	0.49	7.57	5.14	0.53	1.11

Table 4.35: All cases- All methods : Signal to Noise Ratio

## AMPLITUDE

Although, applying the methods allows a better visualization of the spectral features than in the original spectrum, it is also important to quantify the results. Indeed, if the line flux amplitudes are not correct, they will mislead the conclusion on these spectral features. In each method's conclusion, the obtained value for the peaks was compared to the intrinsic ones, and their ratios were compared to the ones from the observed spectra w.r.t. the intrinsic ones. Table 4.36 and corresponding Figure 4.86 summarize the overall best results of each method for each case (i.e. Region 1 for Fourier Filtering method and the Approach II for the sine wave fitting method).

#	Obtained or observed Value/ Intrinsic Value[%]											
	Case (1)				Case (2)				Case (3)			
	Peak 1	Peak 2	Peak 3	Peak 4	Peak 1	Peak 2	Peak 3	Peak 4	Peak 1	Peak 2	Peak 3	Peak 4
FF	102.24	87.93	103.82	105.83	113.37	92.54	88.43	95.05	81.80	84.48	101.16	60.01
SW	107.47	92.57	113.67	93.36	116.29	95.25	93.23	93.34	94.09	98.28	97.41	111.42
Mult.	107.70	92.61	109.10	110.77	116.38	95.03	90.92	97.27	96.75	101.34	109.06	81.07
Obs	110.9	97.9	140.3	93.04	118.21	94.93	90.24	80.38	96.41	95.28	105.86	164.95

Table 4.36: All methods: Match of peaks flux w.r.t. to Intrinsic Fluxes - The best matches are shown in Blue

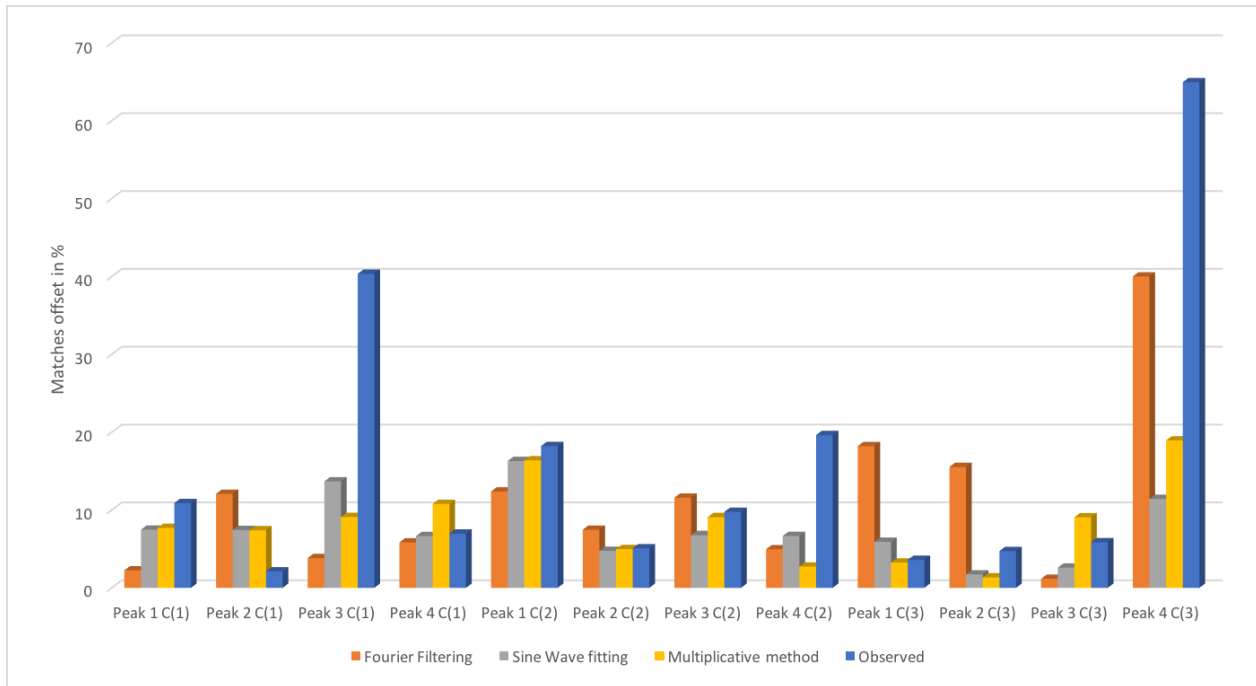


Figure 4.86: All methods: Match of peaks flux w.r.t. to Intrinsic Fluxes - Graphical Representation

From this Table, it is clear that the Sine wave fitting approximates the best the lines flux, followed by the Fourier Filtering method. Although, the Fourier filtering shows the highest number of best matches, its standard deviation w.r.t. the intrinsic values is larger than the one with the sine wave fitting. This can be seen in Figure 4.87. The reader might have noticed that the application of the methods in general leads to better results than the observed ones. Although sometimes, the results might be worst than the observed ones, as it is seen in for example Case (1), multiplicative method for Peaks 2 & 4. It is also interesting to notice that the multiplicative method provides the best results for the third Case, while the Fourier filtering largely decreases the lines flux compared to the observed spectrum. Therefore, none of the methods can be considered as reliable for the lines flux approximations.

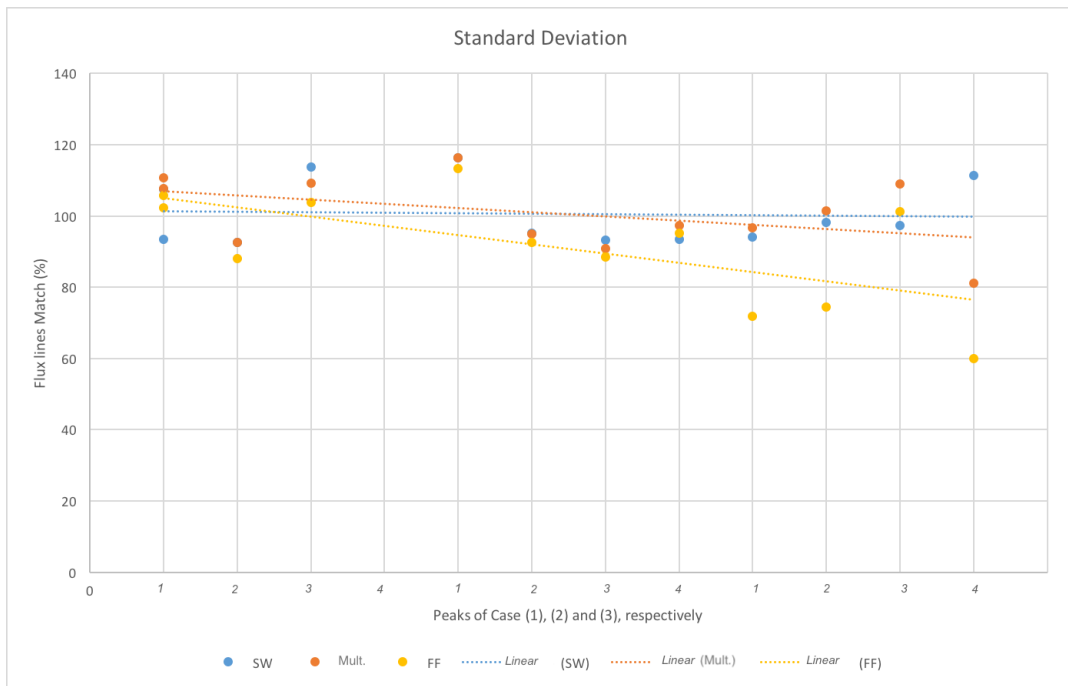


Figure 4.87: Standard Deviation of line flux matches for all methods

The results from the lines flux comparison are opposite to the graphical analysis, from which the Sine wave fitting was ranked as the best. One might conclude that it is not reliable to apply a single method to the data as none of the methods provides optimal results graphically and amplitude-wise. An interesting approach would be to combine the methods together for obtaining the best results w.r.t. to the two qualification criteria. This will be later investigated in Chapter 6.

# 5

## Traditional Defringing Methods - MIRI Application

In Chapter 4, the different methods have been investigated separately on so-called '*fake data set*'. For some methods, different sub-methods (i.e. Filter Region, approach) were studied and the best combination was selected.

In this Chapter, each method developed earlier will be applied to real data sets of MIRI and the outcome will be analyzed. The spectral features of these MIRI data sets being unknown, the only analysis of the 'defringed' data set will consist of a graphical analysis. If the graphical analysis of the MIRI data sets shows a similar pattern than the one from the fake data, it is expected that their spectral features peak analysis would also be similar.

### 5.1. MIRI Data sets

To objectively quantify the impact of the theoretical models developed, it has to be applied to real data sets; in this case data from the MRS of MIRI. In this Chapter, not only the data selection for this study will be explained in Section 5.1.1, but also the quality level of data required for performing the tests, in Section 5.1.2.

#### 5.1.1. Data Selection

Several test data set were recorded for MIRI:

- Flight-model (FM):

Through this campaign, the stability at long-term of the internal calibration of MIRI has been tested. For this test, a source flux was simulated and was measured as well as the source repeatability eight times over 46 days. [19]

- Cryo-Vaccum (CV):

Three cryo-vaccum tests have been performed. The first one was used as a risk reduction test. The second one allowed to perform a first verification of the flight instruments entirely integrated. The last test allows to check the entire system in its final configuration, after the vibrations and acoustic tests performed.[20]

For the data selection, two data sets have been considered: one from the flight model and one from the last cryo-vacuum test (i.e. CV3), with initial high signal-to noise ratio. Furthermore, for each data set, a different channel and exposure was considered. Indeed, MIRI instrument delivers four channels at three different exposures (cf. Figure

5.1) due its internal configuration. For detailed explanation on the internal configuration of the MRS, the reader is advised to read the literature study realized on this subject. [1]

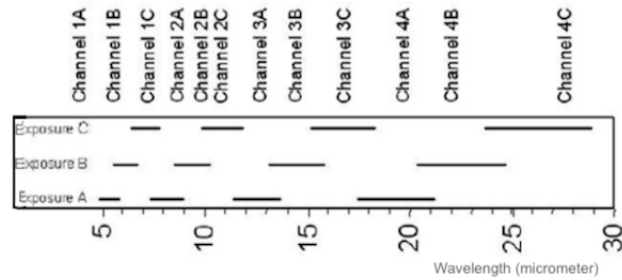


Figure 5.1: MRS - Channel Exposure

For this study, the data sets have been retrieved from data center from SRON - MIRI Team:

With spectral features:

- FM Data Set 1 for Channel 2B → MIRFM1T00010411\_12\_495\_SE\_2011-05-14T12h53m55\_LVL3\_AAR\_CH2\_B.fits
- CV3 Data Set 2 for Channel 1C → MIRM33542-C-C-BG-6019021544\_1\_495\_SE\_2016-01-19T02h27m39\_LVL3\_AAR\_CH1\_C.

Without spectral features (for the multiplicative method):

- FM Data Set 1 for Channel 2B → MIRFM1T00010411\_9\_495\_SE\_2011-05-14T12h36m51\_LVL3\_AAR\_CH2\_B.fits
- CV3 Data Set 2 for Channel 1C → MIRM335102-C-C-8MA-6025180626\_1\_495\_SE\_2016-01-25T18h19m18\_LVL3\_AAR\_CH1\_C.

### 5.1.2. Data Quality Required

In the previous Chapter, single models were developed for correcting the fringes on 1D extracted spectrum of flux intensity vs. wavelength. However, the application of these models requires pre-processing on the data. For using MIRI data in these simulations, the data have to be run through the jwst pipeline for reaching the level-3 data quality from which the 1D spectrum has to be extracted. A detailed explanation of the different stages from the jwst pipeline can be found in Appendix B.

For any other (non MIRI) files, the user is expected to provide a data quality file of the same level as level 3 for MIRI, in order to apply the defringing algorithms of this study. Otherwise, there is no guarantee that the conclusion of this study will be applicable to this data set.

## 5.2. Fourier Filtering

The Fourier filtering method was the first method to be investigated, it was shown to provide graphically good results by removing some or all fringes components, but it appears to also remove some important part of the signal leading to a lake of information (i.e. not correctly calibrated lines flux).

This method consists of selecting different regions in the Fourier amplitude domain and set the values in this region to zero. The new data set is then converted to the initial domain (i.e. intensity vs. wavelength).

### 5.2.1. FM Data Set 1 for Channel 2B

For this set of data, the same steps as explained in Section 4.2 were realized. As expected from the fake data, two major frequency components can be seen in Figure 5.2, the central peak (i.e. low frequency component) and a pair of same amplitude peaks (i.e. high frequency component). Once again two regions have been determined for the filtering, as shown in Figures 5.3 and 5.4 and the outcome of this method can be seen in Figure 5.5.

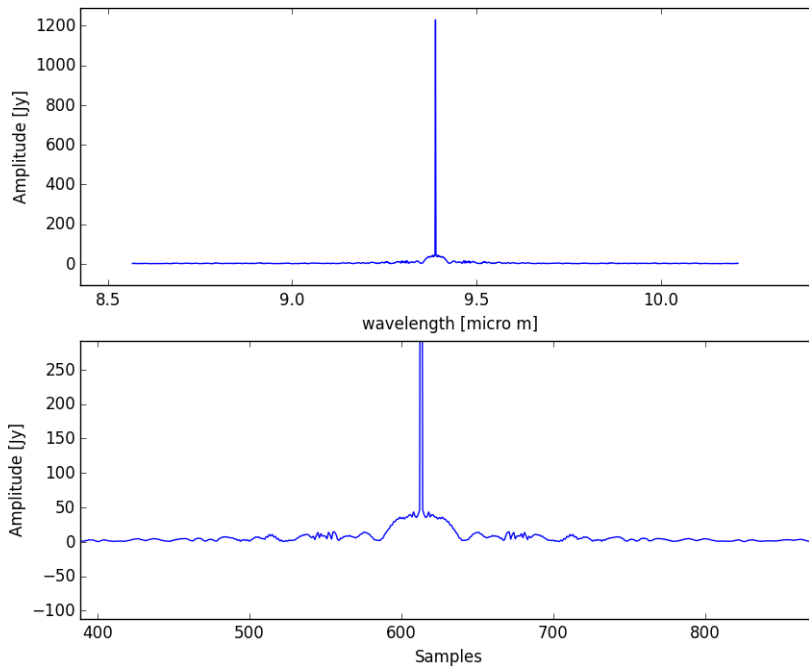


Figure 5.2: FM MRS data - Channel 2B - Amplitude Fourier domain

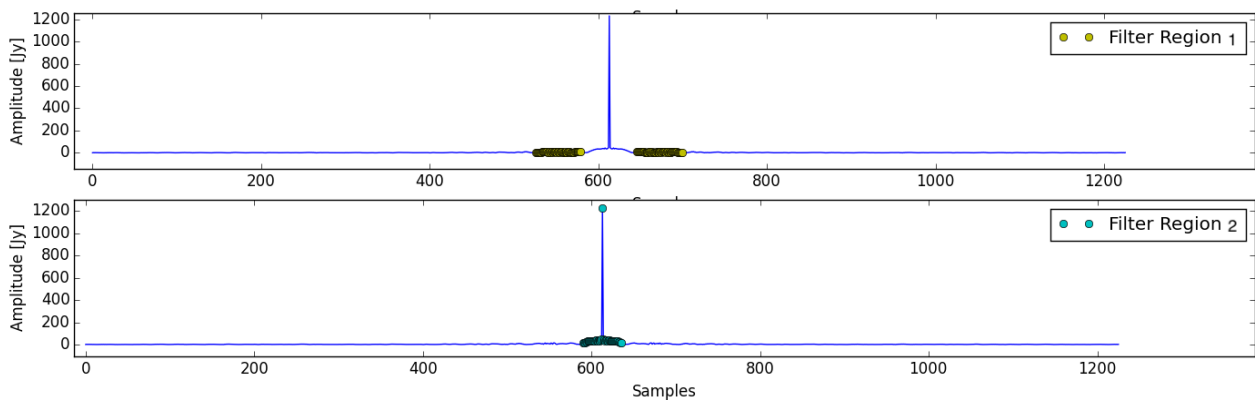


Figure 5.3: FM MRS data - Channel 2B - Amplitude Fourier domain of 2 regions to be filtered

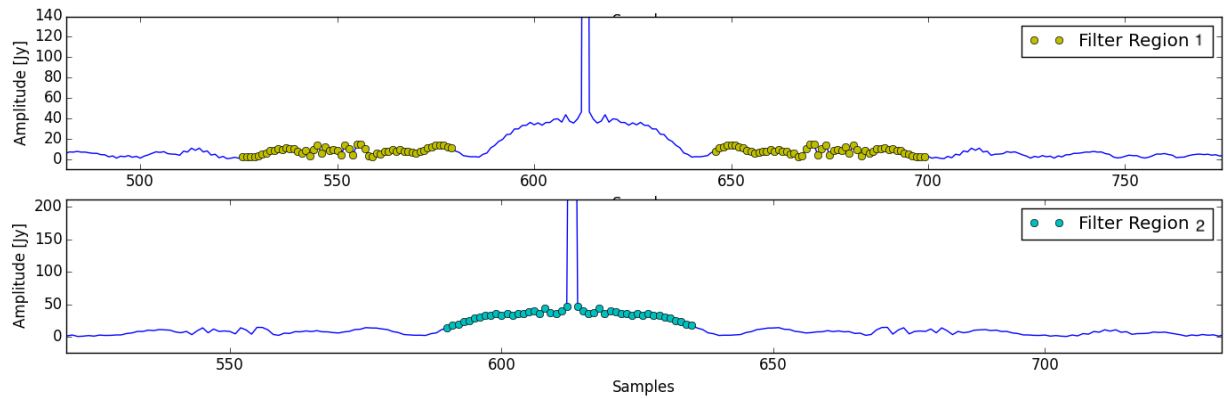


Figure 5.4: FM MRS data - Channel 2B - Amplitude Fourier domain of 2 regions to be filtered - zoom

In Figure 5.5, Region 1 seems to provide the best aesthetical results as the low frequency component is nearly nonexistent in the spectrum, while a high frequency component can still be depicted in the spectrum from Region 2. Furthermore, the residuals tend to spread out at the extremities, which might due to an incorrect recording of the data at the beginning and end of the filter.

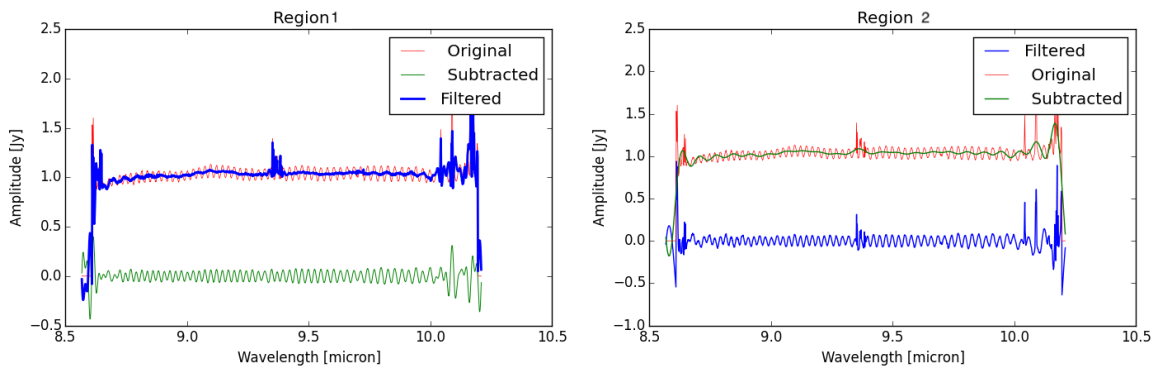


Figure 5.5: FM MRS data - Channel 2B - comparison among the original spectrum, filtered one and subtracted one for 2 different regions filtered

As shown in Figure 5.6, some noise is still present in the data set and it is therefore difficult to spot the weak spectral features. However, some of them are expected at wavelength 9.7 [micron]. The expected weak spectral features are more easily seen in the graph of Region 1 than the one of Region 2; indeed, around 9.7 [micron] the left high frequency component of Region 2 makes it difficult to detect the spectral features. Moreover, when looking closer at the central peaks, their lines flux do vary considerably w.r.t. the different regions.

Therefore, for an overall analysis, Region 1 would be advised, but for a line fluxes analysis a distinction cannot be established between the two Regions, as the real line fluxes are unknown. However, it would be advised to use Region 1 as the same pattern as in the theoretical analysis appears, namely the better graphical analysis and photometric accuracy.

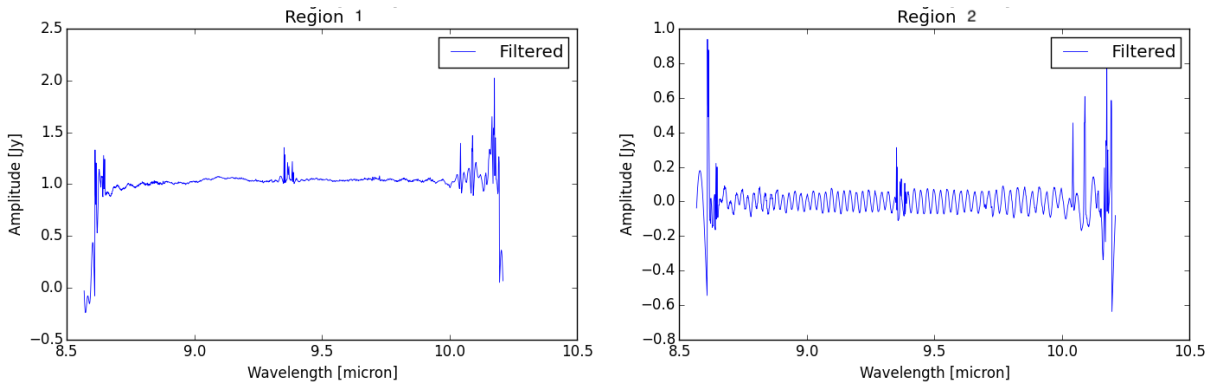


Figure 5.6: FM MRS data - Channel 2B - Filtered spectrum for 2 different regions

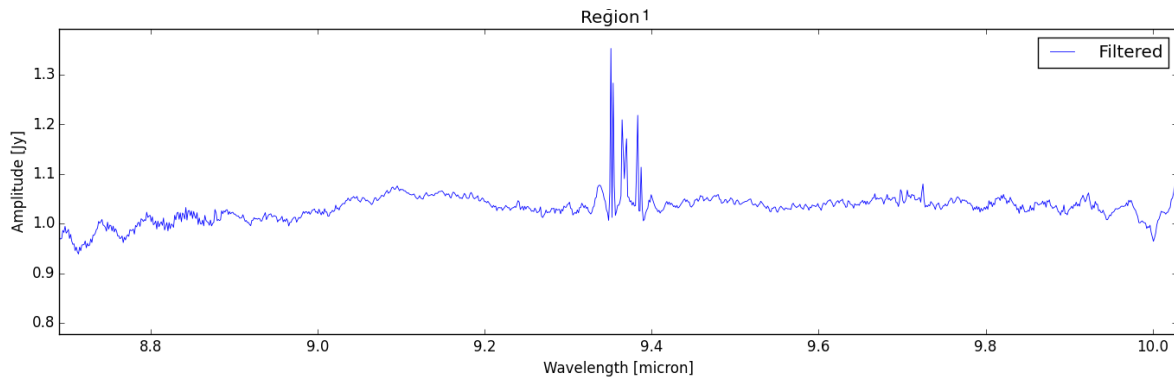


Figure 5.7: FM MRS data - Channel 2B - Filtered spectrum for Region 1 - zoom at interesting spectral feature location (not detected by Region 2)

### 5.2.2. CV3 Data Set 2 for Channel 1C

The first step for applying the Fourier Filtering is to convert the data into the Fourier Amplitude domains, in order to select the amplitude peaks regions as shown in Figures 5.8- 5.9. The two regions selected for the filtering are based on the central peak and the other smaller peaks on both sides of the main peak. A zoom of the different regions selected can be seen in Figure 5.10.

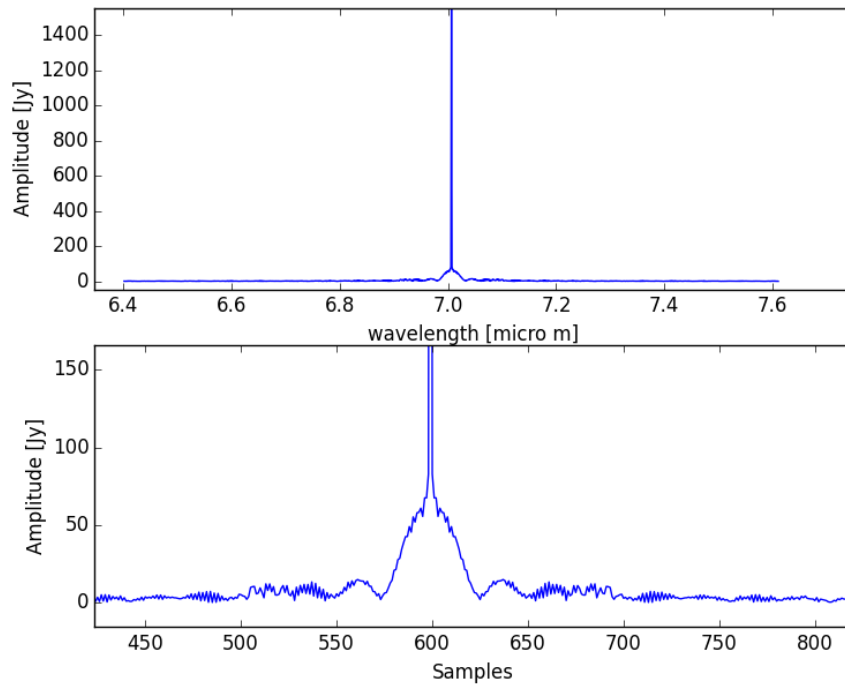


Figure 5.8: CV3 MRS data - Channel 1C -Amplitude Fourier domain

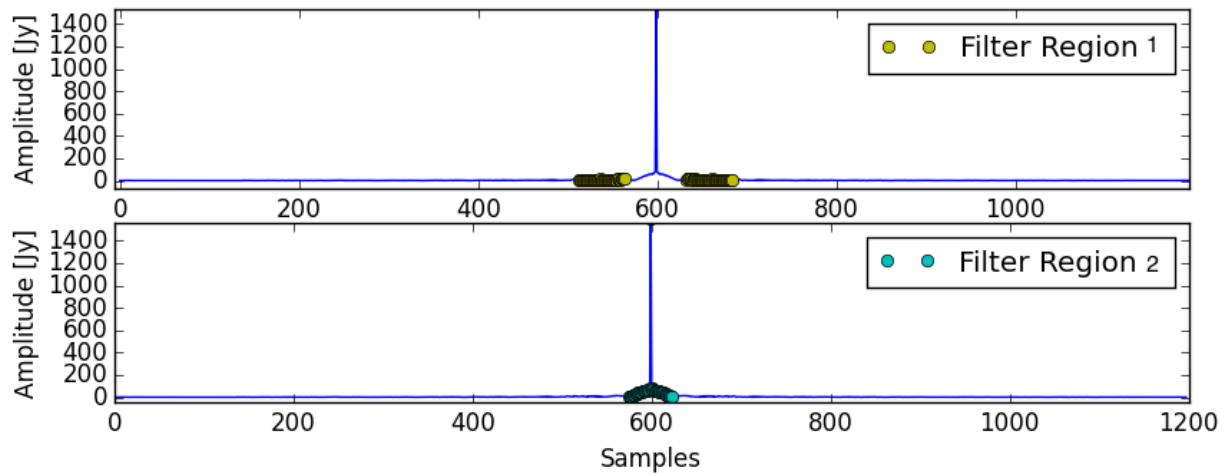


Figure 5.9: CV3 MRS data - Channel 1C -Amplitude Fourier domain of 2 regions to be filtered

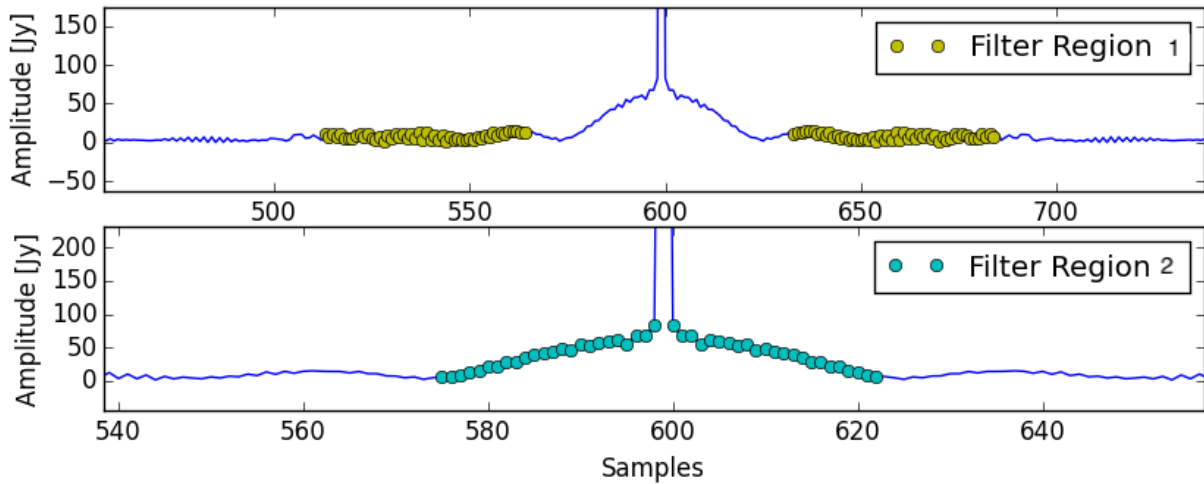


Figure 5.10: CV3 MRS data - Channel 1C - Amplitude Fourier domain of 2 regions to be filtered - zoom

The filter has been applied and the data were converted into the original domain, as shown in Figure 5.11. In this last Figure, numerous spectral features can be detected contrarily to the previous MRS data. Theoretically, Region 2 was not considered as reliable due to its remaining high frequency component, also seen in this data set. While Region 1 seems to have deleted the noise only on one side (cf. Figure 5.12).

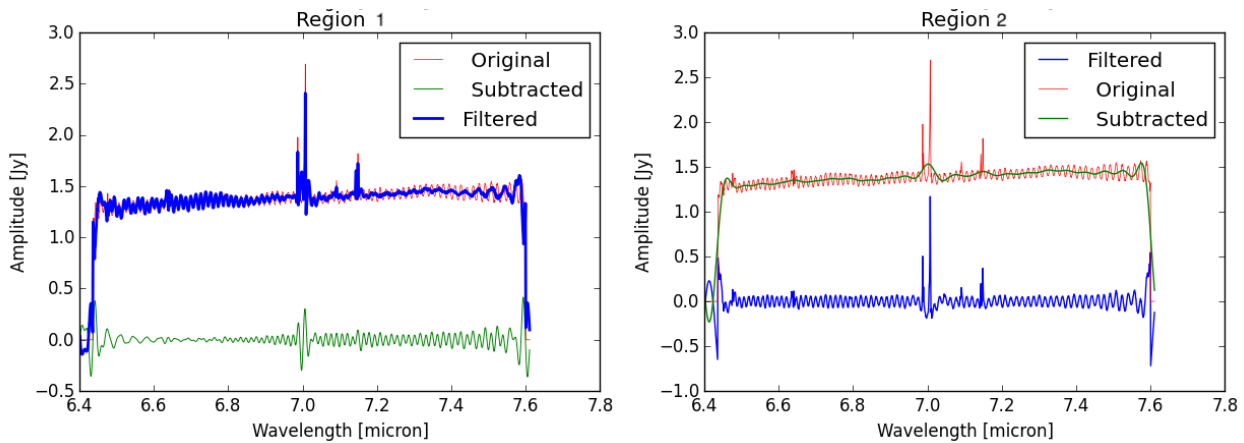


Figure 5.11: CV3 MRS data - Channel 1C - comparison among the original spectrum, filtered one and subtracted one for 4 different regions filtered

Moreover, as indicated previously high residuals are depicted at the end and beginning of the spectrum which might be due to recording offsets. When looking closer at Regions 1 and 2 in Figure 5.13, some spectral features can easily be pointed out although some noise is still present but, this noise makes also difficult to distinguish weak spectral features. Indeed, at wavelengths 6.63 [micron], weak spectral features are expected, but seem to be absorbed by the remaining noise. Furthermore, when comparing the lines fluxes between the two Regions at specific locations ( $\lambda = 7$  [micron] and  $\lambda = 7.16$  [micron]), it was seen that their amplitudes are similar, which would lead to a similar photometric accuracy.

Consequently, the same conclusion as for the previous MIRI data set analyzed can be made. Indeed, for an overall analysis, Region 1 would be advised as the same pattern as in the theoretical analysis appears, namely the better graphical analysis and better match results for Region 1.

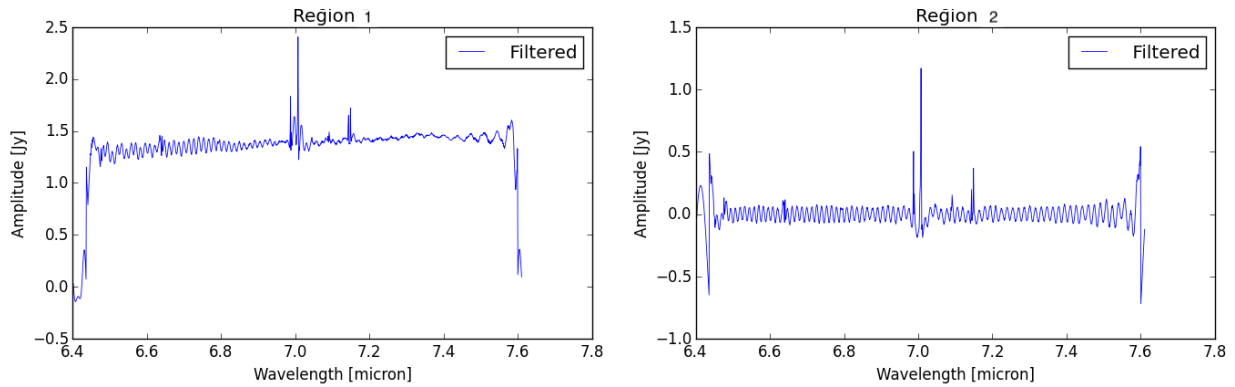


Figure 5.12: CV3 MRS data - Channel 1C- Filtered spectrum for 4 different regions

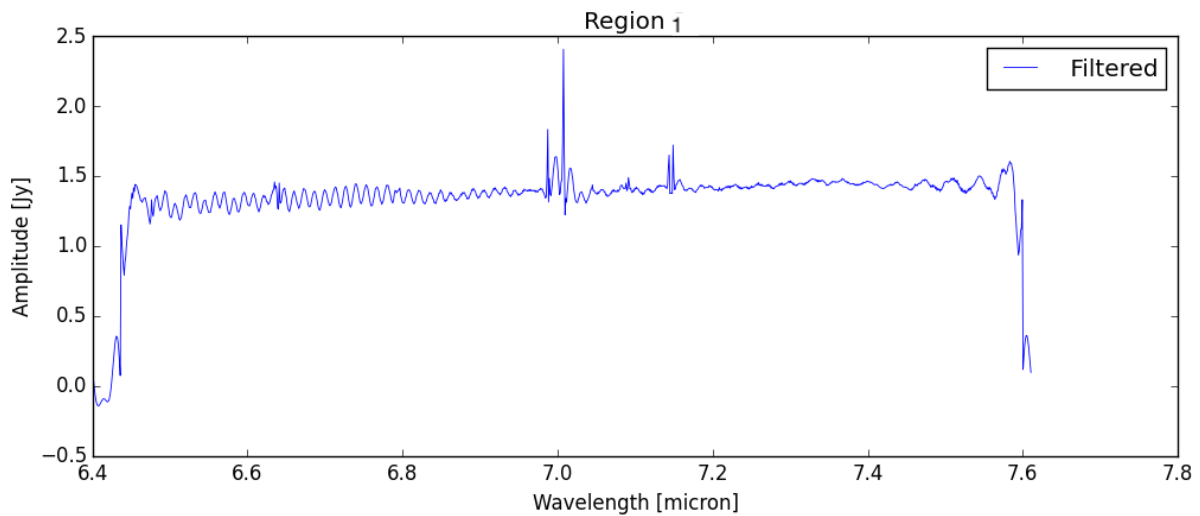


Figure 5.13: CV3 MRS data - Channel 1C - Filtered spectrum for Regions 2 and 3

### 5.3. Sine Wave Fitting

The second method to be applied on MRS data set is the sine wave fitting. As explained at the conclusion of Chapter 4, the best approach is the second which consists of first determining the residuals of the low frequency component and then add them to the high frequency component which will then be estimated by the sine wave fitting method. For a deeper explanation of the method, the reader is advised to look at Section 4.3.

#### 5.3.1. FM Data Set 1 for Channel 2B

The first step was to separate the two main frequency components, as shown in Figure 5.14.

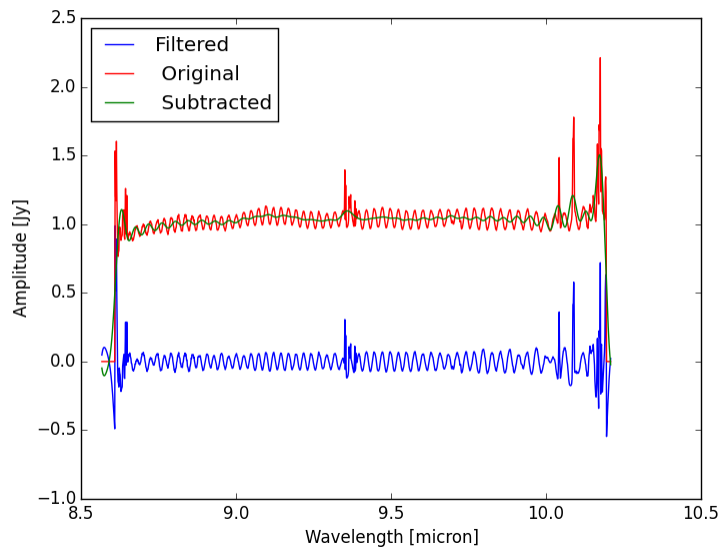


Figure 5.14: FM MRS data - Channel 2B - Sine wave fitting - Low and high frequencies components

In Figure 5.16, the low frequency component and its estimated sine wave fitting can be seen. For this case, the low frequency component seems nonexistent and its subtraction does not modify much the original spectrum. It appears that for this filter the noise is more dominant in the fringe from the detector. For this filter, the same extreme fluctuations as seen with Fourier filtering method can be pointed at the extremities. It is therefore expected to lead to high residuals at this location for the high frequency component. Furthermore, a small bump can be noticed at wavelength 9.4 [micron], which is characteristic of the location of a strong spectral feature. Indeed, for all the Cases analyzed in Section 4.3, the same pattern was present.

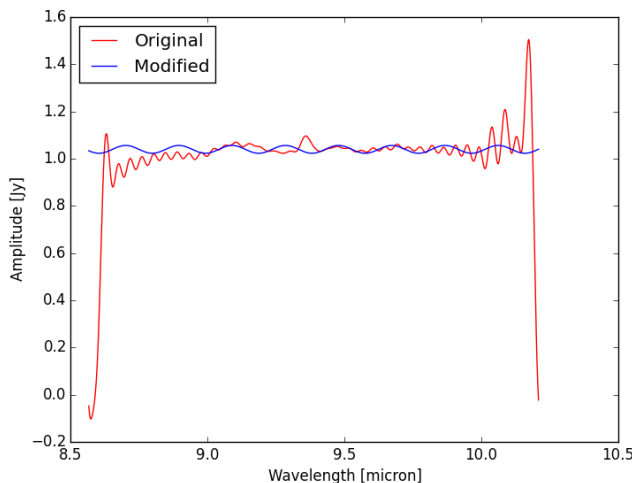


Figure 5.15: FM MRS data - Channel 2B - Sine wave fitting of low frequency component

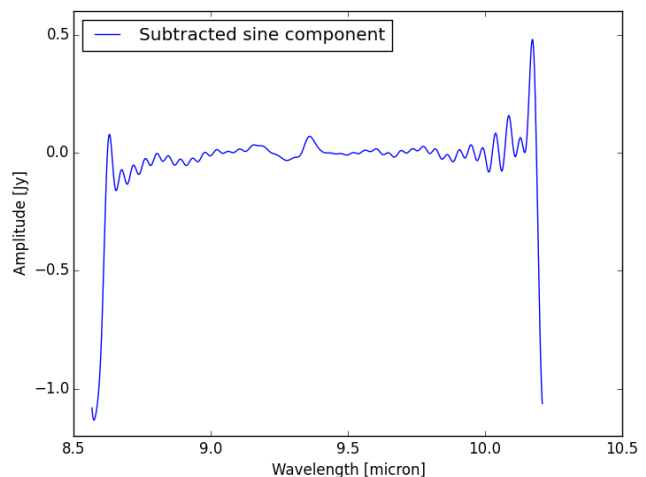


Figure 5.16: FM MRS data - Channel 2B - Sine wave fitting - Residuals of the low frequency component

The residuals are then added to the high frequency component and a sine wave is fitted. As expected, the fitting is not perfect due to notably the remaining low frequency and the noise originally present with the high frequency component. The small bump seen in the low frequency component was, indeed, a spectral feature. This can be clearly seen in Figure 5.18. The final spectrum shows still some residuals and it is hard to distinguish any weak

spectral features.

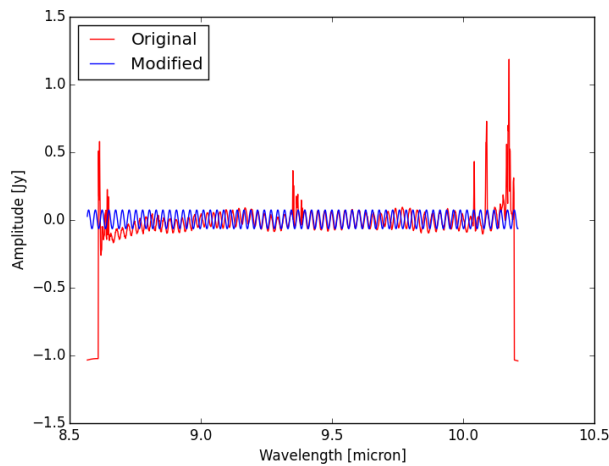


Figure 5.17: FM MRS data - Channel 2B - Sine wave fitting of high frequency component

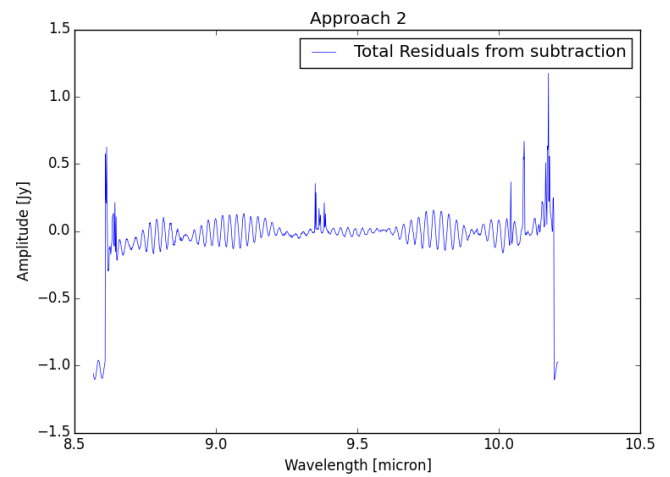


Figure 5.18: FM MRS data - Channel 2B - Sine wave fitting - Total Residuals of the spectrum

### 5.3.2. CV3 Data Set 2 for Channel 1C

The same initial step as realized for Channel 2B was undertaken. Once the frequencies have been separated (as shown in Figure 5.19), first, the low frequency component is fitted with a sine wave and its residuals are determined, as can be seen in Figures 5.20 and 5.21, respectively.

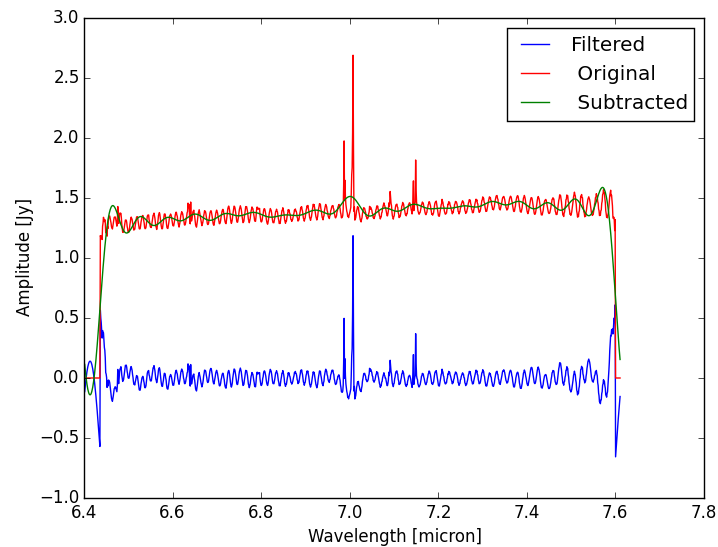


Figure 5.19: CV3 MRS data - Channel 1C - Sine wave fitting - Low and high frequencies components

Figure 5.20 shows the low frequency component and its sine wave fitted. As was the Case for the previous Channel analyzed, the low frequency component is nearly non-existent, making it harder to fit a sine wave to it. That explains the small difference between the original low frequency spectrum and its residuals, shown in Figure 5.21.

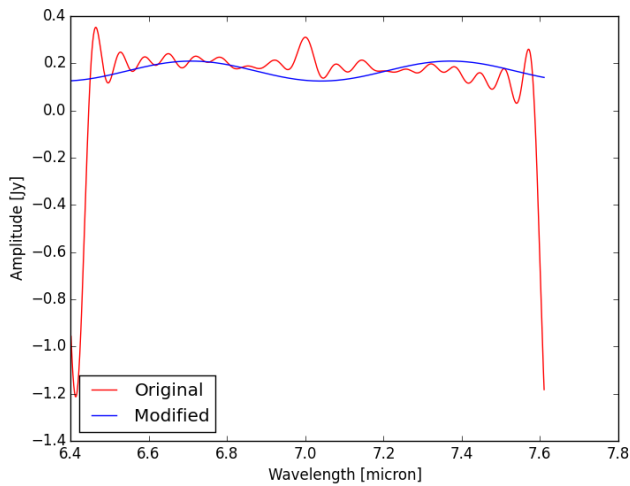


Figure 5.20: CV3 MRS data - Channel 1C - Sine wave fitting of low frequency component

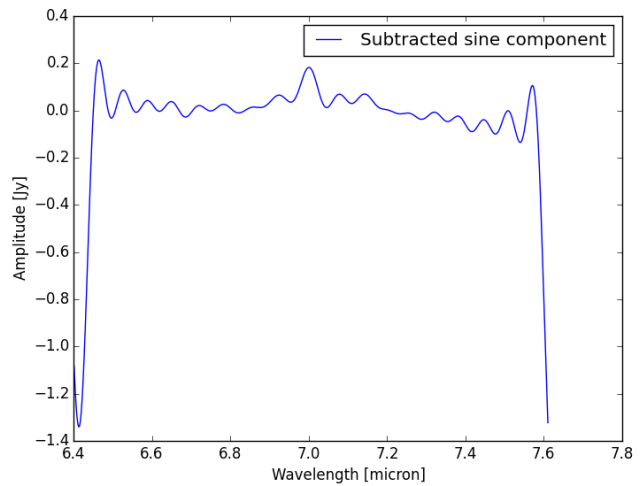


Figure 5.21: CV3 MRS data - Channel 1C - Sine wave fitting - Residuals of the low frequency component

The residuals are now added to the high frequency data set and a new sine wave is fitted to it. The new spectrum allows to better detect some spectral feature and their lines flux (at  $\lambda = 6.47, 6.61, 6.97, 7.0, 7.14$  [micron]), but worsen the detectability of other spectral feature (at  $\lambda = 7.1$  [micron]). When analyzing Figure 5.22, the reader might have noticed that the fitting is not perfect. Although the amplitude seems correct, the fitted sine wave appears to be shifted on the left side and extreme right side of the continuum ( $\lambda = 6.4-7.0$  [micron]) compared to the spectrum to be fitted. Therefore, the final spectrum shown in Figure 5.23 shows accordion-shaped residuals at these locations, which might "absorb" the weak spectral features. This phenomenon was already depicted in the final spectrum of the other Channel and can be explained by a difference of the fringe behaviour in reality than in theory. Indeed, it appears that the phase shift of the fringe varies, while the spectral fringe theory considers it as constant. Understanding why this occurs would be the second step of this study, but this will be explained in the Conclusion, in Chapter 9.

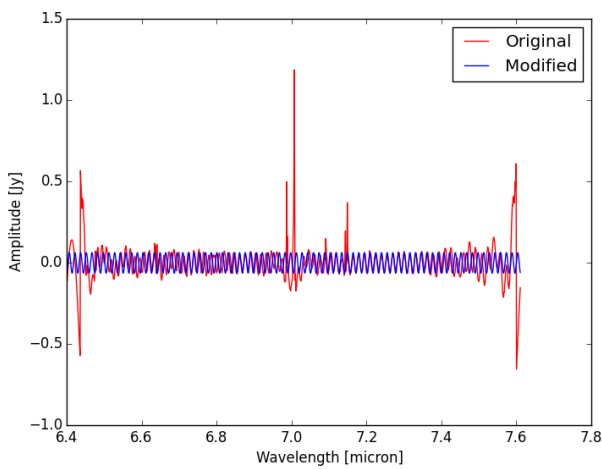


Figure 5.22: CV3 MRS data - Channel 1C - Sine wave fitting of high frequency component

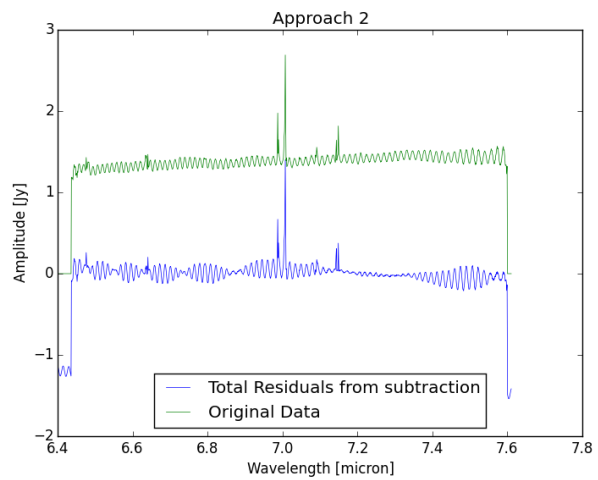


Figure 5.23: CV3 MRS data - Channel 1C - Sine wave fitting - Total Residuals of the spectrum

## 5.4. Multiplicative method

The third method to be applied to MIRI data sets is the multiplicative method, which consists of dividing the observed spectrum by a spectrally flat source for determining the amplification factors and then adjusting the observed spectrum w.r.t. these factors. A complete description of this method can be read in Section 4.4.1.

### 5.4.1. FM Data Set 1 for Channel 2B

The first step of this method is to determine the spectrally flat source and takes its inverse. An ideal flat source with only spectral fringes could not be found, therefore the used file includes some noise, as can be seen in Figure 5.24. The second step is to determine the amplification factors, which are shown in Figure 5.25.

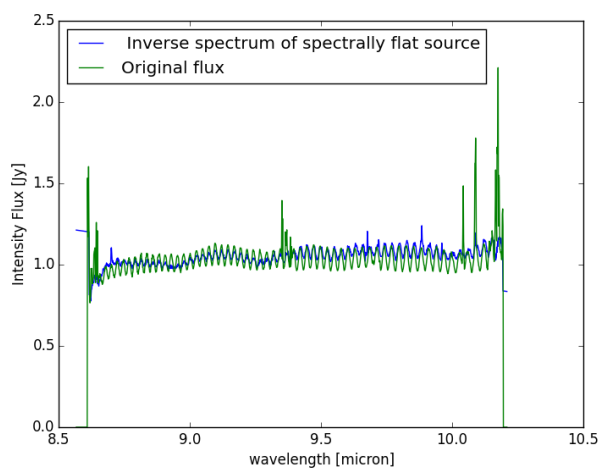


Figure 5.24: FM MRS data - Channel 2B - Multiplicative method - observed spectra with spectral features and spectrally flat source

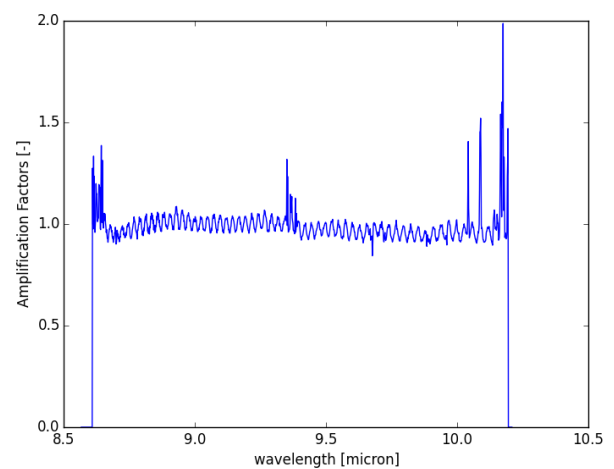


Figure 5.25: FM MRS data - Channel 2B - Multiplicative method - amplification factors

Now that the amplification factors have been determined, the observed spectrum can be corrected for each wavelength, as shown in Figure 5.26. The spectrally flat source used not being ideal as in the theoretical models, the final spectrum was expected to not be as good as the theoretical. Indeed, in Figure 5.26, there is remaining noise on the continuum. Aesthetically speaking, the observed spectrum looks better than the defringed one, as the noise is seen as clear sinusoidal shapes. However, the reader might remember that the noise of the observed spectrum does not consist of a constant sine-wave as explained in the sine-wave fitting, while, in the new spectrum, the remaining noise does not show a constant shape. However, its noise width is smaller than the one of the observed spectrum which allows a better detectability of the spectral features.

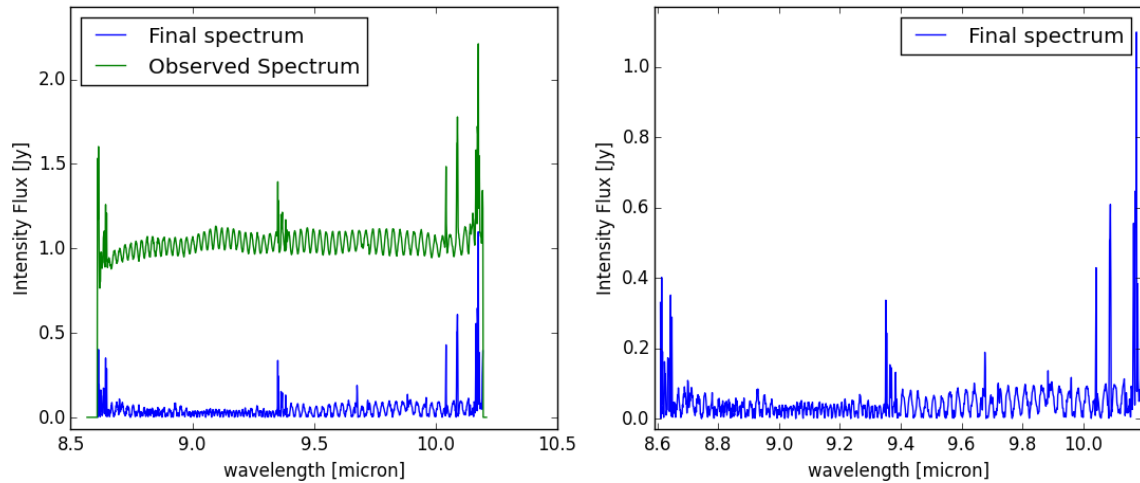


Figure 5.26: FM MRS data - Channel 2B - Multiplicative method - on the right side: the final spectrum. On the left side: the final spectrum compared with the observed one

### 5.4.2. CV3 Data Set 2 for Channel 1C

The second data set has also been defringed using the multiplicative method. As shown in Figure 5.28, the observed data to be treated and the spectrally flat source used are displayed. It is clear from this Figure that the flat source used is not free of extra noise and the results are therefore expected to be as for the previous Channel case.

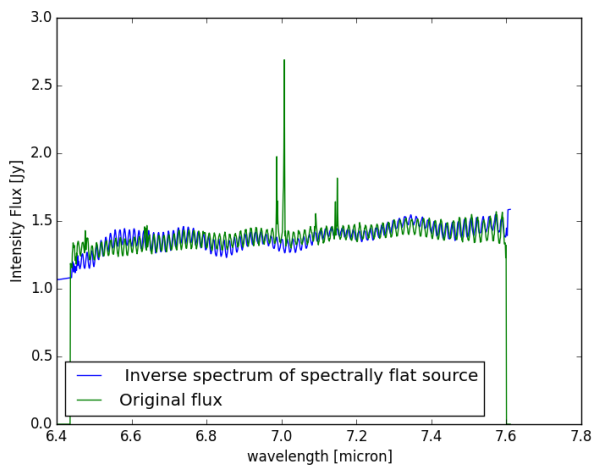


Figure 5.27: CV3 MRS data - Channel 1C - Multiplicative method - observed spectra with spectral features and spectrally flat source

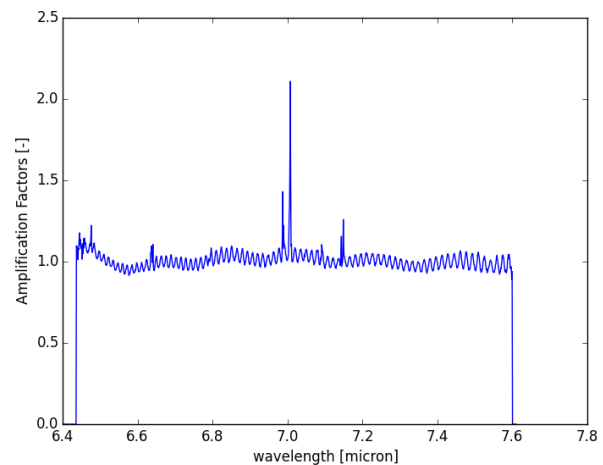


Figure 5.28: CV3 MRS data - Channel 1C - Multiplicative method - amplification factors

In Figure 5.29 the final spectrum and the original observed spectrum can be seen. As expected, there is remaining noise in the final spectrum which is less uniform than in the original observed spectrum. However, the reader might have noticed that the fringe amplitude has been reduced in the new spectrum, allowing to better point out some of the spectral features. Nevertheless, this non-uniform noise might also lead to worse detectability of some spectral features as it is the case for  $\lambda=6.65, 7.1$  [micron].

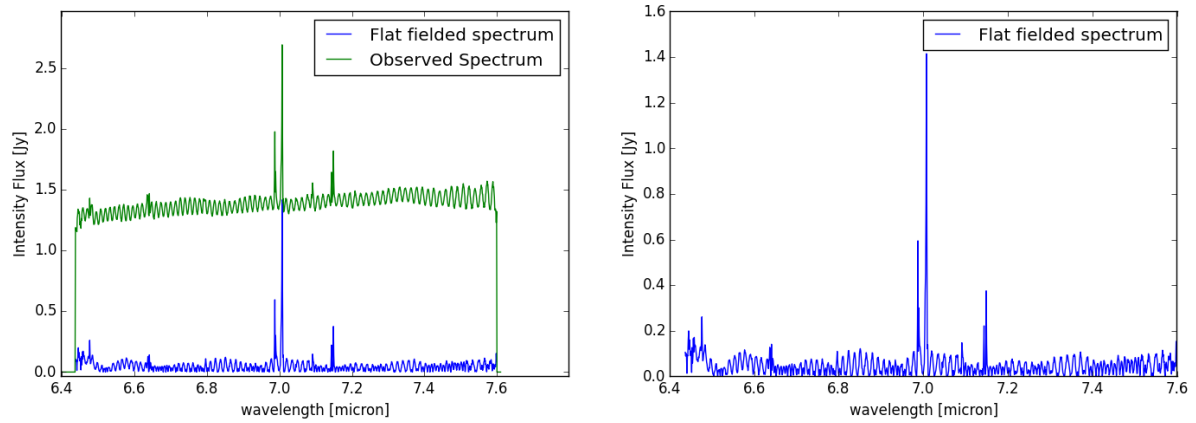


Figure 5.29: CV3 MRS data - Channel 1C - Multiplicative method - on the right side: the final spectrum. On the left side: the final spectrum compared with the observed one

## 5.5. Conclusion

In this Chapter, the three defringing methods have been applied to two MRS data sets, which have been selected from different testing types: cryo-vacuum and flight model.

The intrinsic values of the spectral features, their number and position are not known, therefore it will not be possible to compare the obtained values with the intrinsic ones. However, some conclusions can be drawn on the different methods based on a graphical analysis only, especially the width of the remaining noise and its final spectrum shape.

First of all, it appears that for all methods, the new spectra of MIRI data vary slightly from the theoretical values due to extra noise in the observed spectra. In some cases, the spectra were improved, but sometimes these were worsened.

Concerning the Fourier Filtering method, the results for the two data sets match the outcome from the theoretical analysis, namely the best graphical representation and line flux estimation were expected from Region 1, but this last point could not be verified due to the lack of information on the intrinsic value for MIRI data sets. This method provides a cleaner spectrum allowing to point major spectral features in general. However, the noise present in the Region 2 seems to hide "expected" spectral features pointed out in Region 1. Therefore, some spectral information might have been misinterpreted or missed from this last Region filter. For both Regions, it is important to underline that the fringe amplitude has considerably been reduced, and it would be advised to use this method rather than analyzing the original observed spectrum.

The second method tested is the sine-wave fitting. Contrary to the Fourier filtering method, its outcome for both MIRI test cases were more deviating from the theoretical analysis, although it was expected to be the most promising method out of the three. Indeed, both test cases have an original observed spectrum with a dominant homogeneous sine components, but the sine-wave fit led to flat (i.e. clean) spectrum at some locations and to accordion-shaped residuals at other locations. This unexpected residuals shape was explained by the change of the phase shift with the wavelength. This shift does not match with the spectral fringe theory; that is why it was not seen in the models used in the theoretical approach. Furthermore, it appears to not vary constantly, explaining the accordion-shapes at several locations of the spectrum. The origin of this varying phase is at this stage unknown and shall be further investigated in future work, as explained in the conclusion, in Chapter 9. Despite the final residuals left in both data sets, some spectral features appeared to have a better detectability from the observed spectrum. Indeed, in the Channel 1C data set, out of the six clear spectral features, five were more easily identified after the sine-wave fitting while only

one had a worse detectability.

The last method investigated was the multiplicative method, which required a second file for each case. Contrary to the theoretical testing, the first difficulty faced for this method was to find an appropriate spectrally flat source file compatible with the observed spectrum to defringe. It is therefore a negative point for this method as not all users might have access to such a file. Furthermore, the quality of this spectrally flat source will determine the quality level of this method on the observed spectrum. Indeed, for the two MIRI test cases, the data quality of these files were different: poor quality for channel 2B and acceptable quality for channel 1C. Consequently, the final spectrum of Channel 2B was not extremely improved from the original contrary to the final spectrum of 1C. However, in both cases, the width of the residuals amplitude was decreased and the spectral features were clearly distinguishable. Thus this method improved the graphical quality of the observed spectra.

To conclude, after applying the different algorithms to the MIRI data sets, it was seen that the real application varies slightly from the theory, especially because these data are more noisy than expected. However, the conclusions were found to be similar; therefore the theoretical analysis appears to be objective and further development on defringing methods can be carried out theoretically.

# 6

## Method Combinations - Theoretical Model

In Chapter 4, three different defringing methods were considered independently and their outcome was quantified. From their study, it was concluded that applying each method separately did not lead to satisfying results. Therefore, it was decided to investigate their combination, in order to determine if the artifacts left by one method could be corrected by another one.

Based on the three methods, twelve combinations are possible: six dual and six triple. Out of these twelve combinations, four will be selected and their outcome will be compared to the ones found in the previous Chapter and to the initial spectrum values. From Section 4.5, it was seen that the Fourier Filtering and the Sine wave fitting provided the best lines flux approximations and the multiplicative method the best graphical representation of the cleaned spectrum. Therefore, for each combination selected the last method would be the multiplicative method as first the lines flux amplitude shall be corrected and then the spectrum represented. For the line flux correction, all possible combinations of the Sine wave and Fourier methods will be investigated. These are summarized below:

- **COMBINATION 1:** Sine Wave fitting - multiplicative method
- **COMBINATION 2:** Fourier Filtering - multiplicative method
- **COMBINATION 3:** Fourier Filtering - Sine Wave fitting - multiplicative method
- **COMBINATION 4:** Sine Wave fitting - Fourier Filtering - multiplicative method

The reader might have noticed that in the Previous Chapter, several approaches were considered for each method. However, for each of the following combination, the best approach of each method was selected ( as stated in Section 4.5).

### 6.1. Combination 1: Fourier Filtering - multiplicative method Modification

The first combination to be tested is the Fourier filtering followed the multiplicative method. Thus, first the Region 1 in the Fourier amplitude domain was filtered (namely set to zero); the new set of data excludes therefore, the high frequency component. This new data set is then transformed by the multiplicative method, as realized previously (cf. Subsection 4.4.1).

### 6.1.1. Case (1)

This Combination has been applied to Case (1). The results of the first method are similar to the ones shown in Chapter 4, as can be seen in Figure 6.1. Furthermore, the spectrally flat source of Figure 6.2 used is also the same as developed in Section 4.4.2.

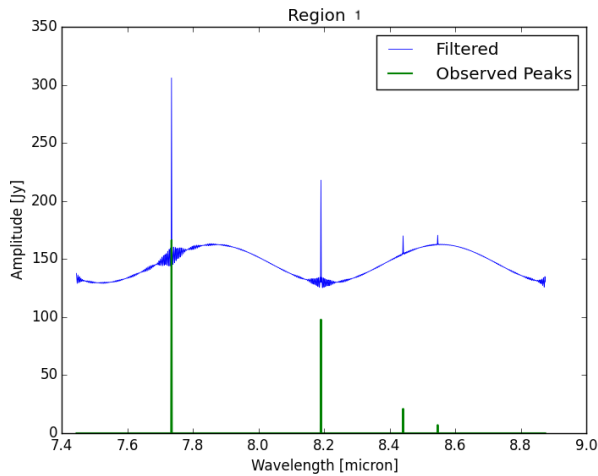


Figure 6.1: Case (1) - Combination 1 - Filtered Spectrum using the Fourier Filtering of Region 1

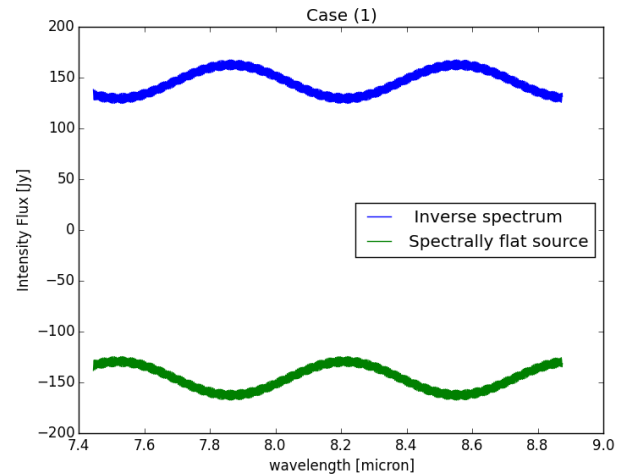


Figure 6.2: Case (1) - Combination 1 - Spectrally flat source spectrum

When analyzing Figure 6.3 which displays the amplification factors of this Case, it is clear that the results differ from the one found when applying this method only. Indeed, this graph shows a high fluctuation spectrum. As the reader might know, this graph describes the division of the outcome from the sine wave fitting to the inverse of the spectrally flat source; and ideally, a value of 1 would be expected everywhere, except at the spectral features locations. On Figure 6.4, it is clear that the new outcome from the multiplicative method is not as clean as when applying this method alone. The weak spectral features are hardly distinguishable and noise is still dominant in the spectrum.

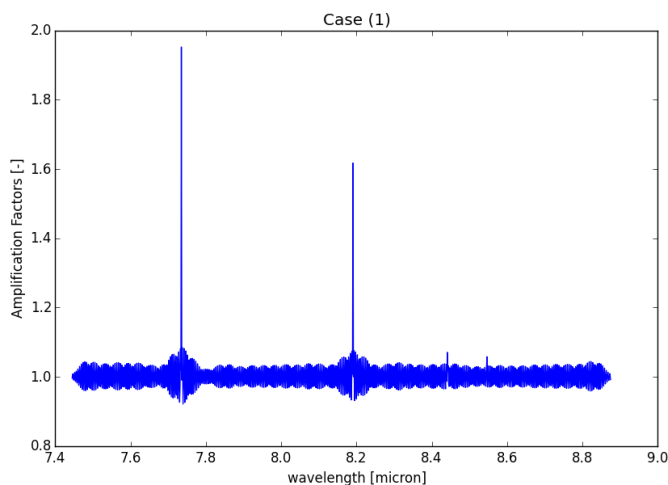


Figure 6.3: Case (1) - Combination 1 - Amplification factors from the multiplicative method

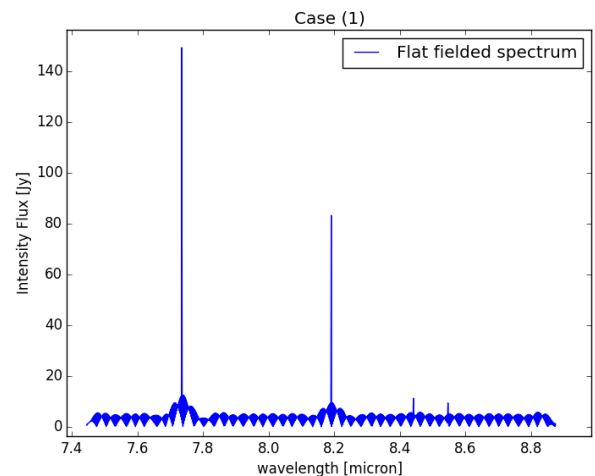


Figure 6.4: Case (1) - Combination 1 - multiplicative method spectrum

Graphically, the outcome from this combination is not satisfying, but let's have a closer look at the lines flux approximations, shown in Table 6.1. The results correspond to the graphical conclusion. Namely, no improvement has been noticed; the results are even worse than the ones found from each method individually. This combination would therefore not be advised for this Case.

#	Obtained or reduced Value/ Intrinsic Value[%]			
	Case (1)			
Method	Peak 1	Peak 2	Peak 3	Peak 4
FF	102.24	87.93	103.82	105.83
Mult.	107.70	92.61	109.10	110.77
Combination 1	98.08	82.65	59.36	110.9
Obs	110.9	97.9	140.3	93.04

Table 6.1: Method Combination 1- Case (1): Match of peaks flux w.r.t. to Intrinsic Fluxes - The best matches are shown in blue

### 6.1.2. Case (2)

The second Case was tested with this combination. As explained for Case (1), Figure 6.5 displays the final spectrum found after the Fourier Filtering method and Figure 6.6 shows the spectrally flat source of Case (2) and its inverse.

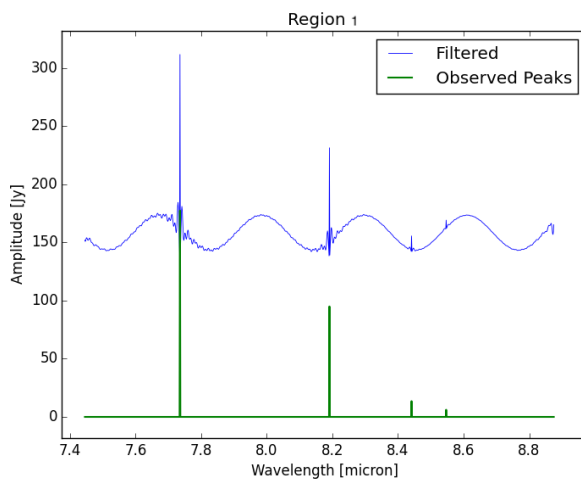


Figure 6.5: Case (2) - Combination 1 - Filtered Spectrum using the Fourier Filtering of Region 1

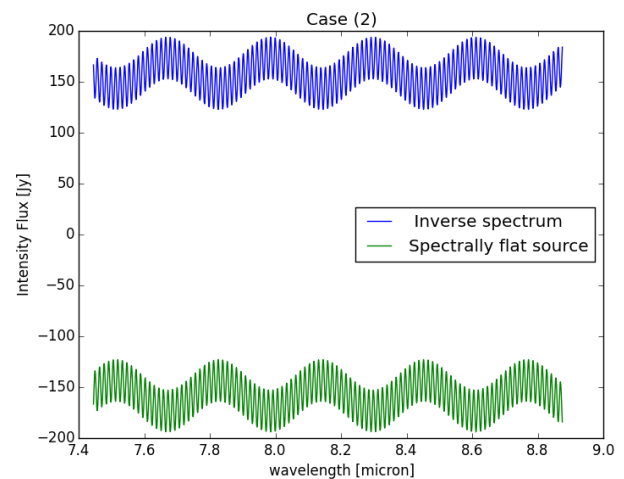


Figure 6.6: Case (2) - Combination 1 - Spectrally flat source spectrum

As was seen with Case (1), the amplification factors shown in Figure 6.7 do not match the ideal case (i.e. 1 at non spectral features locations and not 1 at the spectral feature locations). On Figure 6.8, it is clear that the final spectrum has not been improved, as the weak spectral features are still indistinguishable and the continuum includes several noise components.

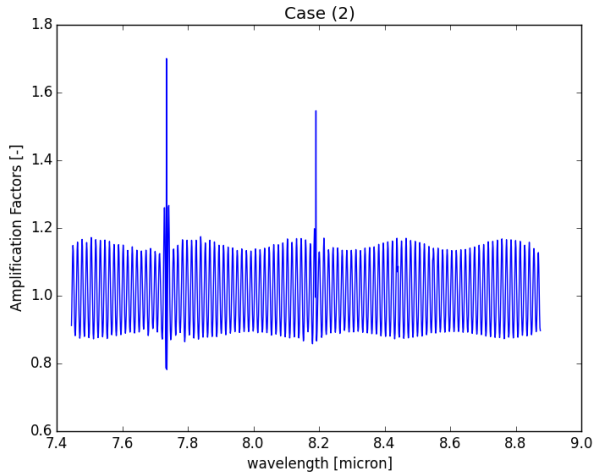


Figure 6.7: Case (2) - Combination 1 - Amplification factors from the multiplicative method

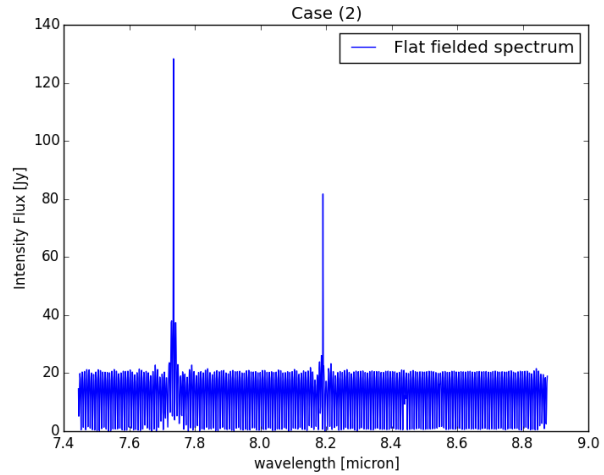


Figure 6.8: Case (2) - Combination 1 - multiplicative method spectrum

Analyzing the new lines flux found with this method also leads to a non-viable outcome. Indeed, the results have gotten worse for every peak. Although it shows a small improvement for the strong spectral features compared to the Fourier Filtering method, its strong offsets for the weak features make it less reliable than the Fourier Filtering method. For this Case also, this combination would not be advised.

#	Obtained or reduced Value/ Intrinsic Value[%]			
	Case (2)			
Method	Peak 1	Peak 2	Peak 3	Peak 4
FF	113.37	92.54	88.43	95.05
Mult.	116.38	95.03	90.92	97.27
Combination 1	82.49	70.79	14.12	190.08
Obs	118.21	94.93	90.24	80.38

Table 6.2: Method Combination 1- Case (2): Match of peaks flux w.r.t. to Intrinsic Fluxes - The best matches are shown in blue

### 6.1.3. Case (3)

The last Case to analyze is the most complex one as it regroups not only the fringe components but also additional noise. In the Fourier filtered spectrum of Figure 6.9, the noise effect was already detectable. Furthermore, due to the poor results of this Combination for Case (1) and Case (2), this combination is expected to provide worse results due to the extra noise of this Case.

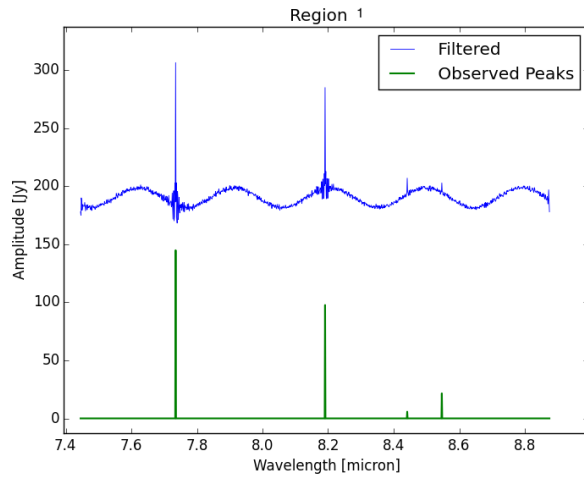


Figure 6.9: Case (3) - Combination 1 - Filtered Spectrum using the Fourier Filtering of Region 1

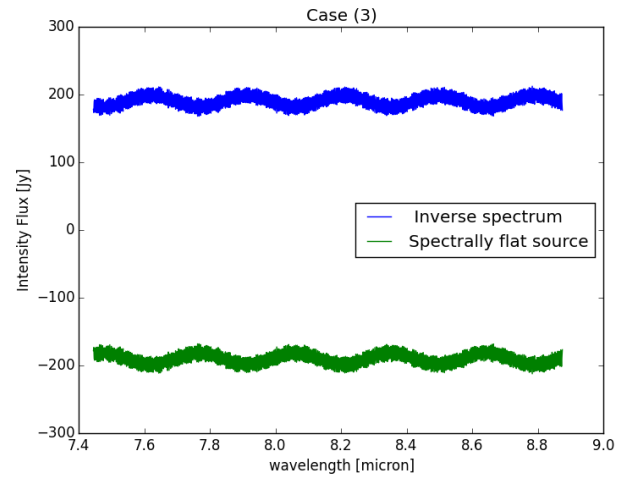


Figure 6.10: Case (3) - Combination 1 - Spectrally flat source spectrum

In Figure 6.11, the amplification factors graph has smaller amplitude of its fluctuations than was the case previously. The final spectrum from the multiplicative method is then slightly better than the one of Case (2), but still shows important left residuals. This last does not allow to point out one weak spectral feature (i.e. peak 4). Furthermore, the graphical quality of this multiplicative method is less accurate than the one found from the Sine wave fitting only (cf. Figure 6.9), which was already of a poorer quality than the multiplicative method spectrum (i.e. multiplicative method applied individually).

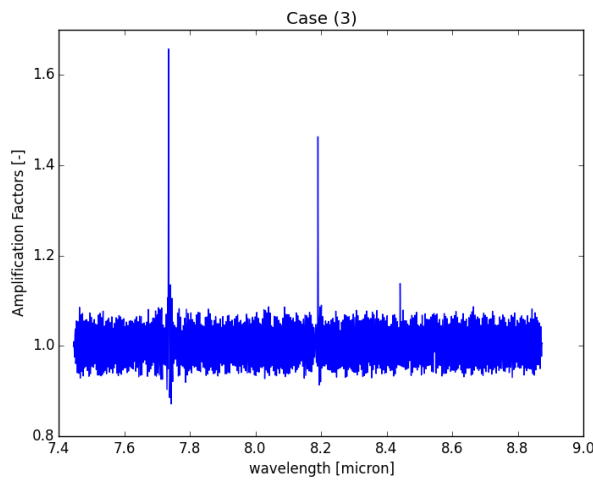


Figure 6.11: Case (3) - Combination 1 - Amplification factors from the multiplicative method

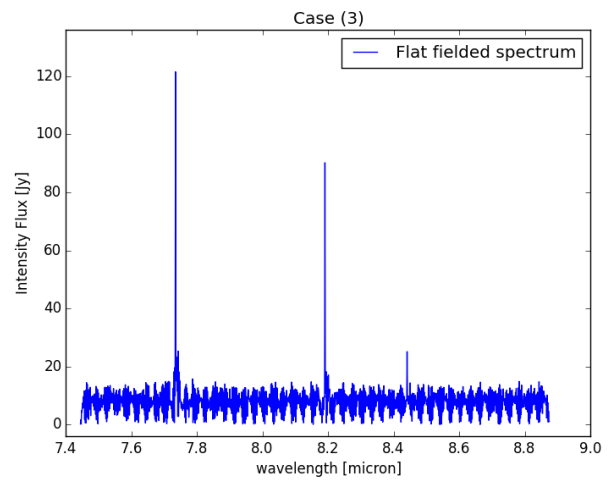


Figure 6.12: Case (3) - Combination 1 - multiplicative method spectrum

As expected, the lines flux analysis regroups the previous conclusions, namely the combination does not provide any improvement in the line flux approximations. Moreover, the weakest spectral feature has a completely different flux amplitude than the expected. For this Case, it would therefore be advised to use the reduced data set or applying any of the previous methods individually.

#	Obtained or reduced Value/ Intrinsic Value[%]			
	Case (3)			
Method	Peak 1	Peak 2	Peak 3	Peak 4
FF	81.80	84.48	101.16	60.01
Mult.	96.75	101.34	109.06	81.07
Combination 1	72.68	80.13	117.00	25.50
Obs	96.41	95.28	105.86	164.95

Table 6.3: Method Combination 1- Case (3): Match of peaks flux w.r.t. to Intrinsic Fluxes - The best matches are shown in blue

### 6.1.4. Conclusion

Throughout the three Cases analyzed, it was clear that this combination did not provide reliable results for the line fluxes nor a cleaner graphical representation. It is surprising that the multiplicative method generated such a noisy spectrum as it was the best method graphically (cf. Conclusion of Section 4.5).

At first sight, this method was promising as the Fourier filtered spectrum had a low frequency component left, which perfectly matches the low frequency component of the spectrally flat source spectrum for all Cases. However, when dividing the two spectra (i.e. generating amplification factors graph), artifacts could be seen, which are due to the high frequency component present in the spectrally flat source spectrum. The multiplicative method would be therefore more reliable on an reduced spectrum, than on the defringed one.

## 6.2. Combination 2: Sine Wave Fitting - multiplicative method Modification

The second combination to be studied is the Sine Wave fitting followed by the multiplicative method. For the first method application, the approach II was used which consists of fitting first the low frequency component and adding the residuals to the high frequency component, then, the fitting of the 'new' high frequency can be realized and the residuals determined.

### 6.2.1. Case (1)

The first step is to determine the sine wave fitting of the low frequency and add its residuals to the high frequency data set before fitting a sine wave. This step being similar to the one in Subsection 4.3.2, only the final residuals graph is shown (Figure 6.13). On Figure 6.14, the spectrally flat source, its inverse and the total residuals from the sine wave fitting are shown. From this comparison, it is clear that the spectrally flat source component is not matching the residuals spectrum. Therefore, it is expected not to provide reliable results.

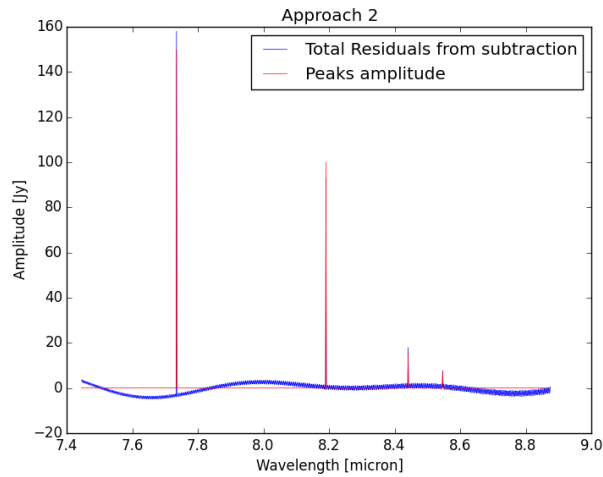


Figure 6.13: Case (1) - Combination 2 - Total residuals set from sine wave fitting of high component (Approach II)

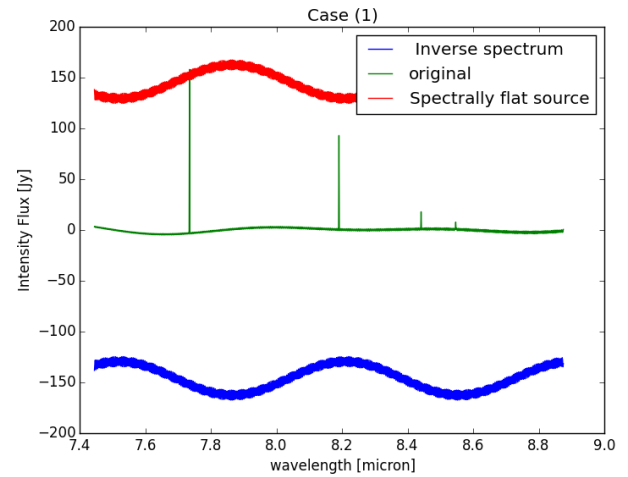


Figure 6.14: Case (1) - Combination 2 - Spectrally flat source spectrum and its inverse compared to the residuals spectra ("original") from the sine wave fitting

The amplification factors graph shows values near zero for the non spectral features, while the ideal value would be 1, which would translate the perfect correspondence of the fringes. The multiplicative method fringe thus will not be as the expected one. This is confirmed by Figure 6.16, in which it is clear that the multiplicative method spectrum has not been improved compared to the original version. On the contrary, more artifacts seemed to be introduced in this spectrum. Indeed, a low and high frequency components are more dominant in this Spectrum than the one after Sine fitting (cf. Figure 6.13). Moreover, the spectral features are wrongly represented as absorption lines instead of emission ones. The graphical representation being flawed, this combination has been considered unreliable for this Case.

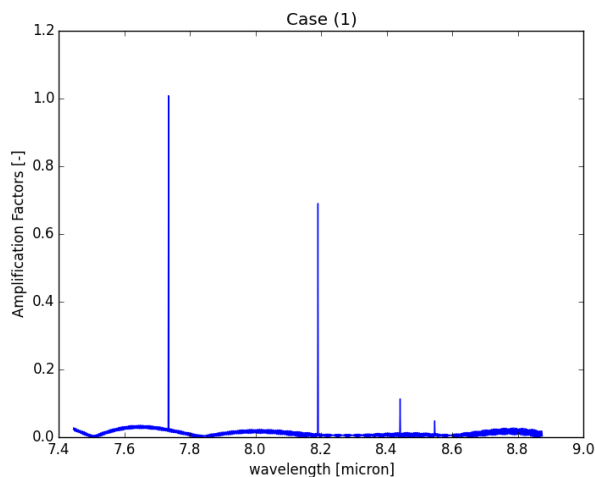


Figure 6.15: Case (1) - Combination 2 - Amplification Factors

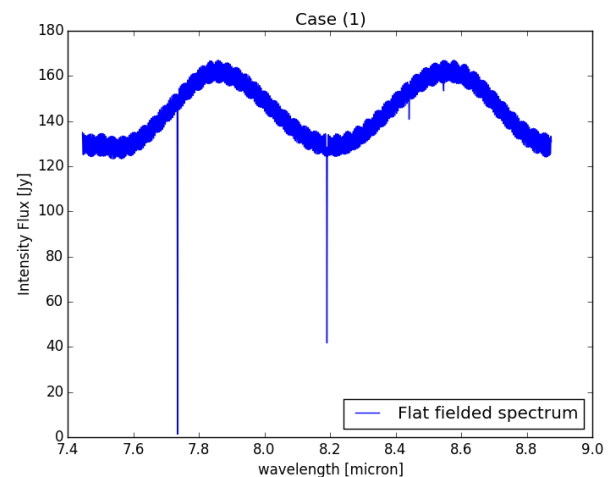


Figure 6.16: Case (1) - Combination 2 - multiplicative method spectrum

### 6.2.2. Case (2)

In this Subsection, Case (2) has been analyzed with this combination. As previously, the first step being similar to Sine wave fitting in Subsection 4.3.3, only the final residuals graph has been shown in Figure 6.17, while Figure 6.18 represents the spectrally flat source, its inverse and the residuals spectrum from the Sine wave fitting. As was seen for Case (1), the spectrally flat source is not superimposed on the residuals spectrum, which might suggest poor final results.

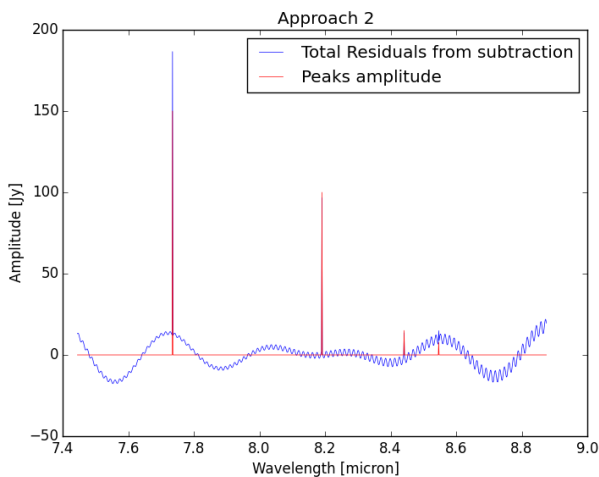


Figure 6.17: Case (2) - Combination 2 - Total residuals set from sine wave fitting of high component (Approach II)

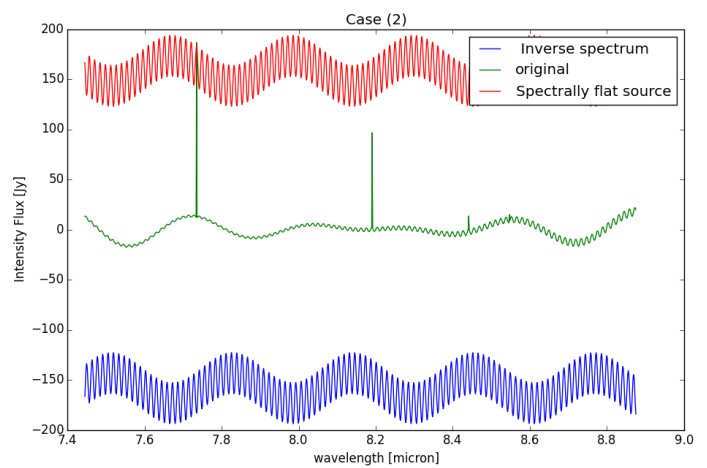


Figure 6.18: Case (2) - Combination 2 - Spectrally flat source spectrum and its inverse compared to the residuals spectra ("original") from the sine wave fitting

On Figure 6.19, the amplification factors graph is displayed. As expected, the results are inconclusive as for the non-spectral peaks, the factors are different than 1 but, closer to zero. This can be translated by a non correction of the spectrum. Indeed, Figure 6.20 confirms it. The spectrum is worse than the original one as the artifacts amplitude has increased and the spectral features, originally emission lines, as become absorption ones. For this Case, the lines flux amplitude have not even been determined as the graphical results are already unreliable. It is therefore not advised to use this Combination for this Case.

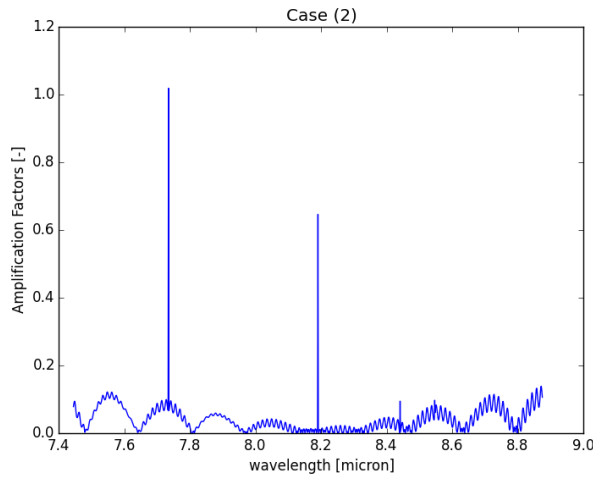


Figure 6.19: Case (2) - Combination 2 - Amplification Factors

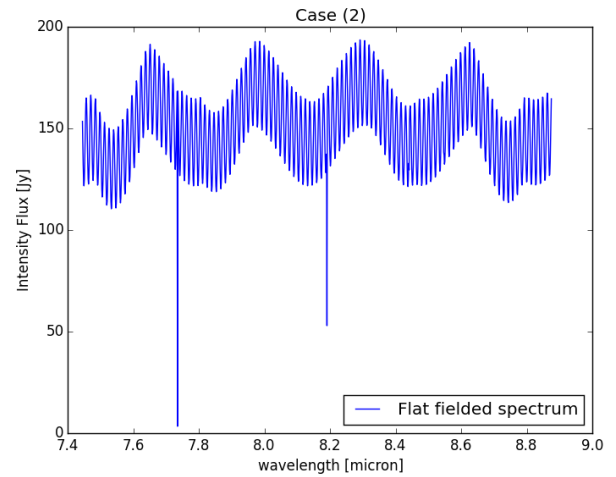


Figure 6.20: Case (2) - Combination 2 - multiplicative method spectrum

### 6.2.3. Case (3)

The third case to be analyzed is the most complex one as it also includes noise as compared to the previous two Cases. As specified previously, Figure 6.21 displays the residuals from the sine wave fitting using Approach II, while Figure 6.22 shows the spectrally flat source, its inverse and the sine-wave fitted spectrum. Once again, the fitted spectrum is not matching the spectrally flat source, which suggests poor results.

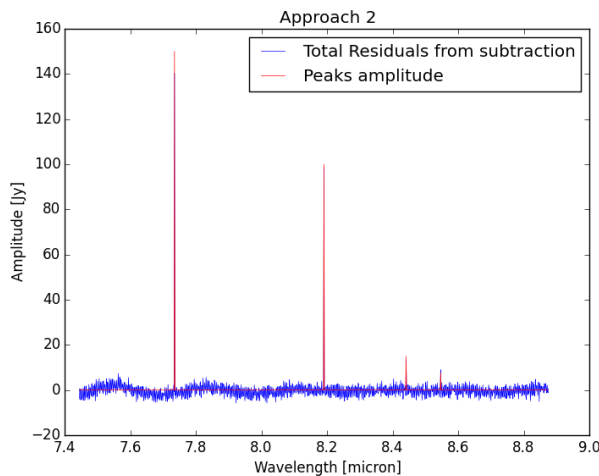


Figure 6.21: Case (3) - Combination 2 - Total residuals set from sine wave fitting of high component (Approach II)

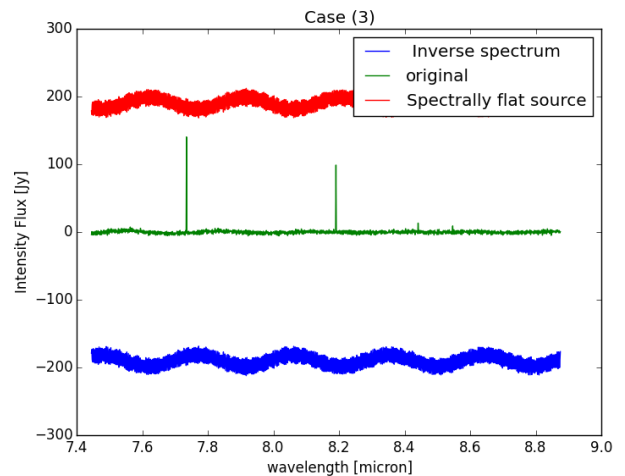


Figure 6.22: Case (3) - Combination 2 - Spectrally flat source spectrum and its inverse compared to the residuals spectra ("original") from the sine wave fitting

The same scheme as for the two other Cases appears here, namely amplification factors close to zero for non spectral features and a final poor graphical quality, with strong artifacts and unreliable spectral features.

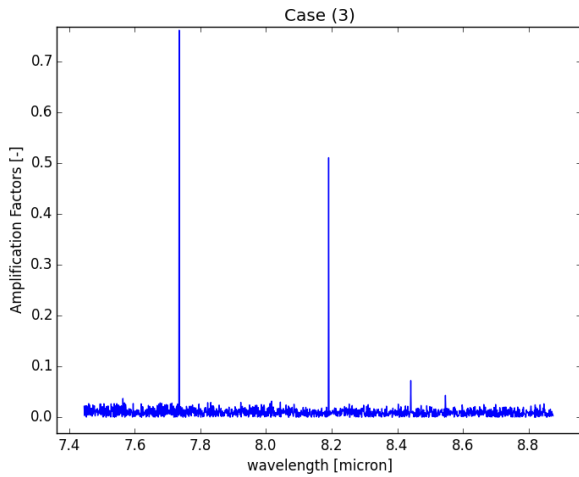


Figure 6.23: Case (3) - Combination 2 - Amplification Factors

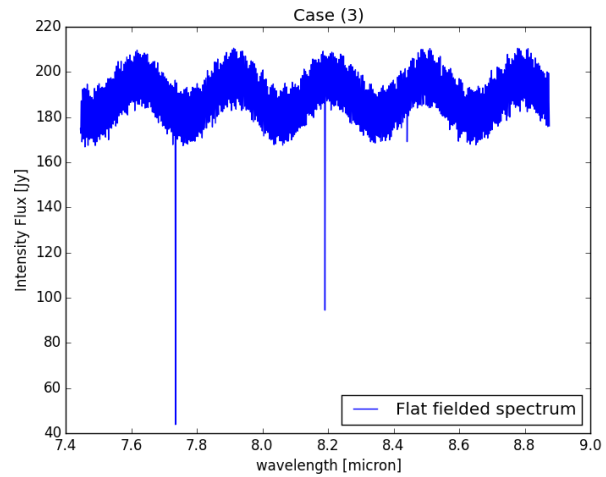


Figure 6.24: Case (3) - Combination 2 - multiplicative method spectrum

#### 6.2.4. Conclusion

The application of this combination on the three Cases was not more successful than Combination 1. Indeed, for all the Cases, the graphical results were extremely worse so that it was not even necessary to determine their lines flux. The first step of the method worked well (i.e. the sine wave fitting) but, the second method seemed not adapted to the data type from the first method. This was seen in the second graph displaying the spectrally flat source, its inverse and the outcome from the sine wave fitting. For the multiplicative method to be optimal, the spectrally flat source has to partially be super-imposed with the spectrum 'to be treated'. However, in these cases, they were not which led to artifacts introduced in the spectrum when applying this multiplicative method. Furthermore, in all Cases, the spectrally flat source showed more dominant components than the residuals from the sine fitting, which also generated the artifacts when dividing the two.

It is clear from the Cases that simply combining these two methods was not optimal, because both models are based on original defringed data. Nevertheless, the second method input is already partially defringed and thus the spectrally flat spectrum taken as fringe components reference is not corresponding anymore to the fringe component from the sine-wave fitted spectrum. This combination might thus provide better results if the second method is adapted to its input, by for example applying the sine-wave fitting to the spectrally flat source.

### 6.3. Anticipated Conclusion

The combination of the two methods clearly provide worse results than using the methods individually. Indeed, the final spectrum was more noisy than the initial one and the lines flux approximations were in most of the cases worse than the reduced ones. It would therefore be advised to study the reduced data set than applying any of the above combinations. Therefore, it was considered irrelevant to study the triple combinations, namely combinations 3 and 4, nor to apply these combinations to the MRS data sets.

The methods applied in a chain structure did not work efficiently because each single method is developed to correct

the fringe pattern, considering the two major components (low and high frequencies). However, in the combination, the second method did not correct the fringe anymore but its residuals and in some cases, a left frequency, which leads to the poor outcome accuracy.

The idea of combining the methods consecutively did not provide the expected results and was, therefore, wrong. Taking the best of each method, namely good graphical results and good lines flux estimations, it would be interesting to create a mix of the methods for optimizing the results. Or, to adapt the method to the previous outcome: for example, applying the Fourier filtering or sine wave fitting to the spectrally flat source spectrum and then use this new model for the multiplicative method. These will be the focus of Chapter 7.

# 7

## Optimization - Theoretical Model

In Chapter 4, each of the three methods presented were tested for removing the fringe effect on the data. However, the outcome of each method was not perfect and an optimization of them was considered. Therefore, in Chapter 6, their combinations were tested in order to optimize the output. Nevertheless, it was seen that simply applying the methods successively worsened the results compared to the original ones.

The purpose of this Chapter is to develop optimization of the methods analyzed previously in order to achieve the best results graphically and quantitatively. This Chapter will be divided into three parts; first, the optimization of two combinations described earlier will be investigated. Then, the optimization of single methods will be considered. Finally, conclusions will be drawn on the optimizations in order to quantitatively rank them.

### 7.1. Combinations

In the previous Chapters, the simple method's combinations were studied but, the study was stopped due to the poor results of Combinations 1 and 2, which were due to the multiplicative method not being adapted to the preliminary defringed data set. The ultimate goal of these combinations was to reach good photometric accuracy (or better) of the sine wave fitting or Fourier filtering and the accurate graphical representation of the multiplicative method.

#### 7.1.1. OPTIMIZATION 1 - Combination 1: Fourier Filtering - multiplicative method

For this combination, the Fourier Filtering is normally applied to the observed spectrum, using the Approach II then its residuals are treated by the multiplicative method. However, contrarily to Section 6.1, the spectrally flat spectrum is also Fourier filtered in the same way as applied to the observed spectrum (i.e. Region 1).

##### Case (1)

The first part of this combination consists of Fourier filtering, which has already been described in Subsection 4.2.2. The reader is thus advised to look at this Subsection for the details of this method on Case (1). The output of it is shown in Figure 7.1 while Figure 7.2 displays the Fourier Filtering output of the spectrally flat spectrum (i.e. "Filtered" spectrum). In Figure 7.3, the new spectrally flat source, its inverse and the data set to be further defringed are shown. The reader might have noticed that the flat source spectrum and the residuals one are now superimposed as it should be in the multiplicative method. Therefore, the outcome of the multiplicative method is expected to provide good results.

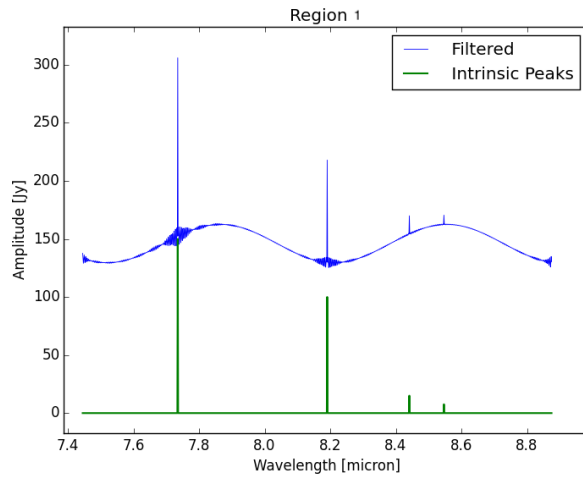


Figure 7.1: Case (1) - Optimization Combination 1 - Filtered Spectrum using the Fourier Filtering of Region 1

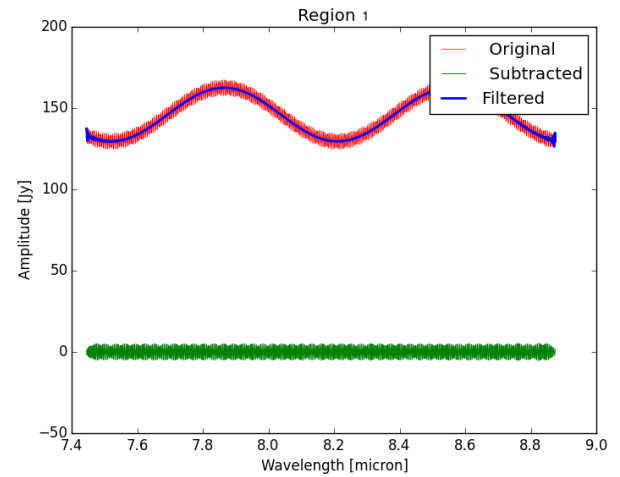


Figure 7.2: Case (1) - Optimization Combination 1 - Spectrally flat source spectrum (i.e. "original"), its Fourier Filtered spectrum using Region 1 (i.e. "Filtered") and the subtracted spectrum resulting from the subtraction of the original flat source spectrum and the Fourier filtered one.

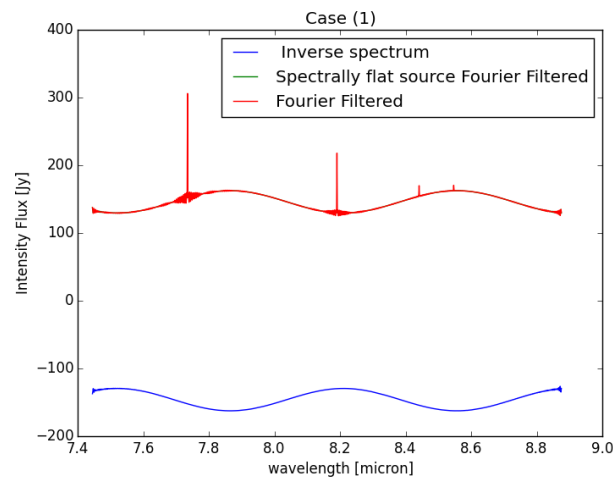


Figure 7.3: Case (1) - Optimization Combination 1 - Filtered spectrally flat source, its inverse and the residuals spectrum from method 1

The amplification factor graph (Figure 7.4) shows promising data, as values non related to the four spectral features are equal to one (i.e. due to the superimposing of the spectrally flat source and the residuals data), and at the spectral features locations, the factors are greater than one, which reflects the emission lines introduced in the intrinsic spectrum. Finally, in Figure 7.5, the spectrum from multiplicative method can be seen. This last feature is close to the one from the multiplicative method only, except that some small residuals can still be depicted preventing the continuum to be flat. The spectral features are clearly represented and nearly all the fringes components are removed. Graphically, this method is reliable but, to be efficient, it has also to provide accurate results for the lines flux estimations.

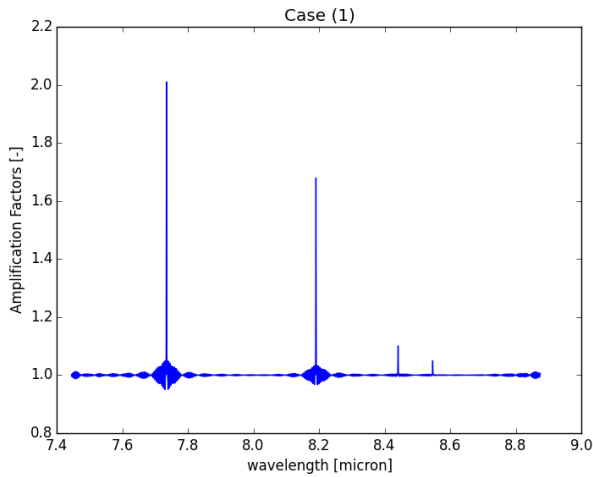


Figure 7.4: Case (1) - Optimization Combination 1 - Amplification factors from the multiplicative method method

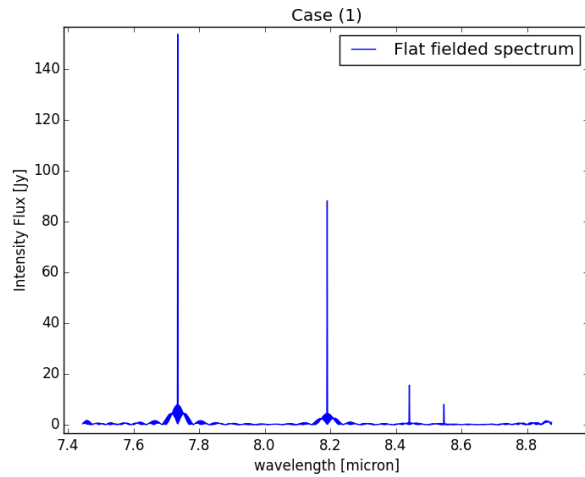


Figure 7.5: Case (1) - Optimization Combination 1 - spectrum from multiplicative method

From Table 7.1, the reader might have noticed the good accuracy of this method, which provides the best estimates for the weak spectral features and good values for the strong ones. It is clear that this optimized combination exceeds its simple version and the methods used separately. Although the lines flux are well approximated and allow to reach the best results so far, it is true that the matches are not perfect and therefore investigation on other optimizations should be continued. Furthermore, the reader might have also discerned that the results obtained are similar (slightly improved) to the ones from single Fourier Filtering method. It can be therefore said that this combinations combines the best attributes of its methods (i.e. graphically and quantitatively).

#	Obtained or observed Value/ Intrinsic Value[%]			
	Case (1)			
Method	Peak 1	Peak 2	Peak 3	Peak 4
FF	102.24	87.93	103.82	105.83
Mult.	107.70	92.61	109.10	110.77
Combination 1	98.08	82.65	59.36	110.9
Optimization 1	102.22	87.94	103.69	104.89
Obs	110.9	97.9	140.3	93.04

Table 7.1: Optimization of Methods Combination 1- Case (1): Match of peaks flux w.r.t. to Intrinsic Fluxes - The best matches are shown in blue

### Case (2)

The second case to be analyzed is as complex as the first one. On Figure 7.6, the final residuals spectrum using filtered Region 1 can be seen, while Figure 7.7 displays the extracted frequency components using the Fourier filtering method on the flat source spectrum. As can be noticed on Figure 7.8, the new spectrally flat source and the residuals spectra are perfectly overlapping, the multiplicative method is therefore expected to be successful.

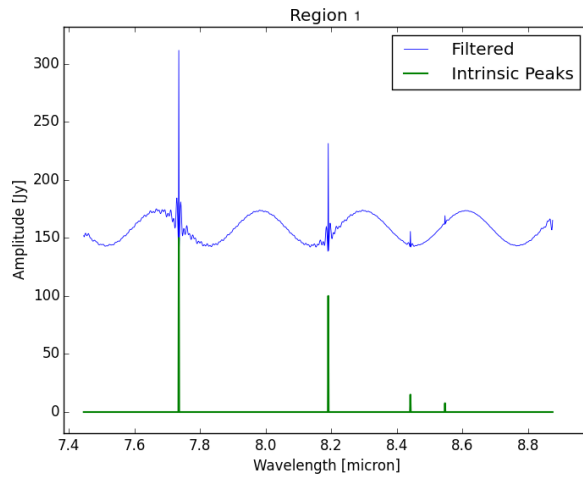


Figure 7.6: Case (2) - Optimization Combination 1 - Filtered Spectrum using the Fourier Filtering of Region 1

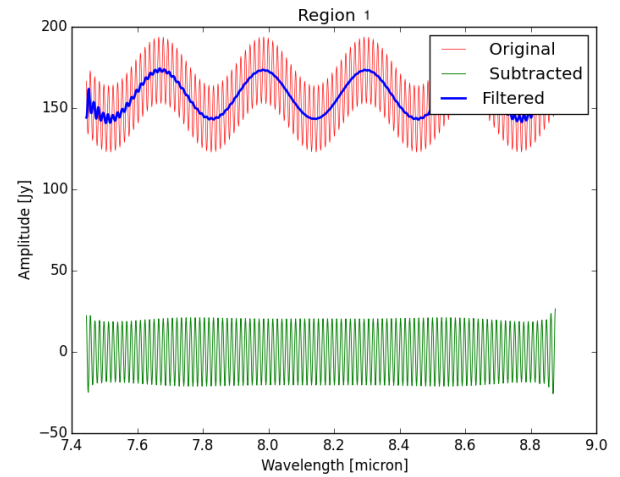


Figure 7.7: Case (2) - Optimization Combination 1 - Spectrally flat source spectrum (i.e. "original"), its Fourier Filtered spectrum using Region 1 (i.e. "Filtered") and the subtracted spectrum resulting from the subtraction of the original flat source spectrum and the Fourier filtered one.

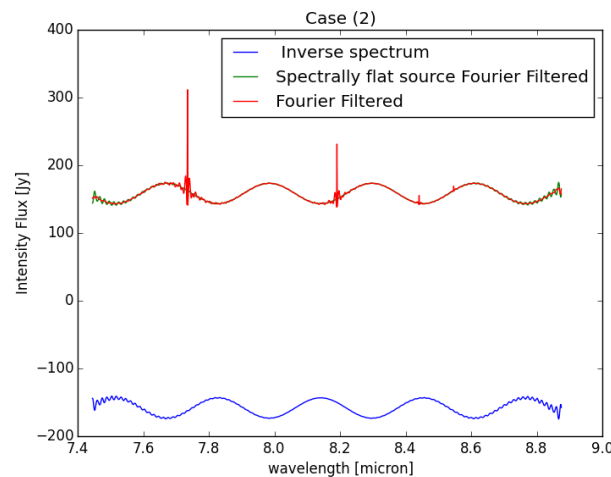


Figure 7.8: Case (2) - Optimization Combination 1 - Filtered spectrally flat source, its inverse and the residuals spectrum from method 1

The spectrum from multiplicative method (Figure 7.10) confirms the expectation. Indeed, the graphical representation is quite close to the spectrum of the spectral features only, as the continuum is in general flat and the peaks are easily distinguishable. The only negative graphical point is the left residuals that tend to spread out at the extremities of the spectrum. In this "fake" data case, the observed data at the extremities are similar all along the spectrum; however, for the real MRS data, it was seen before that strong artifacts were introduced at the beginning and end of its spectrum. Consequently, these artifacts spread out effect is expected to be worse for real data, reducing the graphical quality of the final spectrum.

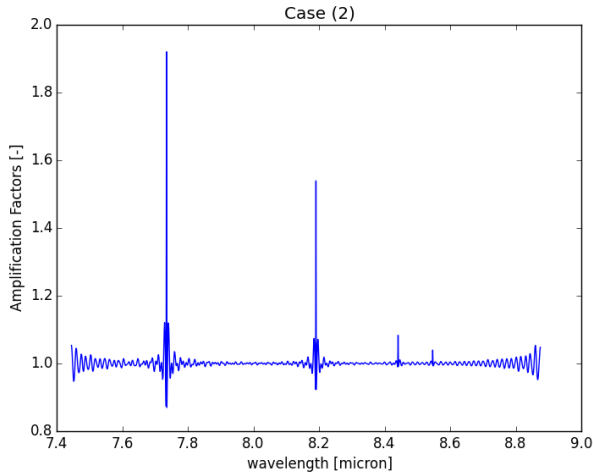


Figure 7.9: Case (2) - Optimization Combination 1 - Amplification factors from the multiplicative method method

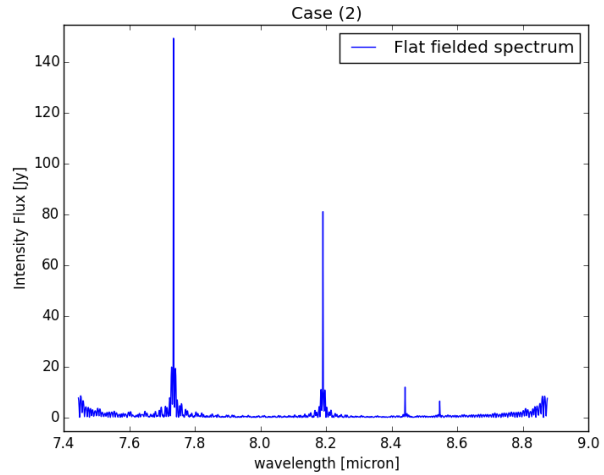


Figure 7.10: Case (2) - Optimization Combination 1 - spectrum from multiplicative method

Graphically, the results obtained are satisfying although there are some artifacts at the extremities. In order to correctly quantify this method, the lines flux approximations have been summarized in Table 7.2. Contrary to the previous Case, this combination does not lead to the best results. It is surprising that this combination of the methods worsen the results as each method provides separately good results. However, it is important to notice that this optimized combination has more accurate matches than the original combination, which proves that applying the Fourier Filtering on the spectrally flat source has a positive influence. However, in this Case, it would preferable to use only one of the two methods which provides better lines flux approximations.

Obtained or observed Value/ Intrinsic Value[%]				
#	Case (2)			
Method	Peak 1	Peak 2	Peak 3	Peak 4
FF	113.37	92.54	88.43	95.05
Mult.	116.38	95.03	90.92	97.27
Combination 1	82.49	70.79	14.12	190.08
Optimization 1	96.29	78.39	77.57	84.79
Obs	118.21	94.93	90.24	80.38

Table 7.2: Optimization of Methods Combination 1- Case (2): Match of peaks flux w.r.t. to Intrinsic Fluxes - The best matches are shown in blue

### Case (3)

The third Case to analyze would be to determine for ranking this combination as it was successful for the first Case but, the opposite appeared with Case (2). The same pattern as depicted previously occurred, namely the filtered spectrally flat source matches the low component left in the residuals data set (cf. Figure 7.13), the amplification factors are thus expected to be equal to 1 except at the spectral features locations.

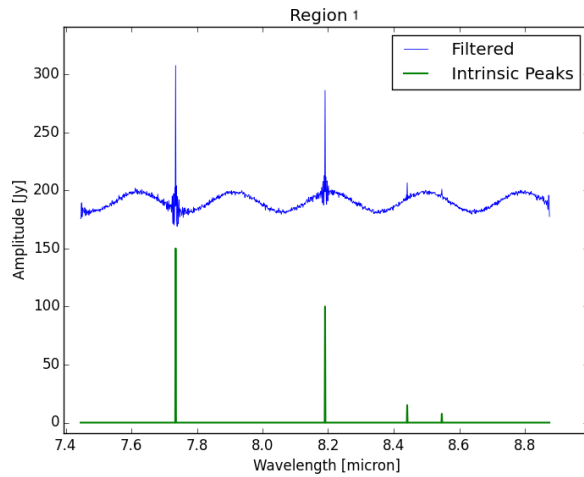


Figure 7.11: Case (3) - Optimization Combination 1 - Filtered Spectrum using the Fourier Filtering of Region 1

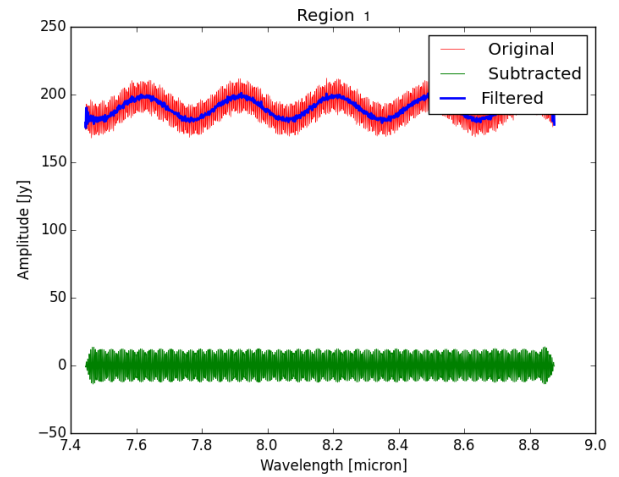


Figure 7.12: Case (3) - Optimization Combination 1 - Spectrally flat source spectrum (i.e. "original"), its Fourier Filtered spectrum using Region 1 (i.e. "Filtered") and the subtracted spectrum resulting from the subtraction of the original flat source spectrum and the Fourier filtered one.

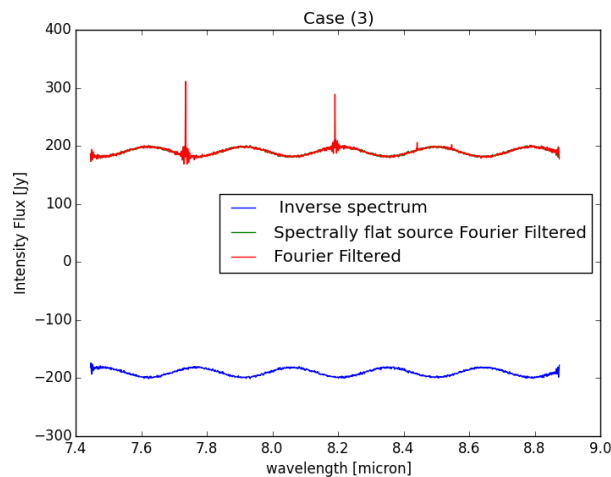


Figure 7.13: Case (3) - Optimization Combination 1 - Filtered spectrally flat source, its inverse and the residuals spectrum from the first method

The final spectrum from multiplicative method (cf. Figure 7.15) is of the same graphical accuracy than when applying the multiplicative method only. It therefore provides satisfying results compared to the initial spectrum, as most all the spectral features are clearly distinguishable, although the weakest one could be confounded with noise. Spectrally speaking the results have not been improved nor worsened by this combination compared to the multiplicative method only.

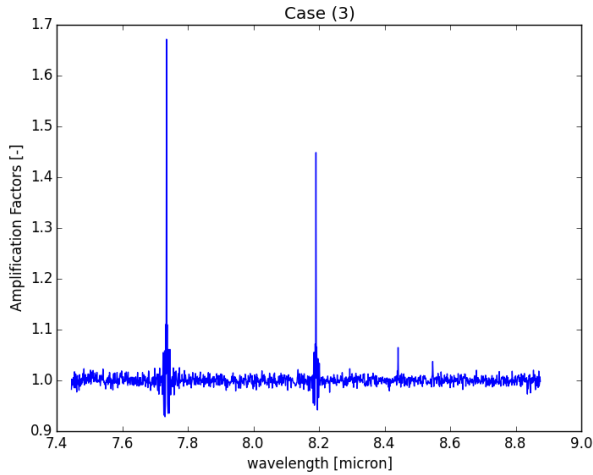


Figure 7.14: Case (3) - Optimization Combination 1 - Amplification factors from the multiplicative method

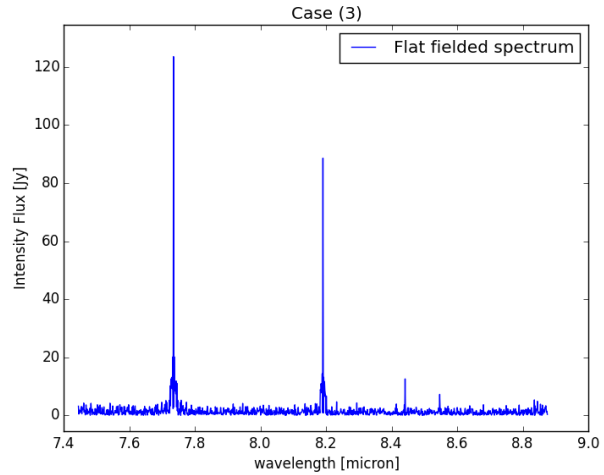


Figure 7.15: Case (3) - Optimization Combination 1 - spectrum from multiplicative method

Comparing the lines flux amplitude will be decisive for classifying this method. The same results as seen for Case (2) are depicted here. Namely, this optimized combination does not improve the lines flux approximations compared to the single methods. For this Case, it would be advised to use the multiplicative method only as it provides the best results (graphically and w.r.t. the lines flux amplitude).

#	Obtained or observed Value/ Intrinsic Value[%]			
	Case (3)			
Method	Peak 1	Peak 2	Peak 3	Peak 4
FF	81.80	84.48	101.16	60.01
Mult.	96.75	101.34	109.06	81.07
Combination 1	72.68	80.13	117.00	25.50
Optimization 1	80.66	87.74	83.38	83.78
Obs	96.41	95.28	105.86	164.95

Table 7.3: Optimization of Methods Combination 1- Case (3): Match of peaks flux w.r.t. to Intrinsic Fluxes - The best matches are shown in blue

### 7.1.2. OPTIMIZATION 2 - Combination 2: Sine Wave fitting - multiplicative method

The second combination to be investigated is the sine wave fitting followed by the multiplicative method. As it was realized for the optimized version of combination 1, the spectrally flat source used as reference of the fringe pattern will also be defringed by the sine-wave fitting method before being used in the multiplicative method.

#### Case (1)

The first step to applied is the Sine-wave fitting on the observed data set and determining its residuals, as shown in Figure 7.16. While 7.17 shows the Sine-wave fitting applied to the spectral flat source spectrum. Both graphical representations can be seen in the next Figure. Compared to Figure 6.14, the spectrally flat source is partially matching the residuals spectrum and the spectrum from multiplicative method is therefore expected to be successful.

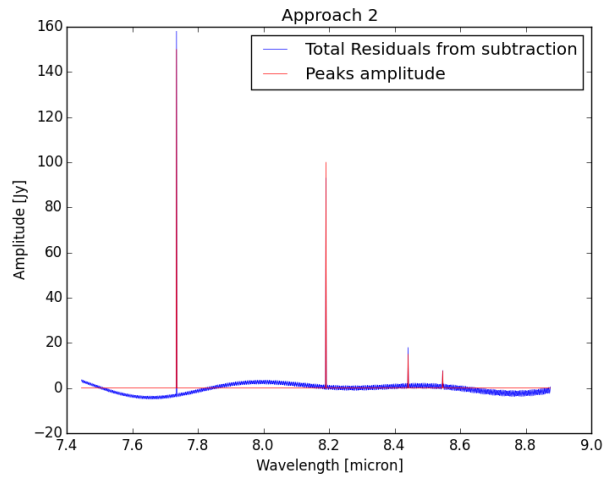


Figure 7.16: Case (1) - Optimization Combination 2 - Filtered Spectrum using the Sine-wave Fitting Approach II

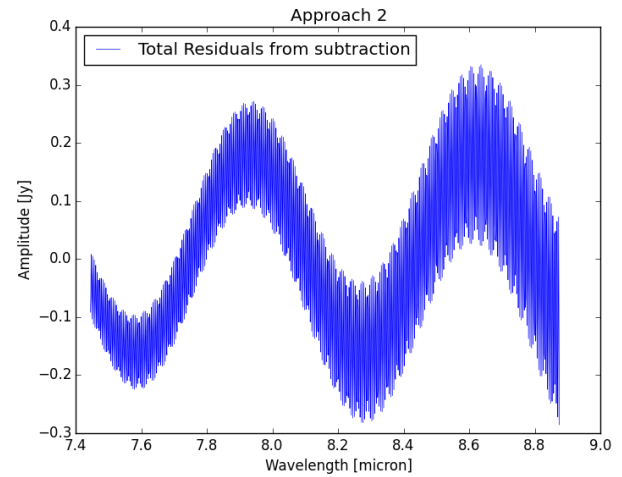


Figure 7.17: Case (1) - Optimization Combination 2 - Spectrally flat source spectrum using the Sine-wave Fitting Approach II

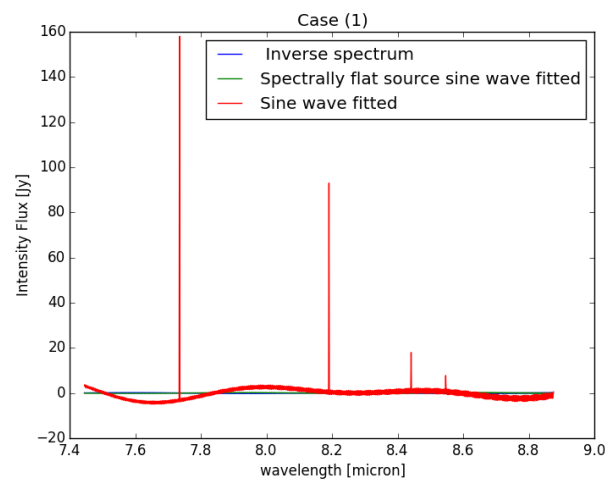


Figure 7.18: Case (1) - Optimization Combination 2 - Spectrally flat source spectrum, its inverse, and the residuals

The amplification factors graph (Figure 7.19) is unexpected as it contains several peaks which are not all related to the known spectral features peaks. However, the final spectrum from the multiplicative method seems reliable as the continuum is nearly flat around zero and the four peaks are clearly positioned. However, a net graphical improvement compared to the new sine-fitted spectrum can not be noticed as the spectrum was already clear from most dominant artifacts.

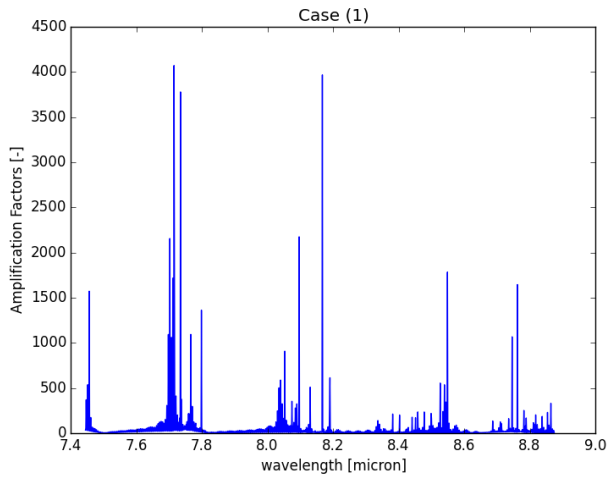


Figure 7.19: Case (1) - Optimization Combination 2 - Amplification factors from the multiplicative method method

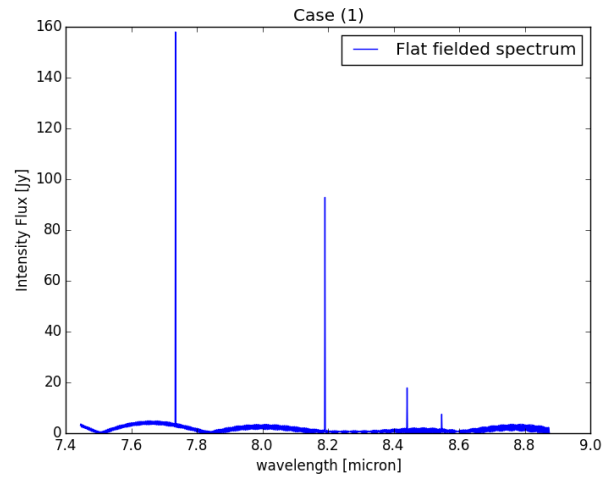


Figure 7.20: Case (1) - Optimization Combination 2 - spectrum from multiplicative method

From Table 7.4, the reader might have noticed that this combination did not improve the lines flux approximations, it actually provides worse result for Peak 3. It would therefore be better for this Case to use the methods independently than combining them.

#	Obtained or observed Value/ Intrinsic Value[%]			
	Case (1)			
Method	Peak 1	Peak 2	Peak 3	Peak 4
SW	107.47	92.57	113.67	93.36
Mult.	96.75	101.34	109.06	81.07
Optimization 2	103.68	92.47	118.94	91.30
Obs	96.41	95.28	105.86	164.95

Table 7.4: Optimization of Methods Combination 2- Case (1): Match of peaks flux w.r.t. to Intrinsic Fluxes - The best matches are shown in blue

### Case (2)

The Case (2) provides less satisfying results with the sine-wave fitting, as strong residual components were still depicted in the final spectrum, as shown in Figure 7.21. The sine-wave model provides similar residuals outcome for the spectrally flat source (Figure 7.22). It appears, therefore, that the combinations of the fringe components makes it more difficult for the sine-wave model to define proper fitting. When comparing the residuals from the observed spectrum and the spectrally flat source, it can be seen that they perfectly match. This would therefore result in excellent spectrum from multiplicative method.

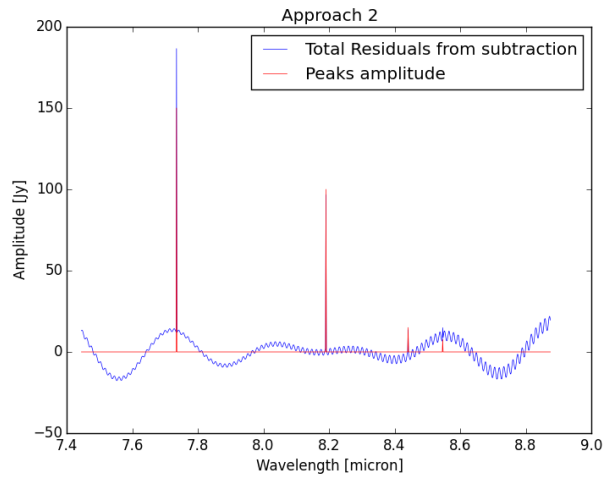


Figure 7.21: Case (2) - Optimization Combination 2 - Filtered Spectrum using the Sine-wave Fitting Approach II

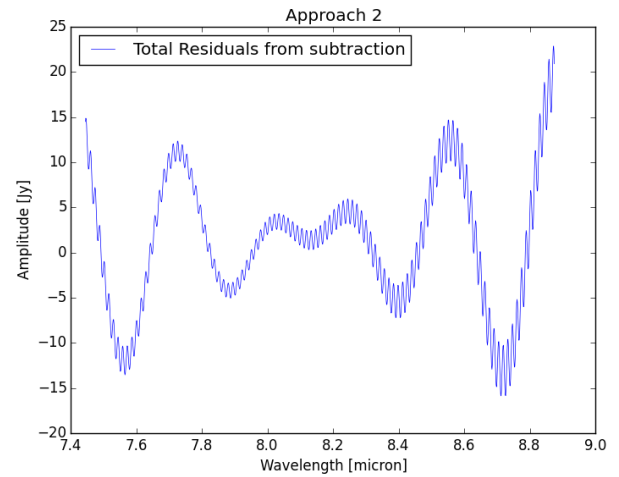


Figure 7.22: Case (2) - Optimization Combination 2 - Spectrally Flat source spectrum using Sine-wave Fitting Approach II

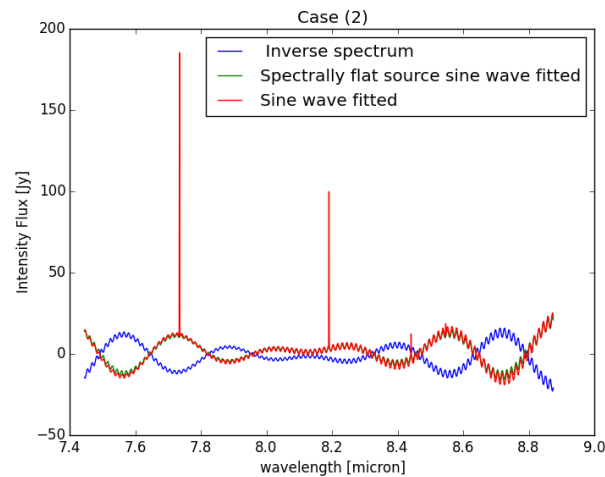


Figure 7.23: Case (2) - Optimization Combination 2 - Spectrally flat source spectrum, its inverse and the residuals

Indeed, as expected from Figure 7.23, the final spectrum shown in Figure 7.25 is excellent and clearly cleans the spectrum from the sine-wave fitting only. The second step of this combination comparison would be to analyze the lines flux approximations, shown in Table 7.5. The results are in general similar to the ones from the Sine-wave fitting, but unfortunately do not surpass the best peaks matches. It would be therefore better for meeting the criteria to use the multiplicative method only.

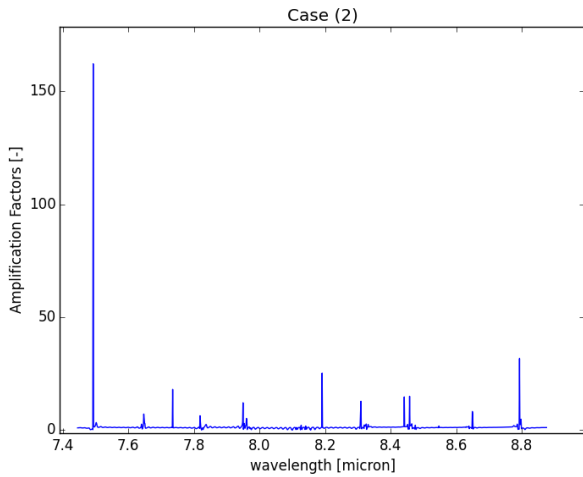


Figure 7.24: Case (2) - Optimization Combination 2 - Amplification factors from the multiplicative method

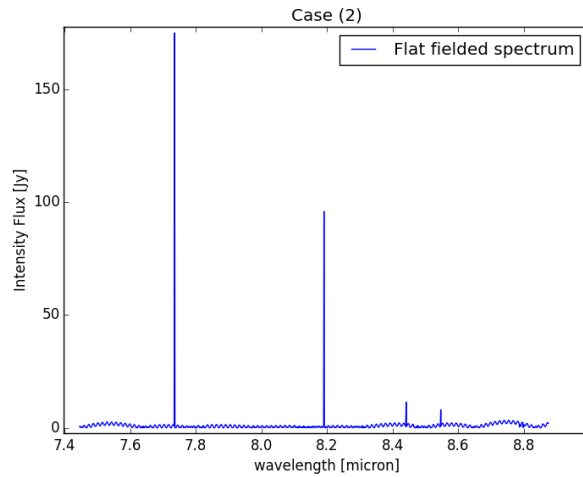


Figure 7.25: Case (2) - Optimization Combination 2 - spectrum from multiplicative method

Obtained or observed Value/ Intrinsic Value[%]				
#	Case (2)			
Method	Peak 1	Peak 2	Peak 3	Peak 4
SW	116.29	95.25	93.23	93.34
Mult.	96.75	101.34	109.06	81.07
Optimization 2	116.36	95.87	72.18	96.26
Obs	96.41	95.28	105.86	164.95

Table 7.5: Optimization of Methods Combination 2- Case (2): Match of peaks flux w.r.t. to Intrinsic Fluxes - The best matches are shown in blue

Case (3)

As has been realized for the previous Cases, the sine-wave fitting method has been applied to the observed spectrum and to the spectrally flat source one, as can be seen in Figures 7.26 and 7.27, respectively. The superimposition of the fitted observed data and the flat source ones (Figure 7.28) predicts good graphical results of the multiplicative method.

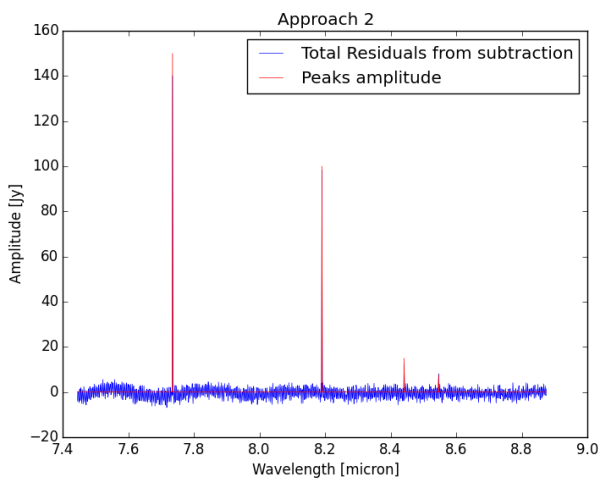


Figure 7.26: Case (3) - Optimization Combination 2 - Filtered Spectrum using the Sine-wave Fitting Approach II

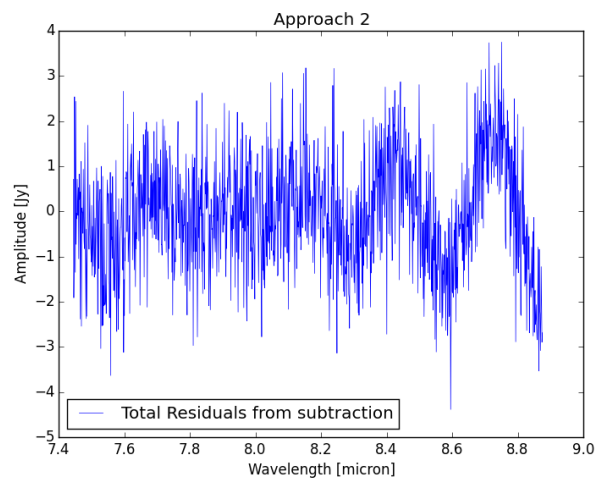


Figure 7.27: Case (3) - Optimization Combination 2 - Spectrally flat source spectrum using the Sine-wave fitting Approach II

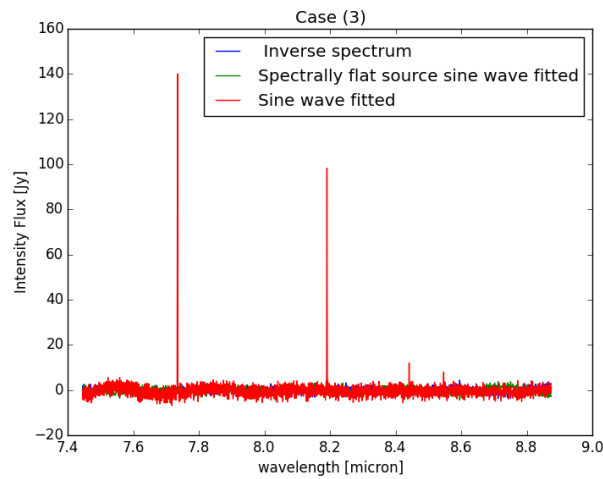


Figure 7.28: Case (3) - Optimization Combination 2 - Spectrally flat source spectrum, its inverse and the residuals

As shown in Figure 7.30, the final spectrum from multiplicative method is slightly improved compared the one after the sine-wave fitting. The continuum is flat and close to zero, but the noise is still present in the spectrum and the weak spectral features can easily be confounded with the noise. However, when applying the multiplicative method only, this problem was already depicted.

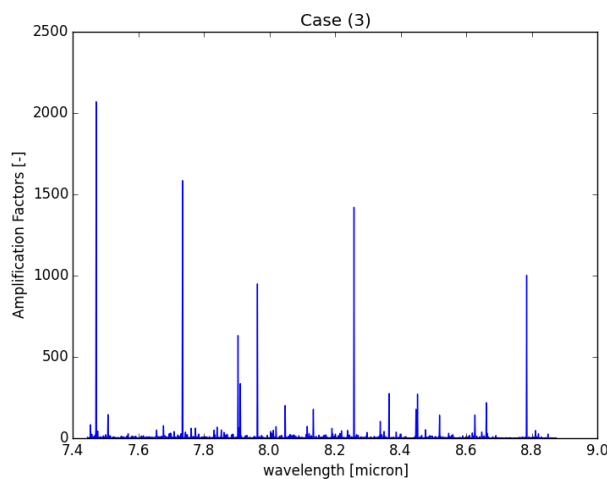


Figure 7.29: Case (3) - Optimization Combination 2 - Amplification factors from the multiplicative method

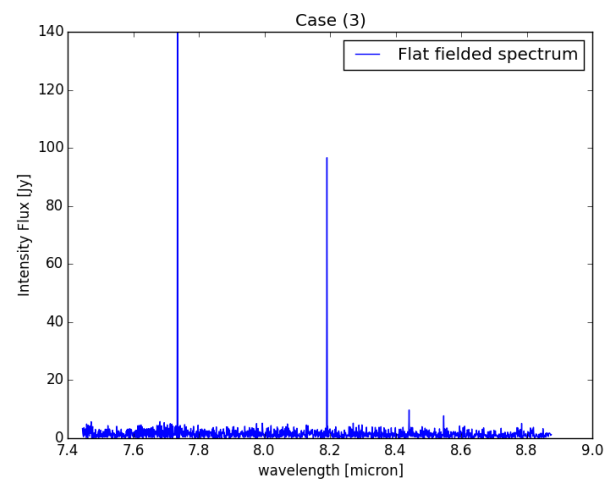


Figure 7.30: Case (3) - Optimization Combination 2 - spectrum from multiplicative method

The peaks matches for this Case are converging to a specific method. Indeed, in Table 7.6, this optimization provides worse results than the application of single method, this bad ranking is mostly due to the third peak offset of 40 %, which is non-negligible. For this Case, it would not be advised to use this combination, but the multiplicative method only would be preferable.

#	Obtained or observed Value/ Intrinsic Value[%]			
	Case (3)			
Method	Peak 1	Peak 2	Peak 3	Peak 4
SW	94.09	98.28	97.41	111.42
Mult.	96.75	101.34	109.06	81.07
Optimization 2	93.26	95.86	60.50	94.90
Obs	96.41	95.28	105.86	164.95

Table 7.6: Optimization of Methods Combination 2- Case (3): Match of peaks flux w.r.t. to Intrinsic Fluxes - The best matches are shown in blue

### 7.1.3. Conclusion

In Section 7.1, the two method's combinations have been improved by applying the first method to the fringe model used in the multiplicative method. Again, two criteria were considered for quantifying these optimizations: the graphical representation and the line flux approximations of the spectral features. This specific method's order was considered for obtained the best results, as if the methods order was inverse, the outcome is expected to be worse. Indeed, if the multiplicative method, which leads to flat continuum spectrum, is applied; then fitting for example a sine wave to this new data from the multiplicative method will not be concluding.

The goal of using the two methods in combinations was to obtain their positive attributes; namely the good graphical representation of the multiplicative method and the good lines flux approximations from the Sine-wave fitting or the Fourier Filtering. For both combinations, the simulations worked as expected graphically, as the resulting spectra have a (nearly) flat continuum of zero and the spectral features are clearly distinguishable.

For the first optimized combination, the residuals left have a strong low frequency component and the multiplicative method allows to remove it leading to a cleaner spectrum. While, for the second optimization, the residuals left do not show in general a dominant frequency component. Therefore, the final spectrum from the multiplicative method is not considerably improved from the sine-wave fitting spectrum. However, it appears that the stronger are the residuals left in the spectrum (i.e. less accurate is the sine-wave fitting), the better is the graphical improvement after the multiplicative method for this combination. The spectral features detectability is described by the SNR of Table 7.7. The optimizations provide, on average, better SNR than the single method (Multiplicative method excluded) and improve considerably the detectability compared to the one of the observed spectrum. Although the final spectrum of Opti. 2 does not seem to be highly improved, as discussed previously, compared to Opti. 1, its detectability is higher in all cases.

#	SNR [-]											
	Case (1)				Case (2)				Case (3)			
Method	Peak 1	Peak 2	Peak 3	Peak 4	Peak 1	Peak 2	Peak 3	Peak 4	Peak 1	Peak 2	Peak 3	Peak 4
FF	12.03	9.77	2.13	1.98	7.34	4.90	1.41	1.25	11.07	7.77	1.71	1.30
SW	111.17	34.7	6.36	2.44	84.55	13.71	1.44	2.16	110.76	31.29	5.74	2.60
Mult.	inf.	inf.	inf.	inf.	inf.	inf.	inf.	inf.	174.17	95.30	11.02	6.10
Opti. 1	48.98	32.89	7.01	4.37	15.66	10.14	1.95	1.87	34.71	29.01	4.93	3.29
Opti. 2	111.89	66.34	12.36	4.68	119.76	94.96	11.53	7.46	68.52	44.02	5.92	4.08
Obs.	20.00	9.01	2.13	1.14	5.25	2.67	0.49	0.49	7.57	5.14	0.53	1.11

Table 7.7: All cases- All single methods and optimized combinations : Signal to Noise Ratio - In red: poor detection, In black: acceptable detection and In Blue: excellent detection

The second point of interest is then to analyze the lines flux approximations at specific locations, namely where the spectral features were intentionally introduced in the original spectrum. The peaks amplitude comparison with the intrinsic ones are displayed in Table 7.8. For each peak, the best match has been colored by the blue color and

matches within 1 % deviation of the best match were colored in green. Graphical representations of the data from Table 7.8 are shown in Figures 7.31 and 7.32, which display comparison among the optimized combined methods and observed data and among all the methods studied at this stage, respectively.

#	Obtained or observed Value/ Intrinsic Value[%]											
	Method	Case (1)				Case (2)				Case (3)		
	Peak 1	Peak 2	Peak 3	Peak 4	Peak 1	Peak 2	Peak 3	Peak 4	Peak 1	Peak 2	Peak 3	Peak 4
FF	102.24	87.93	103.82	105.83	113.37	92.54	88.43	95.05	81.80	84.48	101.16	60.01
SW	107.47	92.57	113.67	93.36	116.29	95.25	93.23	93.34	94.09	98.28	97.41	111.42
Mult.	107.70	92.61	109.10	110.77	116.38	95.03	90.92	97.27	96.75	101.34	109.06	81.07
Combi. 1	98.08	82.65	59.36	110.9	82.49	70.79	14.12	190.08	72.68	80.13	117.00	25.50
Opti. 1	102.22	87.94	103.69	104.89	96.29	78.39	77.57	84.79	80.66	87.74	83.38	83.78
Combi. 2	n.d.	n.d.	n.d.	n.d.	n.d.	n.d.	n.d.	n.d.	n.d.	n.d.	n.d.	n.d.
Opti. 2	103.68	92.47	118.94	91.30	116.36	95.87	72.18	96.26	93.26	95.86	60.50	94.90
Obs	110.9	97.9	140.3	93.04	118.21	94.93	90.24	80.38	96.41	95.28	105.86	164.95

Table 7.8: All Optimized Combinations: Match of peaks flux w.r.t. to Intrinsic Fluxes - The best matches are shown in blue and values close by 1% to the best matches are shown in green

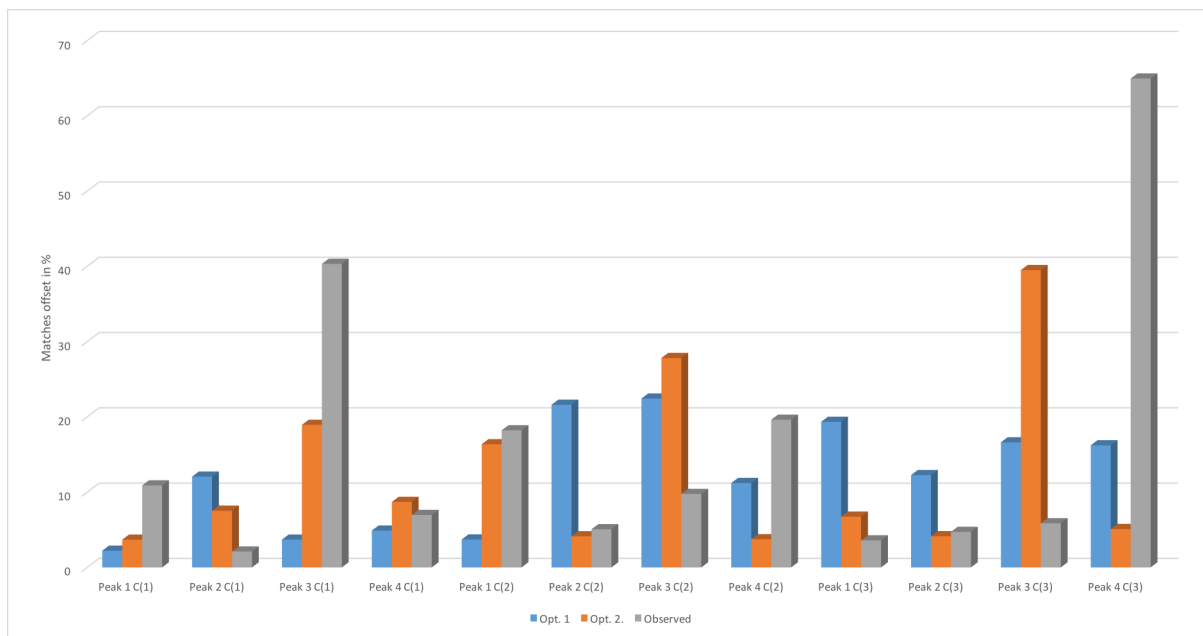


Figure 7.31: All Optimized Combinations: Match of peaks flux w.r.t. to Intrinsic Fluxes - Graphical Representation

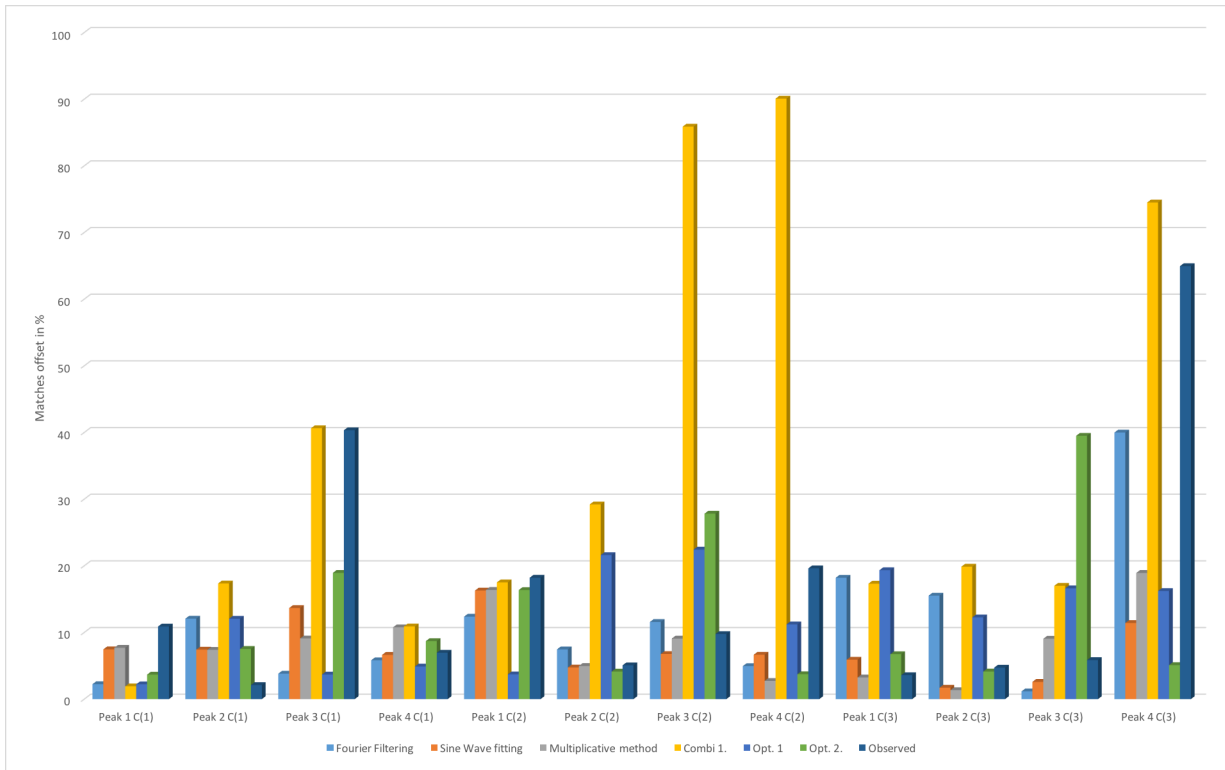


Figure 7.32: All methods investigated at this stage: Match of peaks flux w.r.t. to Intrinsic Fluxes - Graphical Representation

From this Table, at first sight, the method having the most matches is the Fourier Filtering, followed with four matches over 12 by the multiplicative method and the Optimization 1. However, the number of matches is not the only point of focus, the standard deviation of their offsets was also considered. In Table 7.9, it can be seen that the best values are for the Sine-wave fitting, which shows the most constant approximations. In other words, this method might not have the highest number of best matches, but on average, its approximations do not highly differ from the expected values and are constant. This method is followed by the multiplicative method and then the Optimization 1. Furthermore, even-though the Fourier filtering method shows the highest number of best matches, its standard deviation is the worst of all methods. This method does not show a consistency and cannot be considered as reliable. Moreover, from the two tables, it can be clearly seen that both optimizations do not lead to better lines flux approximations than using the method independently, but the optimization 1 surpasses the second one. Finally, the reader might also notice that whatever the method, the results obtained are of a better accuracy than the ones observed.

# Method	Standard Deviation
FF	12.08
SW	4.27
Mult.	5.25
Opti. 1	7.29
Opti. 2	11.44
Obs	18.70

Table 7.9: All Optimized Combinations: Standard Deviation and Average of offset values for all Cases

## 7.2. Single

The second part of the optimization consists of improving the single method and not combined ones as previously.

### 7.2.1. OPTIMIZATION 3 - Sine Wave Fitting

The single method to be developed is the sine wave fitting. As the reader might know, this method consists of the sine wave subtraction from the original spectrum. It was seen that this method provided satisfactory results with the lowest standard deviation w.r.t. the expected results. However, graphically, this method was not optimal and the multiplicative method, based on the division of the spectrally flat source and the spectrum, led to better graphical representations. Therefore, it was decided for the optimization to not subtract the fitted sine wave, but to divide the spectrum by it. First tests were conducted by simply applying the Equation (7.1) to the data set. However, the first tests were not conclusive as they led to only amplification factors.

$$NewSpectrum = \frac{observed}{SWfitted} \quad (7.1)$$

In theory, the spectral features are (de-)amplified by the fringes and then added on top of them, therefore, it was missing a subtraction term in Equation (7.1), which was corrected by Equation (7.2).

$$NewSpectrum = \frac{observed - SWfitted}{SWfitted} \quad (7.2)$$

Testing this new model led to clear spectrum, but the lines flux were incorrectly estimated. The idea was therefore to multiply the spectrum by the amplification generated by the fitted sine-wave. In other words, Equation (7.2) was multiplied by the baseline of the combined fitted sine wave. The Equation used for this optimization is shown in Equation (7.3).

$$NewSpectrum = \frac{observed - SWfitted}{SWfitted} \cdot Baseline \quad (7.3)$$

In which,

*observed* is the entire observed spectrum  
*SWfitted* is the summation of the fitted sine waves for the low and high frequency components  
*Baseline* is the baseline of the *SWfitted*

#### Case (1)

The first step for this method is to determine the sine wave fitting for each frequency components as can be seen in Figures 7.33-7.34.

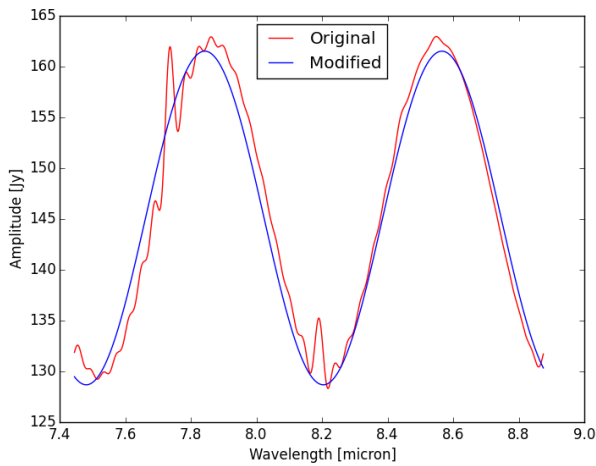


Figure 7.33: Case (1) - Optimization 3 - Sine wave fitting for the low frequency component

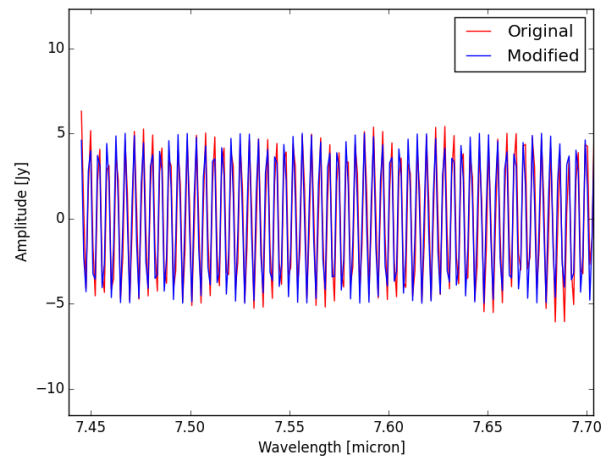


Figure 7.34: Case (1) - Optimization 3 - Sine wave fitting for the high frequency component - zoom

Once the fitted sine waves have been determined, these are added together for forming the "*SW fitted*" and Equation (7.3) can be applied. The final Spectrum is seen in Figure 7.35.

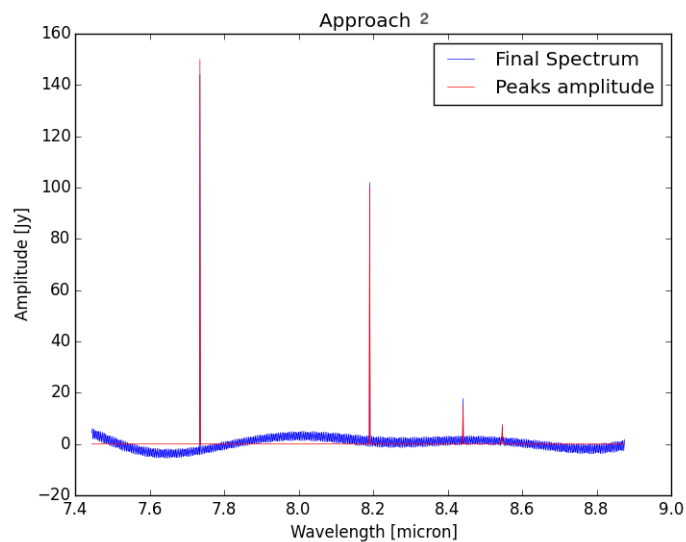


Figure 7.35: Case (1) - Optimization 3 - final spectrum

As can be seen in the previous Figure, the spectrum is in general cleaned, although small low frequency residuals are still left, as was the case when applying the Sine-wave fitting only. Furthermore, the spectral features are clearly distinguishable. Concerning, the amplitude match of the spectral features, one can look at Table 7.10. This optimization provides better matches for the strong spectral features than the other methods. However, one might notice the poor match for the weakest spectral features (i.e. offset deviation of 24.4%).

#	Obtained or observed Value/ Intrinsic Value[%]			
	Case (1)			
Method	Peak 1	Peak 2	Peak 3	Peak 4
SW	107.47	92.57	113.67	93.36
Mult.	96.75	101.34	109.06	81.07
Optimization 3	97.64	100.84	108.89	75.60
Obs	96.41	95.28	105.86	164.95

Table 7.10: Optimization 3 - Case (1): Match of peaks flux w.r.t. to Intrinsic Fluxes - The best matches are shown in blue

### Case (2)

As realized for the previous Case, the different frequency components were extracted from the observed spectrum and sine-wave fitted, as depicted in Figures 7.36-7.37. The reader is advised to look at Section 4.3 for deeper explanations of the sine-wave fitting method.

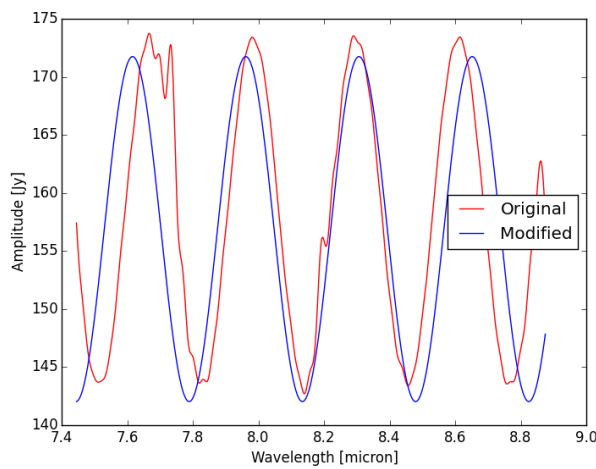


Figure 7.36: Case (2) - Optimization 3 - Sine wave fitting for the low frequency component

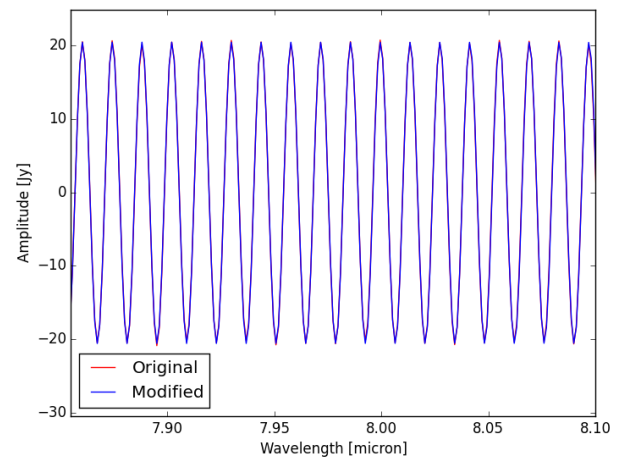


Figure 7.37: Case (2) - Optimization 3 - Sine wave fitting for the high frequency component - zoom

The summed up "*SW fitted*" is then used as this new model for determining the new spectrum shown in Figure 7.38. From this Figure, it is clear that the graphical representation is not meeting the expectations, namely having a flat spectrum at locations with none of the spectral features. But, the reader might have noticed that the final spectrum is similar to the one from the sine-wave fitting method only.

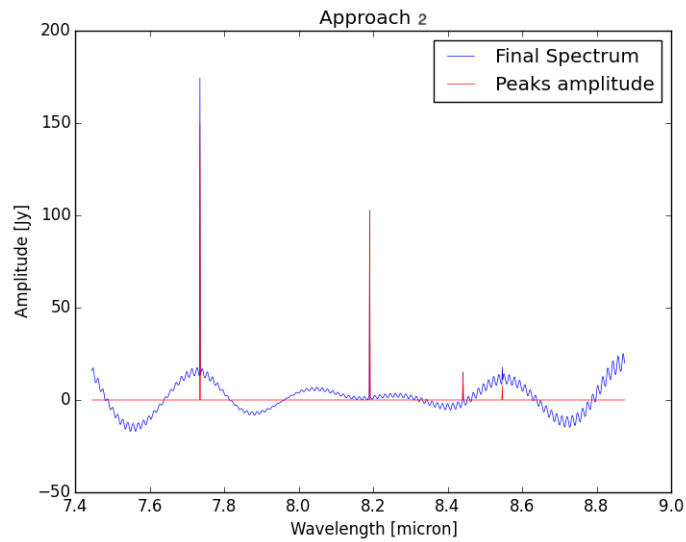


Figure 7.38: Case (2) - Optimization 3 - final spectrum

However, when analyzing the spectral features amplitude match with the intrinsic values (Table 7.11), it is clear that this method provides excellent results for most of the peaks and is obviously improving the results obtained by the single defringing methods.

#	Obtained or observed Value/ Intrinsic Value[%]			
	Case (2)			
Method	Peak 1	Peak 2	Peak 3	Peak 4
SW	116.29	95.25	93.23	93.34
Mult.	96.75	101.34	109.06	81.07
Optimization 3	107.47	100.78	101.28	101.77
Obs	96.41	95.28	105.86	164.95

Table 7.11: Optimization 3 - Case (2): Match of peaks flux w.r.t. to Intrinsic Fluxes - The best matches are shown in blue

### Case (3)

The last case to analyze is the most complex one as it embodies not only the fringes, but also extra noise. Figures 7.39-7.40 show the sine wave fitting for the low and high frequency components, respectively. While in Figure 7.41, the final spectrum can be visualized. As it was seen for the two previous Cases, the final spectrum has the same overall shape than the ones found with the application of the sine-wave fitting only.

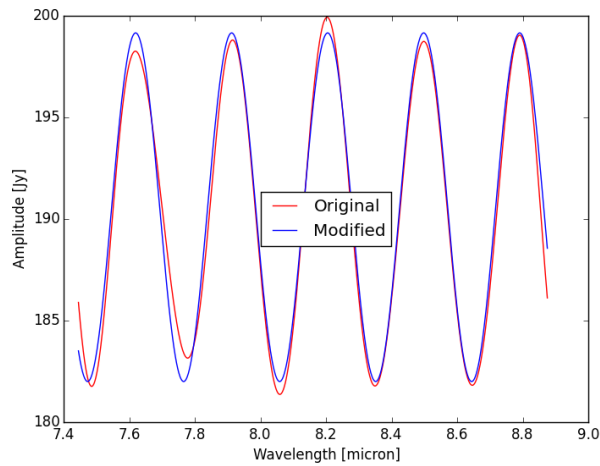


Figure 7.39: Case (3) - Optimization 3 - Sine wave fitting for the low frequency component

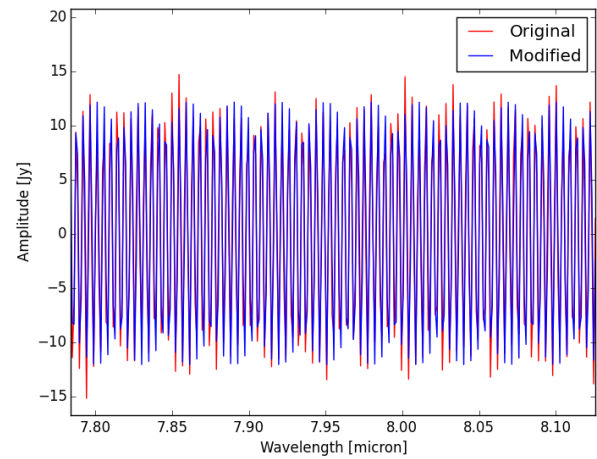


Figure 7.40: Case (3) - Optimization 3 - Sine wave fitting for the high frequency component - zoom

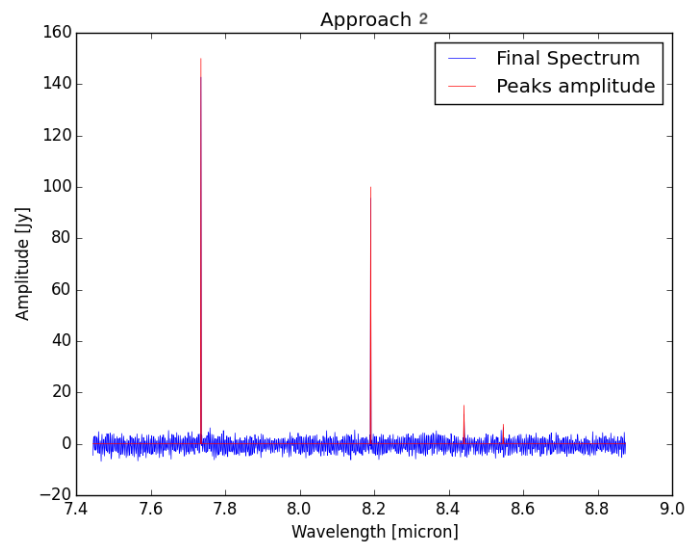


Figure 7.41: Case (3) - Optimization 3 - final spectrum

The distinction between this method and the sine-wave fitting is then seen in the spectral features match with the intrinsic values. As shown in Table 7.12, the results are not as excellent as for Case (2). For this Case, it would be preferable to use the multiplicative method only. Although the results for the strong spectral features are in general satisfying, the offset of peak 3 of 30.77 % is non-negligible and represents the largest offset of the three defringing methods shown in this Table.

#	Obtained or observed Value/ Intrinsic Value[%]			
	Case (3)			
Method	Peak 1	Peak 2	Peak 3	Peak 4
SW	94.09	98.28	97.41	111.42
Mult.	96.75	101.34	109.06	81.07
Optimization 3	95.41	97.09	69.23	104.41
Obs	96.41	95.28	105.86	164.95

Table 7.12: Optimization 3- Case (3): Match of peaks flux w.r.t. to Intrinsic Fluxes - The best matches are shown in blue

### 7.2.2. OPTIMIZATION 4 - multiplicative method

The optimization of the multiplicative method is nearly similar to the optimization 3. Indeed, the structure of Equation (7.3) is maintained, but the data set from the sine-wave fitting is replaced by the one from the multiplicative method, as shown in Equation (7.4).

$$NewSpectrum = \frac{observed - FlatSource}{FlatSource} \cdot Baseline \quad (7.4)$$

In which,

*observed* is the entire observed spectrum  
*FlatSource* is the spectrally flat source spectrum  
*Baseline* is the baseline of the *FlatSource*

However, contrary to the multiplicative method described previously, the Flat source considered also includes some noise for Cases (1) and (2). It was decided for this simulation to include some noise to the spectrally flat source for simulating a realistic environment, as the spectrally flat source file provided for MIRI includes some noise components. For this optimization, the spectrally flat source considered is a so-called 'raw-input', which means that the data set has not been perfectly cleaned from artifacts other than fringes (i.e. level 3 data type).

#### Case (1)

The first step of this method consists of retrieving data, namely the spectrally flat source and the observed data as seen in Figure 7.42. Then, Equation (7.4) is applied leading to the final spectrum shown in Figure 7.43. As can be seen in this last figure, the fringes have been removed leading to a nearly flat spectrum. Furthermore, the spectral features are clearly distinguishable, although some noise is still present in the final graph. This noise is obviously due to the one from the spectrally flat source. Therefore, if preliminary work is realized on the data for perfectly removing non-fringes related artifacts, the final spectrum would be expected to be more flat (i.e. more comparable to the one in Section 4.4.2).

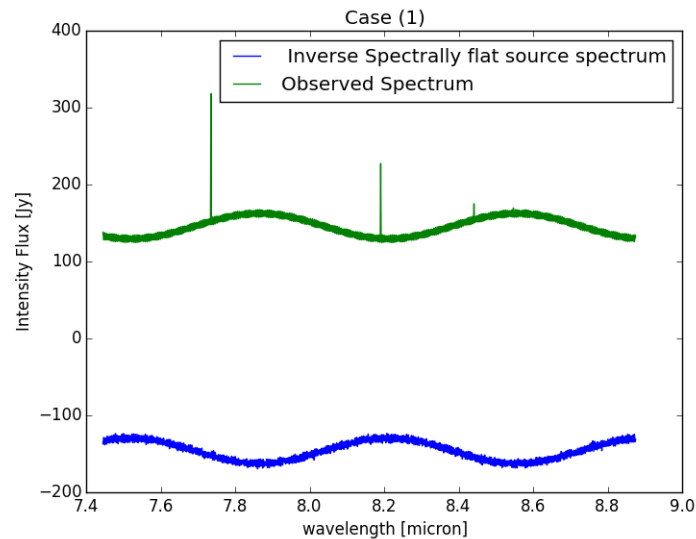


Figure 7.42: Case (1) - Optimization 4 - observed spectrum and Spectrally flat source spectrum with extra noise included.

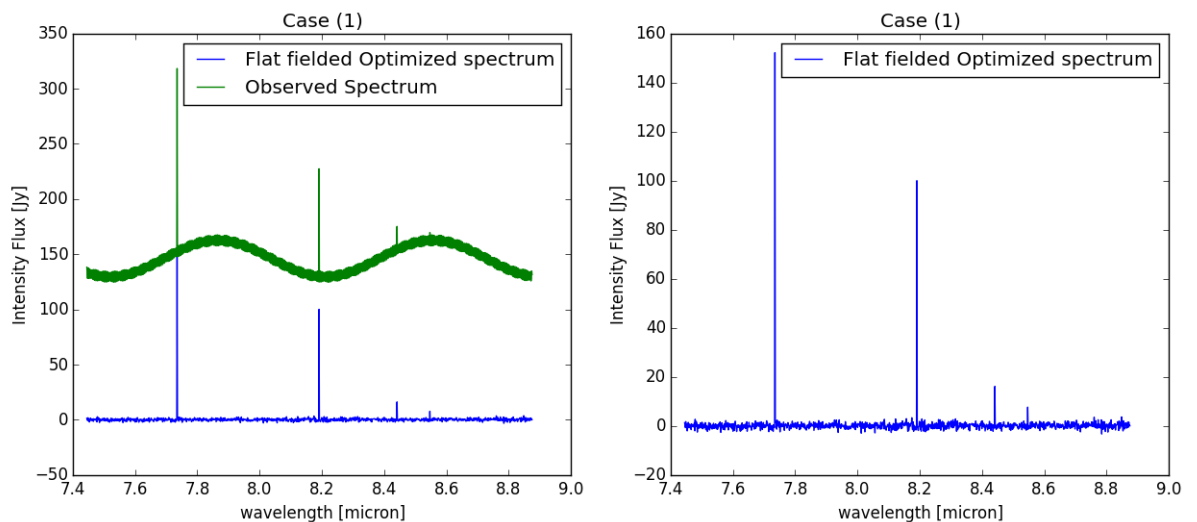


Figure 7.43: Case (1) - Optimization 4 - final spectrum

When analyzing the peaks amplitude match (Table 7.13), one can state that this method clearly improves the amplitudes approximations compared to the observed ones and the ones from the multiplicative method. It is expected to provide better results if the spectrally flat source is perfectly clean.

#	Obtained or observed Value/ Intrinsic Value[%]			
	Case (1)			
Method	Peak 1	Peak 2	Peak 3	Peak 4
Mult.	96.75	101.34	109.06	81.07
Optimization 4	101.27	101.72	114.91	117.98
Obs	96.41	95.28	105.86	164.95

Table 7.13: Optimization 4 - Case (1): Match of peaks flux w.r.t. to Intrinsic Fluxes - The best matches are shown in blue

### Case (2)

As done for Case (1), the spectrally flat source of Case (2) was used in Equation (7.4) to provide the final spectrum, shown in Figure 7.45. Once again, the final spectrum is removed from the main fringes components but, some noise

is still noticeable. The spectral features can clearly be identified; however, the reader might notice that extremely weak spectral features would still be impossible to detect due to the presence of noise in the final spectrum. It would therefore be advised to clean the spectrally flat source from artifacts beforehand. Concerning the amplitude match shown in Table 7.14, the results are not as straight-forward as for Case (1), although in general, it provides the most constant satisfactory results. This optimization would therefore be advised for this Case.

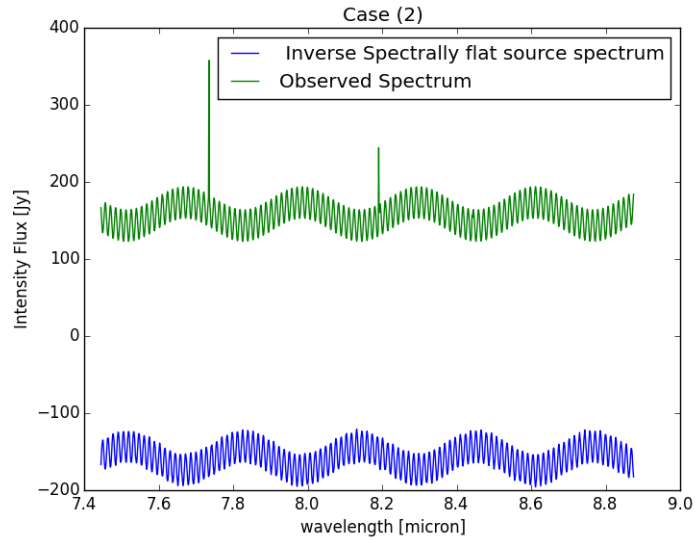


Figure 7.44: Case (2) - Optimization 4 - observed spectrum and Spectrally flat source spectrum with extra noise included.

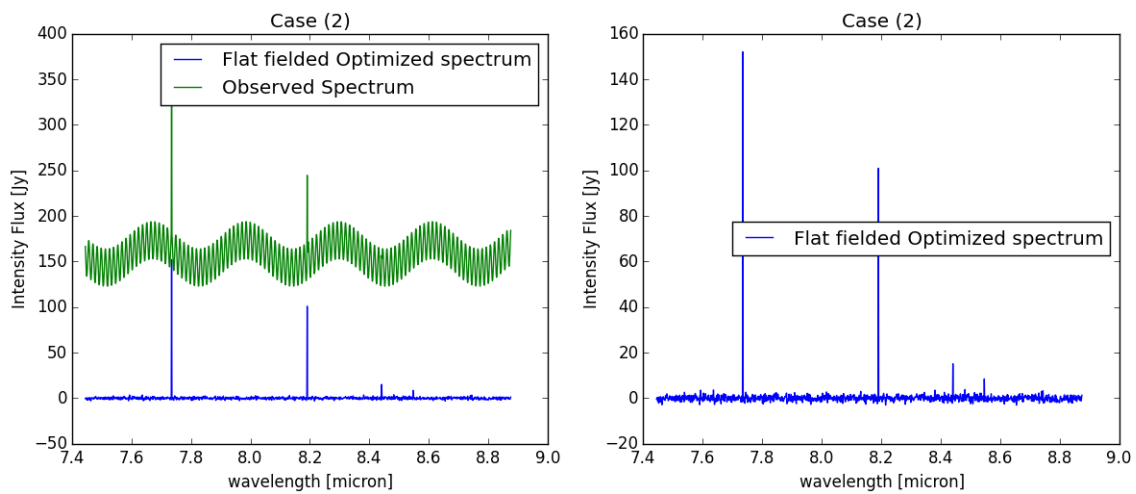


Figure 7.45: Case (2) - Optimization 4 - final spectrum

Obtained or observed Value/ Intrinsic Value[%]				
#	Case (2)			
Method	Peak 1	Peak 2	Peak 3	Peak 4
SW	116.29	95.25	93.23	93.34
Mult.	96.75	101.34	109.06	81.07
Optimization 4	99.51	101.55	89.88	109.89
Obs	96.41	95.28	105.86	164.95

Table 7.14: Optimization 4 - Case (2): Match of peaks flux w.r.t. to Intrinsic Fluxes - The best matches are shown in blue

## Case (3)

In Figure 7.46, it is clear that the weak spectral features are hardly noticeable; they seem to be absorbed by not only the fringes, but also the noise left in the observed spectrum. When looking closer at Figure 7.47, which displays the final spectrum found with the model of Equation (7.4), graphical improvement can be noticed. Indeed, the main fringes elements are removed allowing to distinguish the weakest spectral features with ease. However, as it was pointed for the previous Cases, the noise from the spectrally flat source reduces the final graphical quality of the spectrum and strong pre-processing of this spectrally flat source would be advised.

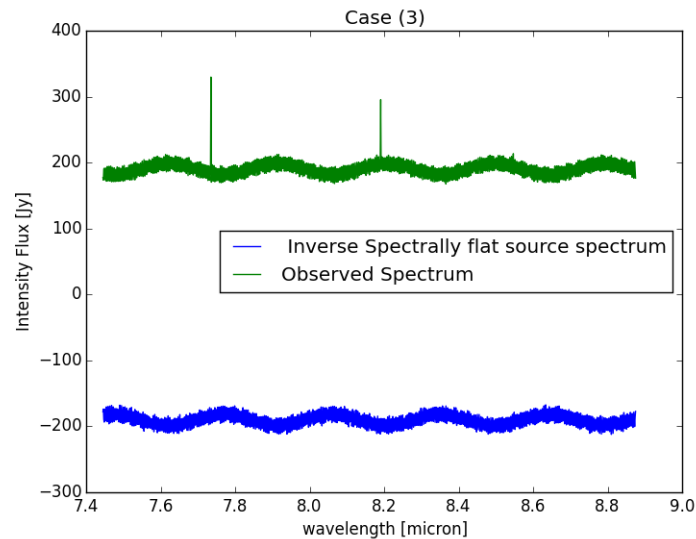


Figure 7.46: Case (3) - Optimization 4 - observed spectrum and Spectrally flat source spectrum with extra noise included.

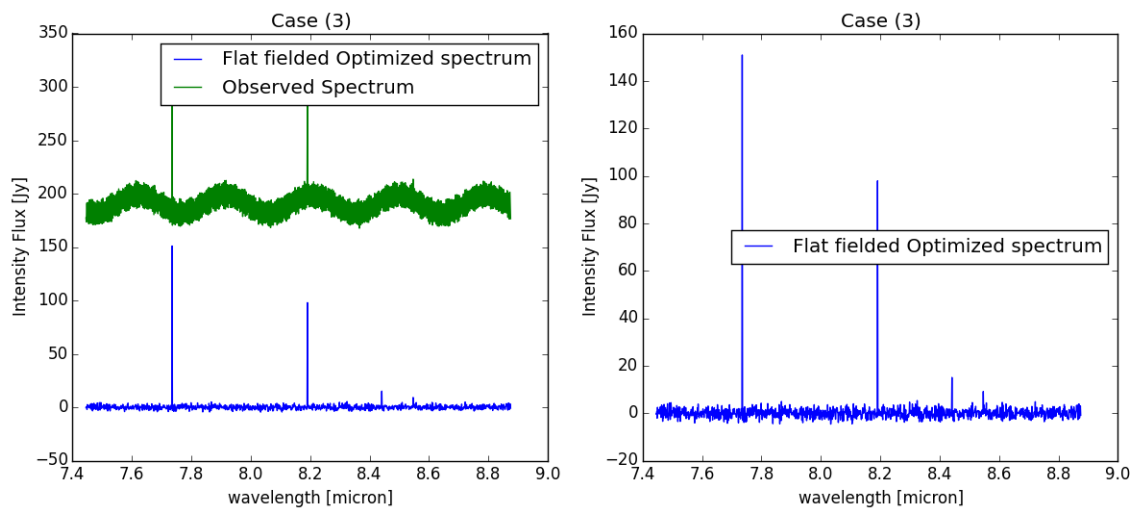


Figure 7.47: Case (3) - Optimization 4 - final spectrum

The analysis of the amplitude matches, shown in Table 7.15, is similar to the one of Case (2), namely the optimization does not provide the best matches for all peaks. But, it provides constant satisfactory results and can be considered as a reliable defringing method.

#	Obtained or observed Value/ Intrinsic Value[%]			
	Case (3)			
Method	Peak 1	Peak 2	Peak 3	Peak 4
SW	94.09	98.28	97.41	111.42
Mult.	96.75	101.34	109.06	81.07
Optimization 4	101.93	98.58	104.44	108.46
Obs	96.41	95.28	105.86	164.95

Table 7.15: Optimization 3- Case (3): Match of peaks flux w.r.t. to Intrinsic Fluxes - The best matches are shown in blue

### 7.2.3. Conclusion

In Section 7.2, two out of the three single defringing methods developed in Chapter 4 were optimized. For the first optimization (i.e. Optimization 3), the goal was to obtain a flat spectrum by dividing the observed spectrum (i.e. multiplicative method principle) and to optimize the spectral features amplitude by using the sine-wave fitting method. However, for this method it was seen that the graphical representation of the spectrum was not improved compared to the spectra obtained with the sine-wave fitting method only. However, a significant improvement of the peak's amplitude was noticed.

The outcome of this optimization was the inspiration for the second single optimization (i.e. optimization 4), which explains the same equation used for both simulations. Indeed, if the graphical properties of the multiplicative method could be conserved and the peak's amplitude improved, the goal of the optimization would be reached. However, for this simulation, as explained in Subsection 7.2.2, it was decided to add noise in the spectrally flat source, contrarily than for the multiplicative method only.

In Table 7.16, the SNR ratio of these optimizations can be seen, this criterion allows to quantify the detectability of the spectral features. It is clear from this Table that the optimization improves the spectral features detection compared to the observed spectrum. Moreover, the second optimized method has better SNR than the first optimization. It is interesting to notice that the detectability is better for the Sine-wave fitting method only than using the optimization 3. However, for all the two optimized single methods, the detectability is considerably better than the ones from the observed spectrum. This aligned with the conclusion of a cleaner spectrum obtained by the optimized defringing methods.

#	SNR [-]											
	Case (1)				Case (2)				Case (3)			
Method	Peak 1	Peak 2	Peak 3	Peak 4	Peak 1	Peak 2	Peak 3	Peak 4	Peak 1	Peak 2	Peak 3	Peak 4
FF	12.03	9.77	2.13	1.98	7.34	4.90	1.41	1.25	11.07	7.77	1.71	1.30
SW	111.17	34.7	6.36	2.44	84.55	13.71	1.44	2.16	110.76	31.29	5.74	2.60
Mult.	inf.	inf.	inf.	inf.	inf.	inf.	inf.	inf.	174.17	95.30	11.02	6.10
Opt. 3	50.05	34.05	5.40	1.74	38.03	9.56	1.92	1.15	26.15	18.63	2.66	1.92
Opt. 4	81.68	52.06	7.44	4.15	97.59	60.48	9.56	4.68	45.53	30.02	4.23	3.36
Obs.	20.00	9.01	2.13	1.14	5.25	2.67	0.49	0.49	7.57	5.14	0.53	1.11

Table 7.16: All cases- All single methods and optimized combinations : Signal to Noise Ratio - In red: poor detection, In black: acceptable detection and In Blue: excellent detection

Table 7.17 summarizes all the peaks match w.r.t. the intrinsic values in % for the single optimizations and the single methods, in comparison with the observed values. The best match are pointed in blue in the Table and the values varying of maximum 1 % from the best match are pointed in green. From this Table, as expected, it is clear that both optimizations provide the best results, especially the last one with six excellent matches over twelve, in addition of the cleaned spectra provided by this method. Furthermore, as stated before, if the spectrally flat spectrum used is cleaned from artifacts, the results are expected to be more conclusive graphically and quantitatively. These

optimizations are, therefore, considered as reliable and more optimal than the single methods develop before.

#	Obtained or observed Value/ Intrinsic Value[%]											
	Case (1)				Case (2)				Case (3)			
	Peak 1	Peak 2	Peak 3	Peak 4	Peak 1	Peak 2	Peak 3	Peak 4	Peak 1	Peak 2	Peak 3	Peak 4
FF	102.24	87.93	103.82	105.83	113.37	92.54	88.43	95.05	81.80	84.48	101.16	60.01
SW	107.47	92.57	113.67	93.36	116.29	95.25	93.23	93.34	94.09	98.28	97.41	111.42
Mult.	107.70	92.61	109.10	110.77	116.38	95.03	90.92	97.27	96.75	101.34	109.06	81.07
Opti. 3	97.64	100.84	108.89	75.60	107.47	100.78	101.28	101.77	95.41	97.09	69.23	104.41
Opti. 4	101.93	98.58	104.44	108.46	99.51	101.55	89.88	109.89	101.27	101.72	114.91	117.98
Obs	110.9	97.9	140.3	93.04	118.21	94.93	90.24	80.38	96.41	95.28	105.86	164.95

Table 7.17: Optimized and non-optimized single methods : Match of peaks flux w.r.t. to Intrinsic Fluxes - The best matches are shown in blue and values close by 1% to the best matches are shown in green

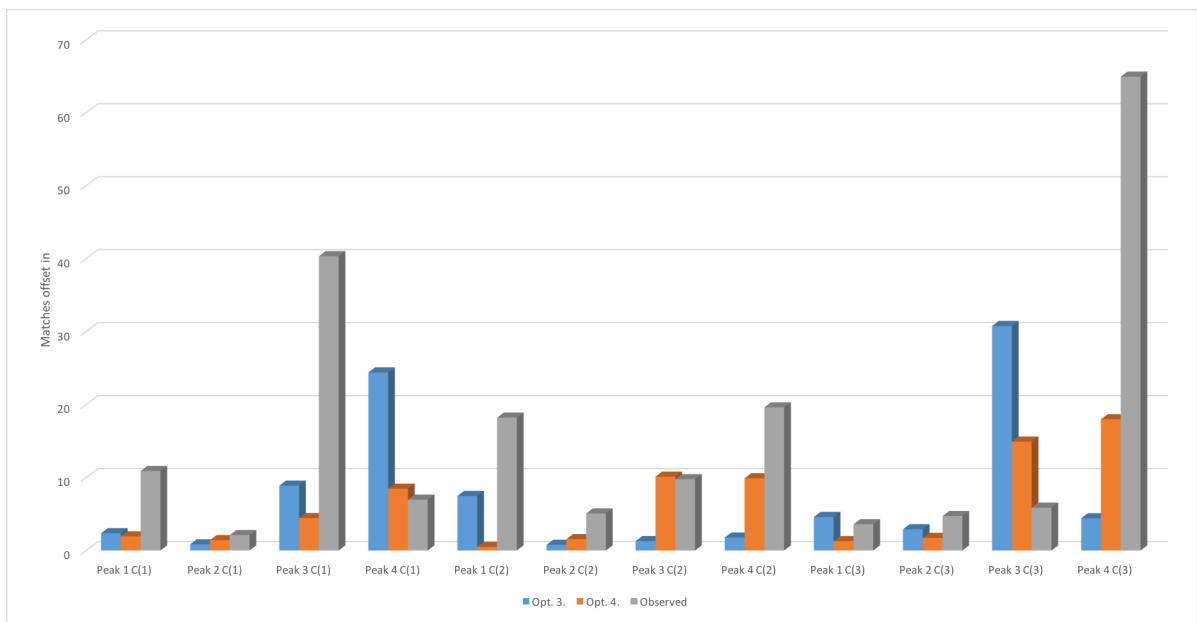


Figure 7.48: All Optimized single methods: Match of peaks flux w.r.t. to Intrinsic Fluxes - Graphical Representation

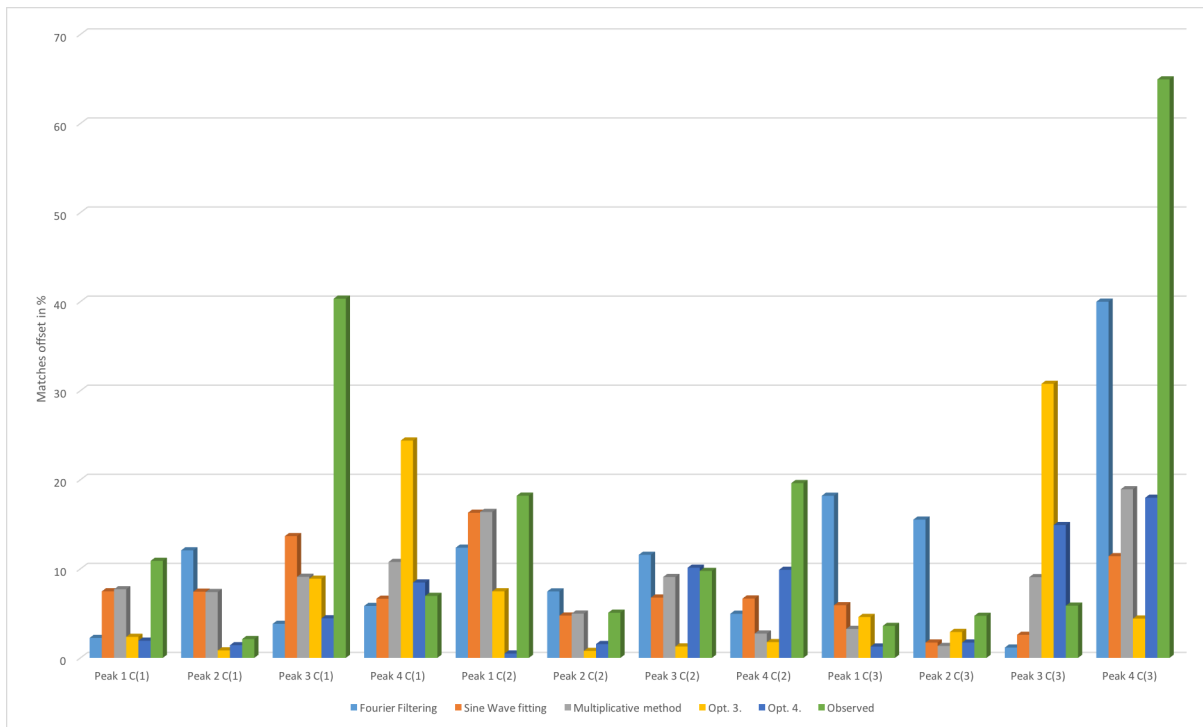


Figure 7.49: All traditional and Optimized single methods investigated at this stage: Match of peaks flux w.r.t. to Intrinsic Fluxes - Graphical Representation

## 7.3. Conclusion

Different optimizations for defringing the data have been considered in this Chapter. The purpose of this Section is to summarize the different outcome of each optimization for ranking them in order to determine if the optimization had improved the data quality as expected. For comparing the different methods, two main criteria have been considered as done in Section 4.5, namely the graphical representation and the amplitude match of the spectral features.

### GRAPHICAL REPRESENTATION

As explained in Section 4.5, five criteria have been chosen for quantifying the spectrum quality:

- **CRITERION 1:** Visibility of the weak spectral features
- **CRITERION 2:** Visibility of the strong spectral features
- **CRITERION 3:** Width of the spectrum continuum → the left residuals
- **CRITERION 4:** Presence of a frequency component left
- **CRITERION 5:** Flatness of the continuum

For each Case, the best configuration of each method (i.e. Region 1 and Approach II) was selected for the graphical comparison. The grading is made on a scale of three components:

- **Good** or [G] as **Green**: shows reliable results
- **Mitigated** or [M] as **Yellow**: does not provide the best results but the outcome is acceptable
- **Bad** or [B] as **Red**: does not provide reliable results nor acceptable ones

# Method	CASE (1)				
	Criterion				
	1	2	3	4	5
Fourier Filtering	[G]	[G]	[G]	[B]	[B]
Sine Wave Fitting	[G]	[M]	[B]	[M]	[M]
multiplicative method	[G]	[G]	[G]	[G]	[G]
Opti. 1	[G]	[G]	[M]	[G]	[G]
Opti. 2	[G]	[G]	[M]	[M]	[M]
Opti. 3	[G]	[M]	[M]	[B]	[M]
Opti. 4	[G]	[G]	[M]	[G]	[G]

Table 7.18: Location Comparison for all single methods and optimizations for Case (1)

# Method	CASE (2)				
	Criterion				
	1	2	3	4	5
Fourier Filtering	[G]	[M]	[M]	[M]	[B]
Sine Wave Fitting	[G]	[B]	[B]	[B]	[B]
multiplicative method	[G]	[G]	[G]	[G]	[G]
Opti. 1	[G]	[G]	[B]	[G]	[M]
Opti. 2	[G]	[G]	[M]	[M]	[G]
Opti. 3	[G]	[B]	[M]	[B]	[B]
Opti. 4	[G]	[G]	[M]	[G]	[G]

Table 7.19: Location Comparison for all single methods and optimizations for Case (2)

# Method	CASE (3)				
	Criterion				
	1	2	3	4	5
Fourier Filtering	[G]	[M]	[G]	[B]	[B]
Sine Wave Fitting	[G]	[B]	[B]	[G]	[G]
multiplicative method	[G]	[B]	[M]	[G]	[G]
Opti. 1	[G]	[M]	[B]	[G]	[M]
Opti. 2	[G]	[M]	[B]	[G]	[M]
Opti. 3	[G]	[B]	[B]	[G]	[M]
Opti. 4	[G]	[M]	[B]	[G]	[M]

Table 7.20: Location Comparison for all single methods and optimizations for Case (3)

From the three matrices shown above, several conclusions can be drawn for the different classification methods. First, the single multiplicative method provides the best graphical results. However, it is important to notice that for obtaining such results, the spectrally flat source used has to be cleaned from all other source of artifacts than the fringes. Therefore, this method would less preferable as having a perfectly clean spectrum will hardly be possible. From the three trade-off matrices 7.18-7.20, it is clear that the optimized methods (except Opti. 3) provide the best graphical representations, especially the Opti. 4 which shows the highest average number of [G]. While Opti. 1 and 2 provide a similar quality level of their final spectra, this might due to the same final step of their combination, namely the multiplicative method. Furthermore, it was explained previously that for Opti. 4, a noisy spectrally flat source was considered which introduced noise in the final spectrum. However, if pre-processing is realized on this data set, the level of artifacts would be reduced which would improve the graphical quality of the final spectrum.

The second point of attention for the graphical analysis is the SNR shown in Table 7.21. As pointed out in all conclusions from the optimizations, the detectability obtained by these are better than the ones from the observed spectrum. Furthermore, for an easier qualification of the SNR, these have been categorized as explained in Section 2.2:

- $2 < S/N < 10$  : acceptable signal quality  $\rightarrow$  Black data
- $S/N = < 2$  : bad signal quality  $\rightarrow$  Red data
- $S/N \geq 10$  : excellent signal quality  $\rightarrow$  Blue data

From all the methods, the multiplicative method and the optimizations 2 and 4 allow the best detectability with no bad signal quality (i.e. red data). From the these two optimizations the second one has the highest number of strong lines, which means that the noise is not dominant in the final spectrum.

#	SNR [-]											
	Case (1)				Case (2)				Case (3)			
Method	Peak 1	Peak 2	Peak 3	Peak 4	Peak 1	Peak 2	Peak 3	Peak 4	Peak 1	Peak 2	Peak 3	Peak 4
FF	12.03	9.77	2.13	1.98	7.34	4.90	1.41	1.25	11.07	7.77	1.71	1.30
SW	111.17	34.7	6.36	2.44	84.55	13.71	1.44	2.16	110.76	31.29	5.74	2.60
Mult.	inf.	inf.	inf.	inf.	inf.	inf.	inf.	inf.	174.17	95.30	11.02	6.10
Opti. 1	48.98	32.89	7.01	4.37	15.66	10.14	1.95	1.27	34.71	29.01	4.93	3.29
Opti. 2	111.89	66.34	12.36	4.68	119.76	94.96	11.53	7.46	68.52	44.02	5.92	4.08
Opt. 3	50.05	34.05	5.40	1.74	38.03	9.56	1.92	1.15	26.15	18.63	2.66	1.92
Opt. 4	81.68	52.06	7.44	4.15	97.59	60.48	9.56	4.68	45.53	30.02	4.23	3.36
Obs.	20.00	9.01	2.13	1.14	5.25	2.67	0.49	0.49	7.57	5.14	0.53	1.11

Table 7.21: All cases- All single and optimized methods : Signal to Noise Ratio

In general, all the methods allow to generate a final spectrum cleaned from a major part of the fringes and therefore easier to interpret than the observed spectrum. Nevertheless, the reader might have noticed that in most simulations, the final spectra are not free of extra noise, which are introduced by the different methods. Sometimes, these added artifacts might lead to misleading interpretation of the results, as is the case for Opt. 3 which has not been considered as graphically reliable due to the important remaining artifacts. The reader might have also noticed that the sine-wave fitting is not optimal for all Cases treated, i.e. some shift of the fitted wave w.r.t. observed wave can be depicted. As explained in Section 4.3, the algorithm developed for this method is not optimal due to the high computational load of the full algorithm. Indeed, a reduced version of the algorithm was run for this study, although the full version is available. If a powerful computer is used for this method, it would be possible to run the full algorithm allowing to reach better precision of the sine wave fitting, thus reducing the level of remaining artifacts (i.e. improving the data quality of Opti. 3).

#### SPECTRAL FEATURES : AMPLITUDE MATCH

The second point of interest is the amplitude match of the found spectral features w.r.t. their intrinsic values. Table 7.22 summarizes all the peak matches for all single methods and optimized ones. As previously, the best matches have been pointed in blue and the matches varying of  $\pm 1\%$  from the best match are pointed in green. All the data summarized in this Table can be visualized in Figures 7.50 and 7.51. At first sight, it is clear that optimizations 3 and 4 (i.e. Opti. 3 and Opti. 4) displays the best matches in general, although Opti. 4 surpasses Opti. 3. In addition to the good score for the graphical representation, Opti. 4 scores also the best result for the amplitudes match. The second aspect to be considered with the data set of Table 7.22 is the variation of the offset w.r.t. the intrinsic values, in order to determine if the method is stable or not. This is done by determining the standard deviation of the offsets (i.e.  $offset = peak\ match\ [\%] - 100\ [\%]$ ), shown in Table 7.23. The same conclusion can be drawn from the standard deviation; Opti. 4 provides the best values which means that in average its peak amplitudes are not highly varying from the expected ones.

To conclude, applying the defringing methods allows to clean the spectrum and reduce the effect of the fringes on the data set (amplitude-wise). In general, the spectra are easier to interpret as the spectral features can be distinguished

despite the remaining noise. When comparing the single traditional method applications to the single optimized ones, the reader might have concluded that the Optimized versions are more reliable than the traditional ones on all aspects. Furthermore, the combinations even optimized do not allow to reach the data quality of the single methods optimization. Moreover, it would preferable to use the traditional single methods than the optimized combinations, as their standard deviations are highest which translate a non-stable outcome, although graphically they provide better results than single traditional methods (multiplicative method not included). Finally, out of both single optimized methods, Opti. 4 leads to the best performance.

#	Obtained or observed Value/ Intrinsic Value[%]											
	Case (1)				Case (2)				Case (3)			
Method	Peak 1	Peak 2	Peak 3	Peak 4	Peak 1	Peak 2	Peak 3	Peak 4	Peak 1	Peak 2	Peak 3	Peak 4
FF	102.24	87.93	103.82	105.83	113.37	92.54	88.43	95.05	81.80	84.48	101.16	60.01
SW	107.47	92.57	113.67	93.36	116.29	95.25	93.23	93.34	94.09	98.28	97.41	111.42
Mult.	107.70	92.61	109.10	110.77	116.38	95.03	90.92	97.27	96.75	101.34	109.06	81.07
Opti. 1	102.22	87.94	103.69	104.89	96.29	78.39	77.57	84.79	80.66	87.74	83.38	83.78
Opti. 2	103.68	92.47	118.94	91.30	116.36	95.87	72.18	96.26	93.26	95.86	60.50	94.90
Opti. 3	97.64	100.84	108.89	75.60	107.47	100.78	101.28	101.77	95.41	97.09	69.23	104.41
Opti. 4	101.93	98.58	104.44	108.46	99.51	101.55	89.88	109.89	101.27	101.72	114.91	117.98
Obs	110.9	97.9	140.3	93.04	118.21	94.93	90.24	80.38	96.41	95.28	105.86	164.95

Table 7.22: All Optimized and non-optimized methods (single and combinations): Match of peaks flux w.r.t. to Intrinsic Fluxes

# Method	Standard Deviation
FF	12.08
SW	4.27
Mult.	5.25
Opti. 1	7.29
Opti. 2	11.44
Opti. 3	9.80
Opti. 4	5.97
Obs	18.70

Table 7.23: All Optimized and non optimized methods: Standard Deviation of offset values for all Cases

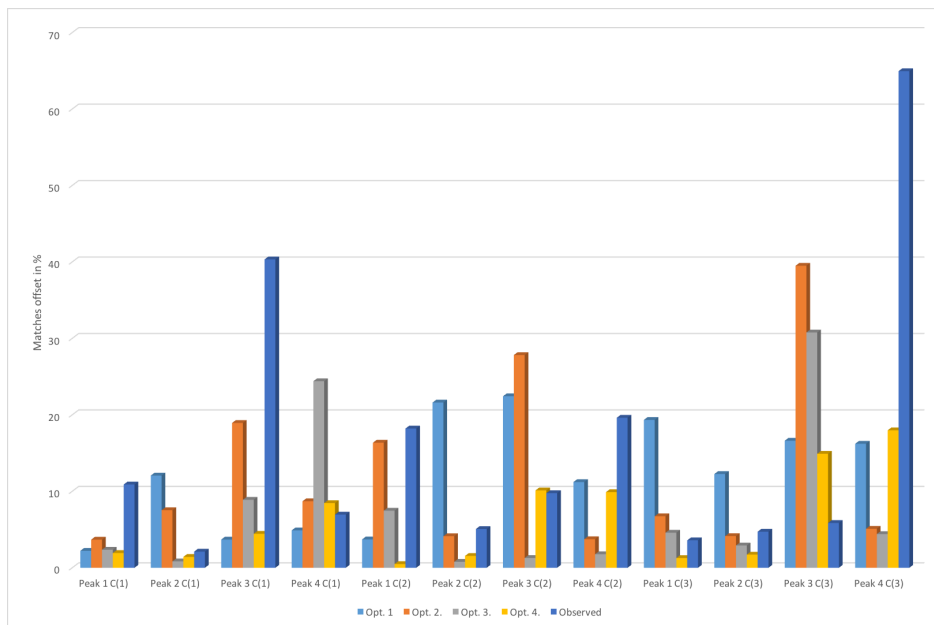


Figure 7.50: All Optimized methods (single and combinations): Match of peaks flux w.r.t. to Intrinsic Fluxes - Graphical Representation

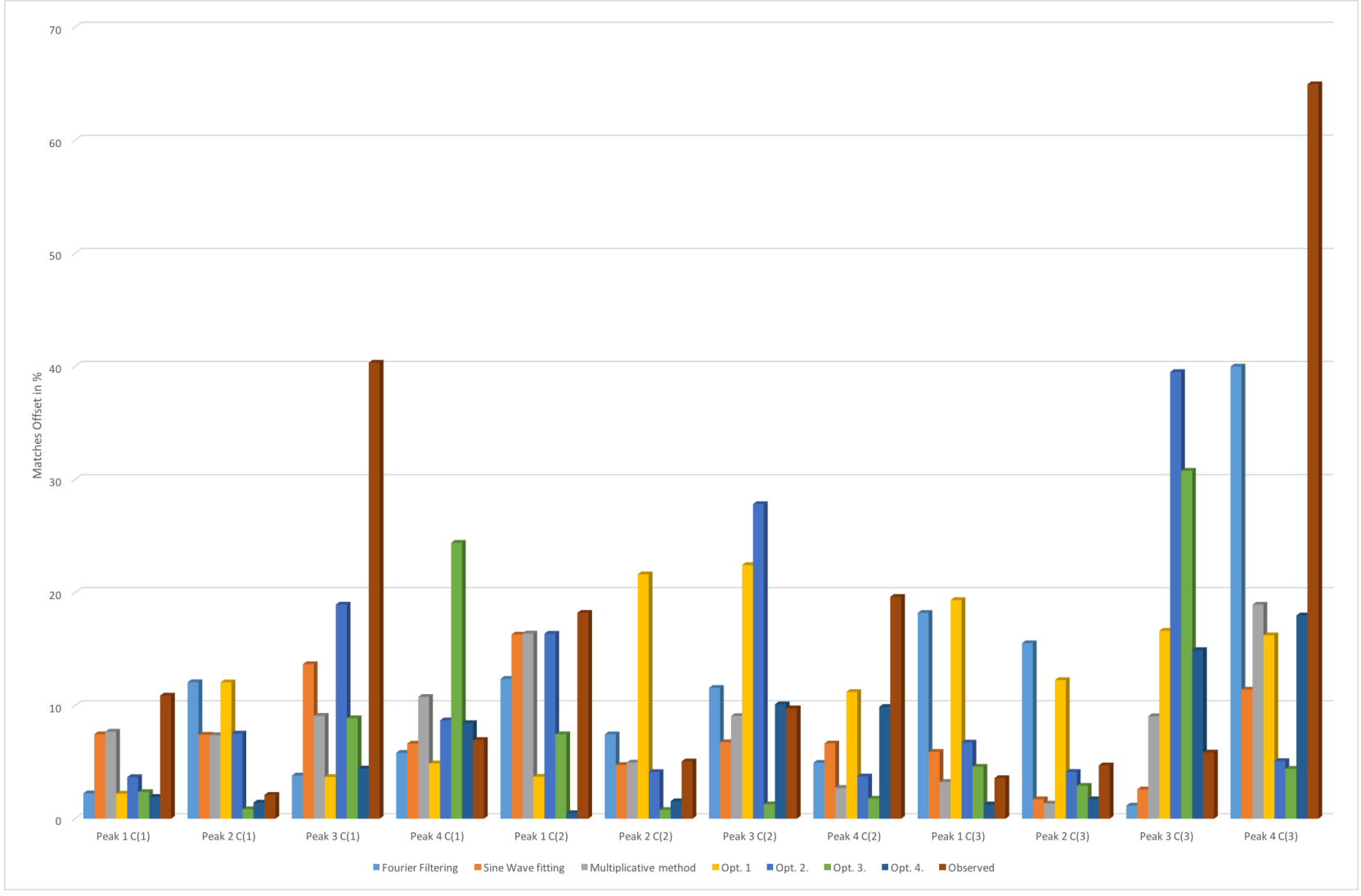
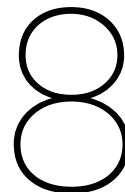


Figure 7.51: All Optimized and non-optimized methods (single and combinations): Match of peaks flux wrt. to Intrinsic Fluxes - Graphical Representation



# Optimization - MIRI Application

In this Chapter, the four optimized models defined and tested theoretically in Chapter 7 will be applied on two data sets of MIRI through four Sections corresponding to each optimization. As explained in Chapter 5, the spectral features (amplitude and locations) present on these data sets being unknown, the analysis of the defringed data will be based only on the graphical aspect.

## 8.1. OPTIMIZATION 1 - Combination 1 : Fourier Filtering - Multiplicative Method

The first optimization to be tested on real data is the Fourier filtering followed by the multiplicative method, in this optimization, both files used (observed spectrum and spectrally flat source) have been processed by the Fourier filtering method.

### 8.1.1. FM Data Set 1 for Channel 2B

First, the Fourier filtering using Region 1 filter has been applied to both data sets: spectrally flat source and observed source, as shown in Figures 8.1-8.2.

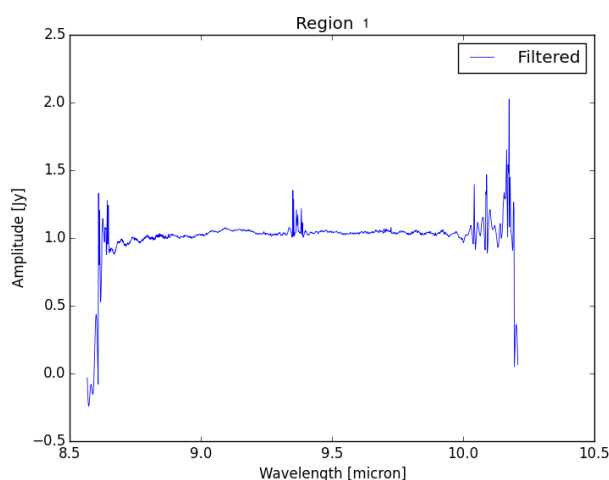


Figure 8.1: FM MRS data - Channel 2B - Optimization 1 - Fourier filtering (Region 1) of observed spectrum

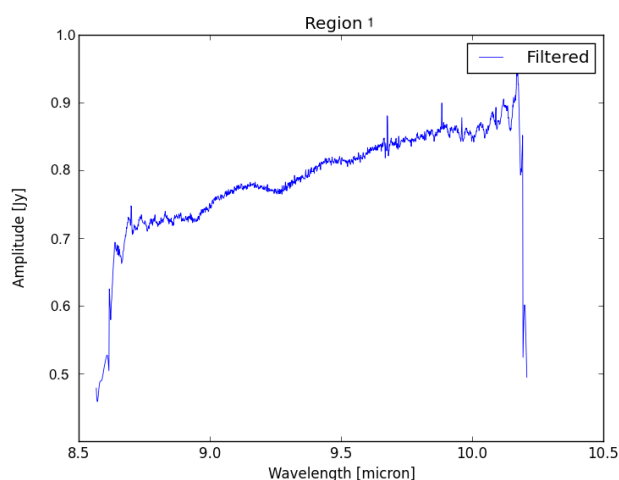


Figure 8.2: FM MRS data - Channel 2B - Optimization 1 - Fourier filtering (Region 1) of spectrally flat source spectrum

The two Fourier filtered spectra are shown in Figure 8.3. The first difference that the reader might have noticed from the theory is the poor presence of the low frequency fringe component, which was more present in the theoretical analysis. Furthermore, it was seen in this previous analysis that more discreet is the left residuals from the Fourier filtering, less important is the graphical impact on the final spectrum but, the improvement on the lines flux approximations is not affected.

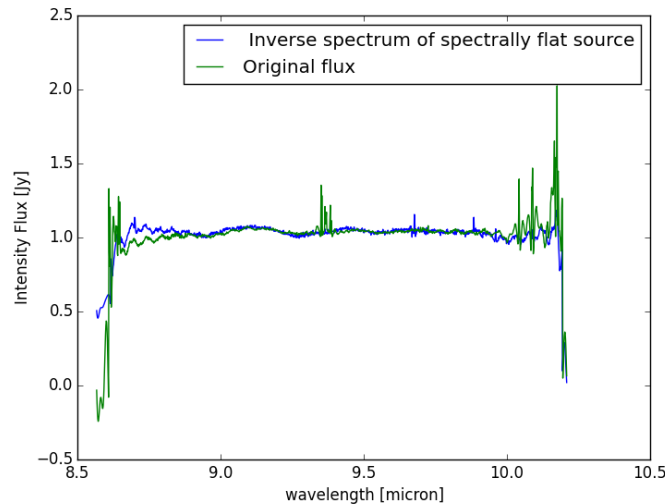


Figure 8.3: FM MRS data - Channel 2B - Optimization 1 - Fourier filtered spectra of spectrally flat source and observed spectrum

The final spectrum of optimization 1 can be seen in Figure 8.4. As expected, the final spectrum does not show major improvement compared to the one after Fourier filtering. However, the continuum appears to be more flat and some spectral features are more distinguishable at  $\lambda=9.73, 9.86$  [micron]. The number of spectral features present in this spectrum being unknown, it is hard to confirm that these two lines are spectral features or introduced artifacts. However, if we referred to the theory, these are indeed spectral features.

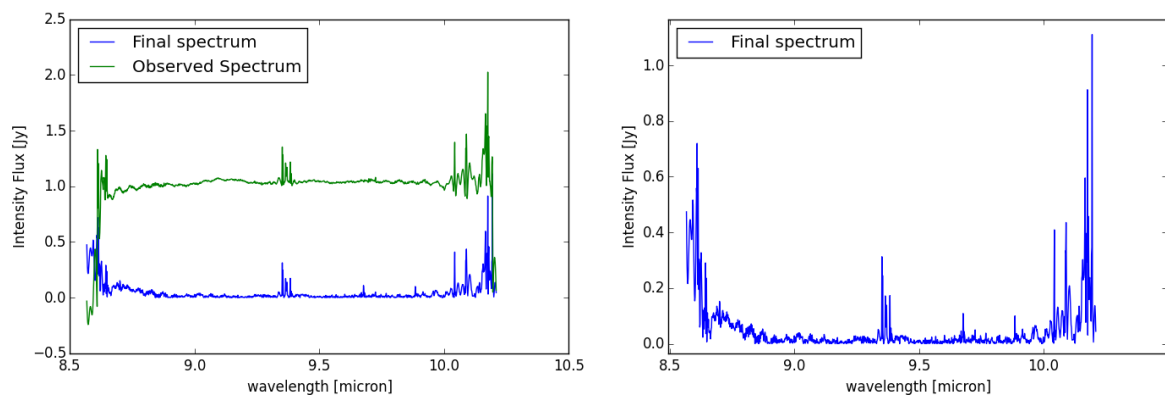


Figure 8.4: FM MRS data - Channel 2B - Optimization 1 - on the left: final spectrum and original observed spectrum after Fourier filtering. On the right: final spectrum

### 8.1.2. CV3 Data Set 2 for Channel 1C

The second channel to be analyzed is the 1C from test CV3. The first step was to filter each file separately with the Fourier method, as shown in Figures 8.5-8.6, while Figure 8.7 provides a general overview of both spectra. As can be seen from this last Figure, both spectra are superimposed at several locations; therefore the multiplicative method is expected to provide a nearly flat spectrum at these locations.

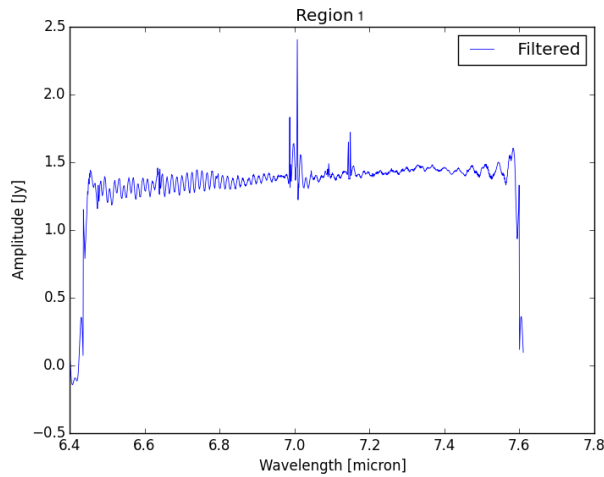


Figure 8.5: CV3 MRS data - Channel 1C - Optimization 1 - Fourier filtering (Region 1) of observed spectrum

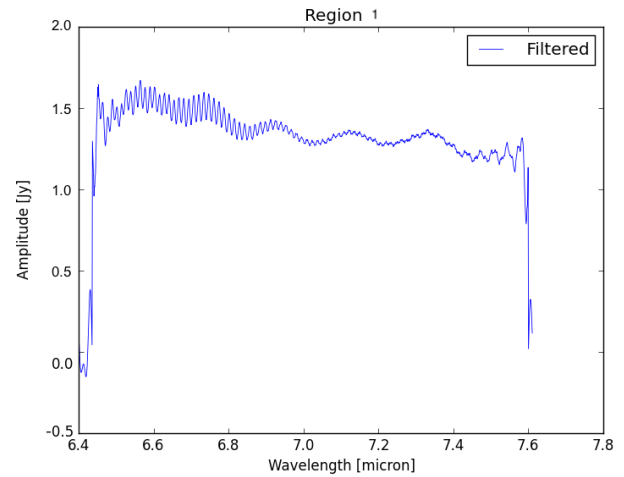


Figure 8.6: CV3 MRS data - Channel 1C - Optimization 1 - Fourier filtering (Region 1) of spectrally flat source spectrum

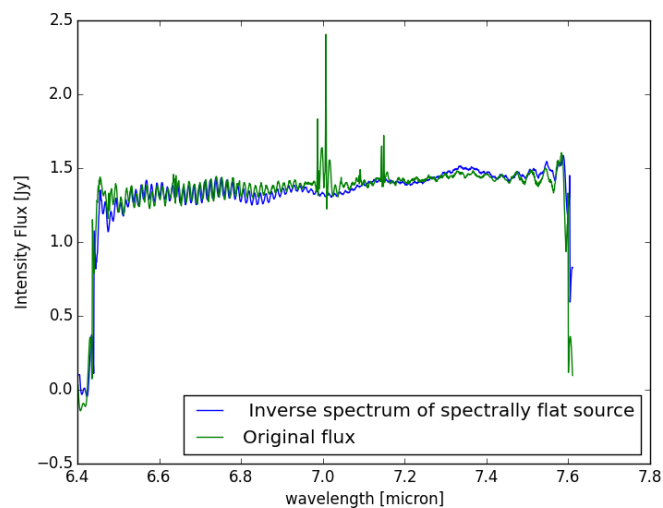


Figure 8.7: CV3 MRS data - Channel 1C - Optimization 1 - Fourier filtered spectra of spectrally flat source and observed spectrum

The multiplicative method has been applied to both Fourier filtered files and the final spectrum is seen in Figure 8.8. As expected the spectrum has a more flat continuum than the one from the observed spectrum. Furthermore, the spectral features are more easily distinguishable, although some residuals are still present in the spectrum. However, the amplitude of the residuals have decreased compared to the initial ones. This method works therefore as anticipated theoretically.

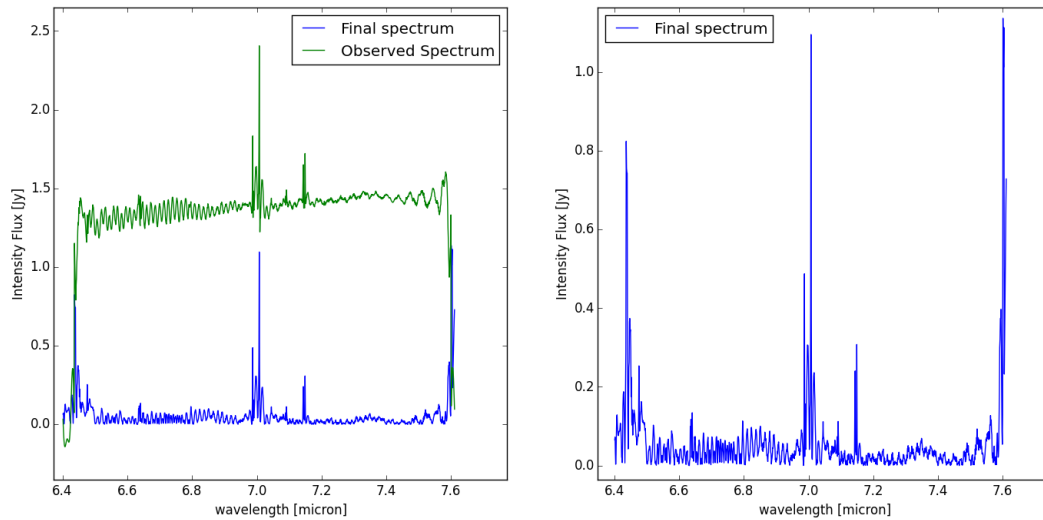


Figure 8.8: CV3 MRS data - Channel 1C - Optimization 1 - on the left: final spectrum and original observed spectrum after Fourier filtering. On the right: final spectrum

## 8.2. OPTIMIZATION 2 - Combination 2 : Sine Wave Fitting - Multiplicative Method

The second to analyze is the optimized version of the second combinations. It consists of applying the sine-wave fitting to the observed data set and to the spectrally flat source and then use these two files in the multiplicative method.

### 8.2.1. FM Data Set 1 for Channel 2B

It was seen in Chapter 5 that applying this method did not lead to the expected results due to the varying phase shift seen in the fringes. This phenomenon generated artifacts (i.e. accordion-shapes) in the final spectrum after applying sine-wave fitting. It was interesting to see that this phase shift also occurred in the spectrally flat source, as shown in Figures 8.9-8.10. Therefore, a correspondence of these accordion-shapes could be seen at some locations which would allow to correct the sine-wave spectrum from these artifacts by applying the multiplicative method. Indeed, in this combination, not only the fringe were corrected but also the introduced artifacts by the sine-wave method.

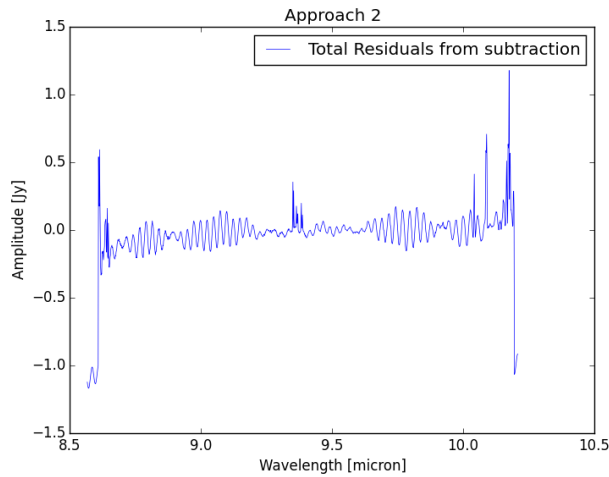


Figure 8.9: FM MRS data - Channel 2B - Optimization 2 - Sine wave fitting of observed spectrum

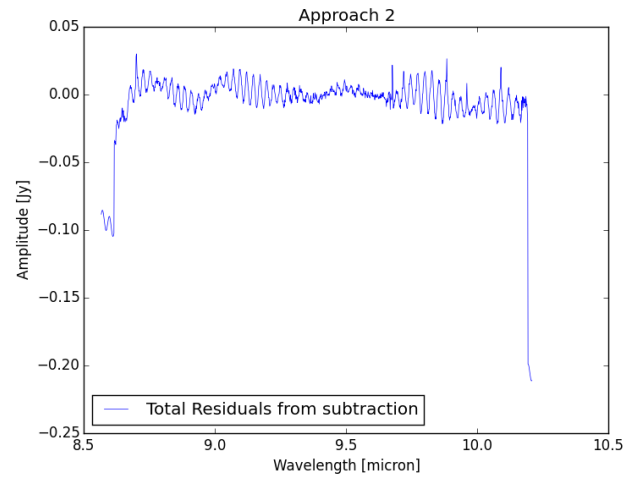


Figure 8.10: FM MRS data - Channel 2B - Optimization 2 - Sine wave fitting of spectrally flat source spectrum

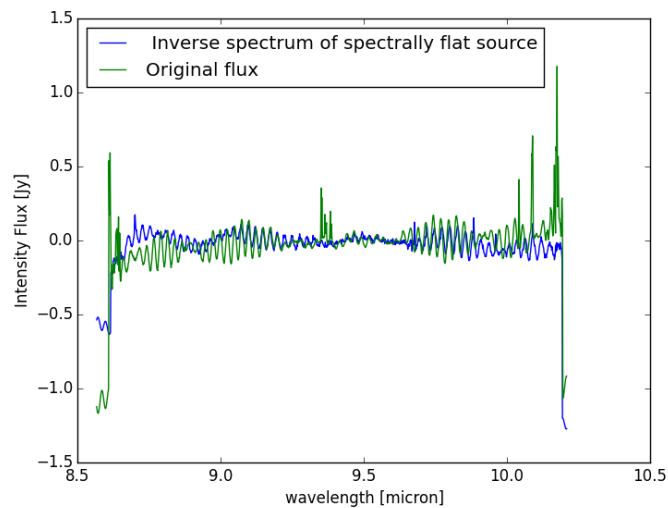


Figure 8.11: FM MRS data - Channel 2B - Optimization 2 - Sine wave fitting of spectrally flat source and observed spectrum

The final spectrum is seen in Figure 8.12 is graphically better than the ones found from the Sine-wave fitting only. Contrary to the theoretical analysis which did not show a considerable improvement of the graphical representation for this method; its application to the MIRI data shows improvement. The spectrum is relatively more flat and the fringe amplitude is highly reduced compared to the initial observed spectrum.

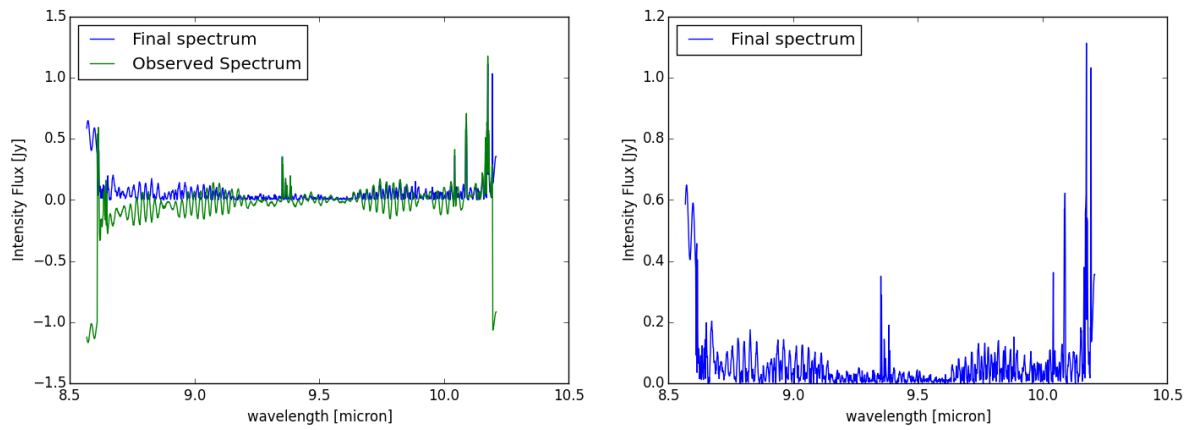


Figure 8.12: FM MRS data - Channel 2B - Optimization 2 - on the left: final spectrum and original observed spectrum after sine wave fitting. On the right: final spectrum

### 8.2.2. CV3 Data Set 2 for Channel 1C

This optimized combination was also applied to the CV3 data set, and showed the same graphical pattern as for the previous case, after the sine-wave fitting. This is shown in Figures 8.13-8.14.

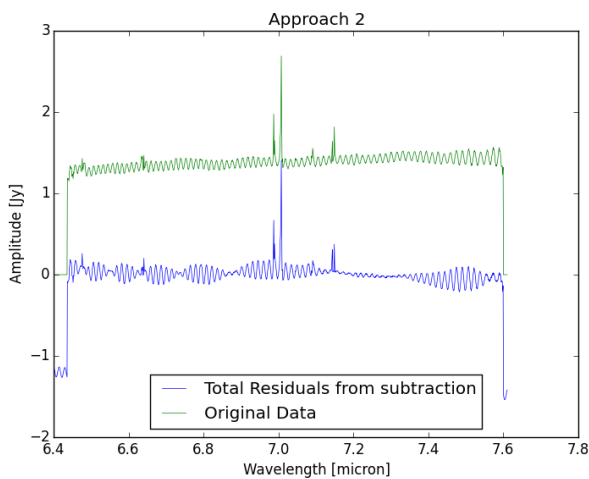


Figure 8.13: CV3 MRS data - Channel 1C - Optimization 2 - Sine wave fitting of observed spectrum

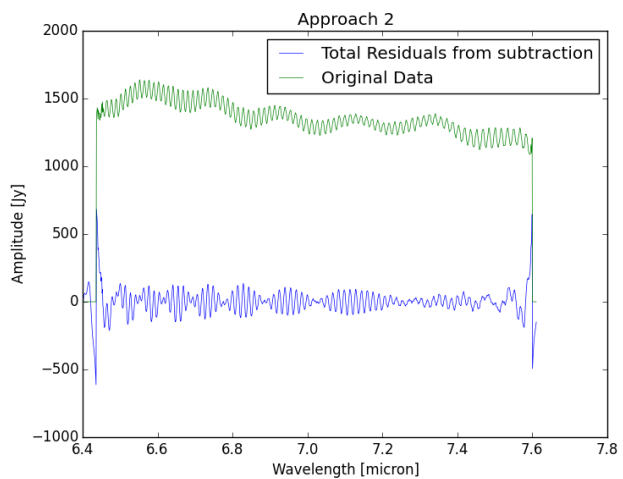


Figure 8.14: CV3 MRS data - Channel 1C - Optimization 2 - Sine wave fitting of spectrally flat source spectrum

In Figure 8.15 both sine fitted spectra are shown. As for the previous data set, the introduced artifacts by the sine-wave method point some similarities between the observed spectrum and the spectrally flat source spectrum. However, it is important to notice that these accordion-shapes of the two files are not similar, which means that the phase shift occurring can not be modeled at this stage for a specific channel and should be further investigated in future work. However, this goes beyond the purpose of this study.

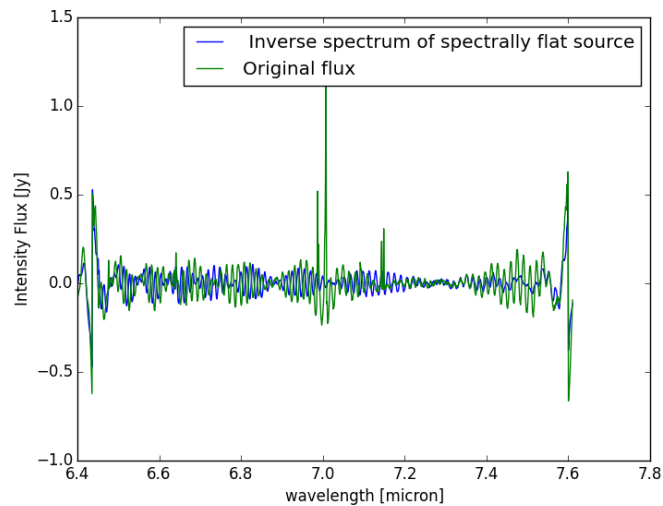


Figure 8.15: CV3 MRS data - Channel 1C - Optimization 2 - Sine wave fitting of spectrally flat source and observed spectrum

Once the two files have been sine-fitted and their residuals determined, the multiplicative method can be applied. Figure 8.16 displays the final spectrum. The strong spectral features can clearly be seen, however, the weak ones are 'absorbed' by the remaining noise. Concerning the noise amplitude, it is clear from the left part of Figure 8.16 that the noise amplitude has decreased and the continuum is more flat.

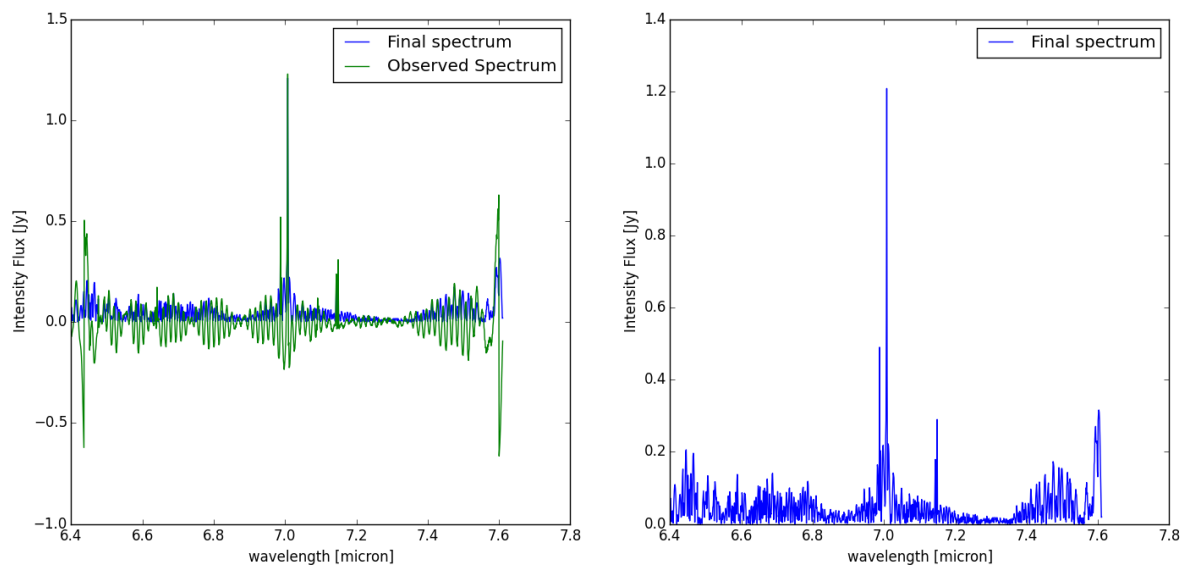


Figure 8.16: CV3 MRS data - Channel 1C - Optimization 2 - on the left: final spectrum and original observed spectrum after sine wave fitting. On the right: final spectrum

### 8.3. OPTIMIZATION 3 - Sine Wave Fitting

The third optimization to test on the MIRI data set is slightly different than from the previous two as it is based on a single method and not on a combined one. The entire theoretical background behind this method is explained in Section 7.2.

### 8.3.1. FM Data Set 1 for Channel 2B

The first step of this optimization is to determine the sine-wave fitting, and the residuals of its subtraction from the observed spectrum. This is shown in Figures 8.17 and 8.18. The final residuals from approach II will consist of the numerator part of Equation (7.3).

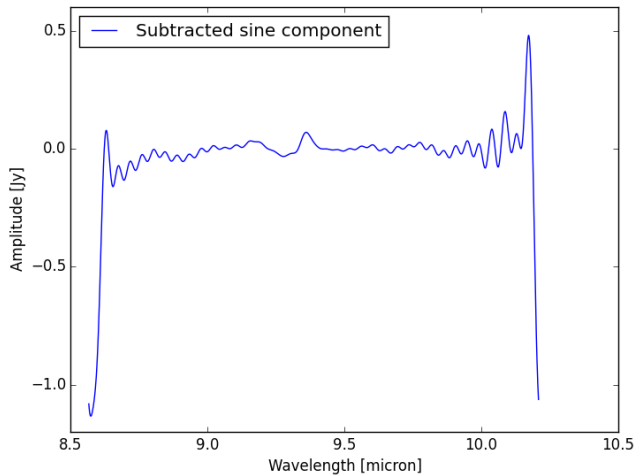


Figure 8.17: FM MRS data - Channel 2B - Optimization 3 -Sine wave fitting - Residuals of the low frequency component

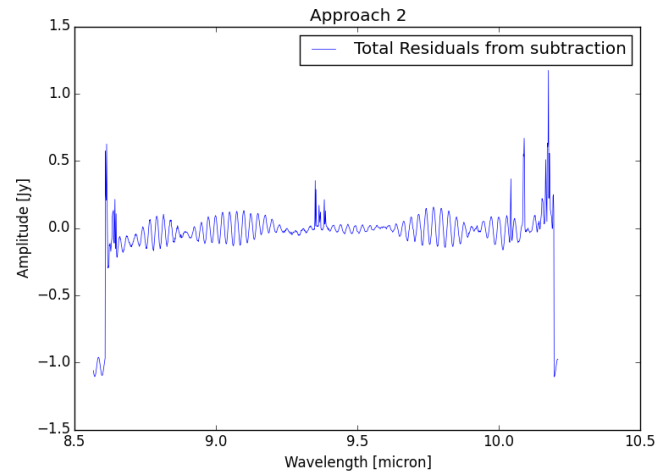


Figure 8.18: FM MRS data - Channel 2B - Optimization 3 - Sine wave fitting - Total Residuals of the spectrum (Approach II)

Once the sine fits have been determined along with the corresponding residuals, the optimization method can be fully applied and lead to the final spectrum of Figure 8.19. This last application has a better overall shape than when applying the sine-wave fitting only as the residuals are more spread out over the spectrum and not concentrated in accordion shapes as seen for the sine-wave fitting (cf. Figure 8.18). This method has therefore improved the spectrum compared to the initial method (sine-wave fitting). Furthermore, at some locations, the residuals have been clearly cleaned (at  $\lambda = 9.2-9.7$  [micron]) allowing to provide a better detectability of the central spectral features. However, it is true that this method is not perfect as some residuals are still strongly present in the spectrum and might hidden the weak spectral features (if any) at these locations. As explained in the conclusion of Chapter 5, the accordion shapes deteriorating the final spectrum graphical quality is due to an unexplained phase drifts at some locations. It is therefore expected that if the sine-wave fitting method is improved accordingly, the results from the methods would be of a higher final graphical accuracy.

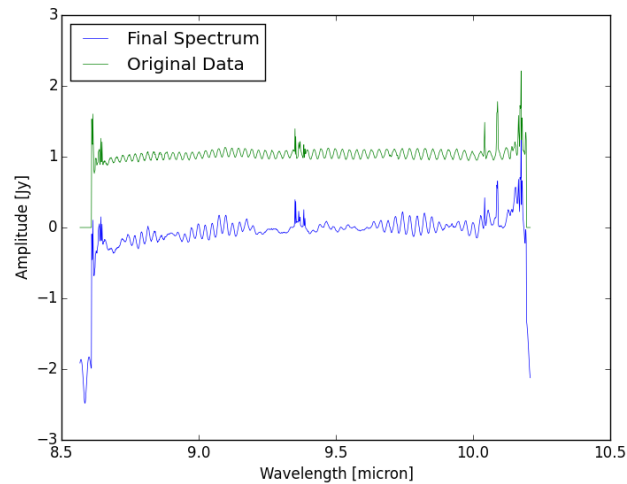


Figure 8.19: FM MRS data - Channel 2B - Optimization 3 - final Spectrum

### 8.3.2. CV3 Data Set 2 for Channel 1C

As realized for the previous data set, the first step for this optimization is to determine the sine-wave fit of the observed spectrum and the residuals (cf. Figures 8.20 & 8.21).

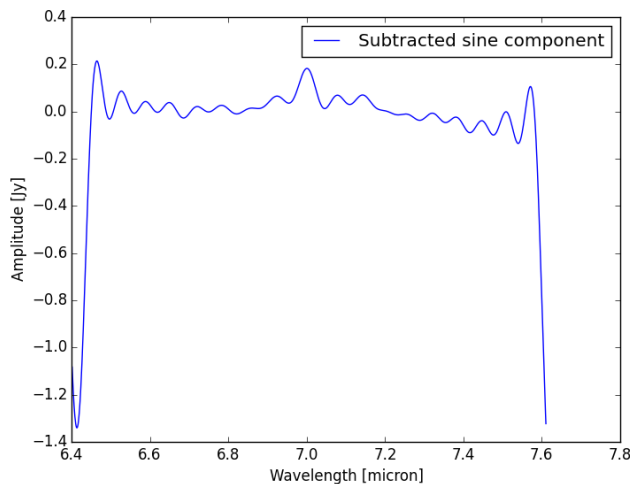


Figure 8.20: CV3 MRS data - Channel 1C - Optimization 3 - Sine wave fitting - Residuals of the low frequency component

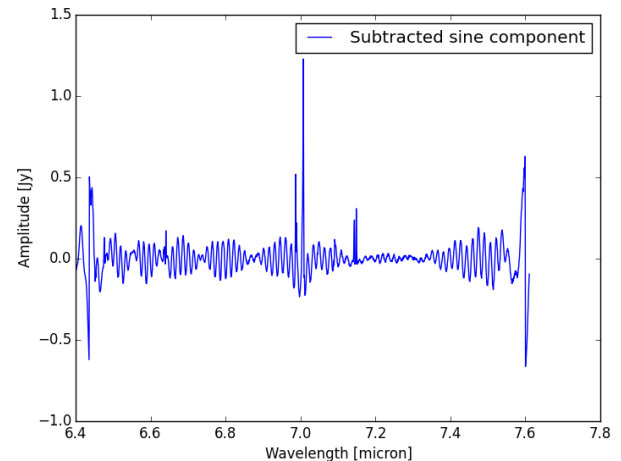


Figure 8.21: CV3 MRS data - Channel 1C - Optimization 3 - Sine wave fitting - Total Residuals of the spectrum (Approach II)

When analyzing Figure 8.22, the same conclusion as for the previous data set can be drawn. First, the final spectrum is cleaner than applying the sine-wave fitting method only, indeed, the amplitude of the accordion-shaped residuals are in general smaller and five out of the six spectral features (that could be noticed from the observed spectrum) are more easily distinguishable than with the sine-wave fitting method. However, contrary to the previous data set, at the central region the fringe amplitude has been amplified resulting to a poor detectability of one the expected weak spectral feature ( at  $\lambda=7.1$  [micron]).

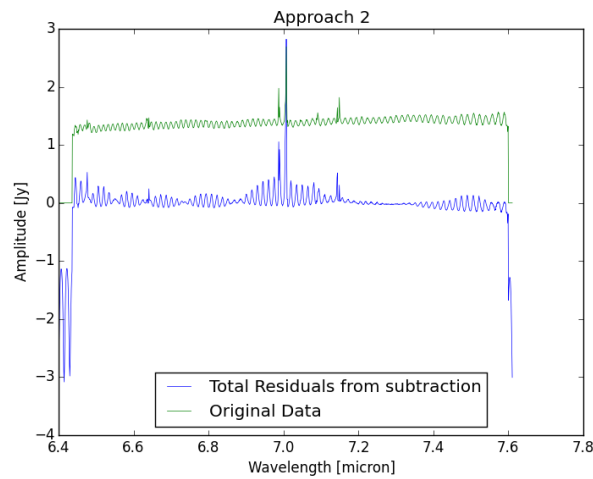


Figure 8.22: CV3 MRS data - Channel 1C - Optimization 3 - final Spectrum

## 8.4. OPTIMIZATION 4 - Multiplicative Method

The last optimization developed in this study is based on the multiplicative method. It follows the same background as used for the optimization 3, but instead of using sine-wave fitted spectrum and its residuals, it uses the new spectrum found by the multiplicative method and determines the corresponding residuals.

### 8.4.1. FM Data Set 1 for Channel 2B

Figures 8.23 displays the two files used for the multiplicative method, namely the observed spectrum and the spectrally flat source. While Figure 8.24 displays the final spectrum. The first thing to note when analyzing this final spectrum, is the poor change of the overall graphical shape. Indeed, the high frequency fringe noise seems to be still present. However, when looking closer at the graph, it can be seen that the fringe amplitude of the spectrum has decreased by a factor of 2 and no major new artifacts have been added to the final spectrum contrarily to the optimization 3. Therefore the detectability of the spectral features has increased. It is expected that if the spectrally flat source was free of noise, it would better match the observed spectrum and the outcome from this optimization would be of a better graphical accuracy.

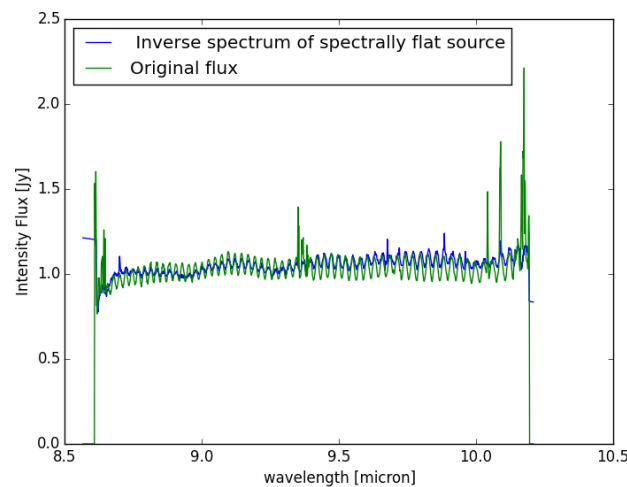


Figure 8.23: FM MRS data - Channel 2B - Optimization 4 - observed and spectrally flat source spectra

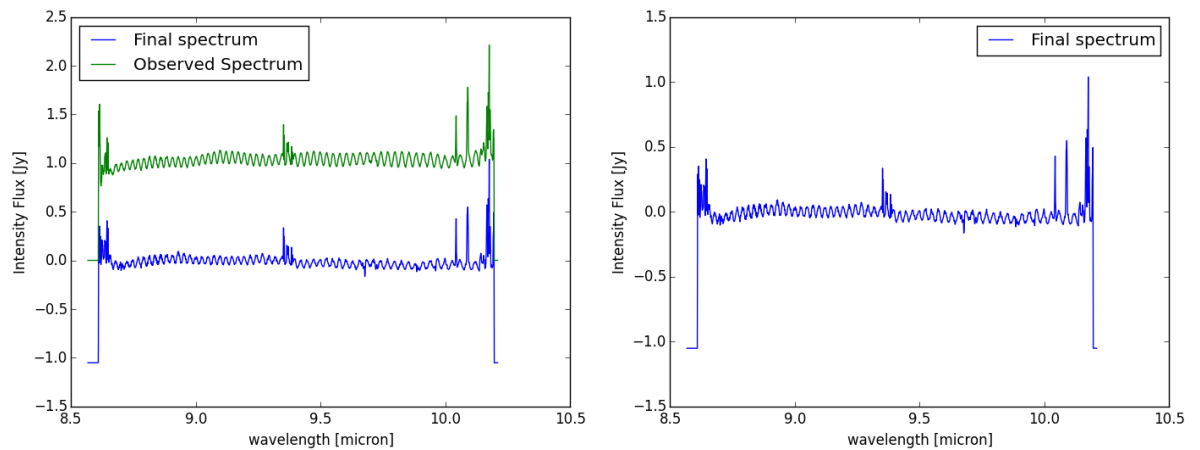


Figure 8.24: FM MRS data - Channel 2B - Optimization 4 - final spectrum

### 8.4.2. CV3 Data Set 2 for Channel 1C

The same analysis used for the FM data set has been applied to this new data set. Namely, first the necessary spectrum files for running the simulation has been gathered as shown in Figure 8.25. And the final outcome from this optimization can be seen in the next Figure. The same conclusion as previously can be stated from this graphical analysis; the overall spectrum shape is similar, at first sight, than the observed spectrum one. But, when quantifying the fringe residuals amplitude, an improvement can be noticed. In this case, the amplitude has been decreased by a factor of 3 compared to the observed spectrum, improving the spectral feature detectability.

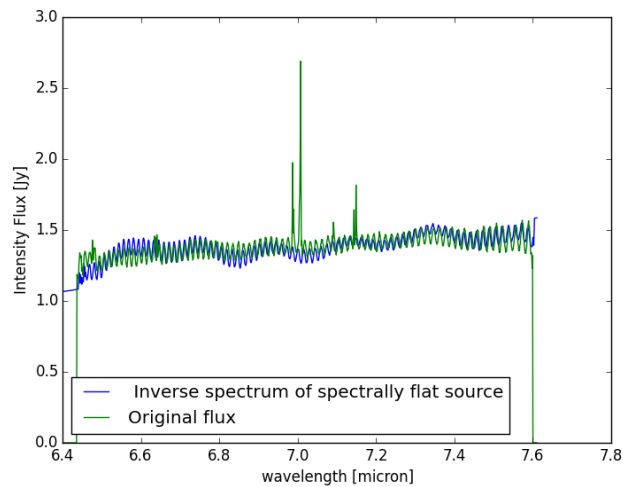


Figure 8.25: CV3 MRS data - Channel 1C - Optimization 4 - observed and spectrally flat source spectra

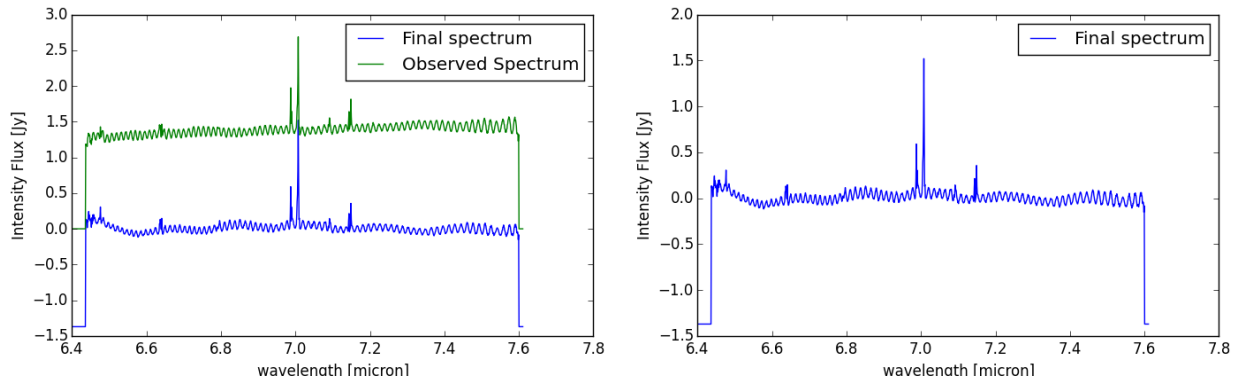


Figure 8.26: CV3 MRS data - Channel 1C - Optimization 4 - final spectrum

## 8.5. Conclusion

In this Chapter, all the optimizations demonstrated theoretically, in Chapter 7, have been tested on MIRI data sets. As realized for the traditional single methods of Chapter 4, two data sets from two different testing conditions have been selected. Furthermore, the same data quality level for these optimizations was required. Therefore, the content of Subsections 5.1.1 and 5.1.2 is also valid in this Chapter.

The first optimization applied was an improvement of the first combination, i.e. applying first Fourier filter to the data (the spectrally flat source included) and then the multiplicative method. For both data sets, an improvement compared to the observed spectrum was noticed as the continuum was flatter and the spectral features were all clearly distinguishable. Furthermore, for both cases, a decrease of the residuals amplitude was noticed w.r.t. the one of the observed spectrum. The detectability criterion has therefore increases in reliability with this optimization.

The second optimization investigated was similar to the first one, except that the files used were pre-processed by the sine-wave fitting instead of the Fourier filtering. In Chapter 5, it was seen that using the sine-wave fitting algorithm led to a final spectrum with accordion shaped residuals. These artifacts introduced in the spectrum were due to the inaccuracy of the sine-wave model developed, which was based on the fringing theory. Indeed, in the real data, it appears that the spectral fringe pattern changes its phase throughout the wavelength, in a non-homogeneous way. In other words, the sine-wave approximating the fringe pattern varies of phase at some locations in, at first sight, an inconsistent way. Although this model is not perfectly accurate, it was shown in Chapter 5, that it allows to reduce the fringe amplitude at some locations. It was interesting to see in this study that the multiplicative method allows to remove not only part of these artifacts introduced but also part of the fringes, and provide a nearly flat spectrum, with a fringe amplitude reduced compared to the observed one. However, a disadvantage of this method was that at some locations these new artifacts introduced by the sine-wave method seemed to absorb the weak spectral features, which could already be pointed in the observed spectrum. It is therefore expected that if the sine-wave fitting method is adapted to this phase shift occurring in the real data, applying this optimization would be positively conclusive, as demonstrated theoretically.

The third method analyzed is an optimization of the sine-wave fitting method. It is based on the fit and uses a multiplicative approach, in order to obtain a closer approximations of the line fluxes w.r.t. the intrinsic values, as explained in Section 7.2. The unexpected results from the sine-wave fitting was already discussed in Optimization 2, due to the phase shift present in the real data sets. Therefore, this method did not provide the expected outcome from the theoretical approach. Nevertheless, using this optimization allows to obtain better graphical representation than using the sine-wave method only, as the residuals were more spread out over the spectrum and not highly

concentrated (i.e. accordion-shapes) at some locations. At locations not influenced by the introduced artifacts, the spectrum was nearly flat and the detectability of the spectral features was excellent (i.e. better than in the observed spectrum). However, at other locations the introduced artifacts seemed to absorb the weak spectral features and their detection became hard. As said for the optimization 2, once the sine-wave method will be corrected for this phase drift phenomenon, the results from this algorithm are expected to be similar to the ones found theoretically. These accordion shapes due to the variations of frequency show that the simple theory of Fabry-Pérot is not perfectly applicable in this instrumentation. A possible explanation of why these changes of frequencies occur throughout the spectrum might be the thickness variation of the detector and filters surfaces. Indeed, as explained in Chapter 3, two flat surfaces are considered in the Fabry-Pérot model but, in reality, one might be flat and the other slightly distorted. Another possible reason for this change of wavelength would be the variation of the incidence angle. [1]

The last optimized method treated in this report was similar to optimization 3, but used the multiplicative method instead of the sine-wave fitting. The results from this simulation were surprising as a flat spectrum was expected, but the final spectrum obtained for both test cases was similar at first sight to the observed spectrum. However, when analyzing closer, it became clear that the fringe amplitude over the all spectrum was decreased by factor comprised between 2 and 3, leading to an improvement of the spectral features detectability. Furthermore, contrary to the previous method, no main artifacts had been introduced in the spectrum. The final spectrum was therefore improved compared to the original one. It is important to notice that the accuracy of this method strongly depends on the data quality of the spectrally flat source. Indeed, in both cases, the spectrally flat sources had fringe amplitudes in general smaller than the ones from the observed spectrum. Therefore, after the application of the multiplicative method, some residuals were left as the spectrally flat source is not ideal (i.e. not having exactly same fringe amplitude than the ones from the observed spectrum).

One might conclude from the different optimizations conducted on MIRI data sets that the obtained results were partially compliant with the outcome from the theoretical analysis of Chapter 7. In general the final spectra have been improved (i.e. fringe amplitude decreased) and although the wrong calibration of the sine-wave fitting method was used, the results were not completely distorted. From this analysis, three major points have been learned. First, the phase drift present in the data set has to be modeled and the sine-wave fitting method should be adapted accordingly for providing high accuracy final spectrum. Then, the optimized methods proposed work on the data as expected and should be applied once the pre-processing method (i.e. sine-wave method) would be optimal. Last, the multiplicative method is promising, but its outcome accuracy depends strongly on the spectrally flat source spectrum, which might be hard to find for any user.

# 9

## Conclusion

The purpose of this study was to provide a first analysis on the different possible algorithms for correcting and providing an accurate measurement of the line fluxes, by defringing data sets. For approaching this goal, the study was carried out in two parallel stages, namely the theoretical and the practical parts. In the theoretical part, fake data sets were generated based on the spectral fringes theory, in which spectral features have been introduced at specific locations. These data sets were then tested with all the defringing methods. While, in the practical parts, real MIRI data sets were tested with the same algorithms.

For analyzing the outcome and quantifying each method, assessment criteria were defined: the detectability of the spectral features and the photometric accuracy. However, these could be correctly quantified only on the fake data sets as the locations and intrinsic line fluxes of the spectral features were known. While, for the practical part, the photometric accuracy could not be realized and the detectability criterion was based on the flatness of the spectrum and the overall fringe amplitude of the continuum.

The methods developed for defringing the data were discussed in three stages. First, three single methods were developed and tested: the Fourier filtering, the sine-wave fitting and the multiplicative method. For the first two methods, different combinations were considered (i.e. different filtering regions for the Fourier filtering method and different ways to approach the residuals from the fitting for the sine-wave method) and the best combination was selected for each method. The three methods proved to provide better results than the observed values on both assessment criteria. Although, the multiplicative method provides the best graphical results (i.e. high detectability), the sine-wave fitting was ranked as the best method theoretically for being optimal graphically and photometrically. When, analyzing the MIRI data sets, some deviations from the theoretical outcome were noticed.

The Fourier filtering method provided the expected results, but after the sine-wave method, some unintended residuals were introduced in the new spectrum. At first sight, these residuals were thought to be from the sine-wave algorithm as it was already seen theoretically that some phase shifts were present due to the algorithm defined. Indeed, because of the high running load from the full algorithm, this algorithm has been reduced allowing to run it on a domestic computer. It was thus expected that running the full algorithm would allow to correct the shift (for the theory and the practical data sets). Nevertheless, it is only at the latest stage of this study (i.e. Optimization part) that the origin of these introduced artifacts was understood as coming from varying phase in the original fringe pattern itself. Although because of these introduced artifacts, the final spectrum shows in general better detectability of (expected) spectral features and at some locations, the fringe amplitude was considerably reduced.

Concerning the multiplicative method, the excellent graphical results in the theoretical model were due to the excellent quality of the spectrally flat source. However in reality, the quality of this file is not as excellent, i.e. the fringe components are not similar to the ones from the observed spectrum. Consequently, the final spectrum is not perfectly flat as some residuals will still be seen. But, in general, the width of the residuals amplitude was decreased and the spectral features were clearly distinguishable and improved in accuracy.

Then, the second stage of this method was to combine the single methods developed in the first stage by using them consecutively. The main goal was to obtain the strong features of the different methods: namely the good graphical representation from the multiplicative method and the good photometric accuracy from the Fourier Filtering and the sine-wave fitting. Nevertheless, the simulations were stopped at a premature stage as the outcome from the two first combinations as the results from the theoretical part were worse than using the single methods only. It was thus decided to not apply these algorithms to real data sets.

Finally, the last stage of this study was the development of optimized methods. The first optimizations developed were based on the previous non-conclusive combinations. The model was improved and the part of the initial goals of these combinations could be achieved with the theoretical values. Indeed, it was seen for all cases analyzed for both first two optimizations that the detectability (determined by the SNR) was improved compared to the single defringing methods and the observed spectrum. However, the photometric accuracy was not ameliorated as expected compared to the single defringing methods. The best algorithm providing constant level of accuracy of line fluxes was the sine-wave fitting followed by the multiplicative method and the optimization 1.

Therefore, it was decided to further investigate the single methods instead of their combinations, resulting in the optimizations 3 and 4, which revisited the concepts of sine-wave fitting and the multiplicative methods. The graphical results were also positive, with higher detectability quantified by high SNR; but the presence of introduced artifacts by optimization 3 made it the less graphically reliable optimization out of the four. Nevertheless, the photometric accuracy of both optimizations was higher than from all the previous methods (optimizations 1 & 2 included). Consequently, the last optimization was considered as the best defringing method from this study.

The application of these optimized algorithms on MIRI data sets showed, as for the application of single methods, some deviations from the theory notably for the sine-wave fitting method (due to the phase shift in the data). However, in general for all optimizations, the fringe amplitude was decreased and the spectral features could clearly be distinguished. The conclusion from the theory were thus considered as reliable for the real data sets.

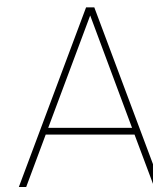
Furthermore, during this study, a new unforeseen element on the fringes behaviour (i.e. change of frequency) has been found, which might be due to a varying incident angle or the non-constant thickness variation of the detector and filters. However, this was not deeply investigated in this report as it did only influence the continuum which was not the main focus of this study.

To conclude, the goal of this study was to determine an algorithm allowing to correct the astronomical line fluxes from the fringing effect and therefore improve their accuracy. Throughout this study, the analysis has been done gradually and a final algorithm (i.e. optimization 4) was considered as the best approach so far and would be advised.

# Bibliography

- [1] M. el Akel. Initial approach for understanding the spectral fringes. *Delft university of Technology*, 2017.
- [2] A. Glasse, G.S. Wright, A. Gallie, and al. The mid-infrared instrument for the james webb space telescope, vi: The medium resolution spectrometer. *The Astronomical Society of the Pacific*, 127(953):646, March 2015.
- [3] S. Kendrew, S. Scheithauer, P Bouchet, J. Amiaux, and al. The mid-infrared instrument for the james webb space telescope, iv: The low resolution spectrometer. *The Astronomical Society of the Pacific*, 127(953):623, 2015.
- [4] A. Labiano, R. Azzollini, J. Bailey, and S. Beard. The MIRI medium resolution spectrometer calibration pipeline. 9910,99102W, 2016.
- [5] A. Lahuis, Eand Boogert. *Chemistry as a diagnostic of star formation: How to get rid of fringes in SIRTf/IRS data*. NRC Research Press, 2003.
- [6] F. Lahuis. Infrared spectroscopy. [http://stsdas.stsci.edu/jwst/meetings/miri\\_edinburgh\\_2008/spectroscopy.pdf](http://stsdas.stsci.edu/jwst/meetings/miri_edinburgh_2008/spectroscopy.pdf), 2008. MIRI Software meeting at ATC, Online; accessed on 9 August 2018.
- [7] F. Lahuis and M. Mueller. personal communication, October 5,2018.
- [8] F. Lahuis, E. Wieprecht, O.H. Bauer, and D. Boxhoorn. ISO-SWS data analysis. *Astronomical Society of the Pacific*, 145:224, 1998.
- [9] F. Lahuis, D. Kester, and D. Lutz. *How To minimise fringe residuals in SWS data*. ISO Explanatory Library. ESA, 2004.
- [10] F. Lahuis, J.E. Kessler-Silacci, N.J. Evans, and G.A. Blake. From molecular cores to planet forming disks, c2d spectroscopy explanatory supplement. *Spitzer Space Telescope Legacy Program*, 2006.
- [11] D. Lee. The miri medium resolution spectrometer for the james webb space telescope. [https://jwst.nasa.gov/resources/spie\\_2006/lee\\_miri.pdf](https://jwst.nasa.gov/resources/spie_2006/lee_miri.pdf), 2017. Online; accessed on 24 July 2018.
- [12] S. Lord. Possible fringe removal methods. Technical report, California Institute of Technology, 1998.
- [13] J.R. Martinez Galarza. *Mid-Infrared Spectroscopy of Starbursts: From Spitzer-IRS to JWST-MIRI*. PhD thesis, University of Leiden, 2012.
- [14] R. Paschotta. *Encyclopedia of Laser Physics and Technology, Fabry-Pérot Etalons*, volume 1. Wiley-VCH, 2008.
- [15] P. Plait, S. Casertano, T. Keyes, and M. Stevens. Fringe science: Creating a STIS CCD fringe flat field. The 1997 HST Calibration Workshop, Baltimore, 1997. Space Telescope Science Institute.
- [16] Space Telescope Science Institute . Jwst pipeline, user manual, revision 7f34b46b. <http://jwst-pipeline.readthedocs.io/en/stable/jwst/introduction.html>, 2018. Online; accessed on 5 September 2018.
- [17] SRON. Research. <https://www.sron.nl/research>, 2017. Online; accessed on 14 June 2018.
- [18] M. van den Ancker, O.H Bauer, S. Drapatz, and A. Heras. *SWS:The Short Wavelength Spectrometer*, volume VI of *The ISO Handbook*. ESA, 2001.

- 
- [19] G. S. Wright, D. Wright, Rieke G. H. Goodson, G. B., and al. The mid-infrared instrument for jwst, ii: Design and build. *The Astronomical Society of the Pacific*, 127(953):686, 2015.
- [20] C. Yew, Y. Lui, P. Whitehouse, and K. Banks. James webb space telescope (jwst) integrated science instruments module (isim) cryo-vacuum (cv) test campaign summary. *Space Telescopes and Instrumentation 2018*, 10698, 2018.



# Code Architecture

In this Appendix, the codes for performing this study will be explained, in two Chapters. First, the requirements necessary on the machine for running the code will be detailed. Then, the different files composing the entire code will be explained and clearly linked to the reader, allowing to any person to run the code by its own.

## A.1. Tool Requirement

Running this tool requires some specific environments (only if using MIRI data) and packages to be installed by the user. The user is advised to check if his machine contains all the necessary packages in order to avoid errors in the codes when running it. Verifying all the environments within anaconda can easily be done by typing `conda-env list` in the terminal. While for checking if the packages are available, go into the desired environment in the terminal (e.g. `source activate miricle`, then call python simply by typing `python`. Once the program is open in the terminal, type `help()`, then after `modules`).

### ENVIRONMENT

- MIRICLE which contains the pre-requisites packages for installing MIRIsim

Besides these specific packages, the user is requested to have anaconda installed in his machine, and preferably using python version 2.7.

### PACKAGES

- From Python:
  1. os
  2. subprocess
  3. pkg\_resources
  4. astropy
  5. getpass
  6. glob
  7. pylab
  8. argparse
  9. numpy
  10. itertools
  11. scipy
  12. matplotlib

## A.2. Tool Overview

For this study, each of the algorithms were generated independently of an external coding source. For running the algorithms, Python tool will be necessary on the machine. The entire code required for this study is made

of the following eight files which overall correlation among the files is shown in Figure A.1:

- MAIN.PY: The main file in which the user chooses the method to run and defines the files or Case to be tested.
- TEST\_CASES.PY: This file regroups all the test cases created for the simulations. The user can modify the fringes characteristics or add another component.
- READ\_DATA.PY: The input data of MIRI are in the form of a .fits file. Therefore, this python code reads this format and convert the data into workable data.
- SINE\_METHOD.PY: This is the algorithm fitting a sine wave to the data and subtracting it from the original spectrum. All the approaches possible discussed in this report for the sine-wave fitting are applicable in this file, the reader can chose which option to run.
- MULT\_METHOD.PY: The multiplicative method algorithm is described in this file. However, the user will have to insert within this file the name of the spectrally flat source used for the simulation, if the simulated file is not from the test\_cases.py file.
- FOURIER\_METHOD.PY: It represents the full algorithm of the Fourier filtering method. It will run by default four different regions to filter as shown in this report. But, the reader can de-select this option and manually select a specific region.
- SINE\_METHOD\_OPT.PY: The optimized version of the sine method is found in this file.
- MULT\_METHOD\_OPT.PY: The file contains the optimized version of the Multiplicative method. As it was the case for the non-optimized multiplicative method, the user has to include the name of the spectrally flat source file within this python file.

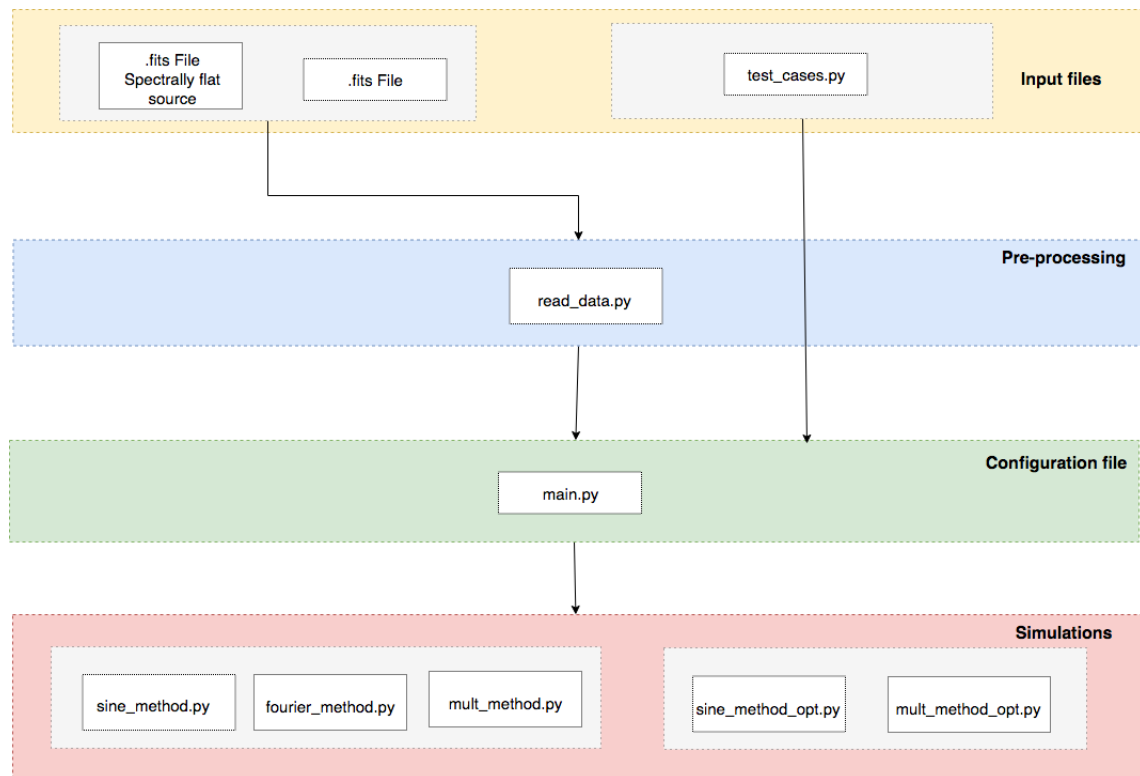


Figure A.1: Architecture of the coding files for this study

All the methods developed are linked within a file called 'main.py' from which the user can select which method to run and the input files. The input data for the user of main.py is shown in Figure A.2.

```
## Determine if the user wants the optimized version or not
optimized = False

## Determine if the user wants to use a single method or a combination
combinations = False

## If combination is True, select the desired combinations :
## 1 for fourier filtering and then flat_fielding
## 2 for sine wave fitting and then flat_fielding
combi = 1 # or 2

## If combination is False, select the single method desired
SW = 0 # Sine-wave fitting method
FF = 1 # Fourier Filtering method
FAF = 0 # Flat-fielding method

## For the Sine-wave fitting: select which approach to use--> 1, 2 or 3
approach = 2

## For the Fourier-filtering: select which region to filter--> 1, 2, 3 or 4
## (If number different than 1,2, 3 or 4, by default all the regions will be run)
filtering = 1

## Determine the type of data:
## if data from test cases: choose a case 1,2 or 3
## if data from MIRI : write MIRI = True and insert the name of the file to be tested
case = 2
MIRI = True
name = 'name_file.fits'

## Determine if the user wants all the plots (1) or restrained number of plots (0)
plot = 0 # or 1
```

Figure A.2: Main.py file layout- input data for the user- detailed version

# B

## Jwst Pipeline

The JWST Science Calibration Pipeline also named the JWST pipeline, consists of three distinct stages. The observations data from all instruments aboard the JWST are processed through this tool for removing the instrumental signatures. Furthermore, this tool transforms the data format to readable and interpretable one.[4]

The pipeline is made of three main stages, namely STAGE-1, STAGE-2 and STAGE-3, which consist of different data reduction levels. Moreover, each stage has optional arguments will allow to skip some steps and save their output.[16]

In the following, the steps used in every stage for each observation mode will be listed; however describing each of these steps is beyond the scope of this report. The reader is therefore advised to refer to [16] for further explanations.

### STAGE 1

In the first stage, the data from all the JWST observation instruments are processed, by performing detector-level corrections. The input data are in ramps format (integration's) (i.e. Level 1B data) containing all the accumulated counts from detector readouts. The corrections performed on this step have to be done on a group by group basis. After this stage, a count-rate (slope) image per exposure or integration (i.e. Level 2A data) is provided. This stage is thus referred as ramp-to-slope process. Depending on the instrument, this stage performs different steps for obtaining slope images. The purpose of this study being testing MIRI instrumentation, only the steps undertaken for this instrument will be detailed in Table B.1.

This stage contains only one optional argument: *save\_calibrated\_ramp*, which allows to save the output from this step.

Table B.1: Functionalities of CALDETECTOR1 for MIRI

Functionalities for MIRI	
○ Data Quality Initialization	○ MIR Dark Subtraction
○ Saturation Check	○ Reference Pixel Correction
○ Error Initialization	○ Persistence Correction
○ Mid-Infrared Linearity Correction	○ NIR NIRNear-Infrared Dark Subtraction
○ MIR Reset Switch Charge Decay Correction	○ Jump Detection
○ MIR Last-frame Correction	○ Slope Fitting

## STAGE 2

The second stage of this pipeline is specific to the imaging and spectroscopic modes, therefore as MIRI provides these two modes, this stage will be further discussed. It consists of processing complementary corrections to the Level 2A data for producing fully calibrated exposures (i.e. Level 2B data). The processes used for imaging and spectroscopy are slightly different depending on the observation mode. An overview of the steps of the MRS can be in Figure B.1, while Table B.2 lists all the steps performed for each observation modes at this stage.

Sub-Steps	Functionalities	
	Imager	MRS
assign_wcs	✓	✓
background	✓	✓
flat_field	✓	✓
srctype		✓
straylight		✓
fringe		✓
photom	✓	✓
cube_build		✓
extract_1d		✓
resample	✓	

Table B.2: Sub-steps for MRS and Imager in stage 2

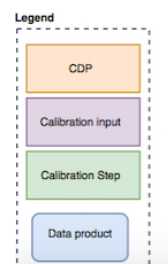
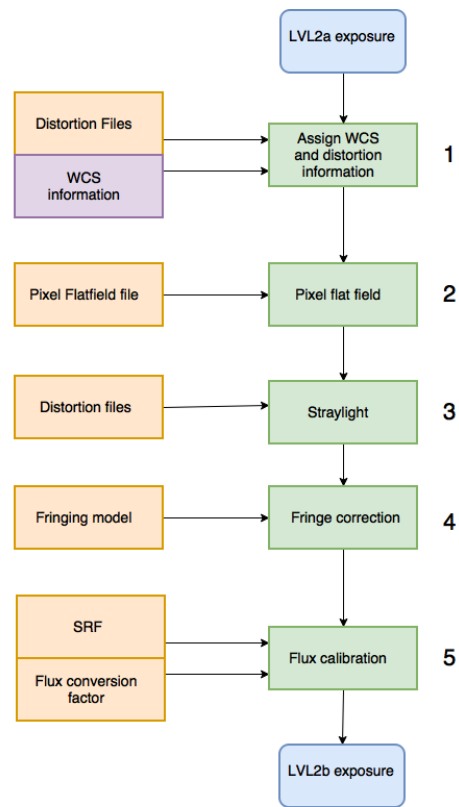


Figure B.1: Schematic description of CALSPEC2

### STAGE 3

The third stage processes more observation modes than the previous stage. Indeed, it will be used for :

- the imager called by the pipeline via *CALWEBB\_IMAGE3*
- the spectrometer called by the pipeline via *CALWEBB\_SPEC3*
- the coronagraph called by the pipeline via *CALWEBB\_CORON3*
- the aperture masking interferometer called by the pipeline via *CALWEBB\_AMI3*
- the time series observations for imager and MRS called by the pipeline via *CALWEBB\_TSO3*

This stage performs routines on level 2 data on several exposures producing a final combined product (i.e. Level 3 data), in other words after this stage the data will be calibrated and associated. As it was the case for stage 2, some steps of this stage are specific to each observation mode, which can be seen in Table B.3.

Sub-Steps	Functionalities					
	Imager	MRS	AMI	Coron	TSO-IMA	TSO-MRS
tweakreg	✓					
skymatch	✓					
outlier_detection	✓	✓		✓	✓	✓
resample	✓			✓		
source_catalog	✓					
mrs_imatch		✓				
cube_build		✓				
extract_1d		✓				✓
ami_analyze			✓			
ami_average			✓			
ami_normalize			✓			
calwebb_coron3				✓		
stack_refs				✓		
align_refs				✓		
klip				✓		
calwebb_tso3					✓	✓
tso_photometry					✓	
white_ligth						✓

Table B.3: Sub-steps for stage 3

The MRS being the principal instrument used in this internship study, an overview of the stage 3 for this instrument has been sketched as shown in Figure B.2.

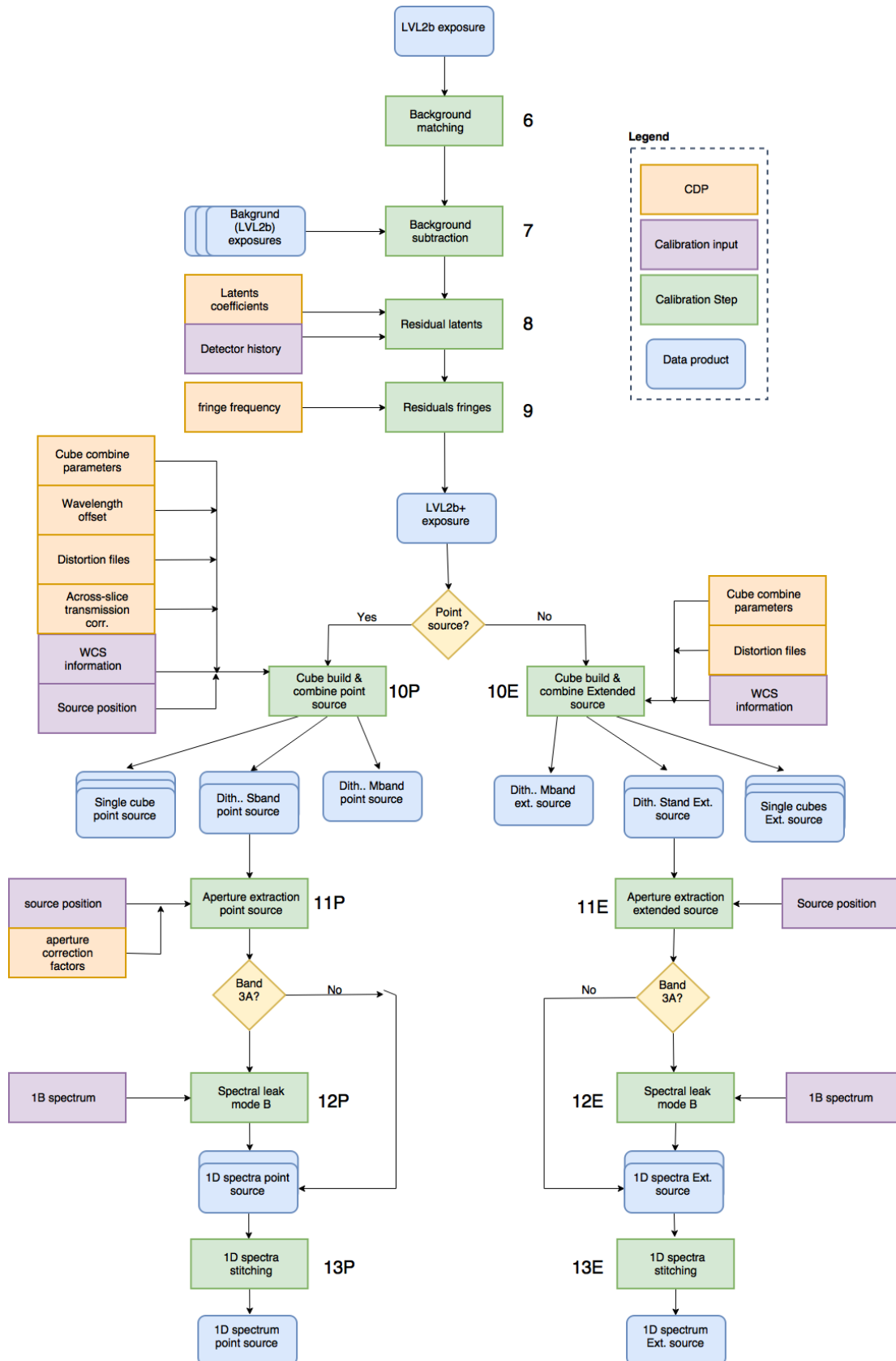


Figure B.2: Schematic description of CALSPEC3